Experimental and Theoretical Analysis of the Performance of Micro Co-Generation Systems Based on Various Technologies

GEORGIOS GKOUNIS

Ph.D.

2015

Experimental and Theoretical Analysis of the Performance of Micro Co-Generation Systems Based on Various Technologies

GEORGIOS GKOUNIS

A thesis submitted in partial fulfilment of the requirements of the University of Northumbria at Newcastle for the degree of Doctor of Philosophy

Research undertaken in the Mechanical and Construction Engineering Department of the Faculty of Engineering and Environment

January 2015

Declaration

I declare that the work contained in this thesis has not been submitted for any other award and it is all my own work. I also confirm that this work fully acknowledges opinions, ideas and contributions from the work of others

Name: Georgios Gkounis

Signature:

Date:

Acknowledgements

The author would like to thank the following people:

First, Prof. K. Mahkamov for encouraging my research and for his valuable advises, support and guidance during the entire course of my studies in UK. Special thanks are due to Prof. C. Underwood for his insightful ideas and help over this project. Special thanks are due to my beloved mother and sister for their continuous psychological and financial support over the course of my academic journey. Special thanks of course are due to my loving partner in life, Miss Theofania Pitta for her unconditional love, support, and patience. Moreover, I would like to express my gratitude to the friends and colleagues I had the pleasure to meet in the UK: Dr A. Alexakis, Dr K. Kraitong, Dr B. Belgasim, Dr M. Al-Maghalseh, Dr I. Mahkhamova and the staff at Thermacore Europe Ltd to name but a few. Additionally, I would like to thank my friends and colleagues who I met and bonded with during my first degree.

Finally, I would like to dedicate my Ph.D thesis to the memory of my beloved father S.G.Gkounis and the greatest influence on my life.

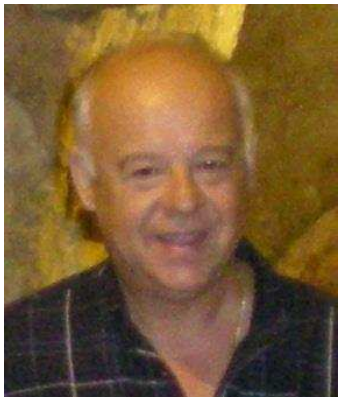

To the memory of my father
S.G. Gkounis 1957-2013

Abstract

This research is focused on the performance evaluation of micro Combined Heat and Power (mCHP) systems based on modern prime mover technologies using both theoretical and experimental analysis. Estimations of the environmental and economic impact associated with their deployment in residential conditions were also carried out.

Experimental work was performed on assessing the dynamic and steady-state performance of the 1 kW_e Stirling based mCHP system (Whispergen), the 0.75 kW_e Proton Exchange Membrane Fuel Cell (PEMFC, PA Hilton Ltd) and the 5.5 kW_e Internal Combustion Engine (ICE) based mCHP (Dachs). Results obtained from experiments (such as partial efficiencies, nominal capacities etc.) were fed directly in a theoretical model. Primary energy requirements corresponding to average UK domestic conditions were simulated based on real life technical data. All theoretical work was conducted using EnergyPlus building simulation tool in which the operation of several hydronic heating systems was modelled. Furthermore, attained experimental data and previously published research results were used to validate the theoretical modelling process.

Several operating strategies of the Stirling based mCHP unit were simulated in order to determine the regime which offers highest reduction in carbon emissions and household expenditures. In addition, variations in a number of parameters that significantly affect the performance of the system were investigated including energy consumption profiles, occupancy characteristics, dwelling thermal requirements, domestic hot water tank volume, etc). For the optimum performance strategy, several configurations of co-generation systems with nominal capacity in the range from 1 to 3 kW_e were simulated. All simulated mCHP scenarios were compared against a conventional heating equipment. Finally, the advantages of a mass installation on a district level, consisting of 60, 120 and 240 dwellings and utilising a mixture of different mCHP units (ICE, Stirling, PEMFC), were estimated.

Table of Contents

List of Tables

Table of Figures

Nomenclature

A_i = Surface Area (m^2)

C_p = Zone air specific Heat (J/K)

Cp_{air} = Molar heat capacity of air (J/Kmol)

Cp_{O2} = Molar heat capacity of Oxygen (J/Kmol)

C_T = Sensible Heat Capacity Multiplier

D = Diameter of the effective area of the anemometer orifice (m)

E_{gen} = Electricity generation (kWh)

F = Faraday constant (9.6485×10^4 C mol^{-1})

$\dot{H}_{air}$ = Total enthalpy flow rate of air introduced to control volume (W)

$\dot{H}_{dilution-air-in}$ = Total enthalpy flow rates of air that is drawn through the cabinet for cooling purposes.

$\dot{H}_{FCPM}$ = Total enthalpy flow rate of produced gases exiting the control volume (W)

$\dot{H}_{fuel}$ = Total enthalpy flow rate of fuel introduced to control volume (W)

$\dot{H}_{liq-water}$ = Total enthalpy flow rate of water required if required for steam reformation (W)

I = Stack current (A)

$[MC]_{cw}$ = Thermal capacitance of encapsulated cooling water and heat exchanger shell immediate thermal contact (J/K)

$[MC]_{eng}$ = Thermal capacitance of the engine control volume (W/K),

$\dot{N}_{air}$ = Air molar flow rate (kmol/s)

$\dot{N}_{fuel}$ = Molar fuel flow rate (kmol/s)

$\dot{N}_i$ = Molar flow rate of gas constituent i (kmol/s)

$\dot{N}_{liq-water}$ = Molar flow rate of liquid water for reformation purposes (kmol/s)

N_{stops} = Number of operation cycles

$P_{el,ancillaries-AC}$ = Power draw of the ancillaries included within the control volume (W)

P_{el} = DC net power generated by FC (W)

P_{inlet} = Air inlet pressure (PA)

$P_{net,ss}$ = Steady-state electrical output of the system (W)

Q_{fuel} = Energy content of the fuel (kWh)

Q_{gen} = Heat generated from the mCHP (kWh)

$\dot{Q}_i$ = Convective internal loads (W)

Q_{LHv} = Molar latent heat of evaporation for water (kJ/kg)

$\dot{Q}_{sys}$ = Air System Output (W)

T_{air} = Air Temperature (°C)

$T_{cw,i}$ = Bulk temperature of the plant fluid entering the heat recovery section (°C)

$T_{cw,o}$ = Bulk temperature of the plant fluid leaving the heat recovery section (°C)

T_{eng} = Temperature of the engine control volume (°C)

T_{flow} = Flow water temperature in the circuit (°C)

T_i = Inside face Temperature (°C)

T_{inlet} = Air inlet temperature (°C)

T_o = Outside face Temperature (°C)

T_{out} = Temperature of air stack outlet (°C)

T_{return} = Return water temperature in the circuit (°C)

T_{room} = Room temperature (°C)

T_s = Surface Temperature (°C)

T_{stack} = Temperature of the fuel cell stack (°C)

T_{sup} = Air system supply temperature (°C)

T_z = Zone Temperature (°C)

UA = Heat loss coefficient (W/K)

UA_{HX} = Effective thermal conductance between the engine control volume and the cooling water control volume (W/K)

UA_{loss} = Effective thermal conductance between the engine control volume and the surrounding environment (W/K)

X_j = Outside CTF coefficient

Y_j = Cross CTF coefficient

Z_j = Inside CTF coefficient

h_i = Heat transfer coefficient (W/m^2K)

$\hat{h}_i$ = Molar enthalpy of gas constituent i (J/kmol)

$\dot{m}_{air}$ = Air mass flow rate through the engine (kg/s)

$\dot{m}_{CH}$ = Mass flow rate of the space heating circuit (kg/s)

$[\dot{m}c_p]_{cw}$ = Thermal capacity of the surrounding environment (W/K)

$\dot{m}_{cw}$ = Mass flow rate of plant fluid through the heat recovery section (kg/s)

$\dot{m}_{DHW}$ = Mass flow rates of the domestic hot water circuit (kg/s)

$\dot{m}_{fuel}$ = Mass fuel flow rate (kg/s)

m_i = Air flow rate due to inter-zone mixing (kg/s)

n = Cycle duration (minutes)

n_{cells} = Number of cells

q'' = Conduction heat flux on the inside face (W/m^2)

$q_{gen,ss}$ = Steady-state rate of heat generation within the engine (W)

q_{gross} = Gross heat input into the engine (W),

q''_{ko} = Conduction heat flux on the outside face (W/m^2)

q_{s-cool} = Heat extracted from system in order to maintain temperature (W)

$q_{skin-loss}$ = Parasitic thermal losses from the control volume (W)

s_i = Coefficients based on manufacturer data or analytic models

$t_{threshold}$ = Time period that FC exhibit no degradation for a given time period (s)

v_{air} = Air flow rate (SLM)

w_i = Coefficient based on empirical data

Subscripts

e = Electrical

gen = Generated

max = Maximum

th = Thermal

Greek Characters

Δh_f = Change of enthalpy (J)

$\Delta_f \hat{h}^o_{H_2O,fg}$ = Latent heat of vaporisation of water at the standard state (J/kmol)

$\Delta_f \hat{h}^o_i$ = Molar enthalpy of the gas i at standard state (J/kmol)

Φ_φ = Flux CFT coefficient

ε_i = Coefficients supplied by user

δ = Time step

η_{co} = Co-generation efficiency

η_e = Electrical efficiency

η_{Nom} = Nominal efficiency

η_q = Thermal efficiency

ρ_{air} = Zone air Density(kg/m^3)

Acronyms

ASHP = Air Source Heat Pump

CCD = Charge Couple Device

CH = Central Heating

CTF = Conduction Transfer Function

DHW = Domestic Hot Water

GDL = Gas Diffusion Layer

HHV = Higher Heating Value

HPR = Heat to Power Ratio

HVAC = Heating Ventilation and Air Condition

ICE = Internal Combustion Engine

LHC = Lower Heating Value

mCHP = Micro-Combined Heat and Power

MEA = Membrane-Electrode Assembly

FIT =Feed-in Tariff

ORC = Organic Rankine Cycle

PEMFC = Proton Exchange Membrane Fuel Cell

SOFC = Solid Oxide Fuel Cell

WTR = Water Transfer Region

Chapter 1 Introduction

1.1 Introduction

Increased energy requirements that the modern lifestyle imposes have raised the greenhouse gases emissions with significant impact in global warming. The continuous decreasing of the fossil fuel reserves combined with the increasing prices of energy contribute to the global energy crisis. Governments with consciousness of the potential problem have a strong interest in renewable and low carbon technologies. Particularly in the UK, households contributes extensively to the net carbon footprint (approximately 74 %) [1]. Greenhouse emission have been increasing 3 % per annum between 1997 and 2004 and it is predicted to continuously increase by 2030 [2]. It has been recently introduced financial incentives when renewable power generation systems are implemented for residential applications such as "Feed-in tariff" and more recently the "renewable heat incentive". These incentives are aimed at increasing the number of installed units and reducing the carbon dioxide emission associated with the burn of fossil fuels as required by the climate change act.

Micro scale Combine Heat and Power systems (mCHP) are an attractive alternative for onsite heat and power generation. Development of such systems was abandoned due to the central electricity generation and national grids, however at the start of the twenty first century the environmental awareness urged for utilisation of efficient technologies that could be used in CHP systems. Primary energy savings and carbon emission reduction could be attained if such systems replace conventional heating systems. Benefits are attributed to high overall efficiency and moderate electricity import from the national grid.

Technologies utilised in such co-generation systems include the Stirling engine, Internal combustion engines (ICE) and fuel cells. Although published research findings predicted significant advantages of proton exchange membrane (PEM) fuel cell based mCHP, technology is far from being commonly available. On the contrary, ICE and Stirling based units have reached commercialisation stage and some units have already been deployed in domestic sector. Systems that reached the commercial level are the Honda Ecowill, Baxi SenerTech Dachs ICE mCHPs and Baxi Ecogen and Whispergen Stirling engine MCHPs.

This research is focused on assessment of the performance of mCHPs based on the three leading prime mover technologies by means of theoretical modelling and experimental work. Obtained results from test-rigs were used for validation of numerical process, whilst both key parameters and real life technical data were applied in theoretical modelling and improved the accuracy of heating systems simulations. This work is concluded by analysing the reduction in carbon emissions and utility expenditures in a mass installation scheme which utilised a mixture of different mCHP units (ICE, Stirling, PEMFC) on the small district (street) scale.

In summary, mCHP systems could offer environmental and financial advantages compared to a convectional heating system. However the magnitudes of the potential benefits are highly depended on several parameters. This research aims to provide insights and to recommend the optimum technology and operational pattern to achieve the maximum benefits.

1.2 Research Aims

The aims of this research are:

1. To estimate environmental and economic impact of modern mCHP units in individual dwellings;
2. To assess the effect of variation in energy consumption profiles, occupancy characteristics, dwelling thermal requirements, domestic hot water tank volume, etc.;
3. To identify mCHP technologies which provide greatest benefits when deployed in individual dwellings;
4. To estimate the ecological and financial impact of deployment of a mixture of different mCHP technologies (ICE, Stirling, and PEMFC) on a district level.

1.3 Research Objectives

The objectives under investigation in this research are:

1. To experimentally assess the performance of three mCHP units; namely Whispergen Mk Vb 1 kW_e Stirling engine, PA Hilton PEM fuel cell 0.75 kW_e and Baxi SenerTech Dachs 5.5 kW_e ICE engine based mCHP units.
2. To model the domestic thermal load of a generic semi-detached, detached and bungalow dwellings under different construction regulations.
3. To model primary energy demand profiles (electricity, DHW) based on measured data.
4. To simulate the operation of a residential hydronic heating system with the co-generation systems.
5. To assess the performance of various configuration and operating strategies of Whispergen Stirling engine based mCHP.
6. To validate the theoretical modelling using obtained experimental data.
7. To simulate a mass installation scheme that consists of a mixture of modern engine based mCHP technologies.

1.4 Research Methodology

This research was conducted in several stages which are outlined:

1. The performance of three leading technology based mCHP units (Whispergen Mk Vb 1 kW_e Stirling engine, Hilton PEM fuel cell 0.75 kW_e and Baxi SenerTech Dachs 5.5 kW_e ICE) was experimentally investigated in respect to steady-state and dynamic operation.
2. Obtained results from experimental set-up such as thermal and electrical output, partial and overall efficiencies, etc. were used in modelling of a hydronic heating systems based on the mentioned mCHP units using Energy Plus software.
3. Real life technical data were used in theoretical modelling of primary energy requirements in three generic UK dwellings.
4. A validation process was carried out in order to ensure the viability of the theoretical simulations.
5. Modelling was expanded to mCHP systems based on three technologies (Stirling and ICE engines, PEMFC) with nominal electrical output in the range of 1-3 kW_e. The modelling was completed for different electrical and thermal requirements of buildings.
6. A simulation of a mass installation scheme on a district level which utilised a mixture of different mCHP technologies (ICE, Stirling, and PEMFC) was finally performed.
7. Annual reduction in both carbon emissions and household expenditures were estimated for all simulated scenarios.

1.5 Contribution to knowledge

The novelty in this research can be summarised as follows:

- Firstly, the modelling of the operation of different types of mCHP systems using measured technical data, including the effect of transitional regimes, considerably improved the accuracy of the simulating process over previous research in mCHP systems.
- Secondly, an operating strategy and configuration of the Stirling engine based mCHP system was proposed that provided enhanced the economic and environmental benefits.
- Thirdly, the comparison of all three technologies, namely PEMFC, ICE and Stirling, was carried out experimentally and theoretically whilst previous works mainly considered just two technologies.
- Finally, for first time the primary energy consumption and carbon emissions reduction were estimated on a district/street level with utilisation of a mixture of different mCHP units (ICE, Stirling, PEMFC)

1.6 Thesis Structure

The outline of this thesis and the investigation process are described in this section. The thesis is separated into the following eight chapters:

Chapter 1 - Introduction: This chapter presents the aims of this research, the methodology followed and highlights the contribution to knowledge and the thesis structure.

Chapter 2 - Literature review: In this chapter previous published research on mCHP systems based on various technologies is reviewed. Results from experimental and theoretical work

on co-generation units and research findings related to the prime mover engine technologies are presented.

Chapter 3 - Theory and Application of mCHP systems: This chapter presents the theory behind the four major co-generation technologies. The fundamentals of operation, the advantages and the application of Stirling and IC engines, PEM fuel cell and Rankine cycle are described in this section.

Chapter 4 - EnergyPlus software: This chapter describes the structure of the building simulating tool used for modelling. The outline of the simulation process and the governing equations followed in each stage of calculations are described here.

Chapter 5 - Experimental results: In this chapter the results obtained from experimental set-ups are analysed. Three cogeneration units (Whispergen Mk Vb 1 kW_e Stirling engine, Hilton PEM fuel cell 0.75 kW_e and Baxi SenerTech Dachs 5.5 kW_e ICE) installed in the laboratory at Northumbria University in Newcastle were tested under steady-state and transitional regimes. Furthermore, the validation process of the theoretical results is presented here.

Chapter 6 - Simulation results: In this chapter the results obtained from numerical modelling are presented and analysed. The discussion starts with the description of the energy demand modelling in a generic UK building in which a number of configurations and operating strategies of the Stirling base mCHP unit were considered. Moreover, simulation was expanded to alternative house types with different energy demands. Finally, the ecological and economic performances of each unit were compared with reference to a conventional condenser boiler house heating scenario in order to identify the most feasible technology and operating regime.

Chapter 7 - District Scheme: This chapter considers the investigation of the primary energy and carbon emissions reduction on a district level with utilisation of a mixture of different

mCHP units, namely ICE, Stirling and PEMFC. Moreover, it introduces the effect of electrical interaction between dwellings.

Chapter 8 - Conclusion and recommendation of future work: The final chapter highlights the main outcome of this research. It includes the summary of the findings and recommendations for further improvement in respect to the experimental and theoretical methodology followed throughout this work.

Chapter 2 Theory of mCHP technologies

2.1 Introduction to micro-cogeneration systems

The origins of combined heat and power (CHP) arise from the factories of the industrial revolution in the late nineteenth century, when engineers utilised the waste heat from power plants for both space heating in winter and facilitation in manufacturing processes. Development of such systems was abandoned due to central electricity generation and national grids, however at the start of the twenty first century environmental awareness issues urged a need for utilisation of efficient technologies that could be utilised in CHP systems. In addition the development of innovative prime movers such as fuel cells, Stirling engines, micro turbines and the necessity for energy decentralisation contributed to the renaissance of interest in CHP [3].

CHP systems can be classified according to their capacity. Large scale includes systems over 2 MW_e, small scale embraces systems with power capacities greater than 100 kW_e and less than 2 MW_e, and Micro scale ('mCHP') refers to units that can be applied in small buildings with a nominal capacity smaller than 50 kW_e [4]. Although 90 % of the units installed worldwide are in the range of large scale, the widest range of technologies is comprehended within the small scale category.

2.1.1 Micro CHP technologies

Micro scale cogeneration technologies are based on Stirling engines, internal combustion (IC) engines, fuel cells (FC), small gas turbines and the Rankine cycle using an organic working fluid (usually referred to as 'organic Rankine cycles' (ORC)). These units are full packages and utilise the waste heat for space heating and domestic hot water applications, mainly

covering energy demands of small buildings and individual houses. Due to low power generation it is crucial to select the adequate technology which will match the application's energy requirements and heat to power ratio (HPR).

Development of the detailed theoretical models of mCHP is beyond the framework of this research, therefore mCHPs operational principles are described only on the simple thermodynamic cycle level.

2.2 Stirling engine based mCHPs

2.2.1 The Stirling cycle

In domestic micro-CHP applications a natural gas burner is used for supplying a high temperature heat at the hot end of a Stirling engine whilst water circulation in the primary hydronic space heating system is used for cooling its cold end. The pressure/volume (PV) diagram in Figure 2.1 shows the ideal thermodynamic cycle of a Stirling engine. The cycle is defined as a closed regenerative cycle with a gaseous working fluid. The working gas is sealed inside the engine, therefore heat is transferred by conduction through the cylinder walls. Due to limited surface areas of cylinder walls, the heat transfer is limited. However the use of a regenerator enhances the thermal performance.

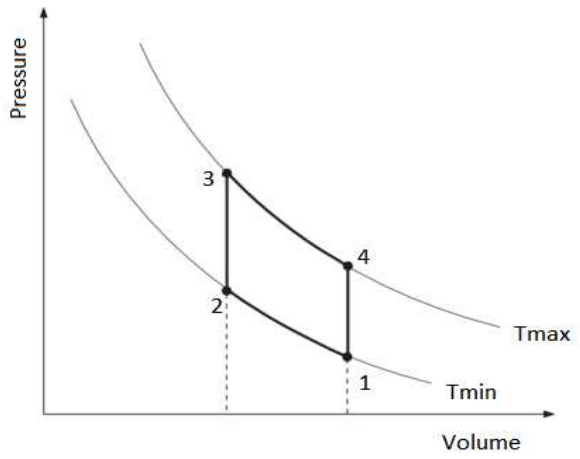

Figure 2.1 Theoretical thermodynamic Stirling cycle [5]

The four thermodynamic processes as evidenced in Figure 2.1are:

1-2 Isothermal compression (compression occurs at constant temperature);

2-3 Isochoric heat addition (heat supply to the gas at constant volume result in pressure and volume rise);

3-4 Isothermal expansion (working gas expands at constant temperature, exerting a force on the working piston and producing useful work)

4-1 Isochoric heat removal (working gas flows through regenerator dispensing heat which will be used in the next cycle)

The PV diagram in Figure 2.2 shows the idealised Stirling cycle upon which the deviation from the ideal cycle due to practical design and material choices is superimposed. This divergence is also attributed to the omission of the volume of both regenerator and in-pipe heat exchangers of the engine (usually referred as dead volume) from the theoretical approach.

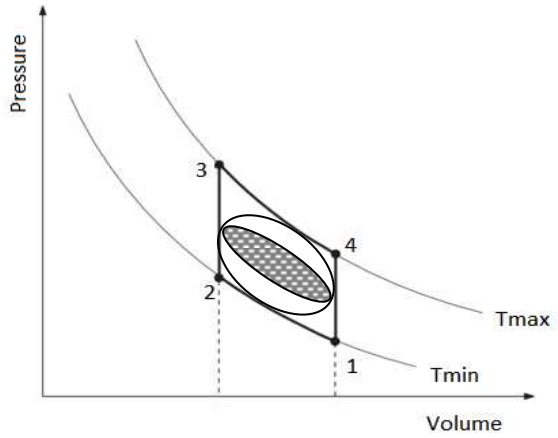

Figure 2.2 Thermodynamic Stirling cycle constrains [5]

In Figure 2.2 the actual cycle is represented by the elliptical shape in the middle of the graph. The gas gradually undergoes through changes in volume, pressure and temperature. As the dead volume is reduced, the cycle moves outwards the larger (light grey) ellipse. Efficiency

of any ideal heat engine is limited by the temperature differential at the hot and cold ends of the engine, as shown by the following equation:

$$\eta = \frac{W}{Q_h} = 1 - \frac{T_c}{T_H} \tag{2.1}$$

where η is the efficiency of Carnot cycle, W is the work done by the system, Q_H is the heating energy entering the system, T_C is the absolute temperature of the cold reservoir and T_H is the absolute temperature of the hot reservoir.

The efficiency of the Stirling engines is depended on the temperature difference between the hot and the cold parts of the engine. The higher temperature difference results in the higher efficiency. However, the upper temperature is limited by the metallurgical limit of materials used for manufacturing the hot side of the engine. In order to avoid the efficiency reduction it is also necessary to minimise the heat losses from the hot to cold components of the engine due to heat conduction, the hot working fluid bypassing etc. Stirling engines operate with the elevated pressure of the working fluid with its level limited by both metallurgical considerations and wear of engine components due to high loads. Finally, further constraints which result in further deviation from the theoretical attainable efficiency are mechanical losses due to friction in the drive mechanism and in bearings, pumping losses, heat losses, etc.

2.2.2 Fundamentals of operation

Stirling engines operate on a closed regenerative thermodynamic cycle, with cyclic compression and expansion of the working fluid at different temperatures [5]. They are external combustion engines, the main advantages of which are that they can be supplied by any source of heat and they could achieve the theoretical thermal efficiency comparable to the maximum efficiency of the Carnot cycle (though in practice numerous losses contribute to lower efficiencies). Other practical advantages include low pollutant emissions, low noise

and vibration levels during operation, long lifespan and service intervals, characteristics which are mainly due to the controlled combustion process that is used for the heat input. A constant heat supply is applied at the hot end of the engine whereas the cold end is cooled down by water circulation. The temperature differential in hot and cold end causes fluctuation in the working gas pressure and therefore forcing the piston to oscillate between the two temperatures zones. Figure 2.3 shows a free piston Stirling engine consisting of a cylinder, power piston displacer, and regenerator. The displacer has a very small mass compared to the power piston and acts to regulate the gas flow through the regenerator. In contrast the power piston's oscillation is maintained due to constant temperature difference across the displacer with a frequency close to the natural frequency of the system. Power in such engines is typically generated in a linear alternator. Although Stirling engines could utilise several types of fuel, in order to obtain maximum performance units are designed to operate with a single heat source. The higher thermal efficiency due to lower heat losses can be attained when a regenerator is applied in Stirling engines. This particular heat exchanger, which consists of a matrix of fine wires, has ability to store and retrieve heat as the working fluid oscillates between its cold and hot ends. Finally, in stationary applications (like mCHP) Stirling engines are designed to operate at the fixed speed of approximately 1200-1500 rpm.

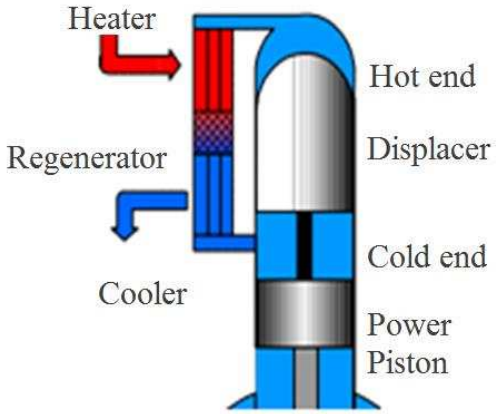

Figure 2.3 Free piston Stirling engine [6]

Mechanical configurations

Stirling engines can be classified in two major categories: (a) single-acting and (b) double-acting engines. Single-acting engines are an assembly of an expansion space, compression space and associated heat exchangers in one or two cylinders with two reciprocating elements

one of which must be a piston [5]. The second category embraces engines of multiple cylinder arrangements where the expansion space of one cylinder is linked through the associated heat exchangers to the compression space of the adjacent cylinder. The main advantage of the double-acting engines is the number of moving parts which is half the number required in multiple arrangements of single-acting engines [5]. The latter can lead to simplified kinematic drives, therefore reducing the cost.

Stirling engines can also have several alternative configurations. Figures 2.4-2.7 [6] show the schematics of Alpha, Beta, Gamma and wobble plate type Stirling engine configurations.

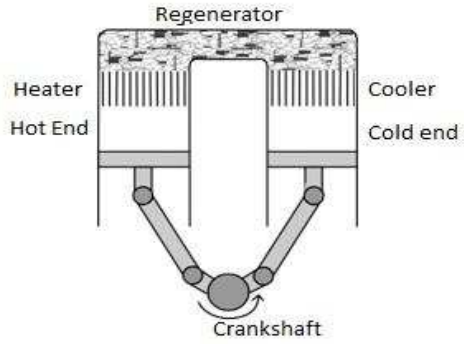

Figure 2.4 Alpha type Stirling engine

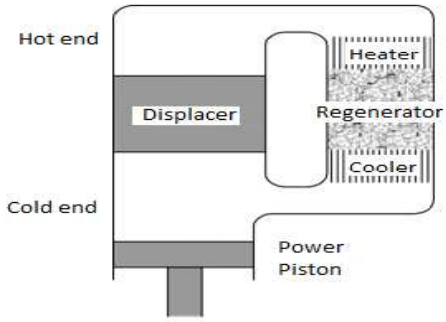

Figure 2.5 Beta Type Stirling engine

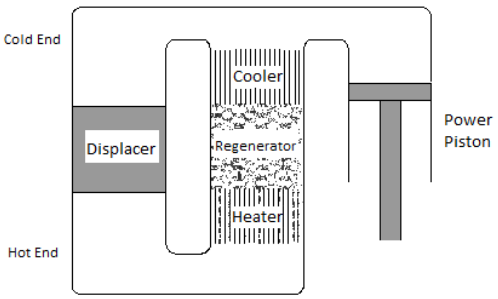

Figure 2.6 Gamma type Stirling engine

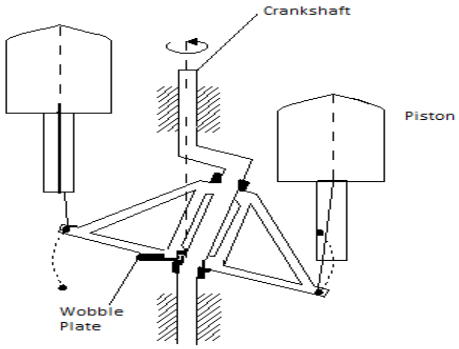

Figure 2.7 Wobble plate Stirling engine [6]

Alpha configured engines can be either single or double acting engines, whereas Gamma and Beta type engines are configured as single acting machines. It has been noticed that Beta type engines are more efficient than the others, however highest efficiency is not always a desirable goal [3]. The preference of the piston-displacer engines is down to the fact that those configurations have simpler reciprocating seals [5] mainly because the sealing around the displacer is smaller than around the piston. Another advantage is the reduced levels of vibrations and mechanical friction losses as a result of lighter reciprocating mass compared to multiple pistons machines.

2.2.3 Applications

The major advantage of external combustion engines, as mentioned, is the utilisation of a wide range of heat sources. In solar application the hot end of a Stirling engine can be placed at the focal point of a parabolic concentrating dish as shown in Figure 2.8. Heat generation from the combustion process of any biofuel can be used to drive a Stirling engine. Stirling engines could be used to convert radioactive-decay heat into electricity in space application for on-board power supply of the spacecraft as shown in Figure 2.9.

Figure 2.8 A 25 kW tracking, concentrating solar power (CSP) dish collector [6]

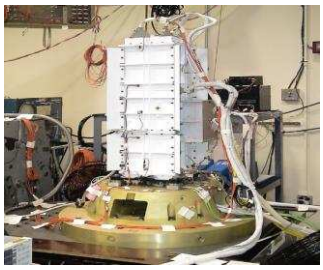

Figure 2.9 An advanced Stirling Radioisotope Generator (ASRG) 130-140 Watts unit which utilises plutonium-238 as heat source developed by NASA [6]

Exhaust gases from the combustion process can be utilised for enhancing the production of bio-gas as shown in Figure 2.10. Finally Stirling engine based mCHP could replace conventional heating systems in domestic sector

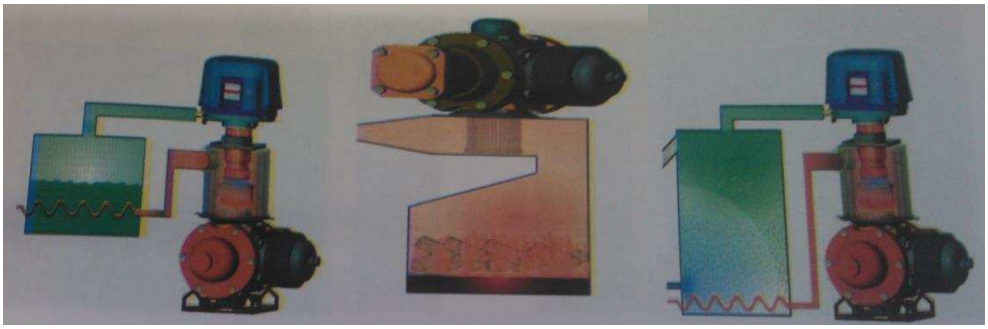

Figure 2.10 Small and micro Stirling engine systems powered by biofuels [4]

2.2.4 Commercially available mCHP systems based on Stirling engines

Micro scale CHP plants have been found to be an attractive option for residential applications. Replacing conventional heating systems based on gas-fired boilers can offer potential environmental and economic benefits in houses. Benefits are mainly attributed to increased energy utilisation and decreased power transmission losses compared to grid connected scenarios as well as reduced carbon emissions.

The Microgen unit was developed by BG Group from US (Sunpower) design, it was taken over by a consortium of gas boiler (Viessmann, Baxi, Vaillant, Remeha) manufacturers. Mass production of engines takes places in China. The engine is based on a Beta type free piston engine with a nominal capacity of 1 kW_e and 5 kWth electrical and thermal power, respectively. However, current models feature a higher thermal output by implementing an auxiliary burner of up to 18 kW_{th} depending on the manufactures. Figure 2.11 shows an 1 kW_e mCHP unit by Baxi. The Disenco mCHP unit (see Figure 2.12) is based on a beta type kinematic design Stirling engine. The design features air-preheater and finned tube heater head both of which contribute to the high efficiency. The unit is characterised by modulation

capabilities and output varies in range of 0.5-3 kW_e and 12-17.4 kW_{th}. A 3 kW_e electrical output mCHP was developed by Sunmachine. The engine utilises the heat from biofuel combustion using a finned tubular heater. The unit is manufactured in Germany and claimed to have a 20 % electrical and 90 % cogeneration efficiency. The Infinia mCHP is based on a free piston engine and was originally developed for incorporation in micro CHP products manufactured by Ariston (formerly MTS) and Bosch in Europe as well as Rinnai in Japan [7]. In 2013 Infinia was acquired by Qnergy which currently has two units available of 3.5 kW_e and a 7.5 kW_e. Thermal capacities are in the range of 3.5-10 kW_{th} and 7.5-22 kW_{th}, respectively. Figure 2.13 shows a 3.5 kW_e mCHP system of Qnergy.

Figure 2.11 BaxiEcogen 1 kW_e Stirling engine based mCHP [8]

Figure 2.12 Inspirit Energy Holdings plc [9]

A unit which is capable to satisfy larger thermal requirements targeting commercial buildings rather than residential installations was manufactured by Cleanergy AB (formerly Solo). The Solo V160 engine is based on a two-cylinder alpha type Stirling engine and it was designed to operate on biogas. Nominal electrical capacity is in the range between 2 and 9 kW_e which corresponds to 8 to 26 kW_{th}. This unit features a claimed efficiency of 22 %. One of the major manufacturers of domestic mCHP units is Whispertech a company based in New Zealand. The unit is based on a four-cylinder double acting, alpha type engine with a

'wobble-yoke' kinematical mechanism to convert the reciprocating piston motions into the shaft's rotation.

The latest MKV model unit has a nominal capacity of 1 kW_e and 7 kW_{th} which corresponds to the electrical efficiency of 12 % and thermal efficiency of 67 %. The mCHP incorporates an auxiliary burner of 5 kW_{th} in order to meet higher thermal loads. The operation of the additional burner is controlled by an outdoor sensor which ensures that the heat primarily is delivered by the engine unless extremely low ambient temperatures are detected. Figure 2.14 shows the design of a Whispergen mkV mCHP unit

Figure 2.13 The Qnergy QB engine mCHP series; [10].

Figure 2.14 Whispergen MKV 1 kW_e Stirling engine based unit mCHP [11]

2.3 Internal Combustion and reciprocating engines based micro CHP

2.3.1 Fundamentals of operation

Internal combustion engines (ICE) convert the chemical energy contained in the fuel into mechanical power [12]. The term "internal" refers to the fact that fuel oxidisation takes place within the engine. After a century of undergoing development ICE technology offers high fuel conversion efficiency and high power-to-weight ratios. Applications of internal combustion engines include transport, stationary power applications, combined heat and

power systems, etc [3]. Numerous criteria are used in the classification of ICE engines which could be presented according to

i. Application: Transport, power generation, cogeneration;
ii. Basic engine design: Reciprocating engines, rotary engines;
iii. Working cycle: four-stroke, two-strokes engines;
iv. Valve or port design and position: Overhead/ underhead valves, rotary valves etc.
v. Fuel: Petrol, natural gas, alcohols, dual fuel, hydrogen, diesel, biodisel, biogas/syngas;
vi. Method of mixture preparation: Carburetion, fuel injection etc.
vii. Method of ignition: Spark ignition, compression ignition;
viii. Method of cooling: Water cooled, air cooled.

Although the above classification illustrates the range of configurations of engines, the method of ignition is commonly used for describing the fundamental operation characteristics of IC engines [12]. Spark ignition engines (also referred as "Otto engines") use a spark plug to ignite the compressed pre-mixed charge in the cylinder. On the other hand, in Diesel engines (compression ignition engines), the ignition occurs when high pressure fuel is injected directly to the compressed air within the cylinder [3]. Both engines can use two-stroke or four stroke cycles. Nevertheless, the four stroke cycle is the most common. However, in applications in which power density is crucial two stroke engines are preferable as they can provide higher power output for a given engine size.

Figure 2.15 shows a basic geometry of the internal combustion engine. In common reciprocating engines the piston moves up and down in a cylinder and transfers power through a connecting rod and crank mechanism to the drive shaft [12]. The piston passing periodically through the top centre crank position (TC) which corresponds to the minimum

cylinder volume and the bottom-centre crank position which corresponds to the maximum cylinder volume.

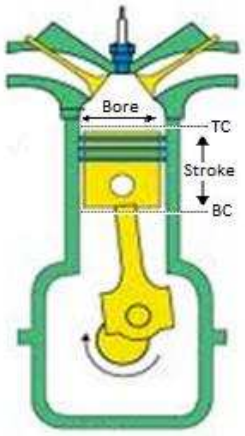

Figure 2.15 Basic geometry of a single cylinder ICE engine [12]

The minimum volume is called clearance volume V_c while the difference of the total volume V_t and the dead volume is referred as the displaced or swept volume V_d. The ratio of the maximum to the minimal volume is the compression ratio r_c. The majority of IC engines operate with a four-stroke cycle, where a complete power stroke is produced when each piston undergoes a sequence of four events as shown in Figure 2.16

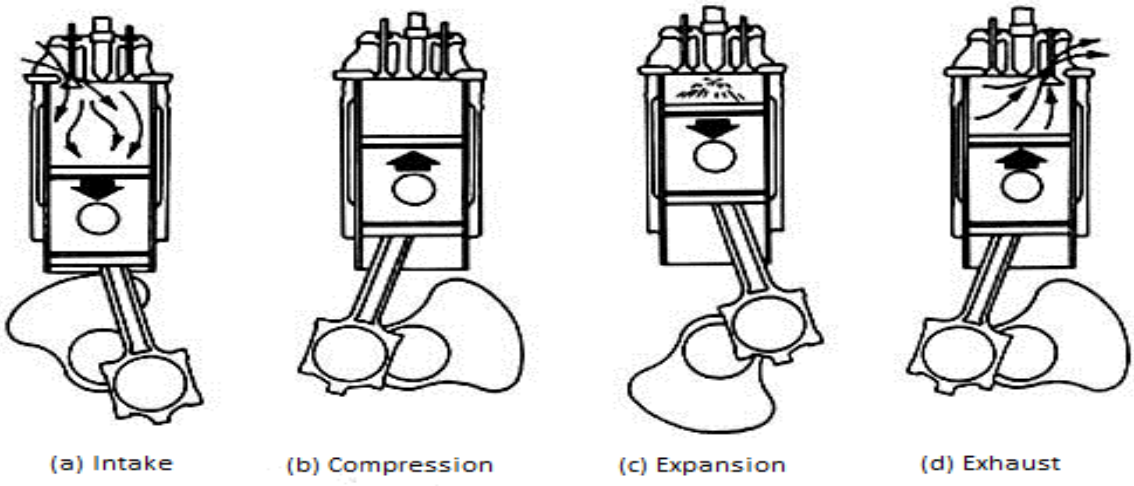

Figure 2.16 The four stages of a four-stroke internal combustion engine [12]

These four strokes could be described as follows:

a) Intake stroke; Mixture of air/fuel enters through the inlet valve into the cylinder while the piston is moving from TC to BC position
b) Compression stroke; The mixture inside the cylinder is compressed to a small fraction of its original volume and ignited. Combustion occurs when the piston is at TC position which causes the temperature and pressure to rise rapidly in the cylinder.
c) Expansion stroke; High pressure and temperature gases exert a force on the piston therefore producing mechanical work.
d) Exhaust stroke; The burnt gases exit the cylinder through the exhaust valve due to pressure difference in the cylinder and ambient and due to piston movement towards TC.

The cycle described is a sequence of processes in which the state of working fluid could be examined and provide quantitative information on engine operation [12].

In the simplest types of two-stroke engines, valves are controlled by the piston motion and the cycle consists of a compression stroke and an expansion stroke only.

2.3.2 Thermodynamic cycle

Figure 2.17 shows an example of an ideal pressure-volume diagram based on a constant volume combustion process.

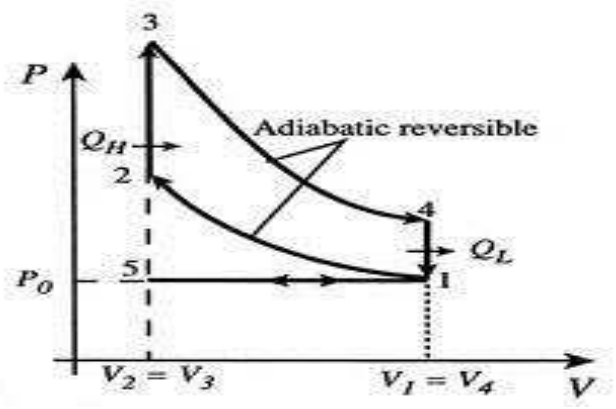

Figure 2.17 Pressure-Volume diagram for an ideal constant volume combustion cycle [13]

The processes in this cycle are described as follows:

- Intake stroke; Air/fuel mixture is drawn into engine (5-1);
- Compression stroke; Pressure and temperature of mixture rises (1-2);
- Combustion occurs over a short time period at the constant volume (2-3);
- Power Stroke; Expansion of the burned mixture result in useful work generation (3-4);
- Heat rejection: the bulk of combustion products leave though exhaust valves (4-1)
- Exhaust stroke: The remains of the combustion products are swept out due to the piston's upward motion (1-5);

A set of assumptions were applied in the analysis of ideal engine processes. These simplifications could be summarised as follows: adiabatic compression and expansion; combustion is considered adiabatic and at constant volume and combustion is complete, constant pressure at the mixture intake process, negligible velocity effects, etc [12]. Figure 2.18 shows an actual engine cycle.

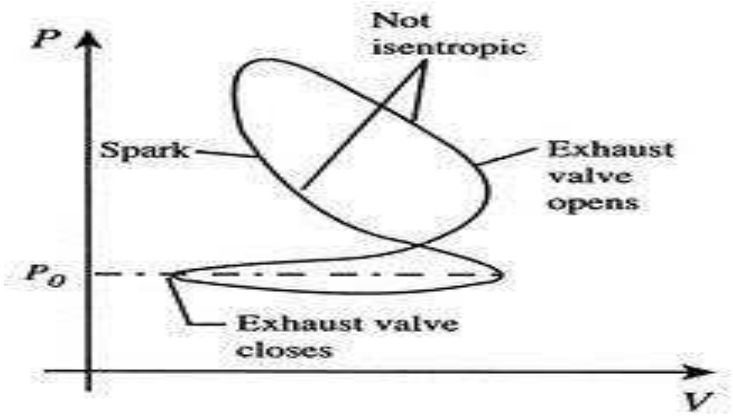

Figure 2.18 Pressure volume diagram for an actual constant volume combustion cycle [13]

As can be noticed in Figure 2.18 an actual engine cycle undergoes a gradual change in pressure, temperature and volumes. Deviation from the ideal cycle can be attributed to friction and mechanical losses and to the omission of all mentioned assumptions.

2.3.3 Commercially available mCHP units based on Internal Combustion engines

Main advantage of the internal combustion engines is the rapid variation of the generated power as a result of the reaction to control. In the automotive application the mentioned characteristic makes them preferable over the external combustion engines. However in stationary applications, IC engines could be improved to reduce engine vibrations and noise levels, emissions, maintenances intervals and raise the reliability. Early mCHP products, based on automotive ICE technology, could not overcome those technical challenges, therefore ICE based mCHPs were not often considered for domestic applications. However, later units demonstrated the increased efficiency, lifespan and low maintenance cost. Available internal combustion engine based mCHP units can be classified according to their nominal capacity. For individual houses a power range of 1 kW_e is considered whereas for multifamily applications and commercial buildings 5 kW_e and 10 kW_e power capacity units are available. In the range of multifamily applications SenerTech Dachs, a company based in Germany, is the market leader in Europe with more than 20000 units installed. Figure 2.19 shows a 5 kW_e ICE mCHP unit of SenerTech Dachs. The unit has a power nominal output of 5 kW_e and thermal output in the range of 10.5-14.9 kW_{th} depending on the version of the unit. Engine operates either with natural gas or diesel fuel, however electrical efficiency is above 26 % for all versions [3]. The Ecopower units manufactured by Vaillant (Figure 2.20) are based on the Marathon gas engine. The manufacture offers two versions with a nominal capacity of 3 and 4.7 kW_e. Both engines feature modulation capabilities which believed to offer significant advantages over competitors. MCHP units with electrical output of 1 kW_e and approximately 3 kW_{th} thermal are suited for individual house applications. The Honda Ecowill ICE engine based mCHP unit has an electrical efficiency of 22.5 % whilst the cogeneration efficiency is 86 %.

Figure 2.19 SenerTechDachs 5 kW_e ICE engine based mCHP [14]

Figure 2.20 The ecoPower 3 kW_e by Vaillant offers modulation capabilities [15]

Figure 2.21 shows the Honda Ecowill system. Its novel design with the incorporation of catalytic converters and acoustic attenuation system overcome the limitation of the IC engines with a drawback on the capital cost. More than 100,000 units have been installed since 2003 with most of the units have been deployed in Japan. The ecoPOWER 1 kW_e mCHP unit from German based Vaillant (Figure 2.22) utilises the same IC engine by Honda but with enhanced performance. It features 3.5 % higher electrical efficiency than the Ecowill unit and its main advantage is that it can be installed indoors.

Figure 2.21 The Honda Ecowill 1 kW_e mCHP unit based on ICE engine [16]

Figure 2.22 Vaillant ecoPOWER 1 kW_e, shares the engine with Honda, with enhanced performance [15]

Figure 2.23 and Figure 2.24 show mCHP units that have been introduced to the European market in the last few years; namely Kirsch, Proenvis, RMB Energie and ESS. Their available capacity is not limited to micro installations (individual houses) but also expands to semi-commercial and commercial applications.

Figure 2.23 The Proenvisprio 5.2 unit has capacity of 2 kW_e and 5 kW_{th} electrical and thermal respectively [17]

Figure 2.24 The 1.9 kW_e micro unit from Kirsch [7]

2.4 Fuel cells

2.4.1 Fundamentals of operation

Fuel cells are electrochemical devices which converts the chemical energy of a fuel into electricity without involving combustion [3].

Figure 2.25 illustrates a simple fuel cell. The simplified diagram of the fuel cell consists of two electrodes at the anode and cathode side respectively and an electrolyte in-between them. Hydrogen flows onto the anode side and splits into electrons and protons. While protons can reach the cathode side electrode through the electrolyte, electrons reach the cathode electrode through a wire that interconnects both sides [18]. In a fuel cell there are two electrochemical reactions.

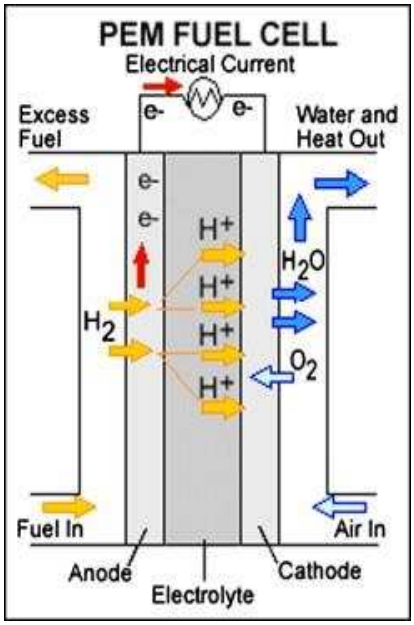

Figure 2.25 Simple Fuel cell [19]

At the anode side:

$$2H_2 \rightarrow 4H^+ + 4e^- \qquad (2.2)$$

At the cathode side:

$$4e^- + 4H^+ + O_2 \rightarrow 2H_2O \qquad (2.3)$$

The electron's flow through the external circuit constitutes a current. At the cathode side electrons, protons and oxygen are recombined and produce water following reaction in Equation (2.3). It is worth noticing that efficient products removal ensures consistent performance during operation.

The energy of the product bond configuration is lower than the energy of the reactants bond configuration, therefore the difference of the energy is released in the form of heat.

2.4.2 Fuel cell performance

The performance of a fuel cell can be graphically illustrated by means of a current and voltage characteristics curve. A polarisation curve is commonly used for this purpose in which the current output of the fuel cell for a given voltage is in the plot. Figure 2.26 shows a typical polarisation curve for a proton exchange membrane fuel cell (PEM FC).

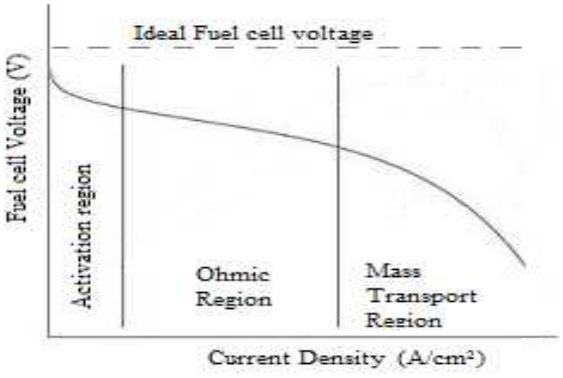

Figure 2.26 A typical polarisation curve (I-V) of a PEM FC [18]

The power output of the fuel cell is dependent on the reaction surface area. A normalised current with respect to that area (A/cm^2) is used instead of the current on the polarisation curve in order to make results comparable. Thermodynamically, a fuel cell can generate any amount of current at constant voltage [3]. However, in a real fuel cell losses that occurring at particular ranges of current densities result in deviation from ideal fuel cell voltage. The real voltage output can be expressed in the following equation.

$$V_{real} = E_{thermo} - \eta_{act} - \eta_{ohmic} - \eta_{conc} \quad (2.4)$$

where V_{real}= real voltage output of fuel cell; E_{thermo}= the ideal (thermodynamically) predicted voltage; η_{act}= activation losses; η_{ohmic}= ohmic losses; η_{conc} = concentration losses.

The ideal voltage is predicted for a reference condition and is dependent on the free-energy change of the reaction ($\Delta \hat{g}^0_{rxn}$), and the number of moles of electrons transferred in the reaction (n) and the Faraday constant (F). It can by expressed as Equation (2.2)

$$E^0 = -\frac{\Delta \hat{g}^0_{rxn}}{nF} \quad (2.5)$$

The reactions occurring in the anode electrolyte in reality occurs at several stages including mass transport of H_2 to the electrode, absorption of H_2 in the electrodes, separation of H_2, etc. The overall speed of reaction is determined by the slowest of the sub-reactions. Losses occurring in the first region of the polarisation curve are associated with the speed of the reaction. Voltage therefore decreases due to electrochemical reaction kinetics by a factor that corresponds to the voltage needed to overcome the reaction activation barrier. The transport of the charge in the cell results in an additional loss called ohmic losses which are attributed to the resistance of the fuel cell conductors.

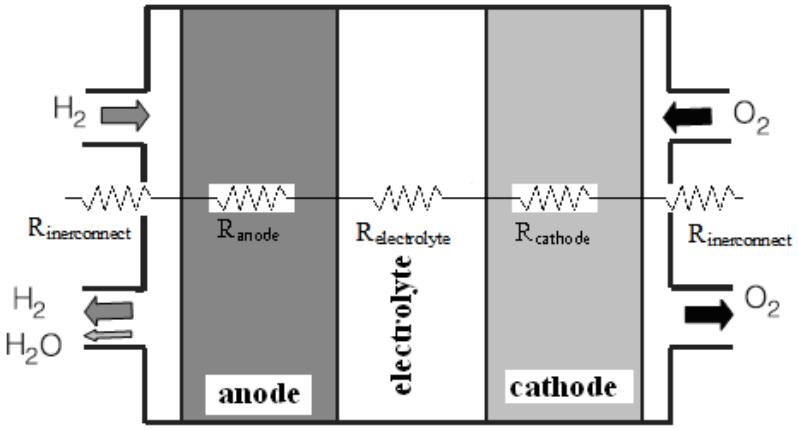

Figure 2.27 Total Ohmic resistance in the Fuel cell [18]

In a total ohmic resistance calculation the resistance of ion and electrons flow through individual components and interconnection within the fuel cell should be considered. The gross resistance is a combination of resistances each attributed to a different component. Figure 2.27 shows the total ohmic resistance as it is divided into interconnect, anode, cathode and electrolyte resistance components. The combination of Nernstian losses and reaction losses in the proximity of the electrodes is referred to as the cell's concentration loss. Both of these losses are a result of depletion and accumulation of the reactants and products in the catalyst layer which leads to reduce fuel cell performance.

2.4.3 Types of fuel cells

Fuel cell can be classified according to the type of electrolyte they use. There are five major types available:

i. Polymer electrolyte membrane fuel cell (PEMFC);
ii. Phosphoric acid fuel cell (PAFC);
iii. Solid-oxide fuel cell (SOFC);
iv. Alkaline fuel cell (AFC);
v. Molten carbonate fuel cell (MCFC).

Although all the above mentioned types are based on the same electrochemical principles, operation characteristics differ from type to type by means of operating temperature, material selection and the supply of hydrogen which can be either direct or indirect (in the case of reforming natural gas). The main advantage of the PEMFC is the high current density and the low operating temperature which makes it attractive for automotive applications. These types use a polymer membrane for proton transport and the cell's performance is dependent on the humidification level of the membrane.

Operating at constant humidification levels are preferable in order to avoid flooding and drying out issues which reduce performance. PAFC cells are at the most advanced state of development [18]. Numerous units have been installed in more than 300 locations worldwide mainly in building power generation applications. They use pure phosphoric acid as the electrolyte and operate at a temperature range of 150 °C – 200 °C. As in the PEM types in order to enhance the reaction for the given levels of operating temperatures noble metal catalyst layers are required.

The need for precious metals in the catalyst is diminished in the case of SOFC due to high operating temperature; in the range of 800 °C to 1000 °C. The excess of generated heat from the electrochemical reaction could be utilised in internal reforming process, therefore hydrocarbons could be used as fuel. However, finding inexpensive materials capable of withstanding those thermal stresses is creating a challenge. Nevertheless, the advantage of these types is the elimination of corrosion issues associated with the PAFC and MCFC and the water management in PEMFC. MCFC operate at lower temperatures, approximately 650 °C. Reactions that occur within the cells are different to those in PEMFC and PAFC as these evolve the transport of negative carbonate ions instead of protons.

One particular interest for MCFC applications is the power generation from gasified coal. However further development is needed in order to increase lifespan of units due to corrosion issues. Table 2.1 can summarise the operating characteristics of the main fuel cell types.

Table 2.1 Operating characteristics of various fuel cell types [3]

Type of fuel cell	PEMFC	SOFC	MCFC	PAFC
electrolyte	Polymer membrane	ZrO_2	$(Li,K)_2CO_3$	H_3PO_4
Charge carrier	H^+	O^{2-}	CO_3^{2-}	H^+
Anode	Pt/C	$Ni+(Zr,Y)O_2$	Ni+10wt%Cr	Pt/C
cathode	Pt/C	$(La,Sr)MnO_3$, $LaCoO_3$	NiO	C
Operation temperature	30~100°C	600~1000°C	600~700°C	150~200°C
System output	1W~200kW	~100kW	~500kW	~200kW
Usable fuels	H2、Natural Gas、Methanol	Natural Gas、Coal Methanol、Petroleum	Natural gas, Hydrogen, Carbon monoxide	Natural Gas、Methanol、Naphtha
Advantages	* long lifetime * quick start-up * high power density	* high stability * can use a variety of catalysts	* high efficiency * impure hydrogen as fuel * Suitable for CHP	* high efficiency * can use impure hydrogen as fuel
Disadvantages	* sensitive to fuel impurities * Requires expensive catalysts	* High temperature enhances breakdown of cell components * Slow start-up	* Slow start-up * High temperature enhances breakdown of cell components	* low current and power * large size/weight

2.4.4 Commercial available mCHP systems based on fuel cell

Of particular interest are mCHP-based fuel cells. The main advantages are considered to be the emission free operation when pure hydrogen is used as fuel and the high electrical efficiency due to the elimination of moving parts and mechanical losses. Stack sizes of such units are in the range of a few kW_e with a heat to power ratio close to one. The main constraint on cogeneration applications is the transient response of the fuel cells. The pre-heating time of a PEM type fuelled by natural gas (in units incorporating a fuel reformer) is approximately one hour whereas in SOFCs a 12 hour period is required in order for the system to reach nominal operation. Sophisticated control logic can be applied to compensate for the relatively long start-up period. While fuel cells have been under development for the last four decades they are still commercially immature. Lifespan of the units, corrosion, performance degrading, and capital cost due to noble metals usage are the major issues

attributing to the fact that fuel cells are the least commercially-available technology among mCHP.

2.4.4.1 Available PEMFC based mCHP units

Figure 2.28 Toshiba 0.7 kWe PEMFC based mCHP [123]

PEMFC mCHP based systems are considered to be the leading fuel cell technology for domestic applications. The low operating temperatures combined with high power densities and efficiency has drawn also the interest in transport applications. Several thousand PEMFC co-generations units have been installed in Japan residential conditions as part of the ENE Farm programme [20] in which the installation cost was heavily subsidised by the government and gas supplying companies. Figure 2.28 shows a 0.7 kW_e mCHP incorporating an auxiliary burner for supplementary heat generation manufactured by Toshiba. The unit exhibit an electrical efficiency of 35 % and sales exceeded 4000 unit in Japanese market. Elcore GmbH company based in Munich, Germany has developed a PEM based mCHP unit (Figure 2.29) with a nominal capacity of 0.3 kW_e and 0.6 $kW_{th.}$ The 0.3 kW_e is considered unusual capacity for domestic application given that most commercial available mCHP units regardless the technology offers a minimum of 1 kW_e electrical output. Nevertheless this particular unit is mainly aiming to cover domestic hot water requirements and therefore is designed to operate continuously and generate 2400 kWh electricity per annum. Figure 2.30 shows a PEMFC unit that was developed by Viessmann Group and Panasonic Corporation collaboration. The fuel cell unit was developed by Panasonic and has been used extensively in ERA FARM program while the incorporated auxiliary boiler system was developed by Viessmann. The unit

features the electrical capacity of 0.75 kW_e which correspond to 37 % efficiency; in respect to the thermal performance, the efficiency of the unit is rated as 53 % at 1 kW_{th}. Finally, the incorporated gas fired boiler can produce supplementary 19 kW_{th}.

Figure 2.29 Elcore 2400 PEMFC based mCHP with nominal electrical output 0.3 kWe [21]

Figure 2.30 Viessman/Panasonic jointly developed 0.75 kWe PEMFC based mCHP [22]

2.4.4.2 Available SOFC based mCHP units

The major advantage of the SOFC mCHP systems is the flexibility in the fuel supply due to the high operating temperatures and the high potential efficiency. However, this particular type of cells exhibits stiffness in modulation of the power output. Galileo of Hexis company, has developed a 1 kW_e SOFC based mCHP unit (Figure 2.31) with a heat to power ratio of two. The system uses an integrated gas fired burner that can generate up to 20 kW_{th} heat in order to cover high thermal requirements buildings. The system can be fuelled either by natural gas or bio methane and features an overall efficiency of 90 % according to the manufacturer. Figure 2.32 shows a particular type of SOFC that has been developed by a UK company named Ceres Power. In their design they applied a metal support cell in order to overcome the thermal cycling issue, reported during operation in SOFC systems. In addition,

the low cost steel is used in the design, reducing the capital cost of the unit. The cell operates at approximately 500 °C to 600 °C and has a nominal capacity of 1 kW_e electrical.

Figure 2.31 Galileo from Hexis features is capable of generating 1 kWe and 2 kWth electrical and thermal power respectively [23]

Figure 2.32 1 kWe SOFC based on steel technology cell mCHP system [7]

Vaillant Group has developed a compact wall-mounted SOFC based mCHP system of the 1 kW_e electrical power output as shown in Figure 2.33.

Figure 2.33 Vaillant 1 kWe SOFC based mCHP system [15]

Operating temperatures higher than 800 °C enable the use of natural gas and the heat recovery is at the range of 2 kW_{th}. Vaillant have several prototypes tested in the laboratory, and these completed more than 12000 hrs of continuous operation. Although electrical efficiency is considerably lower than of competition, the developers were focused on the reliability of the unit and long service intervals.

2.5 Rankine Cycle

2.5.1 Fundamentals of operation

Rankine cycle is a thermodynamic cycle which converts heat into mechanical work. Heat is supplied externally to the working fluid and operation of the cycle occurs in a closed circuit loop. In fossil fuel power plants heat is generated from the fuel combustion process, whereas in nuclear power plant a controlled fusion reaction generates useful thermal energy. Finally in solar power plants the vaporisation of the working fluid is carried out using solar radiation. Figure 2.34 illustrates a schematic of a simple vapour power plant.

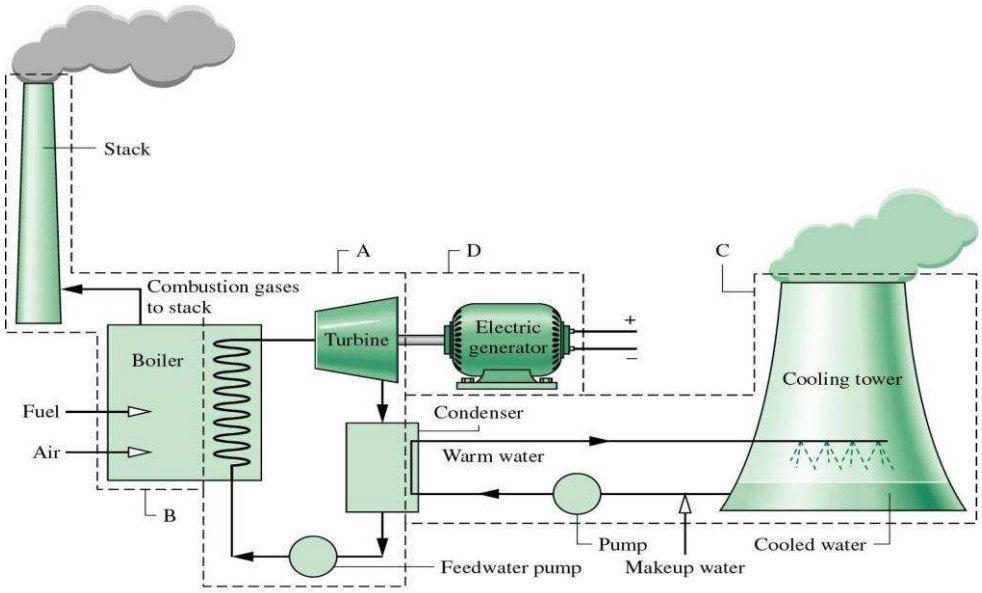

Figure 2.34 Components of a vapour power plant [24]

Of the major issues related to the installation of these power plants are the thermal pollution of the environment and the accessibility to sufficient quantities of water used for cooling requirements. For the reasons mentioned above cooling towers have been employed in recent plants. Nevertheless, control of pollutant discharges and disposal of wastes, particularly in the case of nuclear power plants, are of significant importance in order to ensure operation within acceptable levels of the environmental impact [24]. Solar power plants are considered as non-polluting and operation is classified as safe, however such plants are not yet widely used.

2.5.2 Thermodynamic cycle analysis

The principal work and heat transfers of Subsystem (A) in Figure 2.34 is illustrated in Figure 2.35.

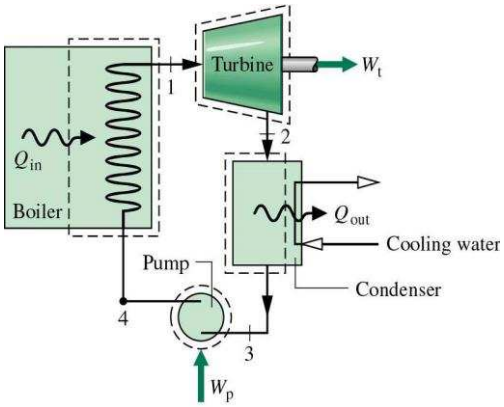

Figure 2.35 Subsystem of the power plant. Main components of the Rankine cycle [24]

For simplicity, the heat exchange between components and surrounding is neglected and kinetic and potential energy changes are not taken into consideration. Arrows in the diagram indicate the positive energy flow and each component is assumed to operate at steady state conditions. Starting from state number 1, high temperature and pressure steam produced in the boiler, passes through the turbine. The steam expands in the turbine and is discharged to the condenser at state 2 at a relatively lower pressure. At this stage useful work ($\dot{W}_t$) is produced by the turbine:

$$\dot{W}_t = \dot{m}(h_1 - h_2) \tag{2.6}$$

where $\dot{m}$ is the mass flow rate of the working fluid and (h_1-h_2) is the enthalpy difference between the two stages.

As the vapour passes through the condenser it is cooled down and is condensed into liquid. The heat dissipated into the cooling water ($\dot{Q_{out}}$) is calculated as

$$\dot{Q_{out}} = \dot{m}(h_2 - h_3) \tag{2.7}$$

The condensed liquid enters the pump where its pressure is increased before entering the high pressure boiler. Assuming that no heat interaction between the pump and surroundings takes place, the work of pump can be calculated as

$$\dot{W}_p = \dot{m}(h_4 - h_3) \tag{2.8}$$

Finally the cycle is complete as the working fluid is pumped to the boiler where it is heated to a saturation level and evaporated. The heat input in the boiler is

$$\dot{Q_{in}} = \dot{m}(h_1 - h_4) \tag{2.9}$$

The ratio of the net work output over the heat input is the thermal efficiency of the cycle:

$$\eta = \frac{\dot{W}_t/\dot{m} - \dot{W}_p/\dot{m}}{\dot{Q_{in}}/\dot{m}} \tag{2.10}$$

2.5.3 Rankine cycle

In an ideal thermodynamic Rankine cycle several simplifications are applied. These idealisations can be summarised as follows: the working fluid is considered to flow through components at a constant pressure; all pressure drops due to friction are neglected; there are no irreversibilities throughout the cycle and the thermal interaction with the surroundings is ignored. An ideal cycle in the temperature- entropy (T-s) diagram is shown in Figure 2.36. The following series of reversible processes could be described in this cycle.

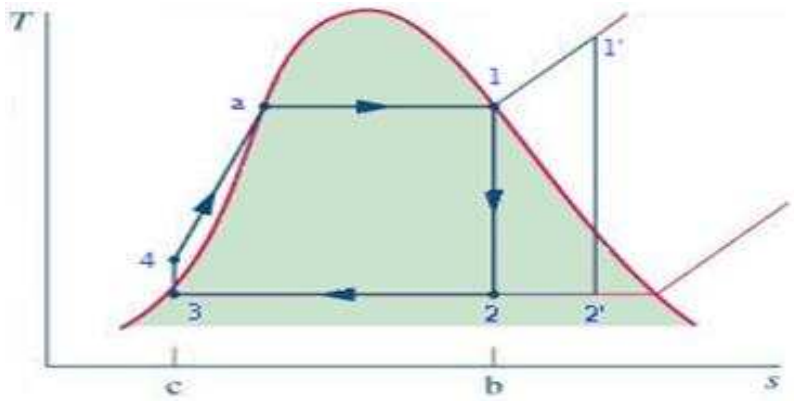

Figure 2.36 An ideal thermodynamic Rankine cycle in the T-s diagram [24]

1-2: Isentropic expansion of the working fluid through the turbine from the saturated vapour to condenser pressure;

2-3: Heat transfer from the working fluid as it passes through the condenser at constant pressure;

3-4: Isentropic compression as the pump increases the working fluid pressure before entering the boiler;

4-1: Heat transfer to the working fluid in the boiler at a constant pressure.

States 1' and 2' in Figure 2.36 exist if superheating of vapour is utilised and which increases the thermal efficiency. The enclosed area 1-2-3-4-a-1 corresponds to the net heat input or to the net work output. Figure 2.37 shows the T-s diagram of an actual Rankine cycle (shown in yellow lines). Deviation from the ideal process occurs due to neglecting the pump losses. Both mechanical and fluid friction within the pump reduces the pump efficiency and the irreversibilities of the processes result in the increase in entropy of the working fluid.

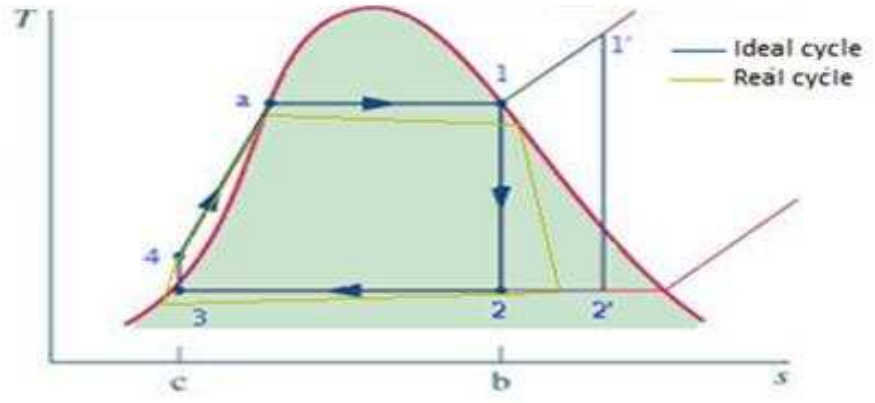

Figure 2.37 Ideal vs real thermodynamic Rankine cycle in the T-s diagram [25]

2.5.4 mCHPs based on the ORC technology

Given the high effectiveness of the Rankine cycle, technology is extensively applied in large scale power plants. In mCHP applications however, a variation of the Rankine cycle is used.

While in conventional power plants water is commonly used as a working fluid, the organic Rankine cycle uses an organic working fluid instead. Despite the fact that water displays exceptional thermal properties at high temperatures, in lower power capacity systems organic working fluids are preferable. At lower mean operating cycle temperatures organic fluids remain in the superheated vapour phase throughout the thermodynamic process. This particular behaviour of the organic working fluids eliminates the condensation issues reported in the low pressure stages of the steam turbine and the higher mean operating temperature result in the higher thermal efficiency. Co-generation units with nominal power output up to 10 kWe are available in the market at the prototype level only. Figure 2.38 shows an ORC based mCHP system tested under laboratory conditions. The power output and electrical efficiency of this particular unit are noticeably low at 0.08 kW_e and 1.66 %, respectively. The test-rig configuration and obtained experimental results could be used for further optimisation and improvement of ORC based mCHP systems.

Figure 2.38 A prototype ORC based mCHP system [26]

An advantage of ORC based mCHPs is the flexibility in the fuel use. A cogeneration unit in which heat is supplied in a 50 kW_{th} biomass-fired boiler has been designed and developed in [27]. The system could generate 0.86 kW_e and 47.26 kW_{th} of electrical and thermal power, respectively. The corresponding efficiencies were therefore calculated to be 1.41 % (electrical) and 78.69 % (cogeneration).

Figure 2.39 a and b show an innovative ORC system developed at the University of Science and Technology of China (USTC). Collected solar irradiation has been used as a heat supply for the ORC. The prototype ORC mCHP system incorporates an innovative solution for the elimination of some reported issues related to the pump operation in conventional ORC cycles. The required operating pressure of this particular gravity driven system is generated by the height difference between the condenser and evaporator. Although there is no indication of the power capacity of the system the developers claim that the efficiency is approximately 10.2 % (higher than the pump driven ORC systems) [28].

(a) (b)

Figure 2.39 A gravity driven prototype installed in USTC with solar collectors supplying useful heat for the ORC operation: (a) solar collectors (b) the engine set-up on the ground.

A major constraint on the development of micro scale ORC based systems is the lack of commercially-available micro-components such as expanders, turbines and alternators. The later result in excessive modification of components that have been primarily designed for various applications in order to be compatible with the ORC process with significant effects on the overall plant performance.

Chapter 3 Literature Review

3.1 Introduction

Published research work related to the theoretical and experimental analysis of mCHP systems based on a range of new technologies was reviewed. Furthermore, a review of building (energy) simulation tools is presented in this chapter.

3.2 Stirling Engine Based mCHP

3.2.1 Operation and modelling of Stirling based mCHP

The operation of Stirling based mCHP units has been assessed in previous research works using various simulation tools. An experimental and numerical analysis of a commercially available Stirling engine based mCHP system was carried out by Valenti et al. [29]. Experimental results were used for validation and calibration of the engine's model. A net electrical efficiency of 9 % and 15 % was predicted from experimental and theoretical data respectively. It was commented that inlet water temperature significantly affects the thermal performance of the unit; thermal efficiency was measured at 90 % and 84 % at water inlet temperature of 30 °C and 70 °C, respectively. Finally, it was noticed a deviation of 4 % between experimental and numeric analysis. A fully dynamic model of a Stirling engine based mCHP incorporating with micro wind and photovoltaic modules was developed by Karmacharya et al. [30] using Matlab/Simulink. Experimental results from operation of a 1 kW_e Stirling based mCHP unit were used in model which was applied to a two typical 3 and 4 bedroom UK houses. The research was to explore the interaction between the power generation modules and to identify the most feasible operating condition which could be used in energy control strategies. They found that the power generation system overall contributed to around 20 % of the domestic electrical demand regardless of the building type. In addition,

they concluded that the power contribution of the mCHP depended on the thermal requirements of the building, whilst the frequency of cycling operations significantly affected the fuel utilisation. Finally, they suggested that an analysis by means of both electrical and thermal optimal sizing was needed. Conory et al. [31] investigated the performance of the Whispergen mk-4 Stirling engine based mCHP. Data from a field trial of the mCHP unit installed in a semi-detached house were used in a Matlab model based on empirical equations. Predicted simulations results were in good agreement with experimental data and the researchers concluded that their validated model could be used as a tool for installers. Kane and Newborough [32] compared Stirling engine based mCHP of various nominal electrical output. They suggested that if a cogeneration unit replaces convectional heating systems, carbon savings could be achieved. However, various parameters directly or indirectly affect the overall performance of the system. A wide range of factors including transient thermal and electrical demand, occupancy pattern, climate etc. significantly influence the primary savings and should be further investigated.

3.2.2 Experimental studies on Stirling based mCHP systems

Several physical tests have been conducted with Stirling based mCHP units. Research was focused on both steady state and dynamic behaviour of the systems. Thorsen et al. [33] designed, manufactured and tested under various load conditions a 3 kW_e Beta type Stirling engine mCHP. The unit used natural gas as fuel and demonstrated 2.3 kW_e power output with efficiency of around 23 %. If a custom made alternator had been used the overall efficiency was expected to reach or even exceed 85 %. In addition, exhaust gas analysis indicated reduced emission compared to ICE engines. Bell et al. [34] tested an actual Stirling engine mCHP under typical Canadian residential condition. They concluded that combining a mCHP with thermal storage tank caused prolonged operation and therefore higher power generation figures. Moreover, higher overall efficiency was noticed for this configuration. Results were

in agreement with previous theoretical research, however, further investigation should be carried out in order to determine the optimum capacity of the thermal storage. An interesting finding was the dependence of the efficiency on the thermal demand profile as a result of fluctuation in the return temperature in the hydronic circuit. Aliabadi et al. [35] examined the performance of the Whispergen Mk III DC Stirling engine mCHP. Although the unit was manufactured to run on diesel fuel, biodiesel was used in their energy balance tests. They found that overall performance in terms of partial efficiencies and emission was poorer when biodiesel was used as fuel. This was attributed to the lower fuel utilisation in combustion process, as fraction of the biodiesel was found in the exhaust. An interesting comment was that even if Stirling engine mCHP features poor electrical efficiency it is comparable with ICE mCHP due to the high engine heat recovery.

Using a renewable fuel, Thiers et al. [36] investigated the performance of a 3 kW_e Stirling engine mCHP. Physical tests of the engine were carried out using wood pellets as fuel and obtained results were applied in theoretical modelling under French residential conditions. Relatively low overall performance of the system was found and sizing of individual equipment should be taken in further consideration. Veitch and Mahkamov [37] investigated the performance of the Whispergen Mk III Stirling engine MCHP. The mCHP was compared to a reference scenario consisting of a non-condensing boiler, hot water tank and electricity from the national grid. More important is that obtained results from experiment had been used in the model. They performed steady-state and dynamic tests and results were used for estimation of overall and partial efficiencies; finally, an exhaust emissions analysis was carried out. Reduction of approximately 9 % in both annual expenditures and carbon emission were predicted. It was found that during the summer period, due to low thermal demand, mCHP is forced to operate in part load resulting in high cycling frequency and

decreasing the overall efficiency. They also recommend that electrical output should be increased in order to bring the heat to power ratio closer to the demand.

3.3 Internal Combustion Engines (ICE) mCHP

3.3.1 Simulation of ICE based mCHP

ICE engine based mCHPs have been simulated over the past years using various theoretical tools. Simulations were based on obtained experimental results and empirical equations. A techno-economic analysis was carried out by Ehyaei et al. [38] in a 10 storey residential building in Tehran city. In their calculation they found that 5 modules were sufficient for meeting the heating and cooling loads of each building. In their model electricity surplus was directed to a heat pump for generating heat during the winter period. During the summer period, the heat recovered from engines was transferred to absorption chillers and used for covering the cooling loads. They found that the annual entropy generation was 2.903×10^4 (GJ/year) and that the cost of electricity in 'CHP mode' could be reduced from 0.11 to 0.05 US$/kWh.

Caresana et al. [39] modelled under different operating modes a mCHP system based on an auto derived internal combustion engine of 28 kW_e electrical nominal output. Buildings with various demands were simulated under Italian climate conditions and results indicated higher performance when variable speed operation of the micro-generator was selected. Both efficiency and economic performance were increased over the constant operation regime. However, it was suggested that financial incentives should be introduced in order to make the mCHP technology feasible. The feasibility of domestic applications of mCHP systems based on IC engines was investigated by Aussant et al. [40]. Several energy demand profiles were modelled using the ESP-r building simulation tool and results were compared with a conventional heating system. It was found that energy and fuel cost significantly affects the

economic viability of the system and that the surplus of heat during summer period operation resulted in higher fuel cost. An interesting comment was that such systems could reduce investments in power generation capacity and power distribution and also avoid transmission losses. Finally, simulation results indicated that carbon emission reduction could be achieved when a provincial electricity emission factor above 400 gCO_2/kWh was considered in their calculation. Onovwiona et al. [41] developed a parametric model based on performance data which could be used on a techno-economic evaluation of a 6 kW_e ICE based mCHP system. Sub-models which simulated the operation of auxiliary equipment (engine, generator thermal electrical storage etc.) were included in their analysis and the model was capable to predict the mCHP performance in 15-min intervals. Two operating scenarios were modelled and a sensitivity analysis carried out in respect to the sizing/capacity of the unit. The co-generation model was implemented in the building simulation program ESP-r which was used for generating thermal and electrical demand profiles. In their analysis they found that regardless of the operating scenario smaller capacity systems had higher overall efficiency. The latter was attributed to higher utilisation of generated heat

3.3.2 Experimental studies on ICE based mCHP systems

An IC engine based mCHP system was assessed in terms of performance by Rosato et al. [42]. The natural gas-fuelled unit featured 6 kW_e and 11.7 kW_{th} electrical and thermal capacity respectively. The engine was experimentally tested and obtained data were used for investigating the system performance during transient periods. It was found that the transient behaviour for both electrical and fuel consumption could be neglected. However, the relatively slow heat generation would lead to overestimation of thermal performance. In addition, experimental data were used for calibration of IEA/ECBCS Annex 42 [43] model

and theoretical predictions were in reasonable agreement with experimental data. Finally, it was commented that under low electrical generation regimes, simulation results overestimated performance compared to the experimental data. Antonio Rosato et al. [44] assessed experimentally the performance of a three cylinder ICE based mCHP system. The system had a nominal power output 6 kW_e and 11.7 kW_{th} electrical and thermal respectively. The unit was operated under electricity led regime and a realistic demand profile was simulated using halogen lamps. Results obtained during a 24 hours dynamic test were compared to a reference scenario; a grid connected building with a conventional heating system. Their exergy and environmental analysis predicted annual carbon emission saving of 2 % in the case of Italian mix power plant technologies even if a higher primary energy consumption was considered. Finally, experimental data was used to calibrate mCHP model in the TRNSYS simulation tool.

The same authors [45] used their experimental results to empirically calibrate and validate the micro-generator module in Annex 42 model [43]. The calibrated model found to exhibit a good agreement with obtained data, however modifications to the mathematical model were suggested due to deviation between the modelling results and experimental data. Results from a field trial with an ICE based hybrid mCHP system were demonstrated by Entchev et al. [46]. In their analysis they found that domestic heat demand was predominantly satisfied by the first stage of the system (ICE based mCHP) while the second stage (furnace) was occasionally in operation. The calculated electrical efficiency of 18.7 % was consistent throughout the trial as a result of the continuous steady-state operation; an overall efficiency between 73-76 % was also found. During the testing period, half of the power generation was consumed onsite (which corresponding to 65.5 % of average daily electrical demand) and the other half was exported to the grid. Finally, an economic analysis predicted savings on

expenditures for the hybrid system over a conventional furnace system during the heating season.

3.4 Organic Rankine Cycle mCHP

Rankine cycle is a type of thermodynamic cycles in which heat is converted into mechanical work. Although in large scale such cycles have proved their effectiveness, in small and micro scale the technology is considered immature.

The energetic performance and the economic feasibility of a biomass-fired Organic Rankine Cycle (ORC) for domestic CHP application were assessed by Algieri et al. [47]. They used decane as the working fluid due to high operating temperature and low critical pressure. In their research better performance was obtained when an internal heat exchanger was applied in the cycle configuration. In addition, the evaporation temperature significantly affects the ORC electrical and overall performance regardless the configuration. Highest partial efficiencies were found at 337 °C: 17.6 % and 63.1 % electrical and thermal, respectively. The capacity of the unit was P_{el}=0.76 kW_e (electric power) and the thermal power of system was Q_{cog}=2.35 kW_{th}. Italian energy tariffs and incentives were taken into consideration in their economic analysis where it was estimated that the payback period was approximately 8 years when a system specific cost of 10000 €/kW_{el} was used. Finally a reduction of 50% on the payback period could be achieved if specific cost could be further reduced.

Wood et al. [48] investigated the economic performance of various CHP systems including ORC. Five different operation strategies were investigated and the sensitivity of the results in various parameters was analysed. They found that the continuous operation for solid fuel systems resulted in higher performance due to cost difference between fuel and electricity. In addition energy sale and import prices, fuel feedstock, discount rates, demand profiles etc. were found to affect significantly the economic performance of such systems. Nonetheless,

they concluded that small scale biomass CHP could be feasible. Uris et al. [49] investigated a biomass-fuelled ORC mCHP system. Several configuration and working fluids were assessed and an economic analysis was carried out. They found that subcritical recuperative ORC systems are technically and economically feasible in Spain. Result obtained using sensitivity analysis indicated that capacity of the system depended on the energy demand and availability of the feedstock and that supercritical cycle should be avoided due to lower profitability. An ORC plan with nominal electric power of 1.25 MW_e and 5.3 MW_{th} thermal used for providing heat to the local district grid was investigated by Stoppato [50]. Various operating modes were assessed (heat led, max electricity etc.) and results from analyses indicated that, following the local incentives, it was feasible to aim at maximisation of power generation rather than utilise the cogeneration aspect of plant. A comprehensive thermodynamic model of a tri-generation system of an integrated organic Rankine cycle was developed by Ahmadi et al. [51]. Obtained results were used in an exergy, environmental and parametric analysis. They found that the gas turbine inlet temperature and compressor pressure ratio were among the major parameters that affect the performance of the system and increasing either of those parameters resulted in higher exergy efficiency. They concluded that a tri-generation system could achieve higher carbon emission reduction compared to conventional mCHP systems or gas turbine cycles.

Liu et al. [52] investigated the performance of a 2 kW_e biomass fired CHP system coupled with ORC. Three dry organic working fluids were used in their thermodynamic models. They found that the thermal efficiency of the ORC was well below the Carnot cycle efficiency. Nonetheless, the overall CHP efficiency of the ORC was in the order of 80 % with all working fluids. In addition the quantity and quality of heat generated from CHP was depended on the organic working fluid and on the modelling conditions. Hot water temperature from biomass burner, ORC fluid, condenser cooling temperature significantly

affect the electrical efficiency of the system which was found to be in the range of 7.5 % to 13.5 %. They suggested that implementing a heat recuperating unit within the ORC could improve the overall efficiency. A small scale biomass fired ORC was experimentally tested by Qiu et al. [27]. The unit was coupled with 50 kW_{th} pellet boiler and produced 861 W_e and 47.26 kW_{th} electrical and thermal power respectively. The corresponding efficiencies were calculated at 1.41 % with respect to the power generation whilst co-generation efficiency was estimated at 78.7 %. The relatively low electrical experimental efficiency (compared to thermodynamics model prediction) was attributed to the poor performance of auxiliary equipments such as micro-expander, alternator, heat exchangers, etc. They suggested that better heat exchangers should be considered in order to achieve the designed hot water temperature and improve the system efficiency and that the lack of commercially available micro scale expanders is one of the main constraints of mCHP ORC systems.

Li et al. [28] assessed the performance of a novel gravity driven ORC mCHP system. In their analysis they used various working fluids with a wide range of pressurisation. The absence of a pump was found to reduce the noise pollution from the system and could eliminate the problems related to its operation. For a given evaporation temperature (120 °C) the gravity driven ORC exhibited higher power efficiency compared to a conventional ORC. Finally, in their required height analysis they found that among the five selected working fluids, PF5060 offered the lowest required height which was estimated at 18.7 m. A small scale solar thermal CHP system based on ORC was modelled and optimised by Quoilin et al. [53]. The system consisted of parabolic though collectors, storage tank and was designed for a power supply in remote areas. The main advantage over the PV technology is the flexibility since such plants could be manufactured locally. Their thermodynamic analysis showed an overall electrical efficiency in steady state conditions between 7 %-8 %. An important comment was that calculations were based using custom made components of efficiency lower than 60 %.

3.5 Fuel cell based mCHP

3.5.1 Fuel cell operation

Fuel cells are electrochemical devices that convert chemical energy of fuels into electric power. Of particular interest are proton exchange membrane fuel cells (PEMFC) due to low operational temperature and high power density [18]. Such systems aim to replace existing power generation systems for stationary and transport applications. Various investigations have been conducted over the last years in order to increase the cells current density and therefore their performance and reduce the production cost. Material selection should also be taken into consideration so that commercial systems can achieve high reliability and ensure market penetration [54-57]. Yongping et al. [58] investigated the dynamic behaviour of a 45 kW_e PEM FC system. In their tests, the load of the 560 single cells system was gradually increased in order to analyse the response of the voltage. They found that although the response of the current was instantaneous, overshoot and undershoot behaviour were observed regarding the voltage response. These particular behaviours were attributed to the effect of electrochemical double layer discharging, gas transferring and membrane hydration or dehydration. They commented that, in all cases, voltage needs around 160 seconds to reach stable conditions. In addition, they found a correlation between the magnitude of change of load and the variation of voltage during the transient "undershoot" behaviour.

Kunusch et al. [59] developed a static model of a PEMFC in which theoretical and semi-empirical considerations were combined. Using experimental data from a 7 cell PEMFC system the authors were able to adjust the governing equations in order for the model to match the experimental performance. They concluded that this simulation methodology could be applied to several FC systems with minor adjustments, despite the fact that model is based on a particular specific PEMFC system. Tang et al. [60] investigated the dynamic performance of a commercially available PEMFC stack. During the regular load variation test

(step-up, step-down) undershoot and overshoot behaviour occurred in both current and voltage response. They concluded that voltage transient behaviour was due to temporary water and gas transport phenomena and that current overshoot accidentally occurred when the air stream was excessively humidified. Ferguson et al. [61] developed a steady state model of a generic PEM cogeneration fuel cell system that could be integrated into existing building simulation tools. Simulations results were validated using prediction data from various fuel cell models as well as experimental data. They found that the thermal model is in a good agreement with a physical GM fuel cell system but approximations used in activation loss formulations resulted in significant difference in the low voltage density region. The authors concluded that their model could be used with confidence.

The performance of a PEMFC system was experimentally investigated by Wang et al. [62]. In their work several parameters, that affect the performance of the fuel cell stack, were evaluated. They found that the performance of the unit was mainly dependent on the reactants, humidification and operating temperature. Using polarisation curves they noticed improved performance of the cell during high operating temperatures, however, performance decreased when a low humidification temperature was applied either to the anode or the cathode side of the stack. They found that experimental results were in a good agreement with a 3-D model which was developed using an unified approach and utilised energy momentum and continuity equations. Iranzo et al. [63] assessed the performance of a 50 cm^2 PEM fuel cell system. In their work they produced polarization curves, Nyquist and Tafel plots for several combinations of operating conditions and bipolar plate design. In addition, an electrochemical impedance spectroscopy analysis was applied for determination of cell Ohmic resistance and charge transfer resistances. Better performance was observed using high humidification rates of reactants and when a serpentine flow bipolar plate was used.

They concluded that their methodology could be applied when model parameters for CFD simulations must be estimated.

A large-effective-area (330 cm^2) and a transparent PEMFC were tested from Junhyun Cho et al. [64]. In their research they assessed the transient response of the fuel cell's voltage to the current step change. They found that the voltage undershoot behaviour exhibits two different time delays until the stack reaches a new steady state. The first time delay (the order of 1 s) was related to the gas transport and the second (order of 10 s) was due to the recovery of membrane water content. Findings were validated using a transparent fuel cell for which the dependency between the transient response of the system and the two-phase flow was established. Finally, by analysing a series of channel images, they observed that the water or vapour production coincided with the voltage undershoot behaviour. Yan et al. [65] evaluated the steady-state performance and the transient response to the current change in a single PEM FC system. They found that among the factors that affect the performance, humidification level of the reactants, operating temperature and air stoichiometric rate significantly influenced the cell performance. Optimum operation was estimated at temperatures between 65 °C -75 °C and pressure range from 1 to 4 atm. They suggested that the enhanced performance was attributed to better membrane humidification levels and water/gas transport in catalyst layer and Gas Diffusion Layer (GDL).

The effect of fuel dilution and reservoirs on the dynamic behaviour of a PEMFC was studied from Kim et al. [66]. They particularly investigated the undershoot after overshoot behaviour of the current density in a fuel cell caused by limited fuel flow velocity. They suggested that diluted anode gas could eliminate the undershoot behaviour and increase the recovery time. In their second hypothesis, different volume fuel reservoirs were tested. They concluded that the geometrical characteristics of the reservoir had a strong influence on the performance of

the fuel cell. Jung et al. [67] investigated the performance of an ambient force-feed air PEMFC system that could be used in automotive applications. A variable flow fan was used for simulating a number of velocities, whilst a high stoichiometric flow rate of hydrogen was applied. They noticed that the environmental conditions such as humidity and temperature significantly affect the performance of the stack. An interesting comment was that low fan speed resulted in the high stack temperature which leads to dehydration of the membrane and degrades the performance. Finally, a humidification section was excluded from the design due to simplicity considerations, despite the fact that could control the water content of membrane.

Kim et al. [68] assessed the dynamic behaviour of a PEMFC during load changes. Neither overshoot, nor undershoot behaviour were observed at excess stoichiometries. However low and normal stoichiometric ratios both resulted in transient behaviours which were attributed to hydrogen transport and utilisation. Finally, dynamic behaviours were modelled using parameters from obtained experimental data and were in good agreement with the test results. A 1 cm^2 active area PEMFC was investigated under load change conditions and steady-state operation. Benziger et al. [69] in their long term test (12000 hr of operation) observed consistency and reproducibly within the first 2500 hr of operation however after 3000 hr the fuel cell started to exhibit various and sundry complexities. Between the 5000 hr and 12000 hr of operation, autonomous oscillation was observed in respect of the current and voltage of the cell. They suggested a simple mechanism based on the mechanical properties of the membrane to explain this chaotic behaviour, where Membrane-electrode Assembly (MEA) eventually became more elastic and permeable due to mechanical stressing and oxidation degradation reaction in both anode and cathode.

Chen et al. [70] experimentally investigated the performance of a commercial 10 cell PEMFC. The stack was tested under various operating conditions. They found a correlation between the stack voltage and the pressure drop using fast Fourier transformation and they suggested that this was due to water flooding removal cycle in the cathode. An interesting comment was that the pressure drop signal could be potentially used as a diagnostic tool for the stack voltage.

The behaviour and the performance under fast load commutations of a PEMFC stack for stationary application was analysed by Hamelin et al. [71]. In addition, mathematical models were developed based on the experimental data in order to predict the voltage response. They commented that transient behaviour could significantly affect the performance of the system and if current or voltage exceeds certain limits, which could lead into shutting the unit down. Jiao et al. [72] assessed the water removal from the gas diffusion layer in a transparent PEMFC system. In their tests a speed Charge Couple Device (CCD) camera was used for recording images of the water flow for different levels of compression of the GDL and air flow rates. They found that under low air flow rate the thicker membrane exhibited better water removal performance due to higher porosity and permeability. At high air flow rate, fuel cell performance was decreased due to larger amount of water retained within membrane. Finally, high compression resulted in decreased membrane pore size and therefore to limited cross flow.

The liquid water formation using visualisation techniques was also investigated by Spernjak et al. [73]. An untreated and a wet-proof membrane was used for a range of air flow rates in a single-serpentine channel transparent PEMFC. Higher performance was observed when the wet-proofed membrane was used due to the ability to expel a larger amount of water and therefore the majority of pores were available to the gas transport.

Yan et al. [74] conducted an experimental study in a commercial size PEMFC. They tested a 256 cm^2 of effective cell area under various humidification conditions and using 2 different thickness membranes. They noticed that the thinner membrane performed better due to smaller water content. An interesting comment regarding the thin membrane was that at low operating temperature (30 °C) cell performance improved using dry reactant gases, however findings were reversed at high operating temperatures (80 °C). The water discharge characteristic of a PEMFC was investigated by using a Neutron imaging technology by Kim et al. [75]. Using a compressed air supply they found increased water removal at the cathode channel however no significant difference was observed in respect to the water management of the membrane. The effect of operating temperature was assessed and it was noticed that decreased water removal performance occurred with an increase in the stack temperature. Although the combination of compressed air supply and heating was superior, the complexity of the system limited the application. They finally concluded that their method is suitable for water management investigations due to high sensitivity to small variations in local water content. Arsalis et al. [76] developed a detailed model of high temperature PEM fuel cell that could be used for residential applications. Components of the mCHP including a gas reformer were modelled. They concluded that among others parameters, fuel cell operating temperature and heat exchanger input temperature caused high uncertainties and significantly affect the overall efficiency. However further validation of the model with experimental data is necessary.

3.5.2 Self-Humidifying MEA

A novel self-humidified membrane for PEMFC application was developed by Wang et al. [77] and its performance was evaluated over a convectional Membrane-Electrode Assembly (MEA). The membrane was surrounded by an inactive Water Transfer Region (WTR) which enhanced the water management and improved the performance of the PEMFC system. The

proposed MEA with the WTR had double power density over the convectional MEA due to the better water transport. The enhanced water management was attributed to the elimination of the drying effect of the anode side and the flooding issue in the cathode catalyst layer. An interesting comment was that that environmental humidity had a small effect on the fuel cell performance however increased ambient temperature resulted in higher performance. Qi et al. [78] investigated the performance of a PEMFC operated under dry reactants. They used a particular flow field design which allowed hydration of the reactant gases by moisture recovered from the outlet gasses. In their tests they found that drying of the membrane at high current was due to electro-osmotic drag at the anode side, since back diffusion could not recover the water content of the membrane. An interesting comment was that flooding issues could not be ignored even if external humidification had not been used. The later was confirmed as performance improved at high air stoichiometries. Despite the fact that operation at the high stoichiometric ratio prevented flooding issues, it resulted in faster dehydration of the membrane.

3.5.3 Mathematical modelling of fuel cells

Several mathematical models have been developed during recent years. Researchers attempted to analyse the operation of fuel cell systems under various operating conditions (humidification levels, temperature, stoichiometries). The earliest models have been developed by Springer et al. [79]. In their isothermal, one dimensional FC model several coefficients (membrane conductivity, diffusion and electro-osmotic drag coefficient, etc) as a function of the membrane water content had been measured and were applied in the model. They found a net steady state molar water flux per H^+ in a 50 cm^2 cell of 0.2 H_2O/H^+ which was validated by measured data and an increase membrane resistance when the current density was increased. The model predicted better performance of a thinner membrane and a fully hydrated membrane was able to reduce the water management issues in PEMFC stacks.

Bernardi and Verburgge in their models [80, 81] investigated the factors that limited the cell performance and the gas/water transport mechanisms. In their mathematical work they applied porous-electrode equations and Stefan–Maxwell diffusion media and catalyst layers. Model predictions of the polarization behaviour were in a good agreement with experimental data. A simple pseudo two dimensional model of a high temperature PEMFC was developed by Shamardina et al. [82]. The isothermal mathematical model neglected the effect of liquid water in the membrane due to the high operating temperature however it accounted for the crossover of reactant gases. The model could be used for estimation of FC properties from the polarisation curve and can be applied in high temperature PEMFC fed with dry gases.

The effect of the primary parameters on the performance of a PEMFC was investigated by Tohidi et al. [83]. Their investigation was carried out using a one dimensional steady state model. Theoretical calculations predicted high ionic conductivity at high operating temperature. The membrane resistance decreases when humidification of reactant gases increased but when a thicker membrane was used performance was limited due to lower membrane resistance. An interesting conclusion was that the bulk of the electrochemical reaction occurred in a thin layer close to the diffusion layer as the ionomer were unable to penetrate deep in the catalyst layer. It was suggested that this behaviour could underutilise the catalyst at normal operating conditions, therefore future efforts should be focused on improving the platinum utilisation.

Rowe et al. [84] developed a non-isothermal, one dimensional model in order to assess the effect of the operating conditions on the PEMFC performance. They found that anode hydration should be ensured in order to achieve optimum performance. However, at high operating pressures and when reformed gases were applied in the model the membrane was unable to maintain adequate hydration due to a moderate water vapour coefficient. They

finally concluded that their model could be used for optimising PEMFC performance for a given operating condition. Water management significantly affects the performance of PEMFC systems. However the water and ion transport requires extensive knowledge of the membrane morphology. Karimi et al. [85] and Das [86] developed mathematical models that could predict the physical liquid/gas transport through the membrane and its characteristics under a variety of operating conditions.

A steady state and a dynamic model were developed by Sfarifi Asl et al. [87]. By taking into account the gases transport phenomena, the effect of the temperature on the stack performance and heat balance equation could to predict the behaviour of the stack under load change conditions. Small deviations from experimental results were observed however researchers concluded that the performance of the stack is highly dependent on the operating conditions. Philipps et al. [88] developed a dynamic model of a PEMFC stack based on non-isothermal, mass and energy balance equations. In order to make the model computationally efficient authors neglected the GDL modelling and they assumed that the membrane is operating at steady state conditions. An operating time of 30 minutes was able to be simulated within 1 sec, and despite the simple approach model predictions of the characteristic stack temperature were in good agreement with experimental results. Yalcinoz et al. [89] assessed the performance of an air-breathing PEM fuel cell using dynamic modelling in Matlab. Their model was based in a steady state non isothermal 1-D model in which dynamic characteristics were introduced in order to predict the transient behaviour of the system. They noticed that the performance of the cell was highly affected by the stack temperature due to correlations between the Nernst voltage, membrane resistance and water concentration and the operating cell temperature. Obtained results of the dynamic model were compared with the original steady-state model and small deviations were observed. A simulation scenario in which a laptop computer was powered by the proposed system was

conducted and it was concluded that an air breath PEM FC system could provide adequate power to cover the transient demand of a portable equipment.

3.5.4 CFD-modelling of fuel cells

Several studies have been conducted using detailed 3D computational fluid dynamic (CFD) models in order to provide a more detailed insight of the physical phenomena and behaviour of a PEMFC. Falcao et al. [90] developed a 1-D and a 3-D model using CFD for a PEM FC system. The 1-D model over-predicted the performance of the fuel cell, whilst the 3-D model was able to reproduce the experimental results more accurately as a two phase flow effects were taken into consideration. They concluded that 3-D numerical calculations should be implemented only if more detailed predictions (such as the spatial distribution and visualization of various parameters) are needed as intensive computation was required. An interesting conclusion was that the simple analytical solution based on semi-empirical equations can always be used for quick prediction of fuel cell performance.

3.5.5 Modelling of Micro CHP based on fuel cells

The implementation of fuel cell technology in micro combined heat and power (micro CHP systems) had been of particular interest in recent years. Due to high efficiencies, fast start-up and zero emissions, fuel cells could replace convectional heating systems and provide economic and environmental benefits. Various operating scenarios of a High Temperature Proton Exchange Membrane Fuel Cell (HTPEMFC) system were modelled by Arsalis et al. [91]. Results from a conventional (for mCHP) operation heat-led regime were compared with an electricity-led scenario as authors attempted to optimise the operating pattern. Parameters that affect the operating regime's performance such as number of switching events, operation at low partial efficiencies, etc., were restricted in an improved scenario. A thermal storage tank was additionally implemented for avoiding the wasting of heat surplus and the highest performance was predicted on the improved scenario. The poor electrical efficiency was

observed with a heat-led strategy was selected and low thermal efficiency was recorded during an electricity-led operation. An interesting comment was that, despite the fact that the heat-led operation resulted in high fuel consumption; the highest power production rate was also predicted. The later could provide financial savings in the household, however economical and environmental performance of the system were not considered in the investigation.

Barelli et al. [92] developed a dynamic model of a 3 kW_e PEMFC system using Matlab Simulink. The model consisted of an auxiliary boiler providing additional heat when required and using onsite reformed hydrogen as a fuel. Primary energy requirements of typical residential conditions were used throughout the simulations whilst the dynamic behaviour of the plant's sub-models was validated with a step change in the electric load. They used a sensitivity analysis in which they found optimum performance when higher relative humidity (RH >70) was applied in the stack. They suggested that an additional heater had to be used in order to meet higher thermal requirements and that higher performance could be attained if the surplus of heat was to be restricted. Snevecan et al. [93] compared the power generation cost of several mCHP systems based on Swedish residential condition. Using current data they found that the cost of electricity when the fuel cell was used could be halved by 2020. They concluded that fuel cells should be further developed by means of capital cost and lifespan in order to compete with conventional systems. An interesting comment was that despite the fact that fuel cells are characterised as zero emission power plants, when a fuel reforming process was applied their ecological advantages were limited. Oh et al. [94] assessed the performance of a 1 kW_e mCHP system based on a PEM fuel cell incorporating thermal storage. The operation of the system was simulated using demand profiles based on energy requirements in Korean residential conditions. In their thermo-economic analysis they found that 20% saving in operational cost of the system could be achieved over conventional

heating equipment. An interesting comment was that the heating capacity of the reservoir should be carefully selected as it significantly affects the overall performance. Finally they concluded that such mCHP systems could potentially offer greater savings when installed within a dwelling with higher electrical demand.

Gigliucci et al. [95] investigated the performance of a residential mCHP system based on fuel cells. The unit featured a nominal electrical capacity of 4 kW_e and used onsite reformed hydrogen as fuel. A mathematical model which simulated the operation of the system was developed and model estimations were in a good agreement with experimental data. They found the global electrical efficiency of 18 % and thermal efficiency of the order of 30 % and they concluded that improvements in fuel utilisation and in heat management could increase the cogeneration performance of the β-prototype unit around 27 %. A hybrid system that consisted of PV arrays, electrolyser and fuel cell system was investigated by Shabani et al. [96]. Such systems could be used for heat and power generation in remote areas. In their techno-economic study, based on experimental data and model prediction, researchers evaluate the feasibility of the system over conventional back-up generators. It was noticed that air stoichiometry and stack temperature significantly affect the co-generation performance. The benefits analysis demonstrated a 10 % reduction in the consumption of the LPG fuel. Finally, they concluded that the carbon footprint could be reduced by 1600 kg CO_2/year compared with traditional diesel or petrol generator.

3.5.6 Experimental results obtained using PEMFC

Briguglio et al. [97] investigated the performance of a low temperature 5 kW_e PEM fuel cell based mCHP for domestic applications. A heat exchanger was used in the experimental setup to remove the heat from the stack. Stack temperature was kept at 71 °C since manufacturers

suggested operation at moderate capacity in order to prevent possible damage. Maximum overall efficiency of 80 % was estimated, however further insulation of the stack was necessary in order to reduce thermal losses and therefore increase the thermal efficiency. Hwang et al. [98] developed a PEM fuel cell based mCHP system fuelled by pure hydrogen. Interestingly, they introduced an integrated thermal management to the unit that controlled the operating temperature of the stack and recovered the dissipated heat. They predicted maximum overall efficiency of 81 % (significantly higher compared to a mCHP system with reformer). Hamada et al. [99] investigated the performance of a prototype 1 kW_e PEM fuel cell mCHP. The unit was used in domestic hot water applications and tests were for steady state and dynamic operation. A gas reformer was integrated into the mCHP converting natural gas in hydrogen ready to be used in the fuel cell. A prolonged start-up transient was highlighted especially when the unit performed from the cold state. A dependence on the temperature condition of the reformer with the start-up period and small variation of the overall efficiency of the system when operating in part load conditions were observed. Overall, a reduction in primary energy and carbon emissions were estimated. Using a natural gas reformer a 5 kW_e PEM fuel cell co-generation system was analysed from Melo Furtado et al. [100]. Physical tests of the unit were conducted under various loads and a polarization curve of the fuel cell was produced. High electrical efficiency predicted in part load operation was found to be due to limited thermal losses.

3.5.7 Fuel reforming effect

The effect of the gas reformer on the overall performance of the low temperature PEM fuel cell based mCHP was investigated by Radulescu et al. [101]. The operation of five identical units of 4.5 kW_e and 6 kW_{th} (at 60 °C) was analysed by means of partial and overall efficiencies. They found that the extended start-up transient resulted in poor cogeneration efficiency (38.2 %). They suggested that although the performance of the fuel cell stack was

adequate, poor reforming process and high electric losses significantly decreased the overall performance of the mCHP

Nogare et al. [102] modelled a small scale hydrogen production unit coupled to a PEM fuel cell. The unit was based on a natural gas steam reforming process and a comparison on two different configurations in respect of the CO removal from the syngas was carried out. In their calculations, which were based on a presumed thermodynamic equilibrium, they found that the physical CO removal configuration (PSA) achieved slightly higher efficiency due to lower fuel requirements. However the chemical CO removal configuration (PROX) required the low operating pressure therefore the compressor could be avoided in this scenario. An interesting comment regarding the efficiencies was that higher efficiencies could be achieved using better hydrogen purification methods and recycling the hydrogen from the fuel cell exhaust. Calo et al. [103] tested and analysed two small stationary reformers for hydrogen production, used in domestic application PEM fuel cell systems. Experimental results of their first generation reformer highlighted the need for further development and improvements. In a second generation, reformer improvements were implemented in respect to the burner, combustion chamber, reactants, cylinders and the hydrogen purification. Analysis of the second unit demonstrated better transient performance, whereas the start-up time was significantly reduced. They found the steady state efficiency of the process (without counting the auxiliary electricity consumption) of 78.6 % however they commented that the unit should be further developed in order to reach the industrialisation stage. Heinzel et al. [104] assessed two reforming processes for hydrogen generation using natural gas. Steam reforming and auto-thermal reforming were thermodynamically analysed and experimental tests were conducted. They found that the higher hydrogen content makes the steam reforming process more feasible for domestic application fuel cell systems and it was estimated that a maximum efficiency of 71 % is achievable. An interesting comment

regarding the auto-thermal reforming process was that the produced syngas was found poor in hydrogen (30 %) however, the process itself offered more flexibility in terms of start-up time and load changes.

Jahn et al. [105] modelled a steam reforming process as auxiliary equipment of a 5 kW_e fuel cell system. Their model was based on simple reaction kinetics where transport delays and pressure drops were not included in calculations. Their model's estimations were in a good agreement with the experimental results in respect of the produced gas concentration and the dynamic behaviour of the process. Small deviations from experimental work were noticed in burner wall and evaporator temperatures; both were attributed to the simple approach of the model and to the assumption of chemical equilibrium used in the calculations. An innovative membrane natural gas reformer coupled with a PEM fuel cell system was assessed by Campanari et al. [106]. The authors modelled and compared membrane reforming process with conventional methods (steam reforming and auto-thermal). They found that higher efficiencies of net electricity could be achieved mainly due to the lower temperature heat recovery. An interesting comment was that the simplicity of the layout (1 stage process instead of 4) enhanced the heat transfer process and reduced the losses in the fuel processing reaction which lead to lower fuel consumption.

Zuliani et al. [107] investigated the performance of a 1 kW_e high temperature PEM fuel cell micro-generation system coupled with a natural gas reformer. Using in their calculations a fixed efficiency of the reforming process of 78 % they found better performance of the overall system at a low operating load. An interesting comment was that HTFC could easily be coupled with a natural gas reformer due to the increased tolerance in content of CO in the fuel mixture. The performance of HTFC predicted was lower compared with the low temperature FC, however the simplicity of its design resulted in the lower parasitic electricity

consumption and therefore overall efficiency could be comparable to the LTFC. Horng et al. [108] assessed the performance of a small methanol reformer for hydrogen production used in fuel cell systems. In their experimental work the cold start response of the reformer was assessed. They found that slow combustion led to reduction in the heat losses due to moderate temperature and also that the reaction temperature of the catalyst was reached faster. Similar findings were attained when a higher fuel rate was used, as a result of increased heat transfer to the catalyst. An interesting comment was that for a given rate of methanol an optimum air supply should be implemented.

3.6 Comparison of mCHP technologies

Several mCHP units based on different technologies (ICE, Stirling, fuel cell, ORC, mCHPs) have been compared over the past years. Researchers were focused on determining the technology that displayed the highest performance. However, results were contradicted as performance was highly depended on key parameters including primary demand requirements, modelling methodology, mCHP configuration, occupancy pattern, etc. The performance of two ICE based and a Stirling engine based mCHP systems were assessed by Rosato et al. [109]. The operation of the systems was modelled using TRNSYS software and a three storey multifamily building was selected for analysis. Simulation results predicted reduction up to 13.4 % and 18.9 % in primary energy consumption and in carbon emissions, respectively, over a conventional gas fired boiler and grid supplied electricity. In addition, the SenerTech mCHP offered the best performance. An interesting comment was that for a given mCHP unit the configuration which incorporates the smaller water tank volume offered greater both environmental and economic performance. Pineau et al. [110] investigated the energetic and environmental performance of six heating systems installed in a low energy requirement dwelling under various European climate conditions. They found that the lack of capacity size availability of mCHP systems reduced the performance of all units and

particularly of heat pumps. They highlighted the importance of mCHP sizing and they commented that the heating strategy did not affect the primary energy consumption. Finally, it was found that regardless the climate conditions, wood fuelled boilers could offer lower emissions over other technologies. Several mCHP systems for domestic application were analysed using the TRNSYS simulation tool by Cao et al. [111]. Units were based on various technologies including Stirling engine, ICE engine, fuel cell and ORC with nominal electrical output in the range 0-2 kW_e. A family house in Helsinki residential conditions was used in modelling and annual results analysis was carried out using a 1h time-step. In addition, they used simplified mCHP models due to lack of detailed models for the commercial units. In the core of their methodology they introduced an interactive utilisation of the matching indices and overall matching criteria which provided a macroscopic view of matching capabilities.

Arteconi et al. [112] developed a model for evaluation of the performance of various mCHP technologies. A detached house in Italy was used for testing the model and estimation of economic and CO_2 emission savings. They concluded that Stirling engines were an interesting option when operating on heat demand; however high capital cost makes mCHP less free market competitive. Cockroft and Kelly [113] also compared fuel cell, ICE, Stirling engine and Air Source Heat Pump (ASHP) mCHP under several space heating requirements. ASHP found to offer the greatest potential in carbon savings. It was stressed that, if any of mCHP operated at overall efficiencies above 80 %, carbon savings could also be achieved. An important comment regarding the overall performance was that dwellings with improved insulations level (and thus moderate heating requirements) displayed reduced potential savings; the latest marks down the heat to power ratio (HPR) and affect the overall performance of Stirling engine mCHP which operate at high HPR. Peacock and Newborough [114] investigated the effect of deploying cogeneration systems in UK dwellings. A Stirling engine of 1 kW_e and fuel cell based mCHP were compared to conventional condensing boiler

heating system and electricity from national grid. They found that Stirling engine mCHP increased the annual carbon emissions due to generation of excess heat. In order to improve the performance they suggested that applying a control logic in the unit not only would increase the lifespan of mCHP as a result of less cycling frequency but also would offer carbon savings up to 5 tonnes per year due to thermal surplus restriction. The restricted utilisation during the mild or low heat demand season, negatively affect the household energy bills mainly due to moderate power generation. Besides, economic performance was strongly depended on the utilisation of the produced electricity. An important comment was that the fuel cell is preferable due to high efficiencies even in part load operation, limited thermal surplus and low HPR.

Donerand Weber [115] investigated the performance of various mCHP technologies using dynamic building simulation tool. In their simulation results a ground source heat pump offered highest energy savings and emission reduction in accordance with [113]. An interesting comment was that economic and environmental benefits could also be attained in all mCHP technologies. Kuhn et al. [116] made an overview of the mCHP technologies and summarised the features and advantages of each technology. They concluded that carbon emission reduction was achieved when high overall efficiency co-generation unit replaced convectional heating systems and network electricity. It was suggested that mCHP should further improve their performance to become competitive and widely accepted to a public not yet familiar with the technology. Roselli et al. [117] in their research summarised the technical specification of several alternatives mCHP systems. Bardieri et al. [118] also investigated the feasibility of deployment of various mCHP systems in two single-family dwellings. Stirling engine based mCHP was highlighted as the best technology with a primary energy saving in the range of 20 %- 28 %. It was stressed that savings are prime mover technology dependent. A particular suggestion, regarding the optimum sizing was that

cogeneration units with lowest electric capacity closest to the peak electric demand should be selected. Similar findings regarding the dependence of the efficiency on the supply temperature and thus the heat demand was noticed by Thomas [119]. Four mCHP units were tested under steady-state, dynamic and partial load (when applicable) operation conditions. Characteristics of the units including thermal and electrical outputs and partial efficiencies were estimated, in addition exhaust gas analysis was carried out. They stressed that when applying moderate return temperature condensation occurred and better overall performance was noticed.

Dorer et al. [120] assessed the performance of several fuel cell based mCHP systems in residential conditions. They concluded that, compared to a boiler as reference configuration, fuel cells could provide up to 48 % reduction in energy demand. Combined fuel cell with back up boiler and thermal storage could improve the overall performance of the system. Interestingly, greater savings attained in buildings with high levels of insulation; this was in contrast with [121] where optimal CO_2 emissions reduction were predicted for high thermal demand dwellings when Stirling engine based mCHP was used as the heating system. In their simulations, they also included fuel cell systems combined with solar collectors dimensioned to cover 65 % of the domestic hot water demand. They stressed that this particular configuration could offer even better performance and thus, greater environmental benefits.

The Carbon Trust [122] reported field test results for domestic mCHP. For this, mCHP units were installed and tested in real domestic environments and results were compared with condensing boiler systems regarding carbon emission analysis and steady state performance. The results indicated that Stirling engine mCHP demonstrated average thermal efficiencies of 71 % but poor average electricity production efficiency of 6 %. Both figures deviate from manufactures claims and are heat demand dependent. The same trend in lower part load

efficiencies was also found for ICE engine mCHP. A significant comment in respect to the operation of convectional heating systems was that, according to the Carbon Trust, a condensing boiler consumes electricity at up to 10 % of its rated power when operating. In addition, the average thermal efficiency of condensing boilers were indicated at 85 % which is lower than the claims of >92 % by manufactures. This divergence occurred mainly due to the design and the set-up of the heating system, where operation at high return temperatures does not enhance condensation. Besides, significantly low efficiency was noticed in the non-space heating season as a result of short operation periods. Although high losses from the casing of the Stirling based mCHP was noticed, it was concluded that this particular prime mover technology demonstrated better environmental performance than condensing boilers for dwellings with high thermal requirements (low levels of insulation).

3.6.1 Operating strategies of mCHP

Newborough et al. [123] in a preliminary investigation summarised the environmental performance requirements for mCHPs in order to reduce the UK national carbon footprint by the 2050. They also investigated several operating strategies of mCHP units and evaluated the feasibility of implementing mCHP systems in individual UK homes. They predicted annual savings in energy cost in the range of £100- £200 and carbon emission reductions of 1 tonne per home for a mCHP unit with around 1 kW_e output. However, they concluded that these figures were achievable when electrical efficiency was 20 % or higher. Another interesting point was that the overall performance was influenced by number of factors including operation mode, energy tariffs, demand profiles, etc. Hawkes and Leach [124] investigated three hypothetical operation scenarios of several mCHP technologies in order to determine an optimal operating strategy. Heat-led and electricity-led operation were analysed for UK residential conditions. They particularly found that commonly applied strategies, such as heat-led, could not provide minimal operational cost. In respect of fuel cell based units, it

was noticed that under the least-cost operating strategy, maximum carbon emission reduction could be achieved. Also, the high heat to power ratio in Stirling engine mCHP caused heat generation to exceed the demand and therefore the least-cost effective strategy did not coincide with decreased carbon emissions.

Lin and Yi [125] investigated the performance of a CHP plant operating under an electricity-led regime. Presuming that room temperatures in buildings slightly changed over the time due to the thermal mass of the building, they suggested that CHP could vary its electrical output and, consequently the thermal output, to meet the load fluctuations. Under this particular operation, power generation was highly utilised which improved the performance of the CHP. In contradiction with previous research findings, Stirling engine based mCHP found to be the most promising of cogeneration systems, among 5 other technologies, when operated under heat-led regime according to De Paepe et al. [126]. It was also noticed that only a small fraction of generated power was used on site and that condensing boilers should not be excluded when governments are aiming to achieve CO_2 emissions reductions.

3.6.2 mCHP configurations

Combining mCHP with thermal storage was considered to be beneficial solution. Zhao et al. [127] investigated the optimal operation of CHP combined with a heat storage tank. They found that possible savings could be achieved. However various parameters such as supply temperatures, load profiles and system configuration strongly affect the savings. Under the same pattern, Haeseldonckx et al. [128] assessed the effect of thermal storage on the environmental performance of a mCHP system. They suggested that prolonged annual operation could be achieved either by using an additional boiler or thermal storage. In both configurations mCHP operated continuously and therefore decreased the switching frequency. When combined with an additional boiler, mCHP operated in order to cover an

'average' base heat demand whilst peaks were fulfilled by an additional burner. These operation strategies resulted in higher energy savings and emission reduction in accordance with [124]. It was stressed that incorporating a small thermal storage capacity resulted in an increase (by a factor of 3) in annual carbon savings and a further increase in storage capacity led to smaller increase in savings. Rolfsman [129] investigated the operation of CHP plants combined with boilers and heat storage. Due to daily variation of electricity prices heat storage (which was discharge at low electricity price periods) was used for maximising the power generation during peak-price periods and decreasing the operational cost. Storage in building fabrics and using a hot water accumulator were suggested as heat storage. Their study included electricity prediction models for feasibility investigation in following years.

Peacock and Newborough [130] investigated the effect of heating saving measures on the carbon savings attributable to mCHP. The importance of the heat demands profiles and the effect on the environmental performance were stressed, in relation to with previous research [1]. They concluded that when a 1 kW_e capacity (10 % electrical efficiency) mCHP was deployed on dwellings where heat saving measures had been implemented, marginal or negative emission savings were achieved. However, in high thermal demand dwellings mCHP could offer savings of up to 150 kg CO_2 per annum.

3.6.3 mCHP modelling approaches

Hawkes and Leach [131] used an alternative approach for mCHP investigation. They measured the fraction of the electricity demand that could be displaced by a cogeneration unit and named the new parameter "capacity credit". Comparing three prime mover technologies systems they found that the heat to power ratio (HPR) significantly affects the capacity credit. Low HPR systems (such as fuel cell) are predicted to have the highest capacity credit of around 92 %; consequently Stirling engine based mCHP has a capacity credit of 33 %. They

suggested that the new parameter is an important indicator regarding cogeneration deployment mainly because it could provide information on the performance of the national electricity system. In addition, the same authors [132] investigated the effect of calculation time step used in mCHP performance analysis and concluded that using 10 minute intervals could provide vital information on the system performance. It was also commented that further increases of the intervals will give marginal or no improvements since changes of demand profiles occur over a minutes time period. Using longer time intervals lead to over-prediction in overall performance of the mCHP.

Newborough et al. [133] analysed electricity demand profiles from UK households in order to evaluate possible ways of modulating these profiles. Reduction in peak power achieved using control algorithms in individual appliances of up to 60 % lead to smoother local and national electricity profiles. They concluded that mCHP deployment could provide significant savings in energy bills. Voorspools and D'haeseleer [134] investigated the impact of deployment of cogeneration units using dynamic simulation rather than static methods to predict the annual performance. It was stressed that static method results were more optimistic due to neglecting the dynamic interaction between cogeneration and centralised electric system. They suggested reviewing individual cases within their own context as results from individual scenarios could not be generalised. Oda et al. [135] investigated a new methodology in calculating the efficiency of a CHP system. Using dynamic data where load fluctuations were taken into consideration their numerical model indicated smaller load fluctuation compared to steady state calculations.

3.7 District Heating

The benefits of the de-centralisation of power generation have been highlighted over the past several years. The effects of heat and electricity savings measures in district-heated buildings

were assessed by Le Truong et al. [136]. Their analysis suggested that switching to high efficiency appliances and lighting could provide electricity savings up to 44 %. In addition, heat-fed washing machines and dishwashers could replace conventional electricity driven units which could result in higher power production and increased heat utilisation. Duquette et al. [137] assessed the potential saving of primary energy and carbon emissions in widespread CHP district energy networks. In their analysis, three widespread district energy and a large-scale wind farms were investigated. Savings in carbon emission and primary fuel utilisation of around 32 % and 8.5 %, respectively, were predicted in the scenario of CHP based district energy compared to a reference case. In their sensitivity analysis, they concluded that combined cycle gas turbines offered greater savings potential compared to back pressure steam turbines due to higher electrical efficiency and lower heat to power ratio. The authors raised the importance of considering large scale CHP plant in district energy networks. Voorspools and D'haeseleer [121] assessed the actual performance of mCHP and the impact of mass installation of mCHP in Belgium. In respect of the individual performance of the mCHP, experimental work was carried out. Poor transient performance and high frequency of switching events during low thermal demand regimes was found. This resulted in reduced economic and environmental performance and reduced lifespan of the system. It was stressed that investing in the development of both co-generation units and gas-fired plant could be beneficial for energy and emission reduction. They finally suggested that increasing the operating period of the co-generation systems could result in higher economic and environmental performance.

3.8 Research conducted using EnergyPlus software

EnergyPlus is well-known energy analysis software. It was introduced in 2000 and since it has been widely used in research studies.

The potential energy saving in an office building at several locations across Europe were investigated using EnergyPlus software by Boyano et al. [138]. The distribution of the primary energy usage found to be 46 % for lighting applications, 23 % for heating and 20 % for cooling loads. Obtained simulation results were in good agreement with previous research. They assessed several energy saving measures in buildings by taking into consideration the residential location. They found that by introducing the total lighting control system the operating time period of the respective application could be reduced thus resulting in a 36 % energy savings. An interesting comment was that improvement in the buildings insulation should be carefully selected in accordance with the climate conditions. Combination of two or more energy savings measurements enhanced the potential savings and significantly reduced the utilities bills.

Fumo et al. [139] developed a methodology to estimate primary energy consumption on an hourly basis. Their research was based on a series of predetermined coefficients. The energy requirements could be dynamically estimated when theses coefficients were applied to monthly consumption data (obtained from utility bills). Coefficients were calculated using EnergyPlus Benchmark Models simulation with a 15 minute data sampling time and the main advantage was that eliminated the need of time-consuming dynamic building simulations. The methodology described earlier was applied in two hypothetical buildings and an error within 10 % was found for both cases in regards the estimated partitions of energy. A validation study of a thermal simulation for a room connected to a naturally ventilated double skin facade was conducted by Mateus et al. [140]. Air and surface temperature were calculated using open source building thermal simulation tool in EnergyPlus. Although simulation results predicted an over-estimation on radiant temperature and under-estimation in respect of the air temperature, compared to experimental data errors were within acceptable limit. The latter contribute to increase the confidence in the use of EnergyPlus.

The average simulation error in air and the average daily maximum temperature error were found to be 1.4 ℃ and 2.5 ℃ respectively. Finally, a sensitivity analysis was performed by applying heat transfer methods in order to optimise the performance and minimise the predicted error of calculation.

A significant review in regards the operating strategy and the structure of the EnergyPlus building simulation tool was given by the developers Crawley et al. [141]. They described in details the capabilities, characteristics and limitation of the software. The module-based structure of the simulations was characterised as more efficient since it enhanced data exchange with other software and allowed the integration of new function/modules. Further details are given in the EnergyPlus chapter. Stadler et al. [142] developed a distributed generation model in order to be implemented in EnergyPlus . Given the flexibility and the coupling ability of the EnergyPlus the development of a module simulating the operation of a co-generation system could be facilitated by SPARK [141]. The latter is a simulation tool capable of modelling building equipment as individual modules. The description of physical configuration and the dynamic characteristics of the system is performed using C++ based functions. Furthermore, SPARK allows for enclosing into the simulation process the effective control strategy based on simple and robust optimisation algorithms. The integration of additional simulation modules contribute to the flexibility and capabilities of EnergyPlus. Up-to-dated HVAC libraries provide to end-user modern building design, renovation and improve the accessibility of the distributed generation systems.

Chapter 4 Theoretical background of EnergyPlus Software

4.1 Introduction

A building simulation tool is essential in order to model the buildings energy requirements and the operation of hydronic heating plants. Simulation results then can be used to calculate the economic and the environmental performance of each scenario. EnergyPlus software is a well-established building simulation tool and has been used in a number of research activities as described in Section (3.8). Despite the fact that several building tools have been developed in the last two-three decades, EnergyPlus offers the most flexibility in modelling and high accuracy as compared with other software, including TAS, ESP-r, TRACE and TRNSYS, as a result of the integrated solution manager and the heat balance algorithms that are deployed [141]. In addition, EnergyPlus offers modules for modelling both IC and Stirling engine based micro-co-generation systems reflecting their dynamic behaviour in each time-step.

Currently EnergyPlus is software of an industrial standard for energy modelling of buildings with incorporation of main conventional and non-conventional heat and electricity production equipment and is widely used in both academia and industry. This software has extensive built-in data base on climatic conditions for different regions across the world and includes detailed information on a wide range of structures and fabrics for various types of buildings taking into account their key elements (roofs, walls, floors, doors, windows etc). Detailed information for calculation of the heat transfer in elements of buildings is also provided as a part of this software. It has also the advantage of capacity to directly import building designs prepared in CAD packages. Additionally, it allows the end user to more finely describe the modular HVAC equipment using available specific experimental parameters. Finally, by

deploying a reliable and fast prediction-correction approach for solving the system of governing equations results in accurate and time efficient numerical simulation.

EnergyPlus [143] was first launched in 2001 and uses the simulation methodologies developed in two pre-existing programs: DOE-2 [144] and BLAST [145]. The most accurate subroutines and features of both DOE-2 and BLAST were further improved in order to capture the best features of both packages to create a new more powerful building simulation tool. The developers aimed to create a well-organised, modular-structured software with accessibility to data and capability to easily couple with other software.

4.2 Structure

The solution in EnergyPlus is obtained in several stages. Of a particular interest during development was the integrated simulation manager, which enables simultaneous solution of both loads and systems equations. This function, according to the design team offers a high accuracy for a given set of input parameters. Heat balance equations from a research version of BLAST are used to calculate loads at a time-step specified by the end user. Information is subsequently passed to the building simulation module in which the response of heating and cooling plant can be calculated. If the feedback from the building module does not meet the calculated loads, adjustments of the space temperatures are made at the next time step. The method described above has a major advantage over the sequential simulation techniques used in other programs. It provides feedback from the HVAC module to the load calculations which results in accurate space temperature calculations. In addition, the simultaneous solution method allows the user to evaluate a number of processes, including realistic system control, radiant heating and cooling systems and inter-zone air flow. Figure 4.1 shows the structure of the EnergyPlus software.

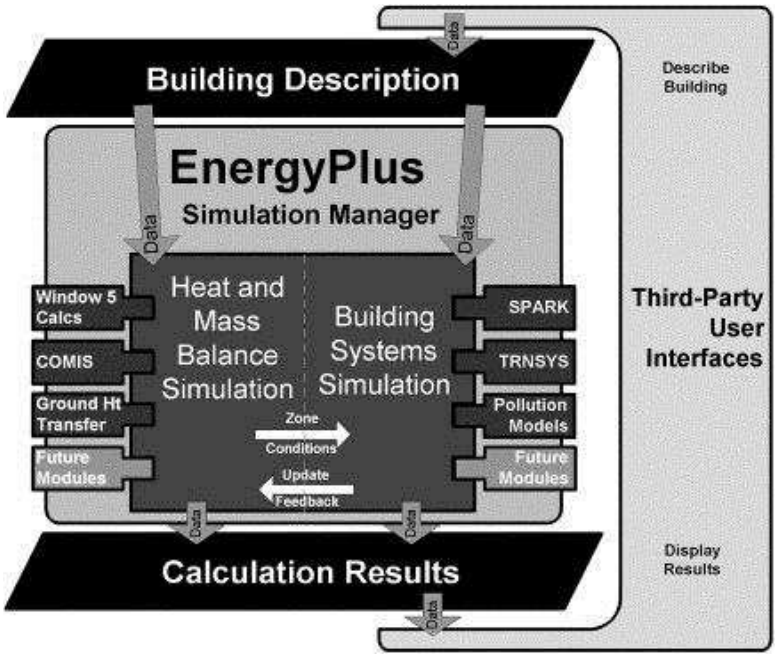

Figure 4.1 Overall structure of EnergyPlus [141]

EnergyPlus incorporates three basic components, namely a simulation manager, heat and mass balance simulations module and building systems simulation tools. The whole simulation process is controlled by the simulation manager.

The major functions of the simulation manager can be summarised as follows:

- Control of loop interaction at the given time-step and over a simulation period;
- Control of the individual modules on decision-making (such as initialisation, simulation, recording data, reports, etc);
- Manipulation of the coupling procedure of EnergyPlus with other simulation software.

The above described structure eliminates the 'spaghetti code' issue [141] reported in predecessor simulation tools. Furthermore, it provides self-contained modules which enhance the flexibility in editing existing modules and adding new features.

The heating and cooling requirements are calculated in the heat and mass balance module. Calculations are based on a fundamental assumption that the air enclosed in thermal zones has uniform temperature. This hypothesis certainly does not occur in realistic conditions, however, it decreases the computational time when compared with simulations including the detailed model of ventilation such as a Computational Fluid Dynamics (CFD) - based models or even less complex zonal network ventilation models. Additional assumptions that are applied in calculations with respect to the heat balance on the room surfaces throughout the simulations are: uniform surface temperatures; diffuse radiating surfaces; uniform long and short wave irradiation; 1-D heat conduction. Figure 4.2 shows the integrated simulation manager structure. The heat balance module consists of the surface heat balance manager which simulates the interior and exterior surfaces heat balance and takes into account the boundary surface conditions and heat transfer modes that occur at surfaces (conduction, convection and radiation). Secondly, the air heat balance manager carries out calculations of various air mass streams within the energy zones, caused by ventilation, infiltration, air exhaust, etc.

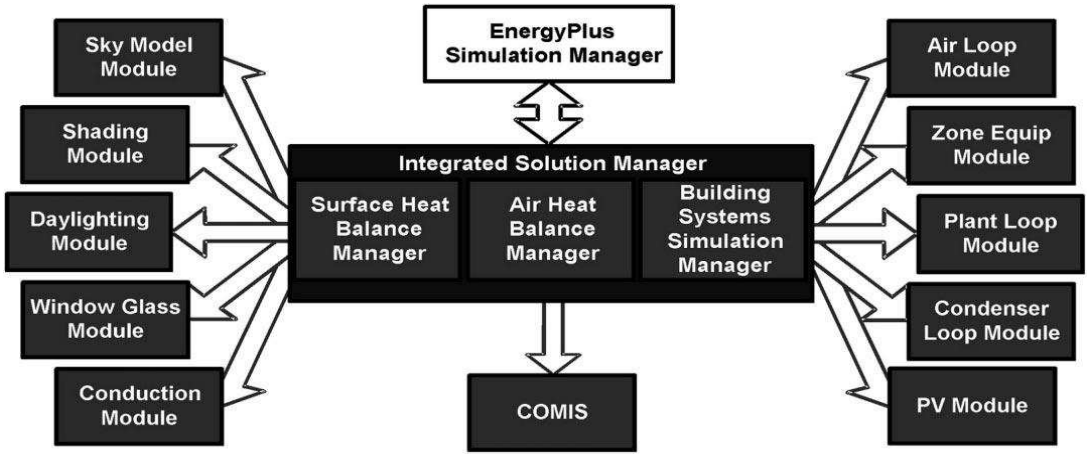

Figure 4.2 Solution manager structure [141]

The surface heat balance module features a daylight sub-module which is capable of simulating interior daylight illumination including inter-reflections both within the zone and due to surrounding objects. A detailed fenestration module allows end users to describe a layer-by-layer window construction allowing implementation of U-values with: a) accurate angular dependence of absorption and transmission for both visible and solar radiation and b) temperature dependency. Finally the implementation of an empirical model that accounts for non-isotropic irradiance as a function of both solar position and cloud cover resulting in improved solar diffuse calculations on tilted surfaces.

The improved mass transfer module provides a detailed layer-by-layer calculation of the mass transfer through surfaces and mass balance in the air within the energy zone. Improved capabilities of the building system simulation manager are due to the additional radiant heating and cooling modules incorporating thermal comfort calculations.

4.2.1 Building systems simulation manager

The inter-communication between the heat balance algorithm module and the various heating and cooling equipment is carried out by the building system tool. The former not only enables the exchange of data between modules but determine the response of the HVAC systems. A dataset from the heat balance manager solution at the given time-step is passed to the building system simulation manager which is responsible for the simulation of the HVAC equipment and components. Energy zone air conditions are subsequently updated (see Figure 4.3). Flexibility of the data input is granted due to the simultaneous solution regime. In contrast, the sequential solution method (building envelope requirements first, then air distribution system, then HVAC equipment) imposes rigid boundaries in software structure and lacks the major advantage of feedback within the modules.

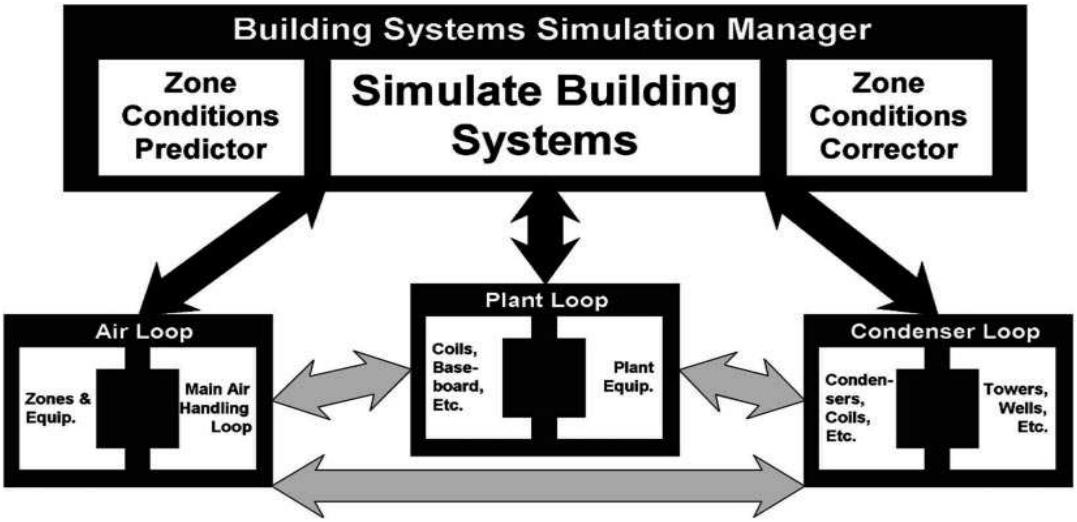

Figure 4.3 Building simulation manager [141]

The building simulation manager allows for fully integrated simulation of systems and plant and features modular and extensible characteristics. Integration functionality accounts for realistic and tight coupling of the air and water side of the system and plant respectively, whilst modularity at both system and equipment levels ensures flexibility when expanding the component library. The interconnection between the equipment and the systems is accomplished through the use of integrating loops within the simulation structure. HVAC air and water loops reproducing the pipe network found in physical systems enable the calculation to include pressure and thermal losses occurred due to turbulent flow within the loops. Although there is no hardwired template system, input (example) files available from the developers offer the end-user an easy starting point in order to develop the desired system configuration.

Air loops are capable of simulating: air transport; heat control and recovery for supply air temperature; outside air economiser; mixing and conditioning; supply and return fans; heating and cooling coils.

Energy zone equipment options are used for connecting the air loops with the zones. Equipment should be specified by users in a priority-based order as used to propagate calculated loads and includes heating and cooling coils, diffusers, supply air control, convection units, high and low temperature radiant/convective units, etc. Figure 4.4 shows the equipment configuration within an energy zone.

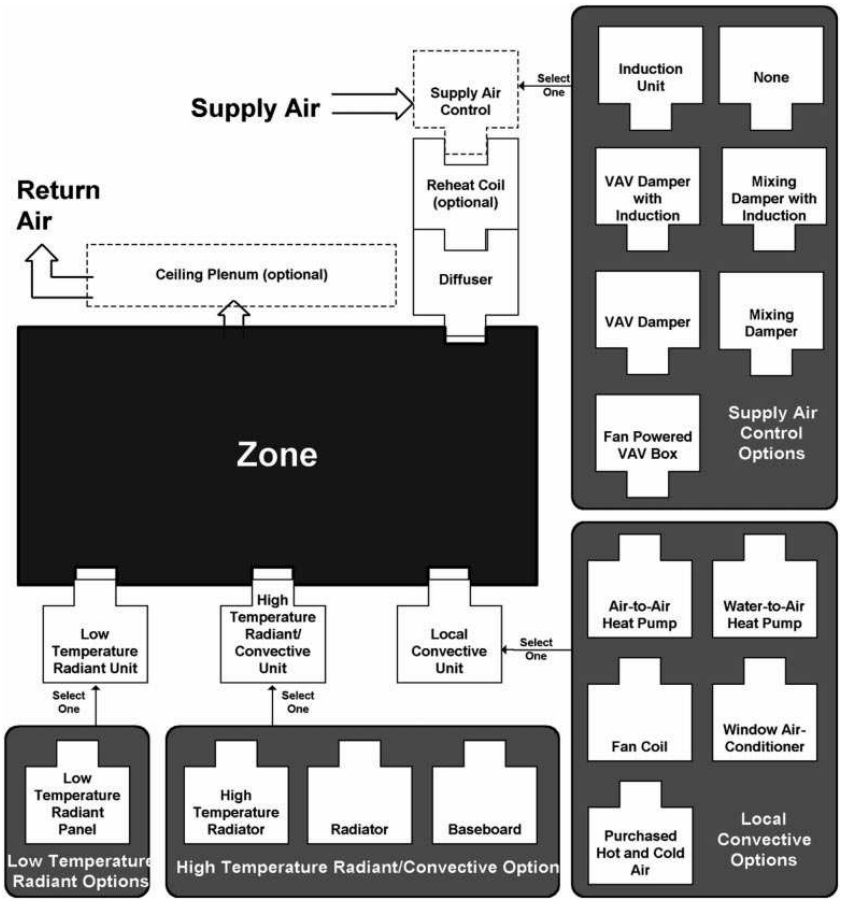

Figure 4.4 Equipment connection to zones [141]

Equipment connections within the loop are defined using nodes at relevant locations and are assigned for numeric identifiers as illustrated in Figure 4.5. Loop state variables and set-point input data are recorded from those identifiers, whereas the unknown state variables are calculated along with control equations variables using an iterative solution method.

At a given node, control representation associates input set-points to a function describing zone equipment. Eventually, the building module initiates calculations with loop components

and updates the control equations using an explicit finite difference method. Calculations carry on until the solution is converged.

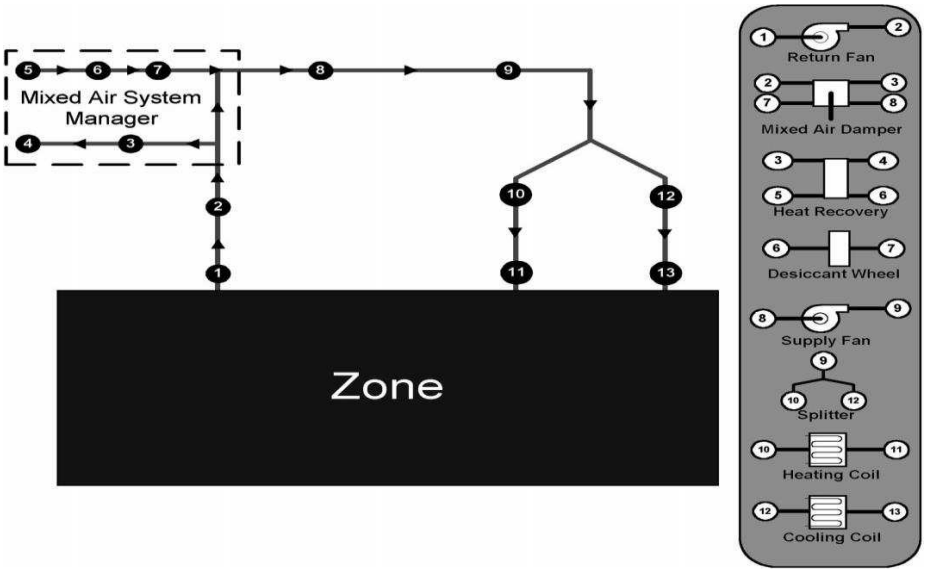

Figure 4.5 Schematic diagram of air loop node [141]

4.2.2 Water loops

A primary HVAC plant equipment loop, used for supply components, and a secondary loop, used for heat rejection equipment, is connecting the zone modules with the heat balance simulation manager. The characteristics of the equipment within the zones are used as criteria for classification purposes. Furthermore, the solution method described in the air loop section is applied for calculating the response of the HVAC plant water loops. A significant function of the nodes is the interconnection between water and air loops. However a distinct node structure should be applied through the input file. EnergyPlus has an integrated HVAC component library which can be expanded with new components as a consequence of the extendable nature of the building simulation module. This can be performed by expert users through a coupling process with an equation based simulation tool named SPARK [141]. Figure 4.6 shows a primary water HVAC plant loop.

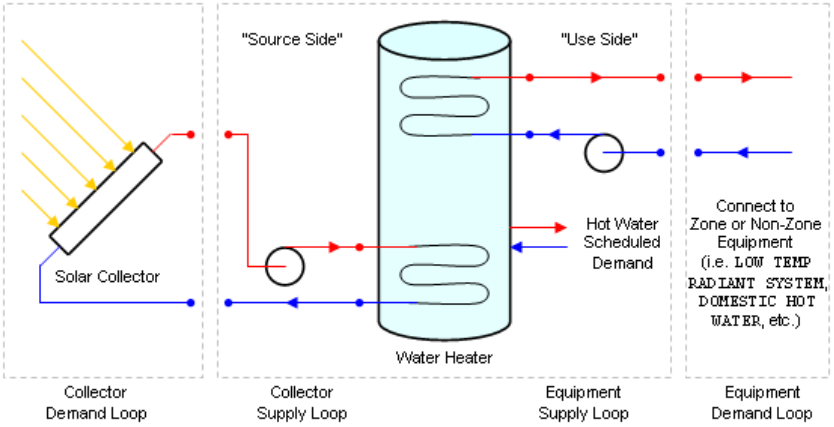

Figure 4.6 Example of a solar collector plant loop connection diagram [146]

4.2.3 Input-output and weather data files

A plug-in module based on the Google sketch-up permits the design and creation of a building geometry in format manageable by the simulation modules. A further development of the file can be performed using the main interface of EnergyPlus either by text editor or the inbuilt “idf" (input data file) editor. The input file consists of an object-based format in which the characteristics of both building and systems are specified in detail. In the text editor the basic system components are defined as ‘objects’ (such as a building surface, coil, boiler) and the characteristic of the corresponding component are described with values (data) organised in particular order, namely object, data 1, data 2, data 3...., data N.

In addition, the idf editor interface offers a less complicated alternative for editing the input data than is the case with generic text editor. Objects and characteristics are visible and well organised in tables whereas the end user can set the perspective values for the components that are applied in model.

The simulation manager saves the results for the given time-step (and for a given simulation period) in an output file with a structure and methodology similar to the one described for the input files. Results follow the same syntax format, using a comma-separated values format

ready to be imported to a spreadsheet for further analysis. Of particular interest is the weather data. The file of input data includes basic location information:

- Peak heating/cooling design
- Location name
- Data source
- Daylight saving periods
- Longitude
- Latitude
- Typical and extreme periods
- Time zone
- elevation

EnergyPlus provides a library of climate data from weather stations all over the world using average values in the format of 'typical meteorological year' (TMY) climate information. Although weather data includes information for every minute interval, EnergyPlus usually reads hourly data records. The self-contained format of all the files associated with energy as described in the previous section is retained throughout the simulation process. These results are in easy to access files and allow a smooth data exchange with other software such as databases and spreadsheets. However, a major drawback is the large size of these files due to data accumulation.

4.2.4 Validation of EnergyPlus

The performance of EnergyPlus has been validated by applying simultaneous paths, during the testing processes. An ASHRAE Standard 140P comparative testing process was applied in the load algorithms. Simulations were conducted on a box with windows and shading together with low and high mass constructions.

Results were therefore compared against other simulation data provided by a classic semi-empirical method. In addition, the heat conduction transfer through a variety of thicknesses and materials was analytically tested under several temperature conditions. The testing process indicated a good agreement between EnergyPlus predictions and those from other simulation tools. This also was confirmed in [140].

4.3 EnergyPlus Mathematical Models Overview

EnergyPlus is used for calculating heating or cooling loads in order to maintain the thermal control set-points specified by the user and the energy consumption of the primary plant equipment. The model utilises a domestic energy use profile through the use of input data that specify the nature and the timing of appliances, lighting, DHW usage and thermal comfort. During the simulation, software uses a heat balance-based solution technique for building thermal loads that allows for simultaneous calculation of radiant and convective effects at both the interior and exterior surfaces for each time step. It also takes into account the transient heat conduction through building elements (walls, roofs, floors, etc.) using conduction heat transfer functions, as well as many other parameter [141] so it is capable to simulate a defined "designed day" or an extended period of time (up to and beyond a year).

The mathematical model used in EnergyPlus software is based on energy balance equations in the form of 1-D time dependant ordinary differential equations. The temperature within the zone is calculated for each time-step using data on the energy stored within the zone, heat input from the heating equipment and heat losses. The heat requirement of the building is calculated by taking into account the dwelling materials characteristics, dimensions of walls, windows, rooms and climate conditions and energy transfer due to interzone interactions and ventilation/infiltration. The building simulation tool predicts the response of the heating equipment to maintain the pre-defined temperature in zones of the building by compensating heat losses due to convection, conduction and radiation from the building.

EnergyPlus solves the equations for building, systems and plants simultaneously. The integrated solution manager, described in the previous section, links all the parameters in a simultaneous solution scheme. Figure 4.7 illustrates the representation of a series of functional elements connected by fluid loops.

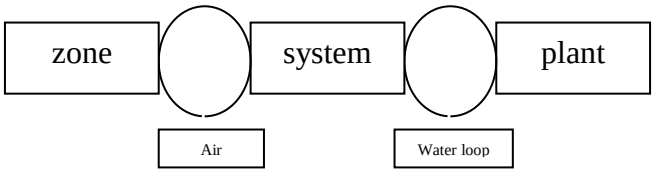

Figure 4.7 Schematic of Simultaneous Solution Scheme [146]

Solution starts with definition of a heat balance equation used for formulating the energy and moisture balance within the zones and is based on using predictor-corrector approach:

$$C_z \frac{dT_z}{dt} = \sum_{i=1}^{Nsl} \dot{Q}_i + \sum_{i=1}^{Nsurfaces} h_i A_i (T_{si} - T_z) + \sum_{i=1}^{Nzones} \dot{m}_i C_p (T_{zi} - T_z) + \dot{m}_{\inf} C_p (T_\infty - T_z) + \dot{Q}_{sys} \quad (4.1)$$

where $\sum_{i=1}^{Nsl} \dot{Q}_i$ is the sum of the convective internal loads, $\sum_{i=1}^{Nsurfaces} h_i A_i (T_{si} - T_z)$ is the convective heat transfer from the zone surfaces; $\sum_{i=1}^{Nzones} \dot{m}_i C_p (T_{zi} - T_z)$ is the heat transfer due to inter-zone air mixing; $\dot{m}_{\inf} C_p (T_\infty - T_z)$ is the heat transfer due to infiltration of the outside air; $\dot{Q}_{sys}$ is the air system output, $C_z \frac{dT_z}{dt}$ is the energy stored in a zone when

$$C_z = \rho_{air} C_p C_T \quad (4.2)$$

Here ρ_{air} is the zone air density, C_p is the zone air specific heat, C_T is the sensible heat capacity multiplier.

The energy output of the system can be formulated from the difference between the supply air enthalpy and the enthalpy of the air leaving the zone:

$$Q_{sys} = \dot{m}_{sys} C_p \left(T_{\sup} - T_z \right) \quad (4.3)$$

Here $T_{\sup}$ is the temperature of the air system supply and T_z is the zone air temperature.

The result of substituting Equation (4.3) in the heat balance Equation (4.1) is

$$C_z \frac{dT_z}{dt} = \sum_{i=1}^{N_{sl}} \dot{Q}_i + \sum_{i=1}^{N_{surfaces}} h_i A_i \left(T_{si} - T_z\right) + \sum_{i=1}^{N_{zones}} \dot{m}_i C_p \left(T_{zi} - T_z\right) + \dot{m}_{\inf} C_p \left(T_\infty - T_z\right) + \dot{m}_{sys} C_p \left(T_{sup} - T_z\right) \tag{4.4}$$

where the sum of zone loads and air system output now equals the rate of change in energy stored in the zone. The simulation manager uses a third order backward difference solution algorithm based on a finite difference approximation in order to solve the Equation (4.4). A 3rd order Euler formula is used as it was predicted to provide good accuracy.

$$\left.\frac{dT_z}{dt}\right|_t \approx \left(\delta t\right)^{-1} \left[\frac{11}{6} T_z^t - 3T_z^{t-\delta t} - \frac{1}{3} T_z^{t-3\delta t}\right] + O\left(\delta t^3\right) \tag{4.5}$$

Equation 4.5 in the solution algorithm eliminates instabilities related to the time step selection and the zone temperature update equation becomes

$$T_z^t = \frac{\sum_{i=1}^{N_{sl}} \dot{Q}_i + \sum_{i=1}^{N_{surfaces}} h_i A_i T_{si} + \sum_{i=1}^{N_{zones}} \dot{m}_i C_p T_{zi} + \dot{m}_{\inf} C_p T_\infty}{\left(\frac{11}{6}\right)\left(\frac{C_z}{\delta t}\right) + \sum_{i=1}^{N_{surfaces}} h_i A + \sum_{i=1}^{N_{zones}} \dot{m}_i C_p + \dot{m}_{\inf} C_p + \dot{m}_{sys} C_p} + \frac{\dot{m}_{sys} C_p T_{Supply} - \left(\frac{C_z}{\delta t}\right)\left[-3T_z^{t-\delta t} + \frac{3}{2} T_z^{t-2\delta t} - \frac{1}{3} T_z^{t-3\delta t}\right]}{\left(\frac{11}{6}\right)\left(\frac{C_z}{\delta t}\right) + \sum_{i=1}^{N_{surfaces}} h_i A + \sum_{i=1}^{N_{zones}} \dot{m}_i C_p + \dot{m}_{\inf} C_p + \dot{m}_{sys} C_p} \tag{4.6}$$

The described algorithm requires zone air temperatures at three previous time steps and uses constant temperature coefficients. The numerical integration over long time simulations may cause a potential truncation error which could be accumulative over many time steps (in addition to the conventional truncation errors evident in the building simulation). This results in zero net error accumulations during each daily cycle simulations.

The heat balance equation without the air system term can be derived as a function of the desired temperature T_z (defined from the user's set points at each zone):

$$\dot{Q}_{load} = \sum_{i=1}^{N_{sl}} \dot{Q}_i + \sum_{i=1}^{N_{surfaces}} h_i A_i \left(T_{si} - T_z\right) + \sum_{i=1}^{N_{zones}} \dot{m}_i C_p \left(T_{zi} - T_z\right) + \dot{m}_{\inf} C_p \left(T_\infty - T_z\right) \quad (4.7)$$

In order for the system to meet the zone conditioning requirements, $\dot{Q}_{load} = \dot{Q}_{sys}$. If the system is not capable of meeting the energy requirements, it provides its maximum output and the zone temperature is allowed to 'float'.

Equation 4.7 is used for sizing of the system as it calculates the capacity for each time step. The method used has predictor/corrector characteristics as the system output is first approximated based on the prediction of the zone temperature and then the change of the zone temperature is determined by the actual air system response.

4.3.1 Summary of time-step model formulation

Simulations are split into a series of discrete time periods commonly referred as time-steps, and software performs calculations for the each time-step. Figure 4.8 shows the basic concept of obtaining a solution through time-steps.

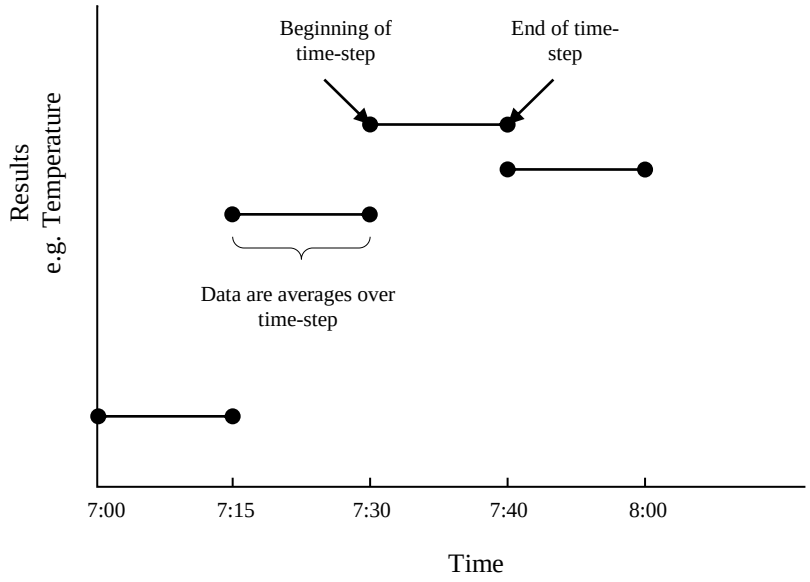

Figure 4.8 Schematic of time-step formulation [146]

The modules participating in a simulation process and predicting the condition for a given time-step, are based on quasi-steady balance equations. During calculations, input data and

time-dependent boundary conditions are taken into consideration at each time step and information is kept constant over that distinct time period. Output data which follows a successful simulation are average values for the respective result. In order for the simulation manager to simplify the solution and due to the simultaneous solution approach, data in some cases lag meaning that some values used in a current time-step were originates during the previous time step.

4.3.2 Surfaces heat balance manager

Conduction through walls

The basic time series solution associates the flux at one surface of a wall to an infinite series of temperature histories at both sides of the wall in order to describe the heat conduction through the wall. The terms in the series decay rapidly, therefore an infinite number of terms only are required for a sufficiently accurate result prediction. The method can be simplified if the flux history is replaced by higher order terms only and by introducing a conduction transfer function (CTFs). The basic form of a conduction transfer function is

$$q''_{ko}(t) = -\mathrm{Z}_o T_{i,t} - \sum_{j=1}^{nz} Z_j T_{i,t-j\delta} + Y_o T_{o,t} + \sum_{j=1}^{nz} Y_j T_{i,t-j\delta} + \sum_{j=1}^{qz} \Phi_j q''_{ki,t-j\delta} \qquad (4.8)$$

for inside surface heat flux;

$$q''_{ko}(t) = -Y_o T_{i,t} - \sum_{j=1}^{nz} Y_j T_{i,t-j\delta} + X_o T_{o,t} + \sum_{j=1}^{nz} X_j T_{i,t-j\delta} + \sum_{j=1}^{qz} \Phi_j q''_{ki,t-j\delta} \qquad (4.9)$$

for the outside surface heat flux.

Here X_j is the outside CTF coefficient, j=0,1,..,nz; Y_j is the cross CTF coefficient, j=0,1,..,nz; Z_j is the inside CTF coefficient, j=0,1,..,nz; Φ_ϕ is the flux CTF coefficient, j=0,1,..,nq; q''_{ko} is the conduction heat flux on the outside face; q'' is the conduction heat flux on the inside face; T_o is the outside face temperature; T_i is the inside face temperature.

The part of subscript which follows the comma in Equations (4.8) and (4.9) indicates the time period for the quantity in terms of the time step δ.

The default solution method in EnergyPlus is known as the state space method which is described by the following linear matrix equations:

$$\frac{d[x]}{dt} = [A][x] + [B][u] \tag{4.10}$$

$$[y] = [C][x] + [D][u] \tag{4.11}$$

where x is the vector of the state variables, u is the vector of inputs, y is the output vectors and A,B,C and D are matrices of coefficients.

In this case the state variables are the nodal temperatures, interior and exterior temperatures are the inputs and the resulting heat fluxes are the outputs:

$$\frac{d\begin{bmatrix} T_1 \\ \vdots \\ T_n \end{bmatrix}}{dt} = [A]\begin{bmatrix} T_1 \\ \vdots \\ T_n \end{bmatrix} + [B]\begin{bmatrix} T_1 \\ T_o \end{bmatrix} \tag{4.12}$$

$$\begin{bmatrix} q_i'' \\ q_o'' \end{bmatrix} = [A]\begin{bmatrix} T_1 \\ \vdots \\ T_n \end{bmatrix} + [B]\begin{bmatrix} T_1 \\ T_o \end{bmatrix} \tag{4.13}$$

where $T_1,...,T_n$ are the finite difference nodal temperatures, n is the number of nodes T_i and T_o are the interior and exterior environmental temperatures respectively and q_i'', q_o'' are the calculated heat fluxes. Figure 4.9 shows a simple one layer slab with two interior nodes and convection on both sides.

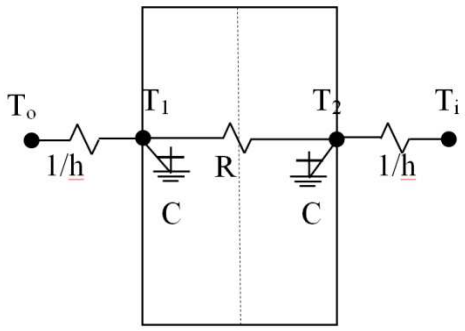

Figure 4.9 Two node state space example

Solutions therefore could be calculated as

$$\begin{bmatrix} \frac{dT_1}{dt} \\ \frac{dT_2}{dt} \end{bmatrix} = \begin{bmatrix} -\frac{1}{RC} - \frac{hA}{C} & \frac{1}{RC} \\ \frac{1}{RC} & \frac{1}{RC} - \frac{hA}{C} \end{bmatrix} \begin{bmatrix} T_1 \\ T_2 \end{bmatrix} + \begin{bmatrix} \frac{hA}{C} & 0 \\ 0 & \frac{hA}{C} \end{bmatrix} \begin{bmatrix} T_o \\ T_i \end{bmatrix} \tag{4.14}$$

$$\begin{bmatrix} q''_o \\ q''_i \end{bmatrix} = \begin{bmatrix} 0 & -h \\ h & 0 \end{bmatrix} \begin{bmatrix} T_1 \\ T_2 \end{bmatrix} + \begin{bmatrix} 0 & h \\ -h & 0 \end{bmatrix} \begin{bmatrix} T_o \\ T_i \end{bmatrix} \tag{4.15}$$

4.3.3 Interior/Exterior heat convection

A basic formula describing the heat convection from the surface is used. In the case of an exterior surface:

$$Q_c = h_{c,ext}\, A\left(T_{surf} - T_{air}\right) \tag{4.16}$$

where Q_c is the rate of exterior convective heat transfer, $h_{c,ext}$ is the exterior convection coefficient, T_{surf} and T_{air} are the surface and outdoor air temperatures respectively. Similar equations are used to describe convection at interior surfaces.

4.3.4 Water loop description

A number of systems can be used for determination of heat requirements in an energy zone. For a conventional heating system, a hot water boiler could be selected and its simple model is used. The user then is required to provide only the nominal boiler capacity and thermal efficiency and the boiler model is based on the following three equations:

$$OperatingPartLoadRatio = \frac{BoilerLoad}{BoilerNomCapacity} \tag{4.17}$$

$$FuelUseTheory = \frac{BoilerLoad}{\eta_{Nom}} \tag{4.18}$$

$$FuelUsed = \frac{FuelUseTheory}{EfficiencyCurve} \tag{4.19}$$

4.3.5 Micro Co-generator Module

The module responsible for the simulation of cogeneration systems is a direct implementation of a model developed by IEA Annex 42 [17]. A design group was formed within the International Energy Agency for the purpose of developing models of building cogeneration systems. The integrated module is capable of simulating combustion based cogeneration devices as well as fuel cell based devices. The operation of a micro CHP unit is simulated using an empirical model including transient periods such as warm up and cool down periods and heat recovery (when performance is a function of the engine temperature). Some of the relevant model equations are:

$$\eta_e = f\left(\dot{m}_{cw,}T_{cw,i,}P_{net,ss}\right) \tag{4.20}$$

$$\eta_q = f\left(\dot{m}_{cw,}T_{cw,i,}P_{net,ss}\right) \tag{4.21}$$

$$q_{gross} = {}^{P_{net,ss}}/_{\eta_e} \tag{4.22}$$

$$q_{gen,sss} = \eta_q q_{gross} \tag{4.23}$$

$$\dot{N}_{fuel} = {}^{q_{gross}}/_{LHV_{fuel}} \tag{4.24}$$

$$\dot{m}_{fuel}^{t+\Delta t} = \begin{cases} \dot{m}_{fuel,demand}^{t+\Delta t} & if \quad \frac{d\dot{m}_{fuel}}{dt} \le \left(\frac{d\dot{m}_{fuel}}{dt}\right)_{max} \\ \dot{m}_{fuel}^{t} \pm \left(d\dot{m}_{fuel}/dt\right)_{max} & if \quad \frac{d\dot{m}_{fuel}}{dt} > \left(\frac{d\dot{m}_{fuel}}{dt}\right)_{max} \end{cases} \tag{4.25}$$

$$\dot{m}_{air} = f\left(P_{net,ss}\right) \tag{4.26}$$

$$P_{net}^{t+\Delta t} = \begin{cases} P_{net,ss}^{t+\Delta t} & if \quad \frac{dP_{net}}{dt} \leq \left(\frac{dP_{net}}{dt}\right)_{max} \\ P_{netl}^{t} \pm \left(dP_{net}/dt\right)_{max} & if \quad \frac{dP_{net}}{dt} > \left(\frac{dP_{net}}{dt}\right)_{max} \end{cases} \tag{4.27}$$

$$[MC]_{eng}\frac{dT_{eng}}{dt} = UA_{HX}\left(T_{cw,p} - T_{eng}\right) - UA_{loss}\left(T_{room} - T_{eng}\right) + q_{gen,ss} \tag{4.28}$$

$$[MC]_{cw}\frac{dT_{cw,o}}{dt} = \left[\dot{m}c_p\right]_{cw}\left(T_{cw,i} - T_{cw,o}\right) + UA_{HX}\left(T_{eng} - T_{cw,o}\right) \tag{4.29}$$

Here η_e is the steady-state, part load electrical conversion efficiency of the engine; η_q is the steady-state, part load thermal conversion efficiency of the engine; $\dot{m}_{cw}$ is the mass flow rate of plant fluid through the heat recovery section [kg/s]; $T_{cw,i}$ is the bulk temperature of the plant fluid entering the heat recovery section (°C); $T_{cw,o}$ is the bulk temperature of the plant fluid leaving the heat recovery section (°C); $P_{net,ss}$ is the steady-state electrical output of the system (W); q_{gross} is the gross heat input into the engine (W); $q_{gen,ss}$ is the steady-state rate of heat generation within the engine (W); $\dot{N}_{fuel}$ is the molar fuel flow rate (kmol/s); $\dot{m}_{fuel}$ is the mass fuel flow rate (kg/s); $\dot{m}_{air}$ is the air mass flow rate through the engine (kg/s); $[MC]_{eng}$ is the thermal capacitance of the engine control volume (W/K); T_{eng} is the temperature of the engine control volume (°C); UA_{HX} is the effective thermal conductance between the engine control volume and the cooling water control volume (W/K), $UA_{loss}$is the effective thermal conductance between the engine control volume and the surrounding environment (W/K); T_{room} is the air temperature of surrounding environment (°C); $[MC]_{cw}$ is the thermal capacitance of encapsulated cooling water and heat exchanger shell immediate thermal contact (J/K); $\left[\dot{m}c_p\right]_{cw}$is the thermal capacity of the surrounding environment (W/K).

Both η_e and η_q are second order polynomials, the method of solution used for these values correlated to engine's mass temperature, T_{eng} and the outlet plant node $T_{cw,o}$. The engine temperature at the given time-step is calculates as:

$$\frac{dT}{dt} = a + b \tag{4.30}$$

where

$$a = \frac{UA_{HX}}{[MC]_{eng}} * T_{cw,o} + \frac{UA_{loss}}{[MC]_{eng}} * T_{room} + \frac{q_{gen,ss}}{[MC]_{eng}} \tag{4.31}$$

$$b = -\left(\frac{UA_{HX}}{[MC]_{eng}} + \frac{UA_{loss}}{[MC]_{eng}}\right) \tag{4.32}$$

The plant node outlet fluid temperature is calculated using

$$a = \frac{[\dot{m}c_p]_{cw}}{[MC]_{cw}} * T_{cw,i} + \frac{UA_{HX}}{[MC]_{cw}} * T_{eng} \tag{4.33}$$

$$b = -\left(\frac{[\dot{m}c_p]_{cw}}{[MC]_{cw}} + \frac{UA_{HX}}{[MC]_{cw}}\right) \tag{4.34}$$

An iteration procedure is used which alternates the calculations of T_{eng} and $T_{cw,o}$ and exits the loop once the energy balance satisfies the following criteria

$$\frac{(q_{gen,ss})_{max}}{10000000} > UA_{HX}(T_{cw,o} - T_{eng}) + UA_{loss}(T_{room} - T_{eng}) + q_{gen,ss} - [MC]_{eng}\frac{dT_{eng}}{dt} \tag{4.35}$$

$$\frac{(q_{gen,ss})_{max}}{10000000} > [\dot{m}c_p]_{cw}(T_{cw,i} - T_{cw,o}) + UA_{HX}(T_{eng} - T_{cw,o}) - [MC]_{cw}\frac{dT_{cw,o}}{dt} \tag{4.36}$$

The simulation of a mCHP module is determined by several operating modes which are controlled by user defined operating modes at each time-step, namely off, standby, warm-up, cool-down and normal.

4.3.6 Fuel cell generator module

The fuel cell module is used for simulating small scale fuel cell based co-generators systems. The module was originally developed by IEA and implemented in EnergyPlus. Detailed description can be found in IEA Annex 42 [17]. Two major types of fuel cell system can be simulated, a solid oxide fuel cell (SOFC) and proton exchange membrane (PEM) fuel cell. Given the recent integration of this module (which is very complex) into software, there are concerns about accuracy and additionally there are uncertainties concerning the input parameters. Input data is extremely difficult to obtain and some sub-systems are currently not widely implemented in practice though they are included in the description of the module.

Large input data results are necessary to introduce separate subsystems within the fuel cell module and each one is responsible for a particular operation during the simulation process. A simulation can incorporate multiple FC generators and all input details are organised in a number of objects which correspond to functions of the FC operation. Figure 4.10 illustrates the structure of the fuel cell module and its separate subsystems. Most of the modules of EnergyPlus use the Higher Heating Value (HHV) of the fuel in the solution. Calculation of the FC model is based on use of the Lower Heating Value (LHV) of the fuel. The fuel cell module is based on the IEA Annex 42 [17] 'The simulation of building-integrated fuel cell and other cogeneration systems'. It is described as a 'grey box' empirical model which compromises a mixture of thermodynamics and empirical performance equations. The fuel cells module interacts with the rest of the model in different ways. The latter accounts for the complexity of the structure as the operation of individual components are assigned to numerous sub-systems. The utilisation of fuel, air and water is carried out within six separate streams. The module not only simulates the heat and power but also the convection and radiation heat transfer to the energy zones through the exhaust node.

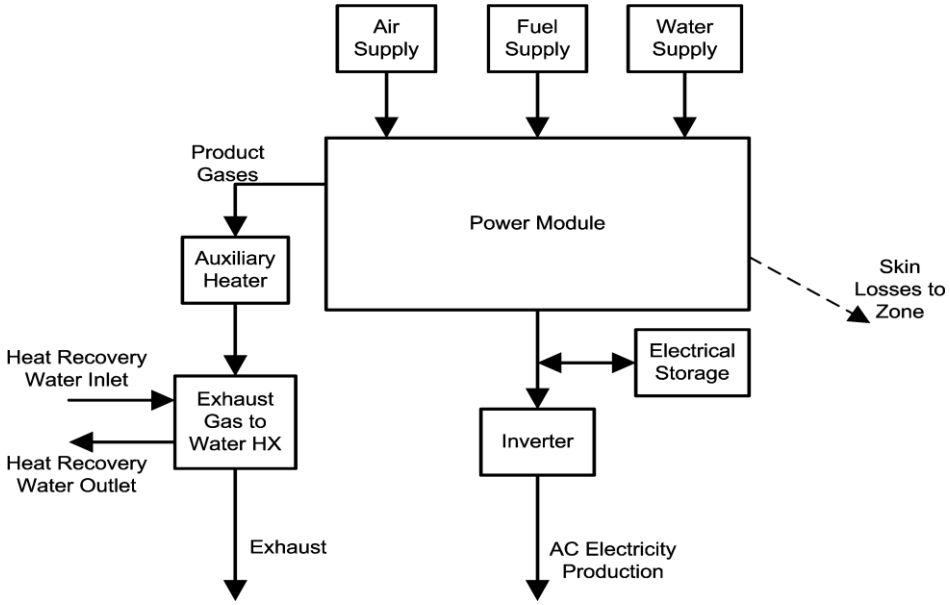

Figure 4.10 Fuel cell module structure [146]

An electric storage can also be applied in simulations when a FC operates as an electricity-led equipment. Such operation eliminates the modulation in power output. The structure of the module makes it possible to describe the interaction of sub-systems with the building's energy and comfort systems.

A summary of relevant equations describing the operation of the module is presented below. Simulations start with solving the main energy balance equation in the fuel cell power module (this equation is used to model the enthalpy of the product gases that leave the FC power module):

$$\dot{H}_{fuel} + \dot{H}_{air} + \dot{H}_{liq-water} + \dot{H}_{dilution-air-in} + P_{el,ancillaries-AC} = P_{el} + \dot{H}_{FCPM-cg} + q_{s-cool} + q_{skin-loss} + \dot{H}_{dilution-air-out} \quad (4.37)$$

where $\dot{H}_{air}$ is the total enthalpy multiplied by a flow rate of air introduced to the control volume (W); $\dot{H}_{fuel}$ is the total enthalpy multiplied by a flow rate of fuel introduced to the control volume (W); $\dot{H}_{liq-water}$ is the total enthalpy multiplied by a flow rate of water

required for steam reformation (W); $\dot{H}_{FCPM}$ is the total enthalpy multiplied by a flow rate of produced gases exiting the control volume (W); q_{s-cool} is the heat extracted from system in order to maintain its temperature (W); $q_{skin-loss}$ are the parasitic thermal losses from the control volume (W); P_{el} is the DC net power generated by the FC (W); $P_{el,ancillaries-AC}$ is the power draw of the auxiliaries included within the control volume (W); $\dot{H}_{dilution-air-in}$ and $\dot{H}_{dilution-air-out}$ are the total enthalpy multiplied by flow rates of air that is drawn through the cabinet for cooling purposes.

In respect to the gas streams the total enthalpy can be substituted from the summation of the enthalpies of their constituent gases. For convenience the enthalpy of each reactant or product gases is expressed as a sum of a standard enthalpy of formation and the deviation between its enthalpy and that at the standard state:

$$\begin{aligned}\sum_i \left(\dot{N}_i\left[\hat{h}_i - \Delta_f\hat{h}_i^o\right]\right)_{fuel} + \sum_i \left(\dot{N}_i\left[\hat{h}_i - \Delta_f\hat{h}_i^o\right]\right)_{air} \\ + \dot{N}_{liq-water}\left(\left[\hat{h} - \Delta_f\hat{h}^o\right]_{H_2O,liq} - \Delta_f\hat{h}^o_{H_2O,fg}\right) \\ + \dot{H}_{dilution-air-in} + \dot{N}_{fuel} * LHV_{fuel} + P_{el,ancillaries-AC} \\ = P_{el} + \sum_i \left(\dot{N}_i\left[\hat{h}_i - \Delta_f\hat{h}_i^o\right]\right)_{FCPM-cg} + q_{s-cool} + q_{skin-loss} \\ + \dot{H}_{dilution-air-out}\end{aligned} \tag{4.38}$$

where $\dot{N}_i$ is the molar flow rate (kmol/s) of gas constituent i; $\hat{h}_i$ is the molar enthalpy of gas constituent i (J/kmol); $\Delta_f\hat{h}_i^o$ is the molar enthalpy of the gas i at the standard state (J/kmol); $\dot{N}_{liq-water}$ is the molar flow rate of liquid water added for reformation purposes (kmol/s); $\Delta_f\hat{h}^o_{H_2O,fg}$ is the latent heat of vaporisation of water at the standard state (J/kmol).

Electrochemical behaviour is commonly described by an empirical prediction of the cell voltage using the Nernst potential which accounts for activation, ohmic and concentration

losses. The electrochemical performance of the fuel cell can be expressed using parameters relating to the electrical efficiency and the net power generation.

$$\varepsilon_{el} = [\varepsilon_0 + \varepsilon_1 P_{el} + \varepsilon_2 P_{el}^2] * [1 - N_{stops} D] * \left[1 - \left(MAX\left(\int dt - t_{threshold,} 0.0\right)\right) * L\right] \quad (4.39)$$

Here ε_i are coefficients supplied by user; P_{el} is the DC net power generated by FC (W); $[1 - N_{stops} D]$ represents the degradation of fuel cell performance due to cycling operation; $t_{threshold,}$ is a user input value representing systems that exhibit no degradation for a given time period.

The flow rate of the process air can be solved either using a power generation-dependent equation or as a function of the fuel flow rate:

$$\dot{N}_{air} = [a_0 + a_1 P_{el} + a_2 P_{el}^2][1 + a_3 T_{air}] \quad (4.40)$$

or

$$\dot{N}_{air} = [a_0 + a_1 \dot{N}_{fuel} + a_2 \dot{N}_{fuel}^2][1 + a_3 T_{air}] \quad (4.41)$$

Here $\dot{N}_{air}$ is the air molar flow rate (kmol/s); T_{air} is the air supply temperature (°C); a_i are parameters based on empirical or manufacturer data. The term $[1 + a_3 T_{air}]$ is used to describe the cooling process when the fuel cell utilises the ambient temperature. The air composition will be considered as constant during simulation period and consist of N_2, O_2, H_2O, Ar and CO_2.

The parametric equation of the liquid water flow rate as a function of the fuel flow rate is given as follows:

$$\dot{N}_{liq-water} = w_0 + w_1 \dot{N}_{fuel} + w_2 \dot{N}_{fuel}^2 \quad (4.42)$$

Here w_i are coefficient based on empirical data; $\dot{N}_{liq-water}$ is the water-liquid molar flow rate (kmol/s).

The above equation accounts for the water-liquid requirements due to any reforming process. In the case of an internally reforming SOFC the inlet flow rate can be neglected.

Product gases

Both electrochemical reactions and combustion process result in gas production which is represented by the term $\sum_i\left(\dot{N}_i\left[\hat{h}_i - \Delta_f\hat{h}_i^o\right]\right)_{FCPM-cg}$ in the equation. Given the operating conditions of the fuel cell the produced gasses mainly consist of hydrocarbons, CO, hydrogen and NO_x. Based on previous research data, it is assumed that hydrocarbons and NO_x emissions account for 0.2 % of the total gases while the CO and SO_x levels are approximately the half of this (0.1 %). Throughout, it is assumed that reactants supplied in the fuel cell are fully react to CO_2 and H_2O.

The parasitic thermal losses to the surroundings via radiation and convection can be calculated as losses at a constant rate, proportional to the temperature differential between the produced gasses and room temperature or as a function of the fuel flow rate as described from in the following equations:

$$q_{skin-loss} = (UA)\left(T_{FCPM-cg} - T_{room}\right) \tag{4.43}$$

Or

$$q_{skin-loss} = s_0 + s_1\dot{N}_{fuel} + s_2\dot{N}_{fuel}^2 \tag{4.44}$$

where UA is a heat loss coefficient (W/K) describing the sum of the convection and radiation loses from the FC surface (or skin) to the surrounding; T_{room} is the room temperature and s_i are coefficients based on manufacturer data or analytic models.

A more detailed analysis of the fuel cell operation can be found in IEA Annex 42 [17]. The heat produced by the selected HVAC systems is directed either to the radiators or to the hot water tank for domestic application through a configuration of pipes and pumps. The simulation of the convective water "baseboard" (i.e. heating radiators) unit follows the standard effectiveness-NTU methodology. The calculation starts by determining the product of the specific heat and mass flow rate for both the air and water sides of the unit (heat exchanger). In the initialisation, the model assumes that the air mass flow rate is equal to 0.42 times of the water mass flow rate. The purpose of this particular selection is to provide accuracy in the performance calculations by providing some reasonable estimate of the air mass flow rate. This rate is kept constant throughout the rest of the simulation.

At each time step, the baseboard should meet any remaining heating requirement of the zone by implementing the following calculations:

$$C_{water} = c_{p,water}\dot{m}_{water} \quad (4.45)$$

$$C_{air} = c_{p,air}\dot{m}_{air} \quad (4.46)$$

Once the effectiveness is determined, the outlet conditions from the unit are determined using the following equations:

$$T_{air,outlet} = T_{air,inlet} + \varepsilon\left(T_{water,inlet} - T_{air,inlet}\right)C_{\min} / C_{air} \quad (4.47)$$

$$T_{water,outlet} = T_{water,inlet} - \left(T_{air,outlet} - T_{air,inlet}\right)C_{\text{air}} / C_{water} \quad (4.48)$$

The user can refer to the ASHRAE Handbook series for general information on different system types as needed. When produced heating energy is directed to the hot water tank, a well-mixed water tank is assumed in calculations. This assumption implies that the whole amount of water in the tank is at the same temperature and the model solves analytically the differential energy balance equation:

$$mc_p\frac{dT}{dt} = q_{net} \quad (4.49)$$

Substituting the q_{net} in equation 4.49 by associated terms dependent on the temperature

$$\frac{dT}{dt} = \left[\frac{1}{mc_p}\begin{pmatrix} q_{heater} + q_{oncy} + q_{offcyc} + UA_{oncyc}T_{amb} + UA_{offcyc}T_{amb} \\ +\varepsilon_{use}\dot{m}_{use}c_pT_{use} + \varepsilon_{source}\dot{m}_{source}c_pT_{source} \end{pmatrix}\right] + \left[\frac{-1}{mc_p}\left(UA_{oncyc} + UA_{offcyc} + \varepsilon_{use}\dot{m}_{use}c_p + \varepsilon_{source}\dot{m}_{source}c_p\right)\right]T \tag{4.50}$$

The temperature of the water tank T(t) at the instance of time t can calculated as

$$T(t) = \left(\frac{a}{b} + T_i\right)e^{bt} - \frac{a}{b} \tag{4.51}$$

where T_i is the initial temperature at time t = 0 and

$$a = \left[\frac{1}{mc_p}\begin{pmatrix} q_{heater} + q_{oncy} + q_{offcyc} + UA_{oncyc}T_{amb} + UA_{offcyc}T_{amb} \\ +\varepsilon_{use}\dot{m}_{use}c_pT_{use} + \varepsilon_{source}\dot{m}_{source}c_pT_{source} \end{pmatrix}\right] \tag{4.52}$$

$$b = \left[\frac{-1}{mc_p}\left(UA_{oncyc} + UA_{offcyc} + \varepsilon_{use}\dot{m}_{use}c_p + \varepsilon_{source}\dot{m}_{source}c_p\right)\right] \tag{4.53}$$

The equation can be rearranged to solve the time needed in order to reach a requested temperature T_f:

$$t = \frac{1}{b}\ln\left(\frac{a/b + T_f}{a/b + T_i}\right) \tag{4.54}$$

All individual components are described as algorithmic models with fixed input and output. They are coupled using air or water loops and allowed to interact as outlined in a schematic approach. Calculations start with zone by zone heat balance simulations where the user's set points are taken into consideration. The solution manager calculates the response of the system for a particular condition of each zone and calculations continue with the component sizing algorithms. It is worth mentioning the importance of correct equipment sizing which is carried out by a solution sizing manager. When a component is called for the first time in simulations, a sizing subroutine is initiated for calculating the auto sizable parameters such as fluid flow rates, temperatures, power output, etc.

Chapter 5 Description of Experimental Work

5.1 Introduction

The performance of three mCHP systems based on IC and Stirling engine and PEM fuel cell technologies were experimentally assessed under both dynamic and steady-state operating conditions. Obtained results such as partial efficiencies, nominal capacities, transient start-up and shut-down periods, were fed directly into the numerical simulation process. The latter allowed to describe the realistic operating conditions. Finally, experimental and theoretical results from building simulations were compared in order to assess the accuracy of simulation methodology. Table 5.1 summarise the main features of the co-generation units that have been experimentally tested. The experimental results presented in this Chapter are representative ones from several tests. Parameters of other cycles were deviating by ± 5 % when compared to the representative curve.

Table 5.1 Main features of the tested micro-cogeneration units based on manufacturer's information

mCHP	Technology	Claimed Net efficiency	Nominal Power (kW)	Nominal Heat (kW)
Whispergen	Stirling Engine	96 %	1	7.5-14
SenerTech Dach	IC Engine	88 %	5.5	12.5
Hilton	PEM fuel cell	/	0.75	/

5.2 1 kW_e Whispergen Stirling Engine Based mCHP

5.2.1 Experimental Facility

For evaluating the actual performance of the Whispergen mCHP, a domestic-scale unit previously installed as a test rig. Both the space heating and domestic hot water loads were

used as in real residential conditions. Figure 5.1 illustrates a schematic of the Whispergen Stirling engine based test rig.

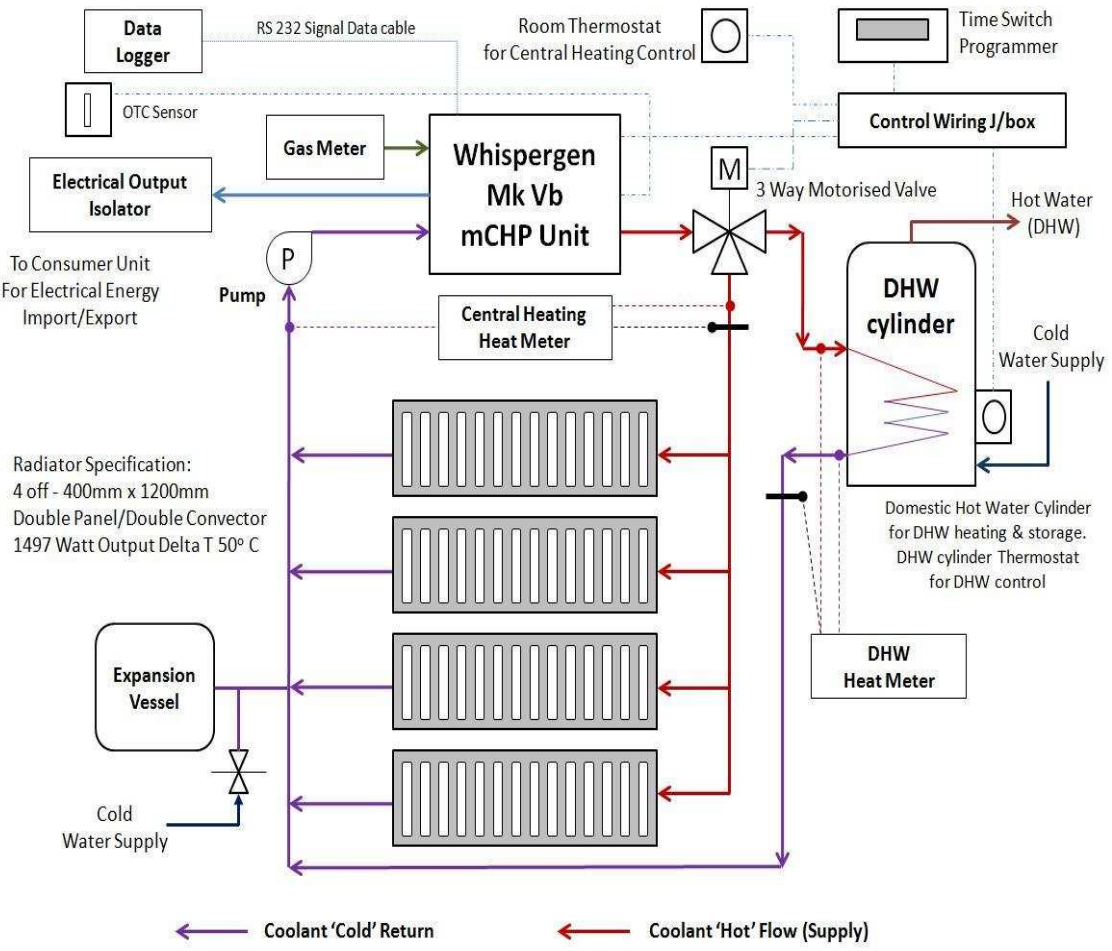

Figure 5.1 Schematic layout of the Whispergen 1 kWe Stirling engine-based mCHP test facility

The Whispergen unit includes the main burner of 6 kW_{th} thermal capacity which is also used for the cogeneration and the auxiliary burner of 5 kW_{th} thermal capacity for use as a top-up heating system. The operation of the auxiliary burner is independent and controlled by a Honeywell Outside Temperature Compensator (OTC) sensor. Temperature readings by both the room sensor and integrated thermostat in the domestic hot water tank were used for controlling the direction of the hot water via a three-way valve. In addition, the operation for

either space heating, hot water production or both simultaneously could be selected using a programmable controller.

The test rig consists of

- A 150 L water tank for domestic hot water production with integrated thermostat;
- A controller for independent signalling of space heating or hot water demand;
- A room thermostat;
- A three-way valve for controlling the direction of the hot water to either space heating radiators or the domestic hot water service (DHWS) storage cylinder;
- Two Gyr & Landis heat meters, installed in both water circuits;
- Data logging via a dedicated RS232- CHP- PC connection using for monitor main parameters.

Figure 5.2 and Figure 5.3 (a-e) shows components of the experimental facility

Figure 5.2 The Whispergen 1 kWe Stirling based mCHP installed in the Energy Lab

a) 150 L insulated hot water storage tank

b) Pressurisation vessel to maintain constant pressure in the hydronic circuit

c) White arrow points to the 3 way valve. The operation of the valve is both temperature and manually controlled

d) Timer/controller signals heat demand

e) Heat meters measure and record the thermal energy supplied for both space heating and water tank.

Figure 5.3 (a-e) Components of the experimental set-up

5.2.2 Experimental procedure

The experimental investigation of the Whispergen mCHP unit considered dynamic (transient) and steady-state operation as well as measurements leading to operational power-generating and overall efficiencies. Two operating strategies were evaluated:

1. The generation of space heating and DHW occurring simultaneously
2. The DHW heat generation was separated from space heating generation and the mCHP was programmed to start prior to space heat demand event and direct all the heat first to the hot water tank and when it is charged, to the space heating equipment.

This method could offer more information in respect to the interaction of the mCHP with the respective equipment (radiators and water tank). The heat meters integrated in two circuits provided both circuit temperature information and total energy generated. The latter can be used for efficiency calculations under steady state operation but was found to be insufficiently responsive for a dynamic performance logging. For this, monitored data from the mCHP engine was used for evaluation of the module operating characteristics in dynamic conditions. The fuel consumption rate measurement (from which the heat input to the unit throughout the operation can be calculated) was carried out using a gas meter. Finally, once heat and power generation values were measured, they were plotted against time using a 1-minute time interval.

The generated thermal energy (in kWh_{th}) was calculated as

$$Q_{gen} = \frac{\sum_{i=0}^{n} Cp_{water}(T_{flow} - T_{return})(\dot{m}_{CH} + \dot{m}_{DHW})}{60} \quad (5.1)$$

where n is the cycle duration in minutes; T_{flow} is flow water temperature in the circuit (°C);

T_{return} is return water temperature in the circuit (°C); $\dot{m}_{CH}$ is the mass flow rate in the space heating circuit (kg/s); $\dot{m}_{DHW}$ is mass flow rate in the domestic hot water circuit (kg/s).

Partial and overall efficiencies are calculated as

$$\eta_{thermal} = \frac{Q_{gen}}{Q_{fuel}} \tag{5.2}$$

$$\eta_{electrical} = \frac{E_{gen}}{Q_{fuel}} \tag{5.3}$$

$$\eta_{overall} = \eta_{thermal} + \eta_{electrical} \tag{5.4}$$

where Q_{gen} is the heat generated from the mCHP; E_{gen} is the electricity generation; Q_{fuel} is the energy content of the fuel.

5.2.3 Start-up and Run-down phase characteristics

Figure 5.4 shows the start-up transition of the Stirling engine-based mCHP test unit. The Whispergen under test rig conditions displayed a quick start up.

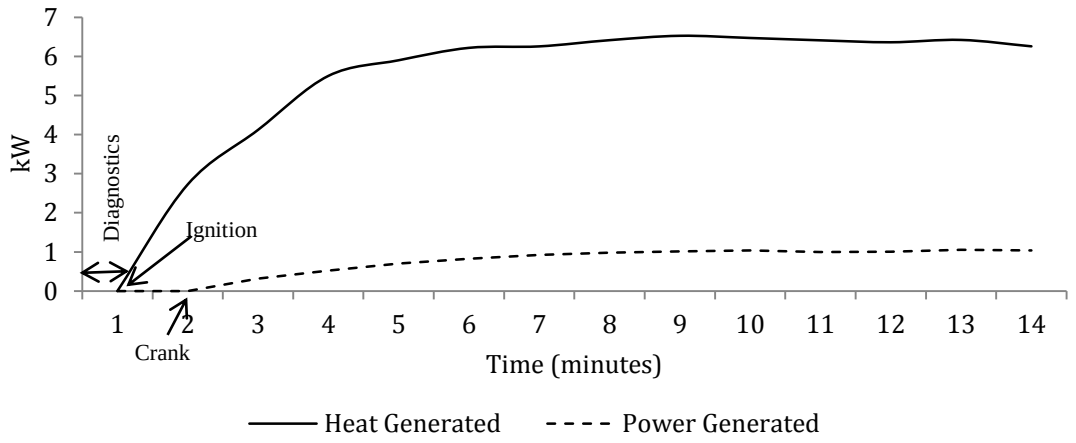

Figure 5.4 The 1 kW_e Whispergen Stirling engine mCHP start-up characteristic

There is an initial 1 minute of diagnostic delay and, if this is discounted, the unit would reach the nominal thermal capacity of the main burner within 7-8 minutes. A delay in power

generation was observed, which is a characteristic of the Stirling engine operation. A total of 10 minutes were required in order to fully reach rated capacities.

Figure 5.5 shows the run-down characteristic. For a period of approximately 6 minutes a significant amount of the thermal energy continued to be delivered to the heating circuit after the burner had been switched off with a beneficial impact on the thermal efficiency of the cycle. This is attributed to the heat transferred from the engine's walls to the hydronic loop. This characteristic operation of the Stirling engines is necessary in order to fully cool down the engine and prevent any thermal damage to engine components such as seals etc. It reflects the high thermal capacity of the engine walls. In addition, the power generation seizes within 4 minute period.

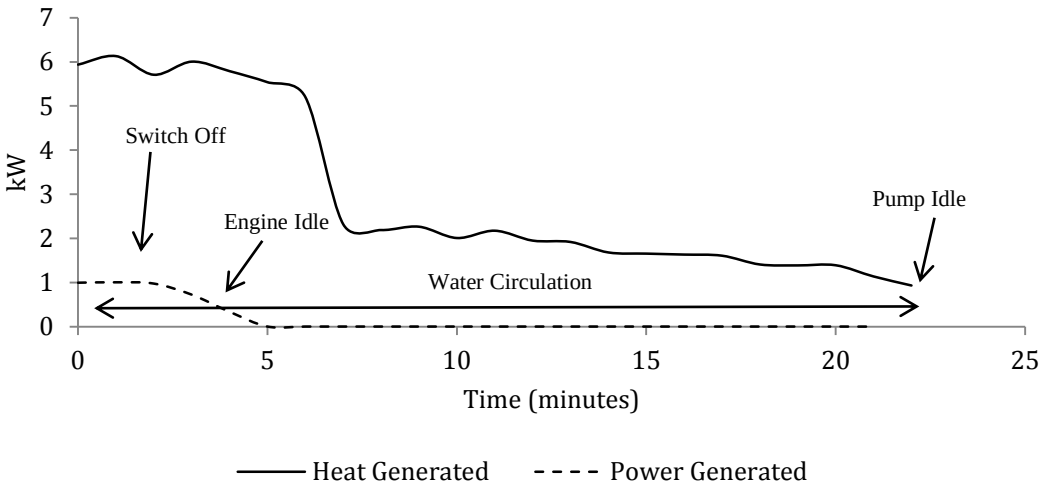

Figure 5.5 The 1 kW_e Whispergen Stirling engine mCHP run down characteristic

5.2.4 Steady state operation

Simultaneous DHW and SH operation mode

Using the installed controller, typical residential operational conditions were simulated on the test rig. The unit was tested under two different operating strategies (as described in Section (5.2.2)) in order to obtain information regarding interaction between the mCHP unit and hot

water tank during its charging and between the mCHP unit and space heating system. In addition, tests were carried out during a cold winter day and a mild autumn/spring day. During simultaneous heat generation mode (both DHW and CH), approximately 1.5-hr and 3.5-hr (5-hr total) experimental runs were carried out for satisfying the morning and evening heat and hot water demands, respectively. Hot water consumption events were simulated by draining the hot water storage tank, however, the volume of water drained was not measured. The mCHP was expected to operate at the full capacity under this particular operating mode in both laboratory and actual domestic conditions. Figure 5.6 shows the heat generated from the mCHP on a winter day.

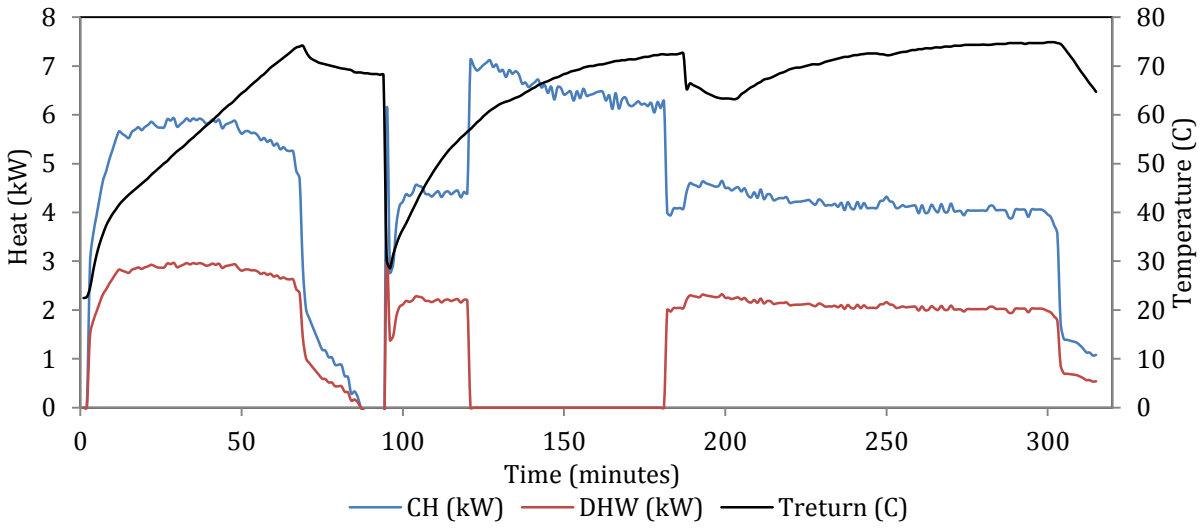

Figure 5.6 Heat generation during the evening of a winter weekday during simultaneous heat generation mode

As it can be noticed in Figure 5.6 the return water temperature fluctuations are due to hot water and heating demand events and resulted in increasing the heat load. The additional heat load was covered by the auxiliary burner which was operating at the beginning of the day for approximately one hour. Figure 5.7 shows the operation of the Stirling based mCHP during milder climatic conditions.

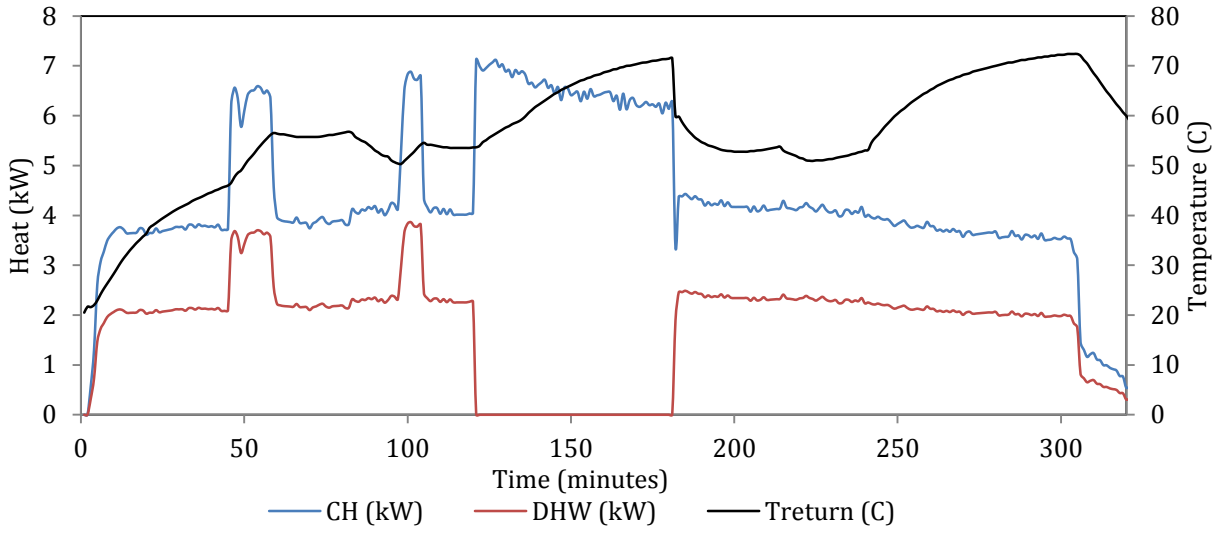

Figure 5.7 Heat generation during the evening of an autumn/spring weekday for simultaneous heat generation mode

In Figure 5.7 it can be observed that the auxiliary burner was not on at the beginning of day as the water tank temperature was higher than in a winter day. However, the two heat generation peaks at approximately 50 and 100 minutes, totalling 11 kW_{th} and 12 kW_{th}, indicate that the auxiliary burner was on. The higher temperature differential during the start-up period during autumn/spring weekdays resulted in the increased thermal efficiency of 70 %. The operation of the auxiliary burner was related to the return temperature. Instantaneous hot water demand resulted in the increased heat load due to a sharp drop in the water tank temperature. When the hot water consumption events lasted longer and therefore the temperature inside the tank was continuously dropping, the operation of auxiliary burner was triggered. However, this was only evident during the first experimental runs in the winter season and when the water circuit had been filled with fresh cold water for the first time. In most tests the auxiliary burner had very little contribution to the heat output of the mCHP unit. The instantaneous rise in the hot water demand was balanced by the thermal inertia of hot water inside the tank thus reducing the impact of fresh cold water flowing into the tank

during the later stages of operation. Finally, the effect of the increasing return temperature on the overall heat generation can be seen in both figures during the last hours of operation. As the return temperature increases, the generated heat decreases, indicating a less effective heat transfer in the engine cooling water jacket. These confirms the advantages of operating the mCHP in a way that the return temperature remains low at the early stages of operation which eliminates the effect of the reduced heat transfer once the unit reaches the steady state operation. The amount of heat generation during the winter and spring-autumn days was nearly the same for the simultaneous central heating and DHW heat generation mode.

Split DHW and SH generation operation mode

Under this operating strategy, extended operation of the mCHP was achieved which was presumed to be beneficial for the potential economic performance due to the increased power generation. The domestic hot water demand was signalled one hour prior to the 6 hours of space heating demand and Figure 5.8 shows the heat generation by the mCHP during a winter weekday.

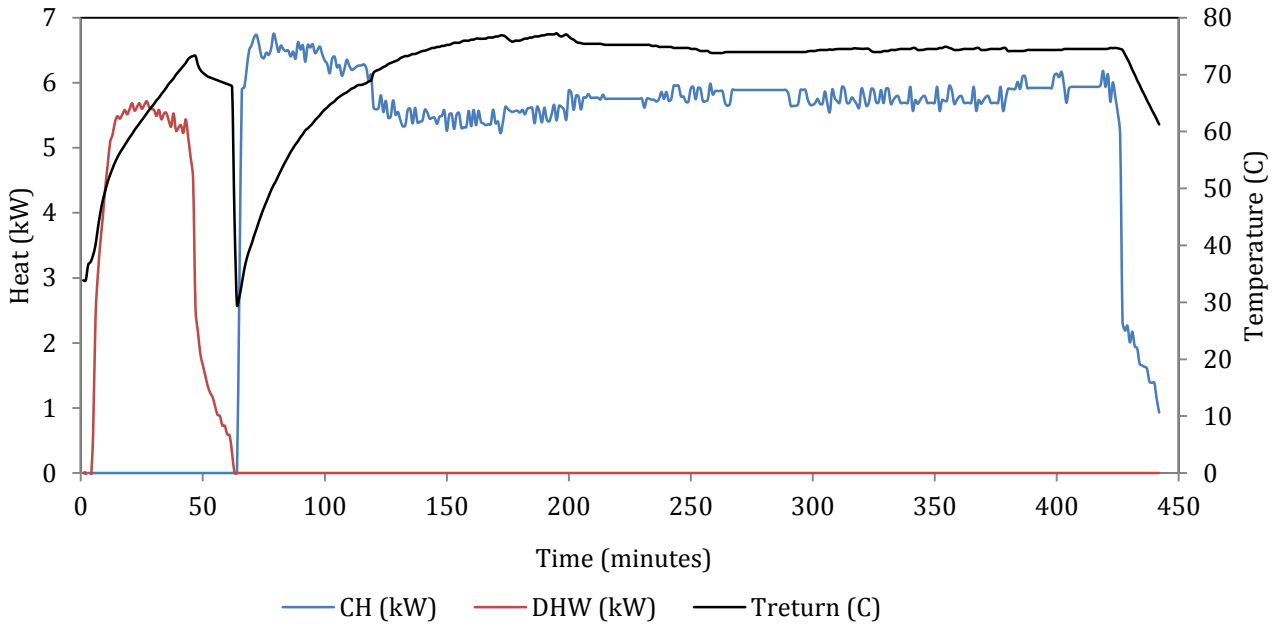

Figure 5.8 Heat generation during a winter weekday in split heat generation mode

In Figure 5.8 it can be seen that in the early stage of operation, when he thermal energy was directed into the water tank only, a slight deviation was noted from the rated thermal output of 6 kW_{th} (approximately 5.7 kW_{th} was generated during this phase). It was assumed that this was due to the limited heat transfer through the coil inside the water tank.

Once the switching to the space heating was signalled, a significant drop in the return temperature occurred. The thermal energy was directed to the central heating circuit and consequently an increased heat transfer rate in the early stages of the space heating operation can been noticed. As the return temperature reached the design level, the thermal output of the Whispergen unit was stabilized at around 6 kW_{th}.

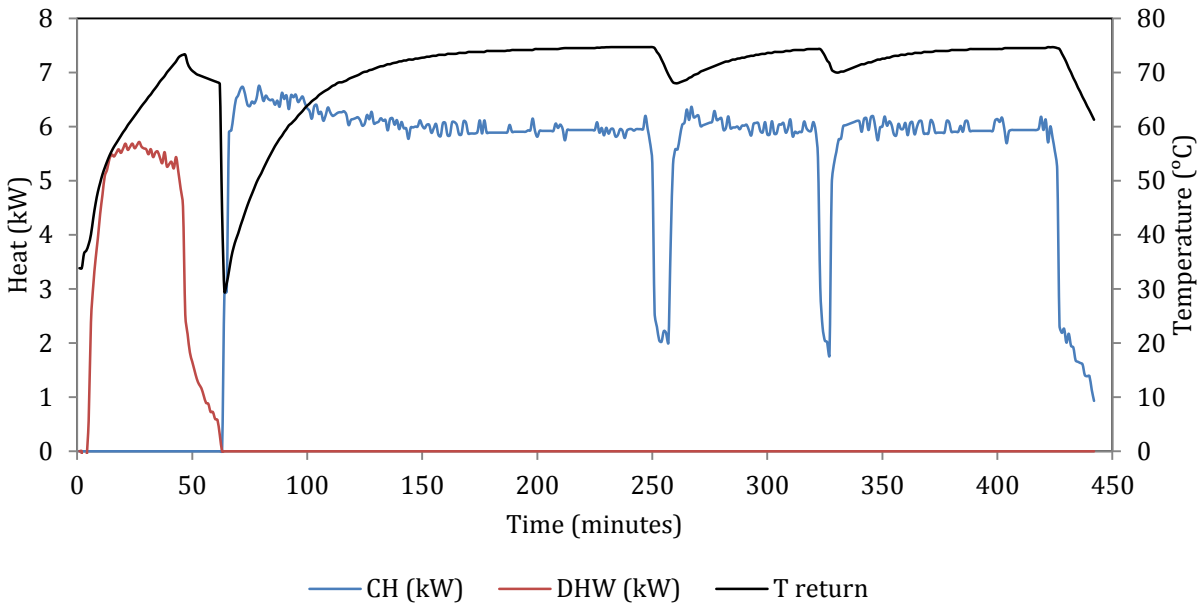

Figure 5.9 Heat generation during a spring–autumn weekdays for a split heat generation mode

Interestingly, in almost all tests the auxiliary burner did not fire up for extended time. Its operation was limited to a few minutes and occurred only on a few occasions as noted in Figure 5.6 and 5.7. This suggests a stiffness in the control logic of the auxiliary burner, limiting the fire events in order to keep low fuel consumption as the auxiliary heat is not associated with additional power generation. Figure 5.9 shows the heat generation by the

mCHP during a mild weekdays. In Figure 5.9 it can be observed that the same trends exist during the operation of the unit during autumn/spring days as in Figure 5.8. Two additional cycling operations were noticed as the outdoor temperature was relatively higher during the tests. Although this mode of operation resulted in higher power generation and very limited auxiliary burner operation, cycling events were present. In actual residential conditions the cycling frequency is expected to be higher. The size and insulation of the laboratory building imposes a considerable heat load during even the autumn/spring period which limits the number of cycling events.

5.2.5 Efficiencies

The methodology used throughout the experimental work was aimed at attaining the most realistic efficiency values. Although the test-rig was designed for simulating domestic conditions the space heating system of the local laboratory environment is quite different to a residential house. The laboratory where the mCHP unit was installed has a large open space room with footprint area of approximately 30x10 m and height of approximately 5 m. This space will therefore have a much higher thermal capacity and higher thermal losses due to a low insulation level when compared with a modern house. Under these conditions, the Whispergen was considered as undersized equipment and consequently was operating constantly at the maximum thermal capacity. This could lead to over-prediction in efficiency calculations, since the number of cycling events (which significantly decrease the overall efficiency) might be expected to be higher in a residential house. The artificial way of triggering cycling operation using drainage of the water tank provided a realistic 'typical domestic conditions' performance.

Figure 5.10 shows the partial efficiency estimations under steady state and transient operation.

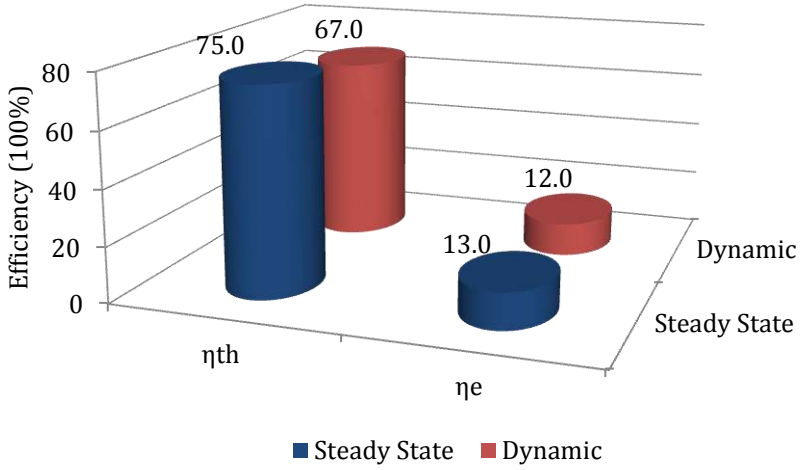

Figure 5.10 Partial efficiencies estimation in dynamic and steady state operation modes for the Whispergen Stirling engine mCHP unit

It can be seen in Figure 5.10 that the average thermal efficiency of 67 % and 12 % for the electrical efficiency were achieved in the dynamic mode of operation. The efficiencies are decreased when the whole cycle has been taken into consideration due to a poorer performance in transient phases. A thermal efficiency up to 75 % with electrical efficiency of 13 % was recorded for steady state operation (without taking into account transient phases). Additional reduction in efficiencies will arise if cycling operation is taken into consideration.

5.2.6 Validation of theoretical simulation results

Obtained experimental results were used to compare these against the theoretical predictions under transient and steady-state operational conditions in order to ensure viability of the simulation process. The Stirling engine features were taken into account in theoretical modelling (the heat generation is dependent on the engine temperature). This method has the advantage of including the dynamic characteristics of real engines into the steady-state equation based solution and it was suggested as the adequate method for application in EnergyPlus for simulating the Stirling engine based mCHP. Such approach resulted in a separation of the mCHP operation into two main regions: a) a warm-up operation, occurring

in the very early stage of operation; b) the normal operation which occurred once the engine's temperature has reached the nominal value. The power generation and therefore the heat generation of the mCHP unit was described with a coefficient (warm-up power coefficient) determined from the experimental results. The power generation as a function including this empirical coefficient is:

$$P_{net,warm-up} = P_{\max} k_p \frac{T_{\text{eng}} - T_{\text{room}}}{T_{\text{eng,nom}} - T_{\text{room}}} \tag{5.5}$$

where $P_{net,warm-up}$ is the power produced during start-up period; $P_{\max}$ is the nominal (maximum) power produced; k_p is the warm-up power coefficient; T_{eng} is the engine temperature; $T_{\text{eng,nom}}$ is the engine temperature during steady state (nominal) operation and T_{room} is the room temperature.

Finally, the distinct regions during transient operation are illustrated in Figure 5.11.

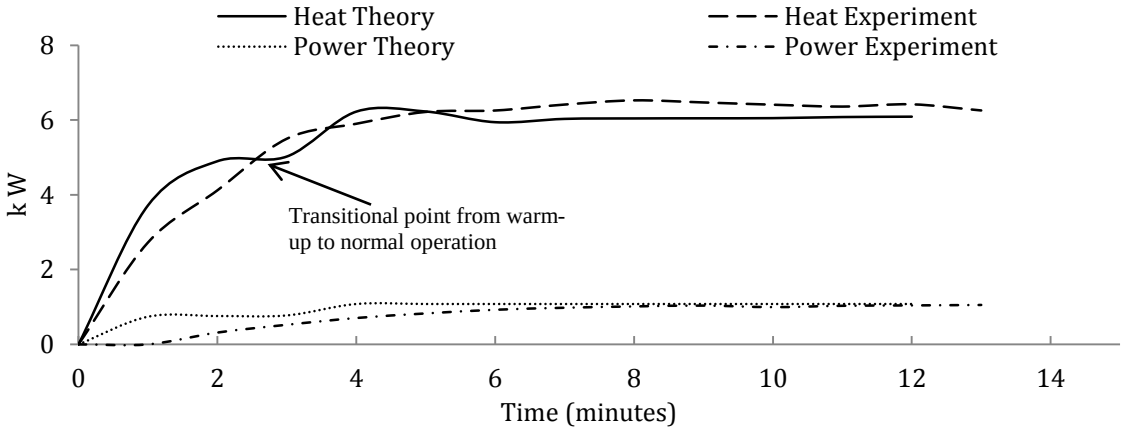

Figure 5.11 Experimental and simulation results for heat and power generation during start-up for the Whispergen Stirling engine mCHP.

Figure 5.11 shows the experimental results against the model prediction for the first 14 minutes of operation (until the engine reaches the steady-state operation). Figure 5.12 shows the validation results with respect to a full operating cycle.

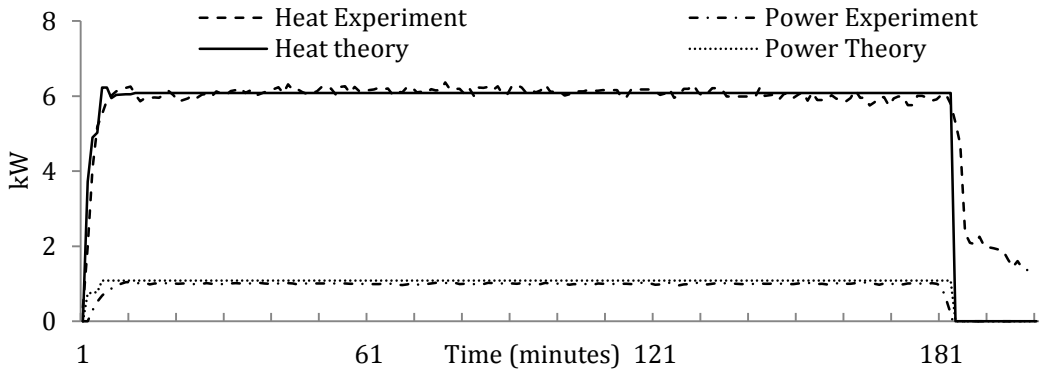

Figure 5.12 Experimental and simulation results for heat and power generation by the Whispergen Stirling engine mCHP unit

As it can be seen in Figure 5.12 there is no significant deviation between the experimental results and model predictions in respect of the heat output rate during the steady state mCHP operation. Constant heat dissipation was predicted by the theory using steady state equations. Fluctuations in experimental heating output were attributed to the change in the circuits water temperature differential. It also can be seen in the experimental curve that the heat is still recovered as result of the water pump running after the mCHP unit was switched-off. This feature is not reflected in the theoretical modelling was as a result of the model's stiffness.

Furthermore, it can be seen in Figure 5.11 that there is a small deviation between theoretical and experimental results during the transient heat generation. The model displays a marginally faster response, however, the error is within acceptable limits. The areas under the theoretical and the experimental lines are approximately equal with a small net error. In respect to power generation a step increase in the electrical power generation was applied in the simulation process. The theoretical results deviate from the gradually increasing experimental electricity generation. It addition, the time delay in the electricity production is excluded in theoretical simulations due to lack of software capabilities. Nevertheless, the errors of 3.7 % and 3.3 % are for a 3 hour and 5 hour runs, respectively. These errors are considered to be within acceptable limits, therefore simulations were thought to be in good agreement with experimental data.

The operation of the Stirling engine based mCHP was modelled using a power time delay approach (normally used in ICE mCHPs) as presented in Appendix A. The simulated heat generation in this modelling approach is significantly faster compared to the experimental results therefore the above approach was no longer deployed in further simulations in this work.

5.3 Baxi SenerTech 5.5 kW_e ICE Based mCHP

5.3.1 Experimental setup

The performance of the Baxi SenerTech Dachs Internal Combustion engine based mCHP was evaluated under laboratory conditions. The unit was installed in the Low Carbon Systems laboratory of the Faculty of Engineering and Environment and used for providing space heating and electricity to part of the campus estate. It has a nominal output of 5.5 kW_e and 12.5 kW_{th}, respectively. The engine is single cylinder natural gas-fired four-stroke IC engine with displacement of 578 cm^3. The unit has 72 cm x 107 cm x 100 cm dimensions (width x length x height) and weights about 530 kg. It has a cylinder bore and piston stroke of 90 and 91 mm, respectively. The heat utilisation is carried out using a combined cooling system and a heat exchanger recovering thermal energy of the exhaust gases at the temperature of 150 °C. The manufacturer recommends the service interval of 3500 hours of operation for engines that use natural gas as fuel with the service life being 80000 hours. The engines with natural gas as fuel models do not require a three-way catalyst due to deployment of the lean combustion process. The rated operating speed is 2400 rpm and the shaft is linked to an asynchronous generator. Net efficiency, in accordance with the manufacturer specification, is 88 %. The operation of the unit was scheduled by the University campus services with some additional local control of the unit on a day-to-day basis.

The experimental setup additionally consist of

- An Apator CQM-III-K compact type heat meter;
- A Grant Squirrel SQ2020 data acquisition unit;
- A gas meter;

Figure 5.13 shows the schematic diagram of the experimental facility.

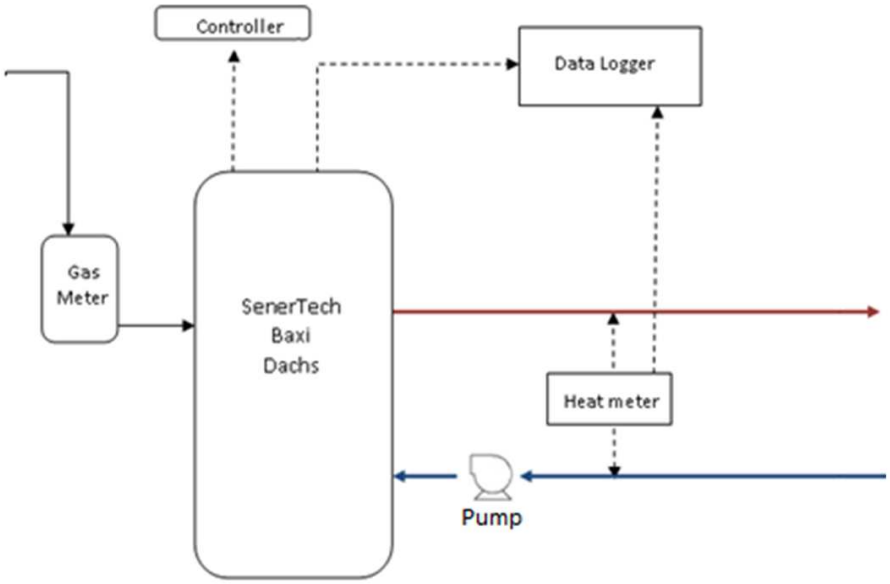

Figure 5.13 Schematic diagram of the test rig of the Baxi SenerTech Dach mCHP unit

Figure 5.14 and Figure 5.15 (a-d) show the components of the experimental facility

Figure 5.14 The Baxi SenerTech Dach mCHP unit installed in the Energy Laboratory

a) The digital display of the unit to monitor key parameters of the mCHP operation

b) The Apator heat meter installed in the hydronic circuit

c) Gas meter

d) Data acquisition connected to a laptop

Figure 5.15 (a-d) Components of the ICE mCHP experimental facility

5.3.2 Experimental procedure

The test rig is capable of providing results for the steady state operation and the transient phases of start-up and shut down. The integration of the heat meter into the hydronic circuit enables recording data on the thermal output and the gas meter provides information on the fuel consumption rate. This data is used for efficiency calculations. The power generated can be directly read off the mCHP control panel.

5.3.3 Start-up and run-down characteristics

Heat and power generated were plotted every 1 minute intervals during start-up transient operation from 15 November to 6 December 2013. Results obtained for several cycles are

presented in Figure 5.16 and Figure 5.17. The heat and power generation by the Seneretch Dach mCHP during the start-up period are shown below.

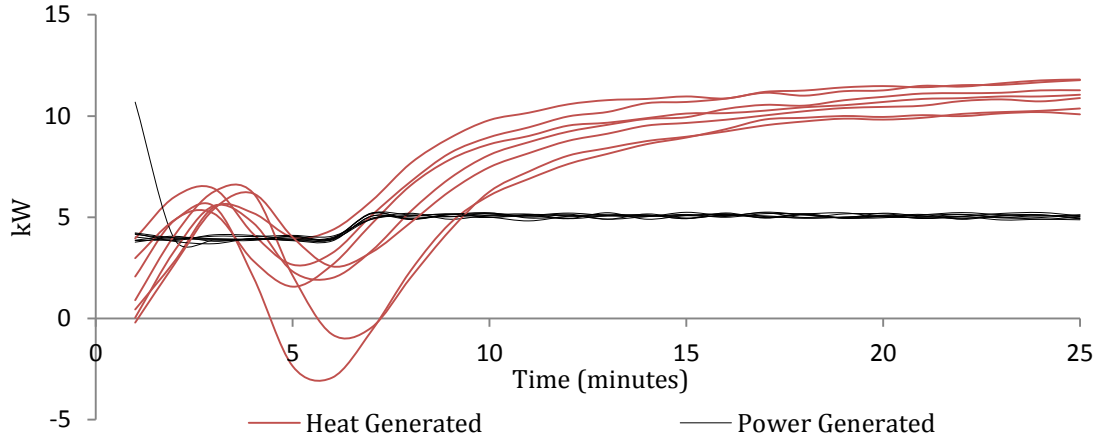

Figure 5.16 Start-up transient regimes of the SenerTechDachs 5.5 kW_e mCHP

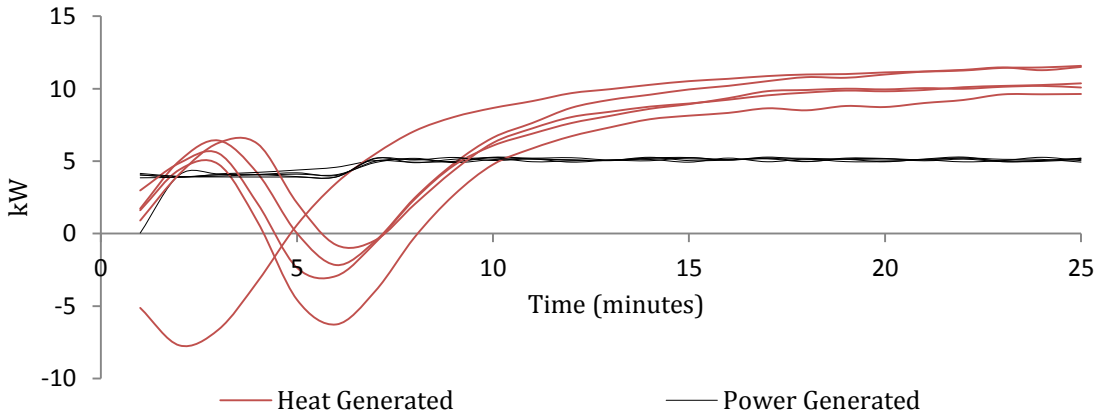

Figure 5.17 Start-up transient regimes of Baxi SenerTech Dachs 5.5 kWe mCHP

It can be seen in Figure 5.16 and Figure 5.17 that heat generation during the transient start-up regime is very poor. Although after reaching the steady state the maximum thermal output stabilises, in the start-up period some irregular behaviour can be observed. As far as a power generation is concerned, no delays in reaching the nominal capacity were noticed – the mCHP unit reached the rated capacity within the first minutes of operation.

The above mentioned significant fluctuations and sub-zero values in the thermal output of the unit in the early period of operation were noticed in all start-up sequences. This was

attributed to the fact that the unit was used as an additional heat source for the existing central space heating system of the building. This central heating circuit is already live when the mCHP is turned on. When the mCHP first starts, the heating pump draws hot water into the engine from the operating central heating system. In the initial temperature of the water entering the engine is higher than that of water leaving the engine. This irregular transient behaviour is observed in the first 6-7 minutes of operation. Measure data for such the operation produced a range of the heat generation curves. It can be seen that there is a time difference in the start-up sections (along X-axis) of different tests. The start-up operation selected for further analysis was considered to be a representative start-up sequence in which the irregular transient processes were discarded. Additionally, this start-up operation was selected as representative one in such a way that parameters of other cycles deviated by ± 5 % when compared to the representative curve. As the mCHP warms up, it starts to generate heat for the central heating system. Therefore data in the first 6 minutes of the mCHP's operation was discarded, see Figure 5.18.

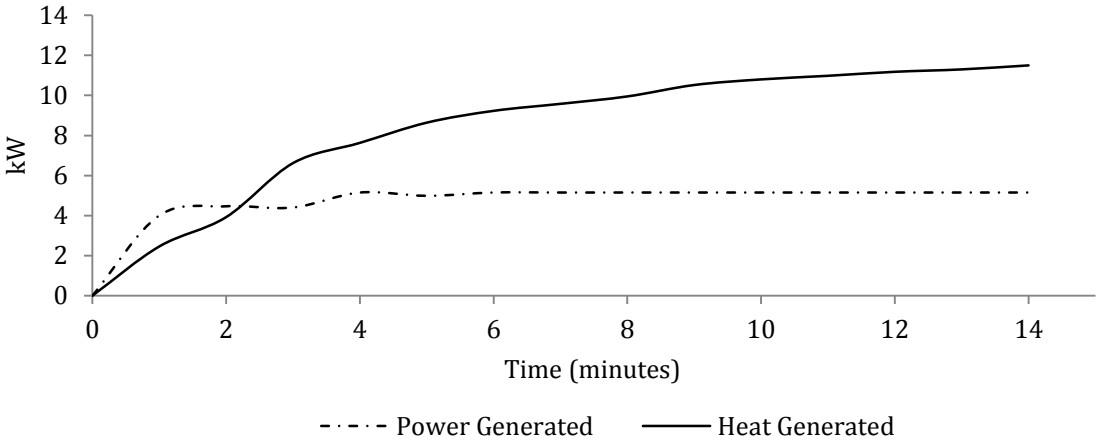

Figure 5.18 Proposed start-up transient regime of Baxi SenerTech Dach mCHP

Figure 5.19 shows the run-down regime characteristics of the SenerTech Dach mCHP unit. After the "heat demand off" signal, thermal and electrical generations reduced to zero within

a 1 minute period. Since it was not necessary to cool down the IC engine, no circulation of the water was carried out by the mCHPs water pump after the unit was turned off. This is different from the run down transient operation of the Stirling based unit.

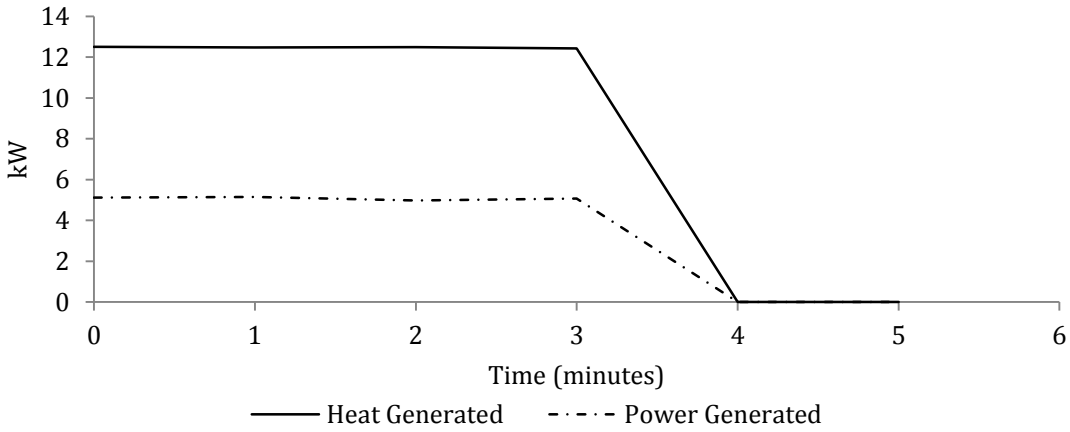

Figure 5.19 Run down regime characteristics of the SenerTech mCHP unit

5.3.4 Steady state performance

Information from a number of runs between the 15th of November and 6th of December 2013 were recorded with a 1-minute sampling interval. Figure 5.20 shows a typical cycle from the recorded runs database.

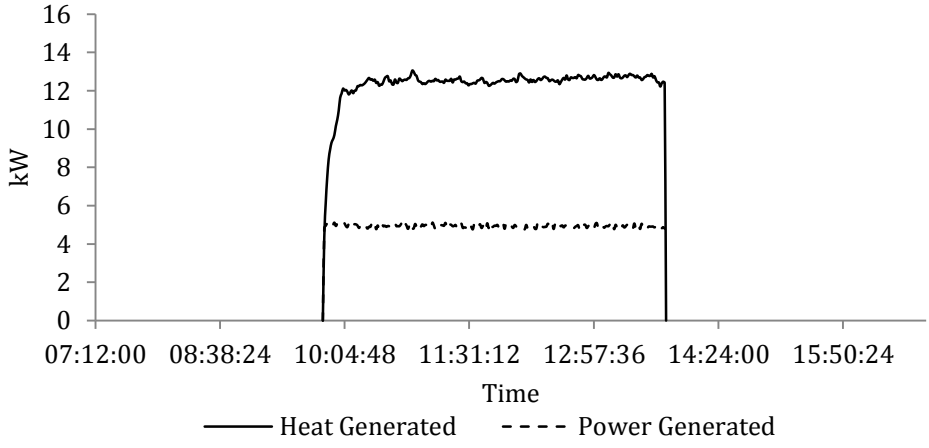

Figure 5.20 Typical cycle of operation of Baxi SenerTech Dach mCHP

In Figure 5.20 it can be seen that the run took place between 10.00 am and 13.50 pm. Due to the increased heating demand in the building switching off during the above interval did not

take place. Once the steady state regime of operation was reached the generated energy level was stable and close to the rated value with very small fluctuation throughout the run time. Output values between 12 kW_{th} and 15.1 kW_{th} and 5 kW_e and 5.3 kW_e were recorded.

5.3.5 Efficiency calculations

Steady state and dynamic regime efficiency calculations were carried out using information obtained during the experimental runs. For the steady state an operating interval of 1 hour was considered, whereas for calculation of dynamic regime partial efficiencies the whole run cycle was analysed. Figure 5.21 shows the thermal and electrical efficiency value estimations.

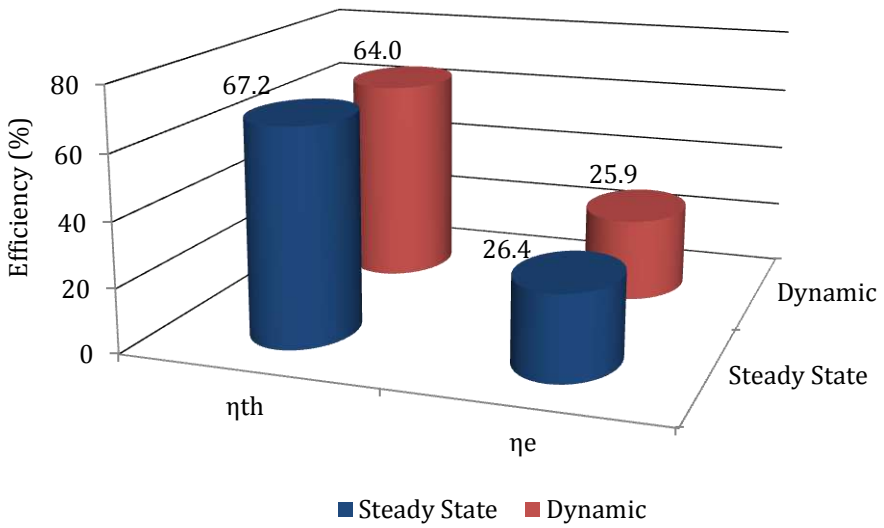

Figure 5.21 Partial efficiency calculations during the dynamic and steady-state regimes of operation for the ICE mCHP unit

It can be seen in Figure 5.21 that during the steady state operating conditions partial efficiencies were estimated at 67.2 % and 26.4 % for thermal and electrical outputs, respectively. When the transitional regimes were taken into consideration, the value of efficiencies decreased – 64 % and 25.9 % for the thermal and electric outputs, respectively.

5.3.6 Validation of theoretical simulation results

The obtained experimental results were compared with that of theoretical simulations. The validation process was focused on the cycle-basis operation and particularly on the start-up phase. Figure 5.22 shows the experimental results compared with the model predictions.

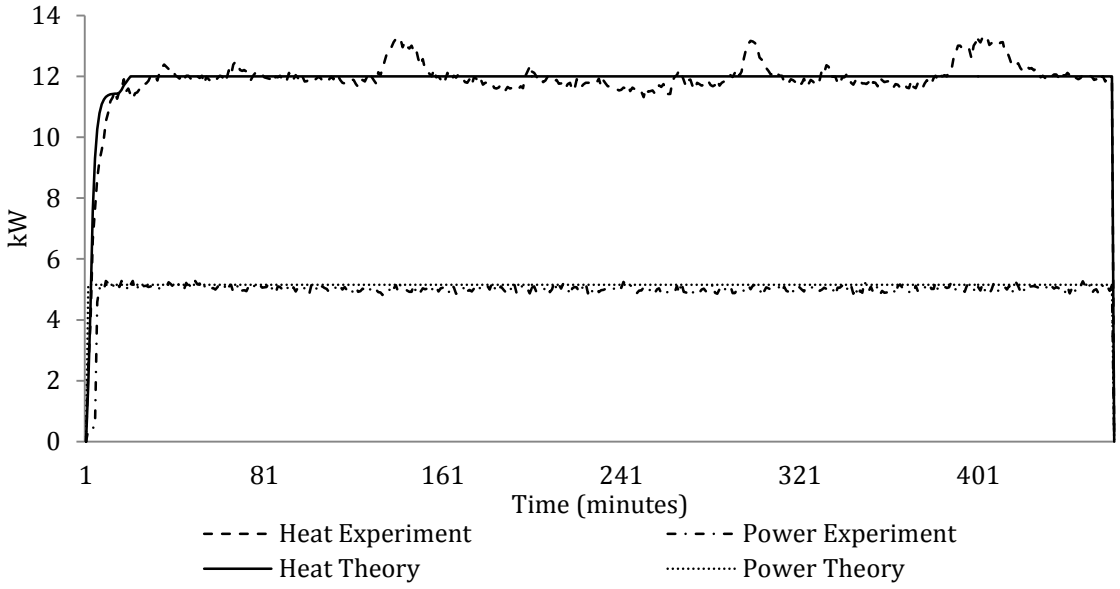

Figure 5.22 Experimental versus theoretical results in a complete operating cycle for the Baxi SenerTech Dach mCHP

It can be noticed in Figure 5.22 that the power generation prediction by the model is in a good agreement with experimental results in terms of the maximum electric output. The simulated heat output of the unit was also found to be close to the experimental data. Small deviations were found in 3 particular regions, in which the heat output from the test-rig was higher for a short period of time. These results can be attributed to the rise in the temperature difference in the hydronic loop due to fluctuations in the water flow in the main heating circuit. The simulated operation of the unit was based on solution of the steady state energy equations therefore a constant output was predicted for both heat and power generation.

Figure 5.23 shows the obtained experimental and simulation results for the start-up transient regime during the first 18 minutes of the unit's operation.

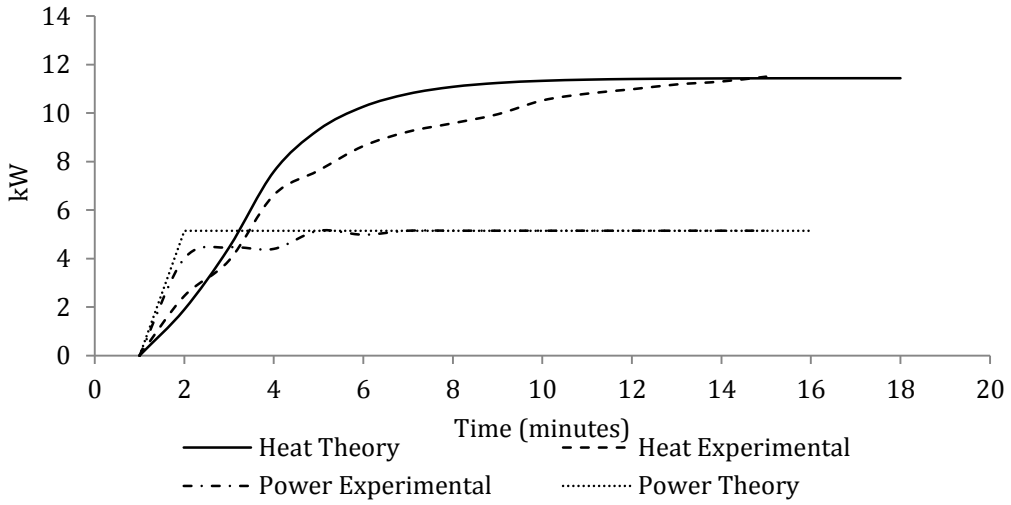

Figure 5.23 Experimental results and model predictions during the start-up for the ICE mCHP unit

It can be seen in Figure 5.23 that model predictions are displaying a marginally faster response with respect to the actual heat generated. This process occurs for approximately 8 minutes before the unit reaches the steady state operation. The same trend was observed for the power generated however in a smaller scale. This inaccuracy in modelling produces an error of approximately 2.77 % and 1.2 % for a 3 hour and 6 hour runs, respectively. It can be concluded that these errors are within the acceptable limits.

5.4 PA. Hilton 0.75 kW_e PEM fuel cell

5.4.1 Experimental Apparatus

Experimental data were obtained using a 0.75 kW_e hydrogen/air PA HILTON Ltd proton exchange membrane (PEM) fuel cell stack. The module consists of 18 Ballard cells connected in series each with an effective area of 50 cm^2. The system had integrated auxiliary subsystems including a bank of resistors for simulating a change of load, a hydrogen supply system with an additional gas regulator, oxidant air circulation system, air cooling supply and an electronic control and safety system with a sensor which can interrupt the operation in the event of leakage detection. Dry hydrogen was supplied from a pressurised cylinder and the

oxidant air was circulated using an electrical fan. The heat produced by the stack was dissipated to the surroundings using air fans on the top of the unit. An integrated data acquisition system was used to monitor and record parameters of the operation. Figure 5.24 and Figure 5.25 show the schematic diagram of the Hilton R510 PEM fuel cell and the experimental set-up, respectively.

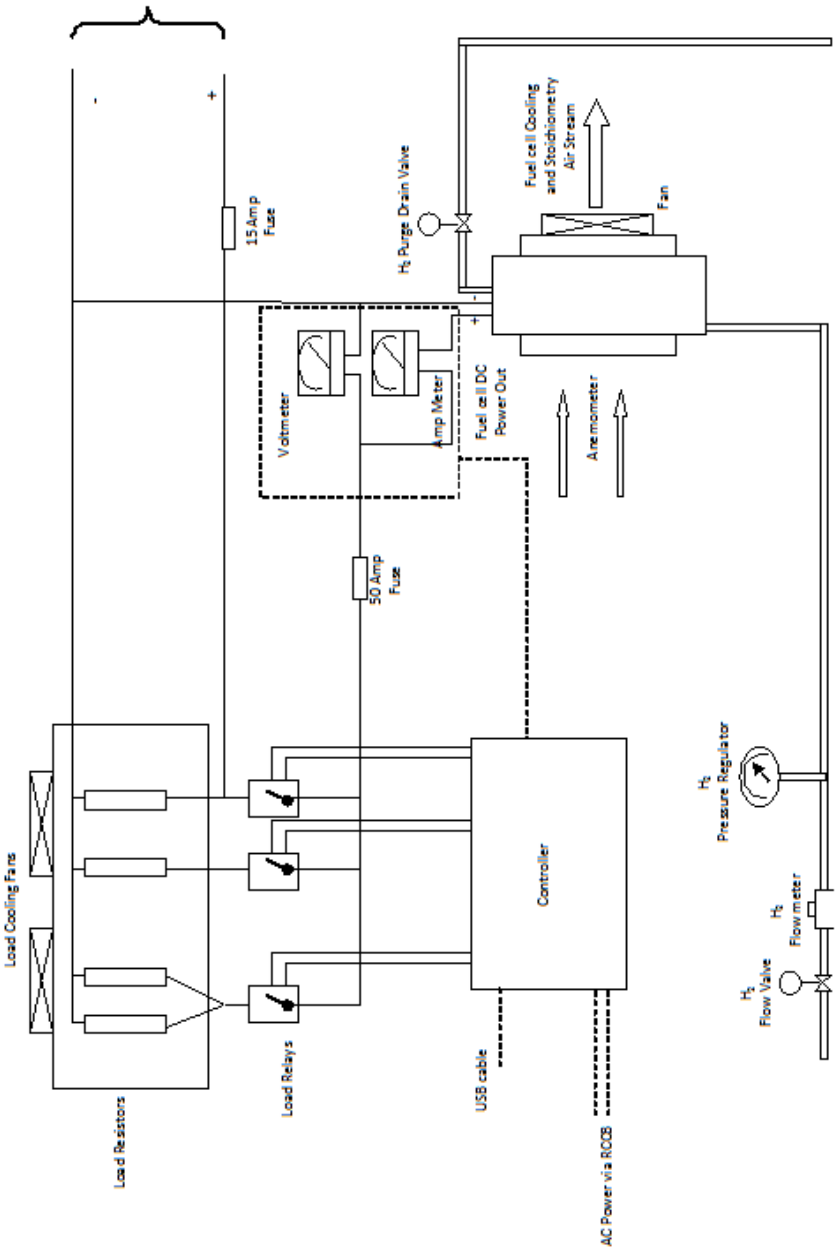

Figure 5.24 Schematic diagram of the Hilton R510 PEM fuel cell

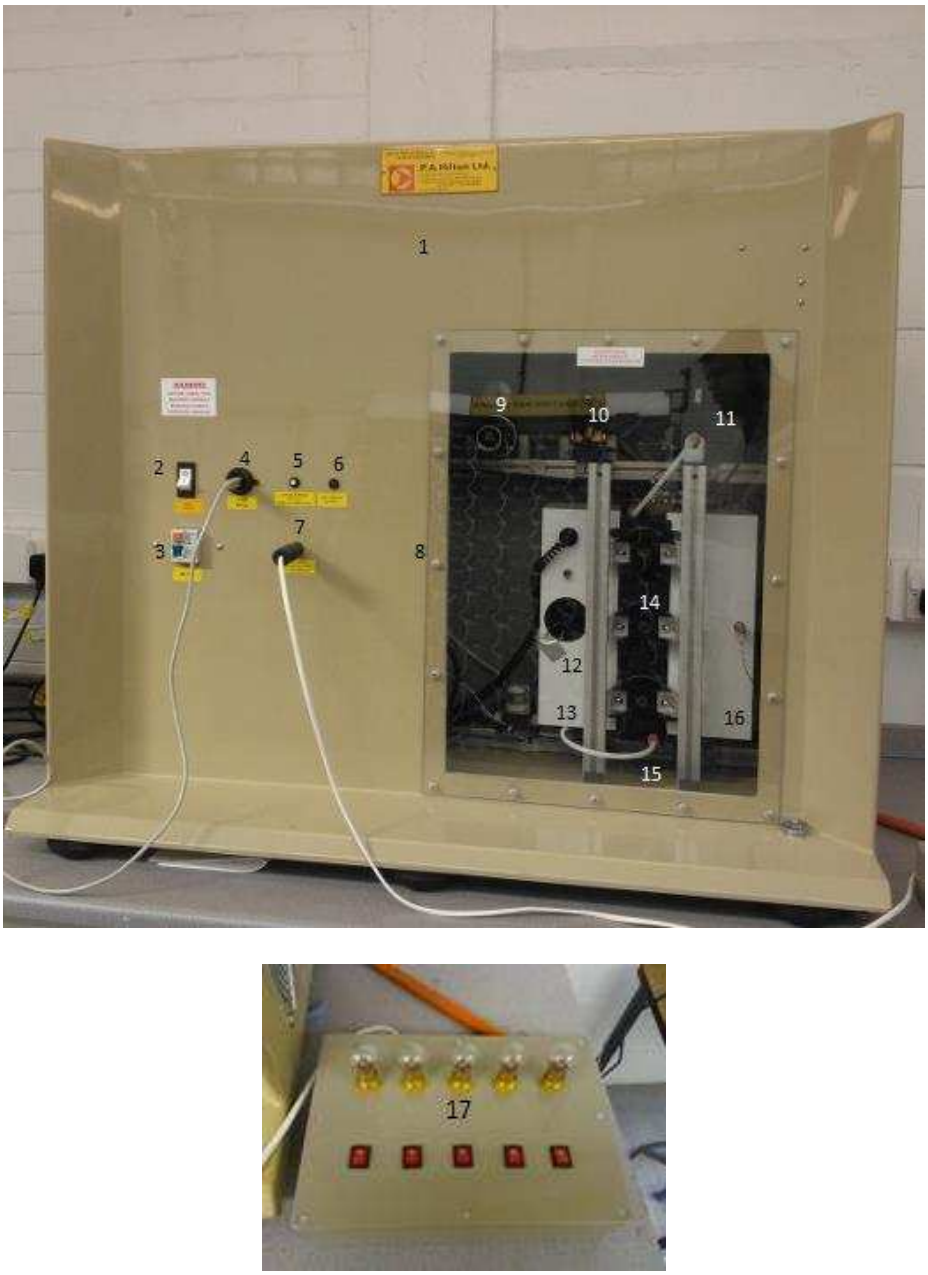

Figure 5.25 Front View of the P.A. Hilton RE510 PEM fuel cell test rig

1. Main panel
2. Moulded case circuit breaker
3. Residual current device (RCD)
4. External power outlet
5. 15 Amp thermal circuit breaker
6. Hydrogen integrity indicator LED
7. USB interface port
8. Perspex window
9. Mass flow meter
10. Pressure regulating gauge
11. Hydrogen control valve
12. Anemometer
13. Air inlet plenum chamber
14. Fuel cell stack
15. Vent valve
16. Air exit plenum
17. External load

Parameters such as flow rates, current, voltage, temperatures, etc. were recorded and software provided by the fuel cell module supplier was used for its experimental observation and real time control.

5.4.2 Experimental methodology

Similar to the previous experiments, the experimental procedure implemented for the fuel cell assembly included dynamic performance and steady state performance analysis with efficiency calculations in accordance with [60]. The electric load was simulated using the integrated resistors and data was logged every 5 s. All variables during the operation of the stack were recorded using the integrated sensors, including the hydrogen flow rate, stack current, voltage and temperature, air inlet and outlet temperatures, air flow rate, blower voltage etc. In calculations, all flow rates were converted into mol/s. The hydrogen flow was measured in standard litres per minute (SLM), and then was converted to a molar flow rate:

$$\dot{N}_{H2} = V\dot{o}_{H2}(SLM) * \frac{1.667 * 10^{-5} m^3 s^{-1}}{0.0224 m^3 mol^{-1}} \tag{5.6}$$

where 0.0224 m^3 is the volume occupied by 1 mol of any gas at STP and $1.667*10^{-5}$ is the conversion factor from SLM to m^3/s

The flow rate required for a given power output was determined as

$$\dot{N}_{H2} = \frac{n_{cells} * I}{2 * F} \tag{5.7}$$

where n_{cells} is the number of cells, I is the stack current, F is the Faraday constant.

The air molar volume at the air inlet temperature was determined as

$$Vo_N = \frac{T_{inlet}}{P_{inlet}} * \left(\frac{P_{inlet} * V}{T_{inlet}}\right)_{STP} \tag{5.8}$$

where T is the air inlet temperature and P is the air inlet pressure.

Thus the air molar flow rate can be calculated as

$$\dot{N}_{air} = \frac{v_{air}}{Vo_N} * \frac{\pi * D^2}{4} \tag{5.9}$$

where $v_{air\ is}$ the air flow rate (gauge reading) and D is the diameter of the effective area of the anemometer orifice.

The stoichiometric oxygen molar flow rate required for the reaction was derived from the hydrogen flow rate using the reaction equation.

$$H_{2(g)} + \frac{1}{2} O_{2(g)} \rightleftarrows H_2O_{(g/l)} + \Delta h_f \tag{5.10}$$

Here Δh_f is the change of enthalpy and positive indicates an exothermic reaction.

The heat generated by the stack was calculated as

$$Q_h = \dot{N}_{air} * Cp_{air} * (T_{out} - T_{in}) - \Delta\dot{N}_{O2} * Cp_{O2} * T_{out} + \Delta N_{H2O} * \left[(Cp_{H2O} * T_{out}) + (Q_{LHv})_{T_{stack}}\right] \tag{5.11}$$

where Cp_{air}, Cp_{O2} are the molar constant pressure heat capacity of air and oxygen, respectively; T_{stack} is the temperature of the fuel cell stack; T_{out} is the air stack outlet temperature and Q_{LHv} is the molar latent heat of water evaporation.

Finally efficiencies were calculated as

$$\eta_{Thermal} = \frac{Q_h}{E_{fuel}} \tag{5.12}$$

$$\eta_{Electrical} = \frac{E_{gen}}{E_{fuel}} \tag{5.13}$$

where E_{fuel} is the energy content of the fuel and E_{gen} is the electricity generated.

5.4.3 Start-up Characteristics

The start-up sequence was triggered by clicking the "start" button on the control panel window of the software. A few seconds later a 'low load' state was activated as the default value and a number of hydrogen purges occurred to remove any water accumulated within the electrolyte membrane and for providing sufficient hydrogen for initialising the chemical reaction. The oxidant/coolant fan was ramped up to supply enough air for heat management and for oxidation processes on the cathode side of the fuel cell. The start-up procedure was repeated several times for both cold start (when the fuel cell was switched off for more than 24 hr) and warm start conditions (the fuel cell was switched off for less than 2hr).

5.4.3.1 Cold start-up

Figure 5.26 to Figure 5.29 show the transient processes during the start-up stage. When the fuel cell is started a voltage of 5.48 V is supplied to the air fan, see Figure 5.26. When the integrated load is switched on the air fan voltage is increased to 12 V, for this to provide sufficient oxygen for maintaining the chemical reaction. The other air components (nitrogen, carbon dioxide, water vapour etc.) can temporarily block the reaction layer and decrease instantly the cell performance. This resulted in an introduction of a measurement of the 'noise' in the electricity generation curve. No flow rates for the reactants were measured for the first 30 seconds. Flow rates of reactants were increased after 35 seconds of operation (see Figure 5.27) and the power generation recording was started. The control algorithm selects 'low load' as a default value during the start-up sequence, therefore an open voltage circuit cannot be not attained. Within 50 seconds the fuel cell reached the steady state condition where the voltage was stabilised at 13 V and the stack current was 12.5 A, see Figure 5.28. The stack temperature reached 27 °C after 100 seconds of operation from its original ambient temperature of 22.3 °C, see Figure 5.29.

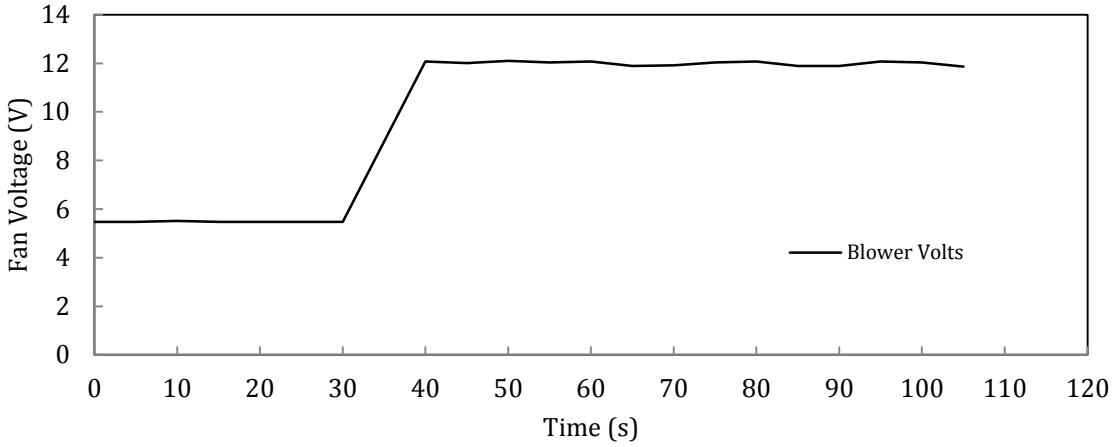

Figure 5.26 Blower Voltage variation during start-up

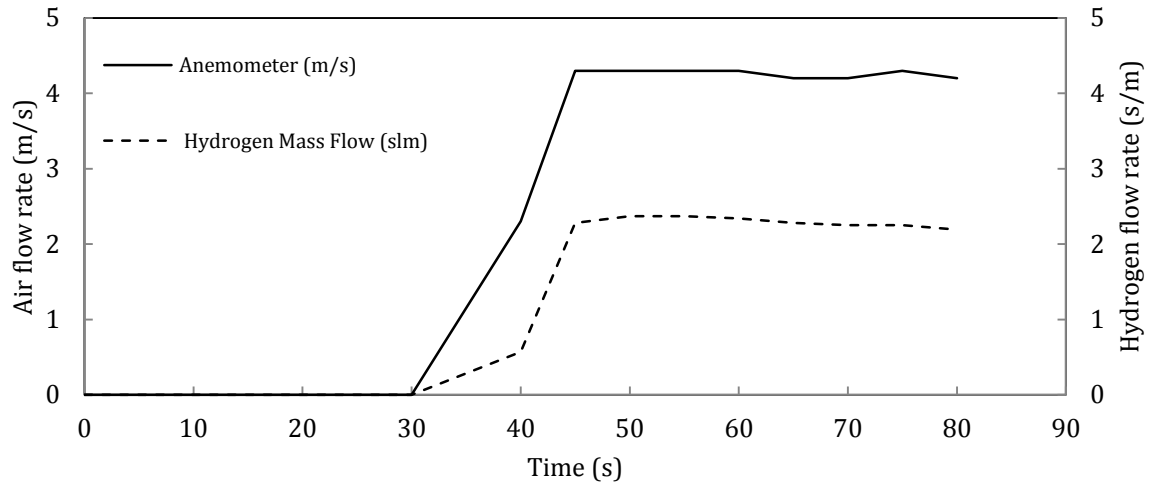

Figure 5.27 Reactants flow rates during start-up

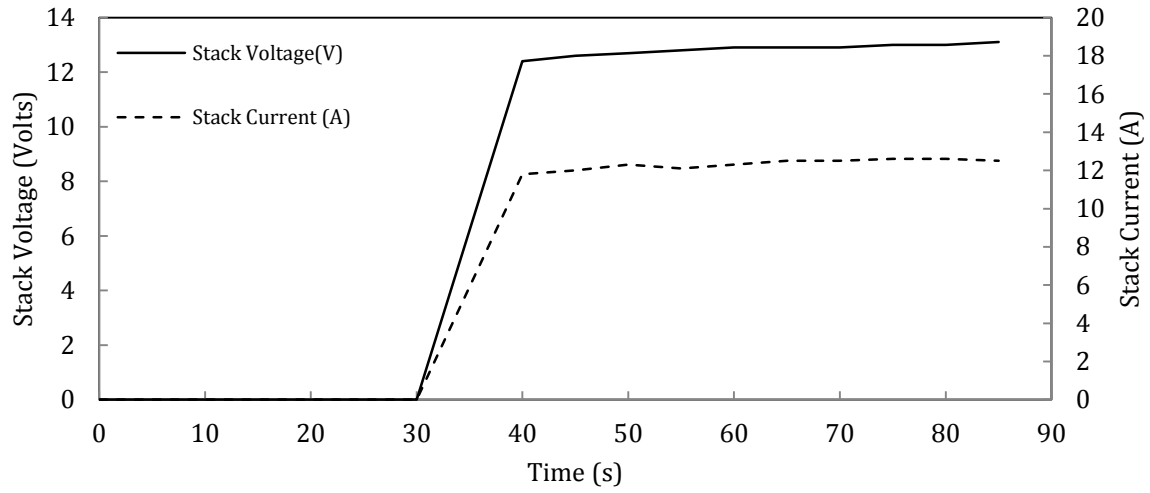

Figure 5.28 Stack voltage and current variations during the start-up

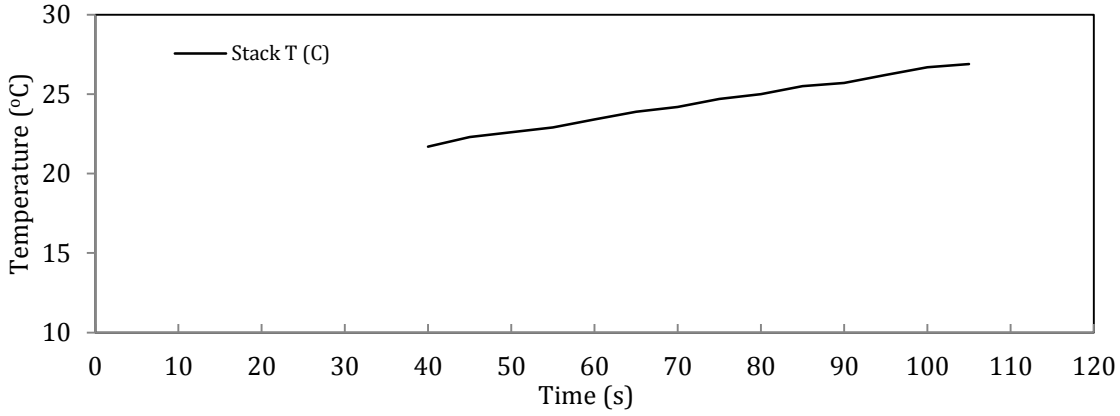

Figure 5.29 Stack temperature variation during start-up

5.4.3.2 Warm start-up

The effect of the warm start-up of the system on the fuel cell transient performance was investigated in a number of tests where the fuel cell operation was started after a maximum 25 minutes break from its previous operation. Figure 5.30 and Figure 5.31 shows the transient response of several parameters during the warm and cold start-ups.

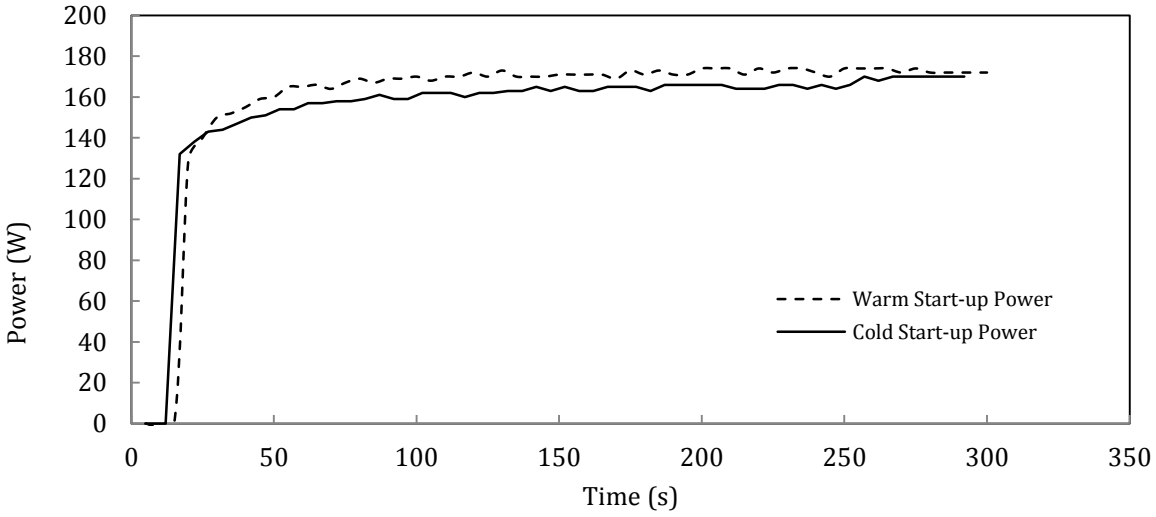

Figure 5.30 Power generation during warm and cold start-ups

It can be seen in Figure 5.30 that there is a very small difference in power generation during the warm and call start-ups. A cold start-up resulted in an approximately 6 % reduction in the electricity produced during the first 200 seconds of operation, though the difference became

negligible later on. It was assumed that this deviation was due to limited kinetics of the reaction and proton transport due to lower stack temperature as shown in Figure 5.26.

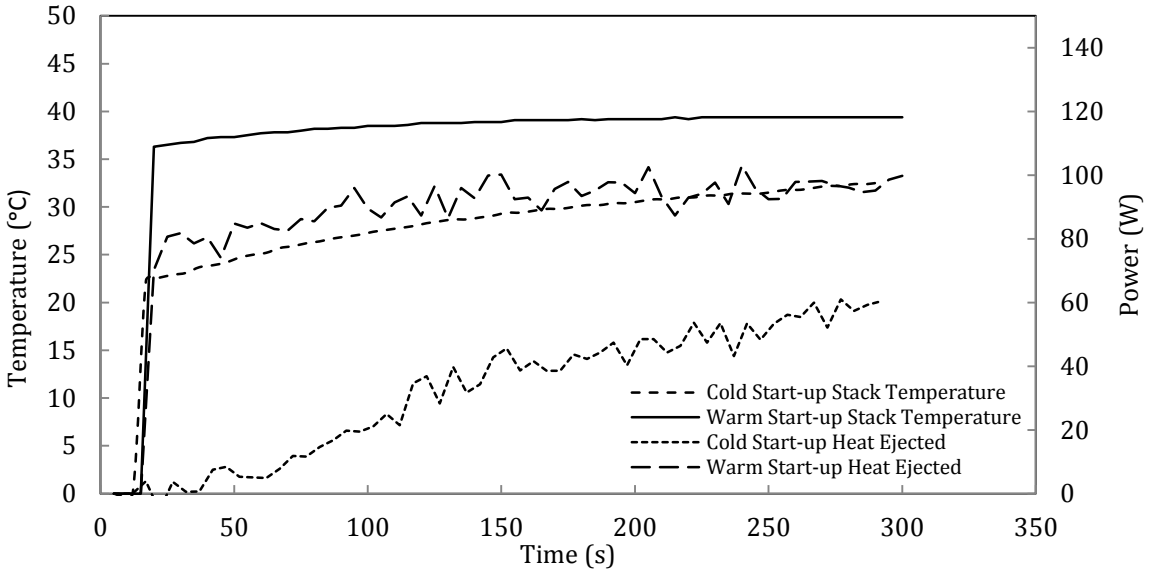

Figure 5.31 Heat dissipation and stack temperature during warm and cold start-ups

It can be seen in Figure 5.31 that there was a difference of 13.4K in the stack temperature during the warm and cold start-ups. Given that the fuel cell was operating at high power densities (the average stack temperature was at 57 °C) for a minimum of 20 minutes before shut down this deviation was expected and was due to the short cool down period (the fuel cell did not reach the ambient temperature). The key temperatures (of the stack, air inlet and air outlet) significantly affect the thermal performance of the cells. In respect of the heat rejected, it was found that the unit reached the steady state operation within 150 seconds in the warm start-up with the thermal power to be stable at 95 W with only small fluctuations around this value. However during the cold start-up when the stack operates starting at the ambient temperature, additional 500 seconds were required in order for the stack to reach the steady state.

5.4.4 Run-down Characteristics

The operation of the fuel cell can be terminated either using the “stop” button on the control panel of software or by turning off the hydrogen supply to the unit. The start of the shut-down

regime results in the current drainage from the stack and hydrogen removal from the anode side. After cutting off the hydrogen supply, the system operates for several seconds using the hydrogen stored within the gas supply pipe work and in the stack itself. Once the measured voltage drops below 5 VDC the internal controller terminates the operation of the fuel cell. Such the control logic was introduced in order to prevent the operation in low membrane humidification conditions which can occur at low current densities and significantly affects the performance of the unit due to the increased membrane resistance. This also leads to limitation of the lifespan of the fuel cells [60, 92]. Figure 5.32 to Figure 5.34 show the transient variation of several key variables during shut-down period in the fuel cell.

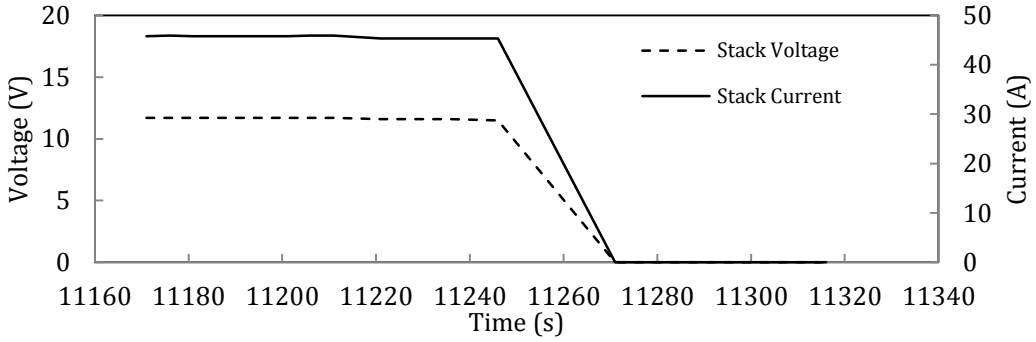

Figure 5.32 Stack Voltage and current during shut-down

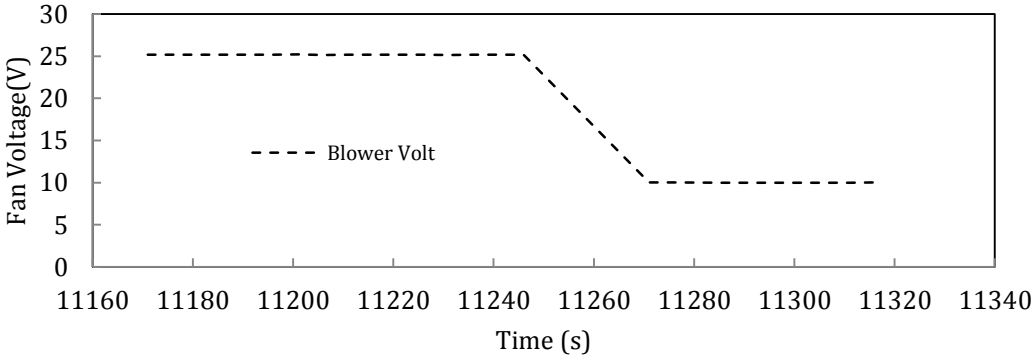

Figure 5.33 Blower voltage variation during shut-down

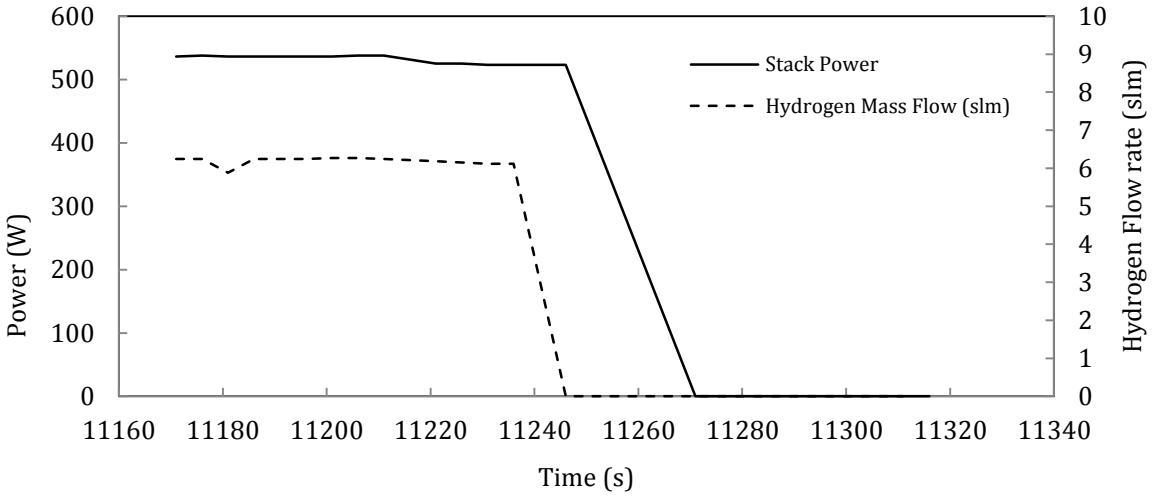

Figure 5.34 Stack power and hydrogen flow rate variation during shut-down

It can be seen in Figure 5.32 to Figure 5.34 that, once the shut-down sequence was initialised via the control panel, within 30 seconds the hydrogen flow rate drops to zero and, consequently, the power generation was stopped. The fan voltage from steady state operation at 25 V decreased to 10 V until the software stops logging data, see Figure 5.33. The sharp reduction to the zero level in all measured parameters occurs synchronously.

5.4.5 Regular load variation

Regular load variation tests are run with progressive increase and then decrease of the load on the fuel cell. Prior to any load change, the fuel cell stack operates in a 'low load' setting for a minimum of 20 minutes in order to reach the steady state operation in accordance with the normal operating procedure of the system. The current and voltage progressively changes from 0 to 46 A and from 13.4 V to 11.6 V, respectively, following a series of step-up and step-down load changes. Figure 5.35 to Figure 5.37 shows the behaviour of the stack during load variations. From Figure 5.35 three distinct load levels can be observed throughout these tests, namely low (13.4 A), medium (25 A) and high load (46 A). The frequency of the purging events increases with the increase in the current in order to prevent water accumulation on the anode side of the cells.

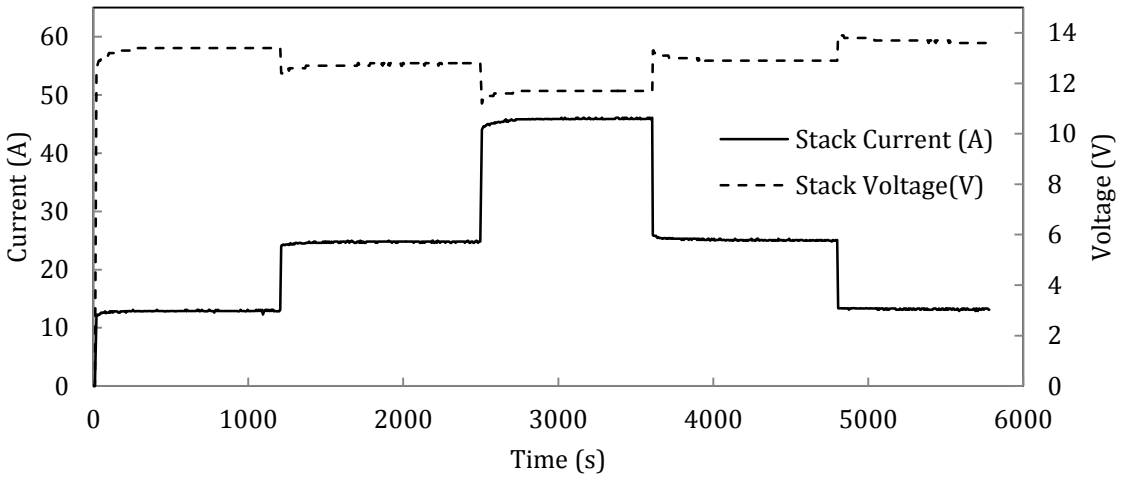

Figure 5.35 Stack voltage and current fluctuations during regular load variation

Purging events were triggered when no more than 2300 ampere-seconds had been delivered from the unit over a period of 200 ms. On the average, at low load conditions the time interval between purging events was 233 s. At medium and high loads, this interval was 122 s and 67 s, respectively.

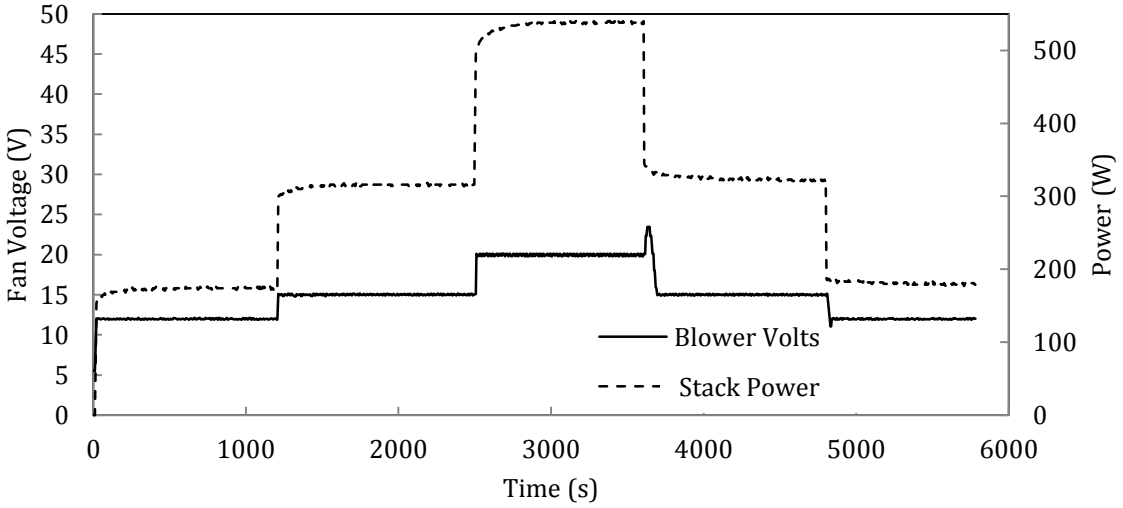

Figure 5.36 Blower voltage and Stack power fluctuations during regular load variation

It can be noted in Figure 5.36 that the fan capacity increases as the power output of the fuel cell stack rises in order to supply sufficient oxygen for the reaction and also for the removal of heat from the stack. The air flow is reduced with the decreasing power. It should be noted that the operation of the blower was controlled by the unit's cooling requirements, which can

lead to a significant increase of air flow in the fuel cell beyond the level needed to maintain a stoichiometric oxygen balance.

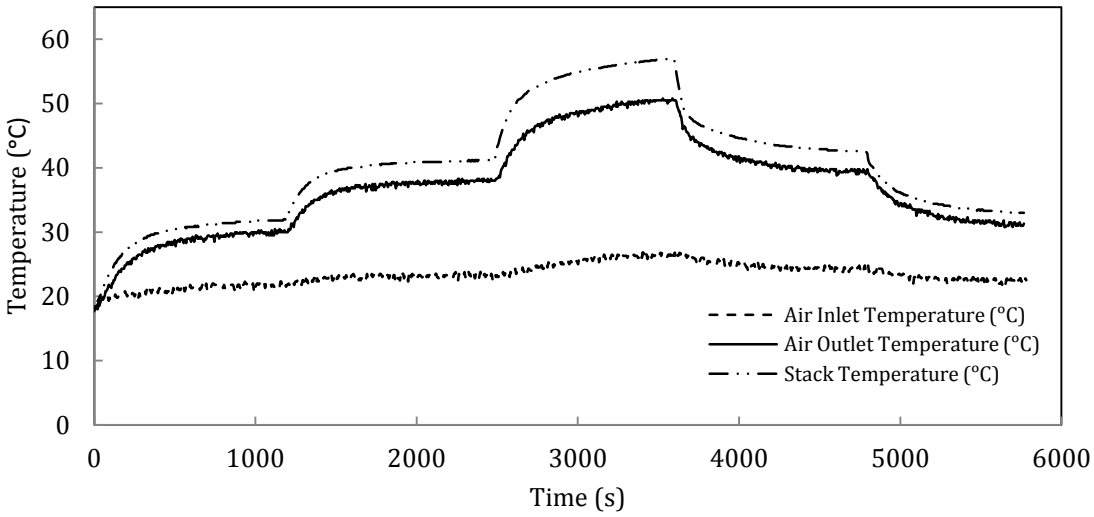

Figure 5.37 Fluctuation in key temperatures during regular load variation

In Figure 5.37 it can be seen that the stack temperature increases with the rise of the current (and hence power) and this is similar to results presented in [60, 94]. The stack voltage experiences undershoot conditions which are triggered by the change in the load. Figure 5.38 shows features of this particular behaviour if the fuel cell.

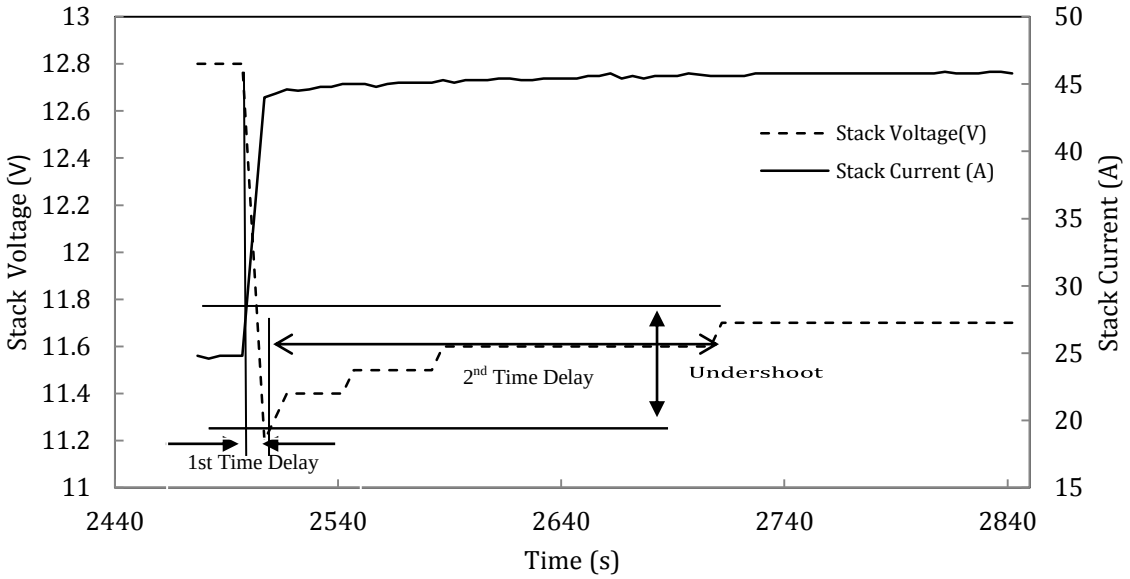

Figure 5.38 Detailed voltage overshoot stack behaviour

From Figure 5.38 it can be seen that during an undershoot transient process, the voltage exhibits two time delays before it reaches a new steady state. It has been suggested in [64] that the first time delay (i.e. the time from the moment when the voltage is in its minimum) usually of the order of 1s is due to gas convection and diffusion processes. An increase in the membrane resistance can be attributed to a moderate water content in the electrolyte resulting in delayed recovery of the voltage. In addition, a higher variation was noticed during the first 40-50 sec of the transient behaviour. Sudden changes in load caused temporary dehydration due to electro-osmotic drag on the anode side and oxidation starvation on the cathode side of the fuel cell. In order for the voltage to recover, the diffusion process had to be activated to restore the membranes humidification level. However, neither overshoot nor undershoot current phenomena were observed during the operation of the unit.

5.4.6 Irregular voltage variation

Further test were carried out to investigate effects of irregular and sudden changes in the load. Irregular voltage variations were result of random change in the load of the fuel cell. Figure 5.39 and Figure 5.40 shows fluctuations of key variables in response to such changes in the load.

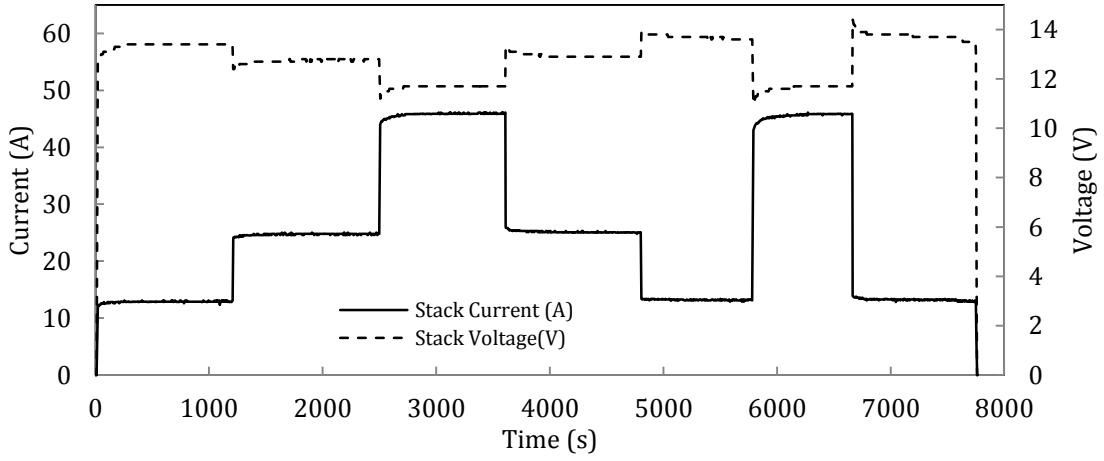

Figure 5.39 Stack voltage and current fluctuation during irregular load variation

An arbitrary load variation pattern was imposed in which the load was switched suddenly from low to high level in several steps and then back to low load as shown in Figure 5.39.The sharp change in both the stack voltage and current were results with the voltage undershoot phenomena visible as discussed above.

In Figure 5.40 it can be seen that the stack temperature increases and decreases with the corresponding change in the load. Heat that was released by the exothermic reaction within the cells can be utilised to improve the performance of the stack according to [65] since it has been established that an increase in stack temperature can improve the gas diffusion and membrane conductivity.

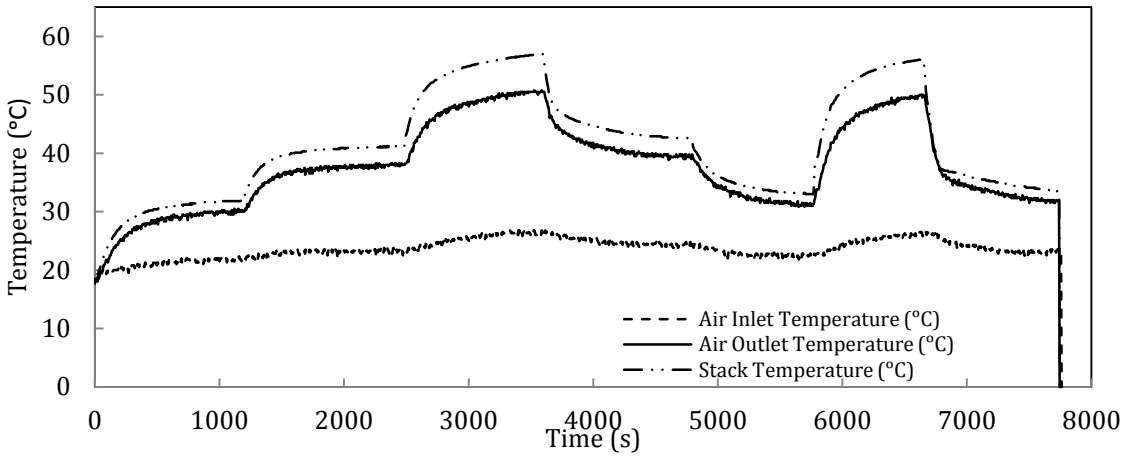

Figure 5.40 Fluctuations in key temperatures during irregular load variation

In addition, the increased heat prevents water condensation which reduces water flooding issues. Controlled selection of the operating temperature strategy can thus improve the transient behaviour of the fuel cell stack and reduce the voltage recovery time [64].

The amplitude of the voltage undershoot observed earlier was noted to be dependent on the magnitude of load change. Figure 5.41 and Figure 5.42 shows the transient regime with the voltage undershoot and overshoot, respectively, for different load changes.

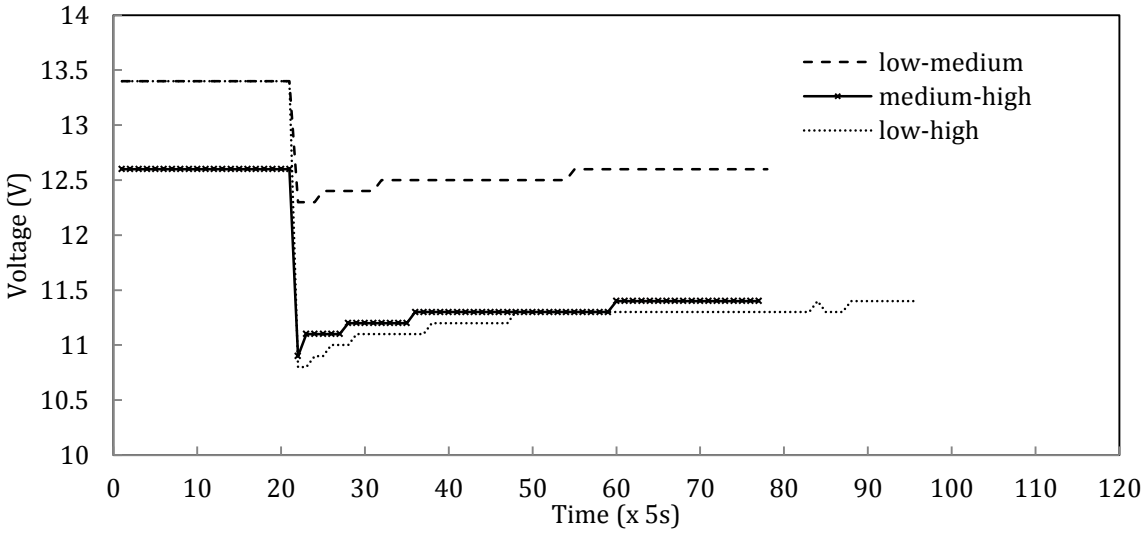

Figure 5.41 Stack voltage undershoot behaviour during a change of load

Figure 5.41 shows that the voltage drops during the following load changes: low-to-medium, medium-to-high and low-to-high. The voltage drops were measured to be 0.3 V, 0.5 V and 0.6 V respectively. Identical trends were observed also in Figure 5.42 in respect of overshoot behaviour following the change in the load. For the load changes from medium to low, high to medium and high to low the voltage overshoot was measured to be 0.3 V, 0.5 V and 0.6 V, respectively.

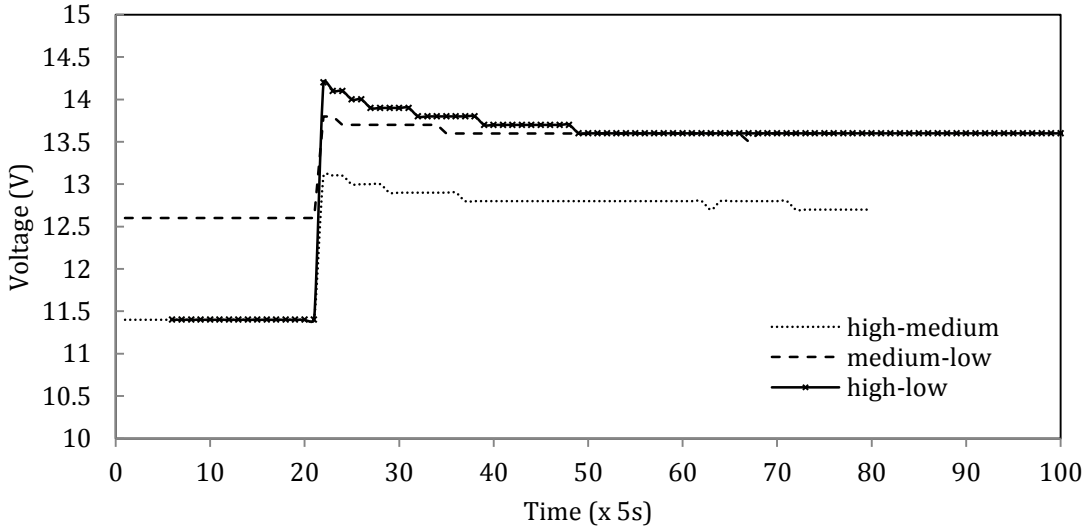

Figure 5.42 Stack voltage overshoot behaviour during a change in load

The stack recovery times were found to be identical during both overshoot and undershoot transient behaviour. Previous research in the transient behaviour of fuel cells that operated with humidified reactants indicated that the stack voltage recovered faster when the load was changed from a higher to a lower level. The latter was attributed to sufficient hydration level of the membrane and to improved mass transport processes. It can be suggested that, when dry reactants were utilised in a self-humidified membrane of the fuel cell stack, the water content of the membrane may not be sufficient, particularly on the anode side. Therefore, recovery of the voltage after the overshoot usually follows the case of an undershoot transient behaviour. It is worth mentioning that the lack of the current transient phenomena supports this hypothesis since an excess of the water content in the membrane increases the possibility of the current overshoot [60]. In addition, the back diffusion from the cathode was probably insufficient for a membrane re-hydration even during the operation at the high load. Although membrane flooding cannot be excluded from the consideration, operation at the high stoichiometric ratio prevents water flooding.

Figure 5.43 shows the gravimetric air/fuel ratio variation during the transient regime caused by step rise in the load.

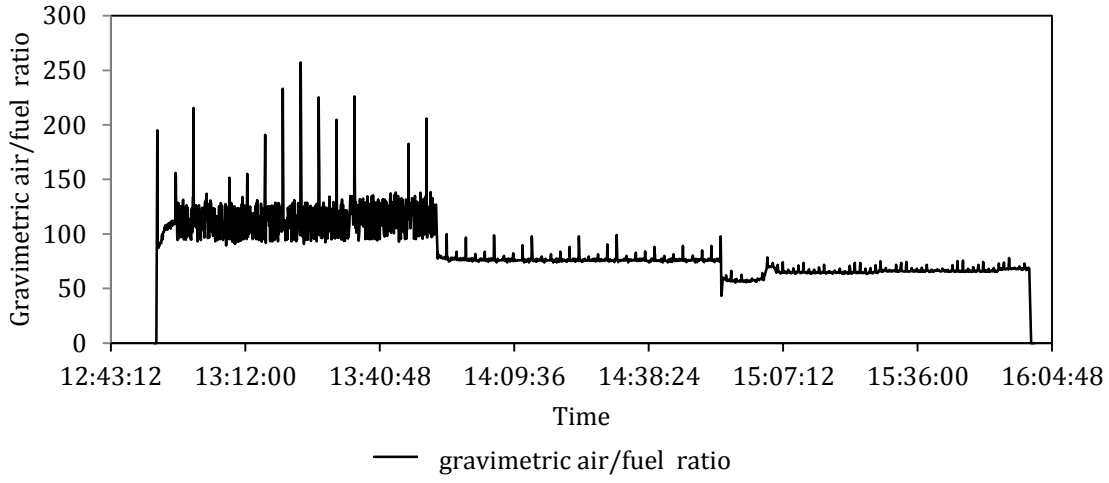

Figure 5.43 Gravimetric air/fuel ratio of the stack during transient operation

Figure 5.43 shows that the stack operated with an average the gravimetric air/fuel ratio of 114 during low load however high fluctuations around the average value can be seen as a result of the unstable hydrogen flow rate. With an increase in the load, stoichiometric ratio was calculated to be 76 and 65 for the medium and high loads, respectively. The operation of the fan in the fuel cell system provides the air flow required for the reaction on the cathode side and stack cooling. For the above reasons the air mass flow rate provided is several times higher than that for the stoichiometric reaction. The high oxidant flow rate possible contributed to faster drying of the membrane [78]. Performance could be improved and stack voltage can recover faster if the reactants side of the stack are fully humidified.

5.4.7 Variation of heat generated during the transient operation

The heat generated during the operation of the stack was calculated using equation 1.6. The cooling requirements controlled the operation of the blower and, as it has been noted, can lead to high stoichiometric ratios. Figure 5.44 shows the variation of heat generated during the operation when the load is increased in steps.

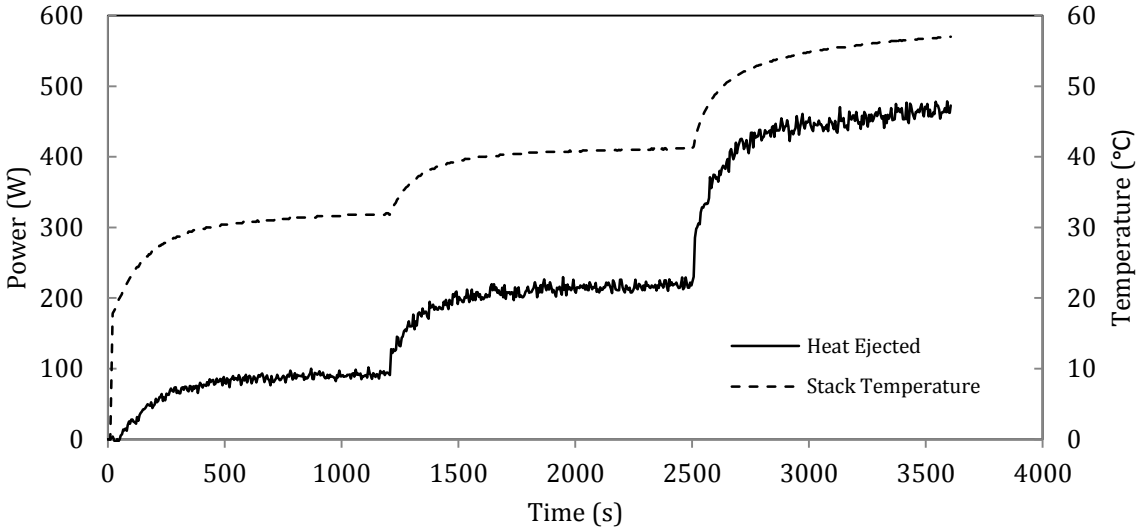

Figure 5.44 Heat dissipation from the fuel cell during the load variation

At the low load the mean value of the heat rejected from the stack was 73 W, at medium load it was measured to be 203 W and at high load it was 434 W as shown in Figure 5.44. Peak values of 102 W, 230 W and 479 W were recorded at low, medium and high loads respectively.

In addition, the heat generation followed the load variation with a slight delay which was due to the time the stack needed to reach new steady state conditions at elevated temperatures. During several tests with the high load small fluctuations in the heat generated were observed. Figure 5.45 shows such a particular behaviour of the stack.

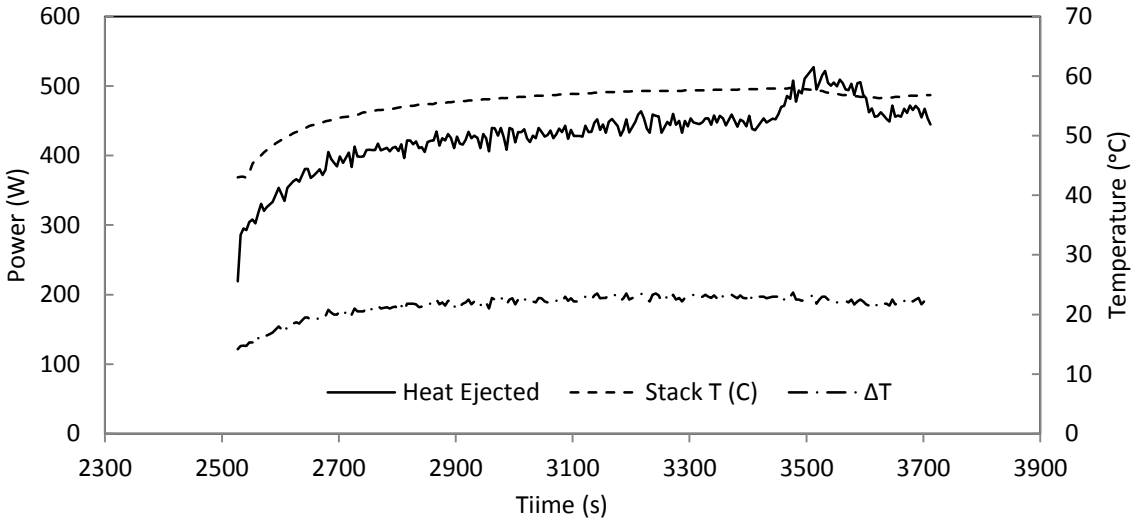

Figure 5.45 Heat variation during operation with high load

From Equation (5.9) it is evident that both the difference between the air temperature in the inlet and outlet and the air flow rate significantly affect the heat rejected from the stack. At a certain points during the high load operation, an increase in the blower voltage can be seen as shown in Figure 5.46. This was found to coincide with an increase in the stack temperature to approximately 58- 58.2 °C. The increase in the air flow rate (to prevent drying of the membrane and due to safety issues) resulted in a steep increase in the heat amount rejected from the unit as shown in Figure 5.45. Once the stack temperature reached an adequate level for safe operation (i.e. values of around 57 °C) then the fan load was adjusted in order to

maintain the stack temperature constant for the rest of the operation. Figure 5.46 shows this sequence during fuel cell operation.

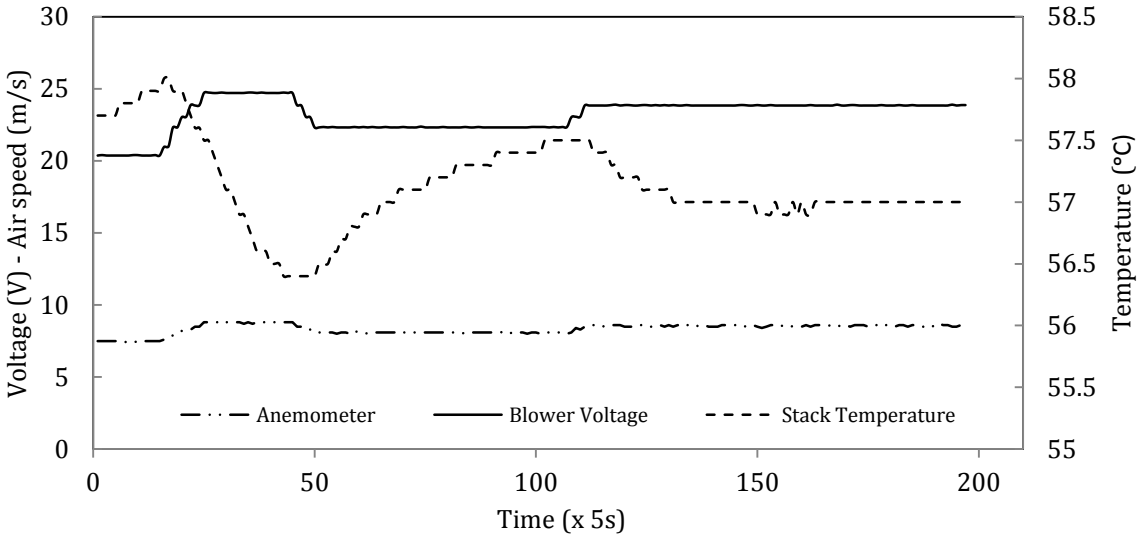

Figure 5.46 Blower performance variation occurring at high load operation

5.4.8 Stack Performance

Data obtained for the steady state operation during a number of tests were used to produce the polarisation curve of the fuel cell stack, see Figure 5.47.

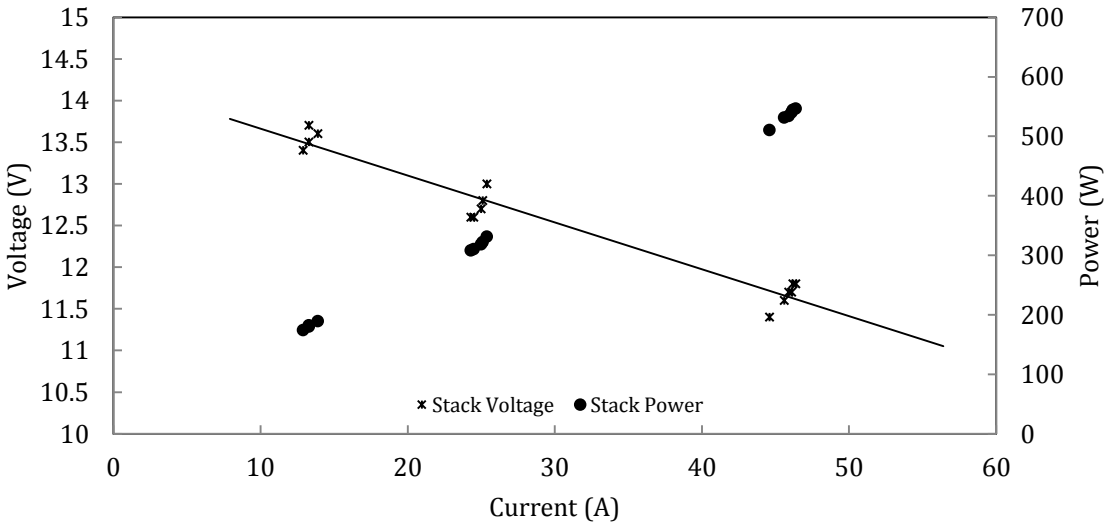

Figure 5.47 Stack polarisation curve

Figure 5.47 shows that the stack performance curve is limited in the ohmic region of the curve due to the fact that 'low load' was selected as the default value and thus the open

voltage circuit couldn't be attained. In addition, the integrated bank of load resistors proved to be insufficient for measuring the performance of the cells close to the maximum capacity and data for the concentrated regions on the diagram was not possible to be to be recorded. As expected, a linear correlation between the stack voltage and current is obtained within the standard operating limits of the unit. Both the membrane's resistance to protons transfer and the electrical resistance in electrodes and collectors resulted in a voltage drop which can be expressed as $V_{ohm} = i * R_{ohm}$ [59].

5.4.9 Efficiency calculations

Figure 5.48 shows the average partial efficiencies calculated using data from all tests. Calculations were based on a standard operation regime in which the load on the fuel cell was increased as a step function followed by similar load decrease. The unit was running for a minimum of 20 minutes at each load level.

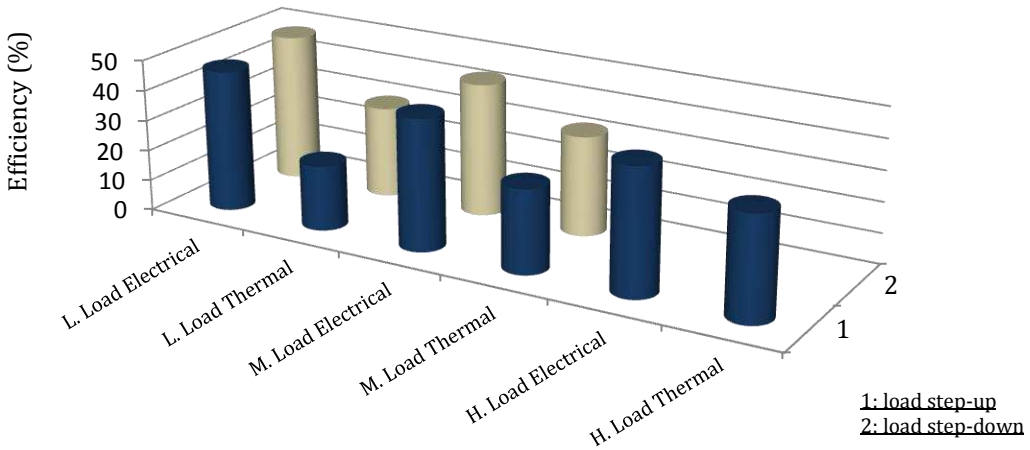

Figure 5.48 Partial efficiency calculations during low/medium and high load operations

In Figure 5.48 it can be seen that there is an increase of 9 % and 2 % in the thermal and electrical efficiencies, respectively, when load was suddenly reduced at low load operation after the transient process following the sudden load increase. It is assumed that such

differences can be attributed to a faster change of the temperature towards the new steady state. In respect to the electrical efficiency, the operation of the stack prior to the sudden decrease in the load increases the stack temperature which was found to be beneficial for the reactants utilisation due to a higher proton conductivity and improved mass transport [62]. In addition the extended operation resulted in better hydration of the self-humidified membrane, due to the high rate of water production at particularly high current densities.

When the load suddenly changed from high to medium level the average stack temperature was 16% higher than the one recorded when the load changed from the low to medium level. This difference improved the thermal efficiency by 5 % during operation when the load suddenly was increased. No change was observed in performance when the unit was operating at the high load conditions. Figure 5.49 shows the individual and overall partial efficiencies during the whole cycle of operation.

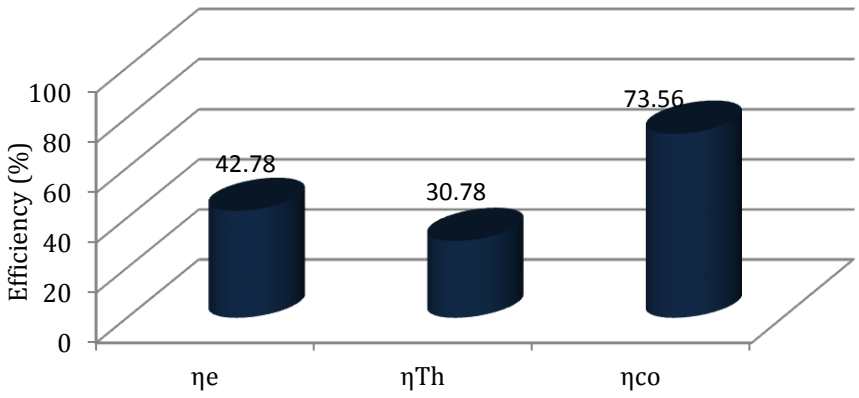

Figure 5.49 Partial and co-generation average efficiencies

Overall, the average electrical and thermal efficiencies for all tests were calculated to be 43 % and 31 %, respectively, and therefore the overall cogeneration efficiency was found to be 73.5 %. It is worth mentioning that the amount of hydrogen utilised during purging was not accounted for in calculations. Purging events lasted for 200 ms and the hydrogen flow rate

exceeded the maximum measurable level by the integrated mass flow rate meter during these events. The manufacturer of the fuel cell assembly has estimated that the purging of the assembly can be expected to result in overestimating the measured efficiency by 2-5 %.

5.4.10 Validation

Experimental results were compared to the outputs of the theoretical model described in Chapter 3. The validation process was carried out for a single run operation. During experimental tests it was observed that the mCHP operated for few minutes in the low load mode before it was switched to the full capacity, in order to achieve the adequate hydration level of the membrane and to avoid performance degradation. However, the mCHP model assumes that the heat should be generated at the maxim output from the beginning of operation. For this reason in the modelling of the mCHP based on a PEM fuel cell it was arranged that the fuel cell assembly would operate at the maximum capacity once the module was switched on. Figure 5.50 shows the experimental results compared with the model predictions. It should be stressed that the operation at the low load mode, corresponding to the membrane hydration, was discarded.

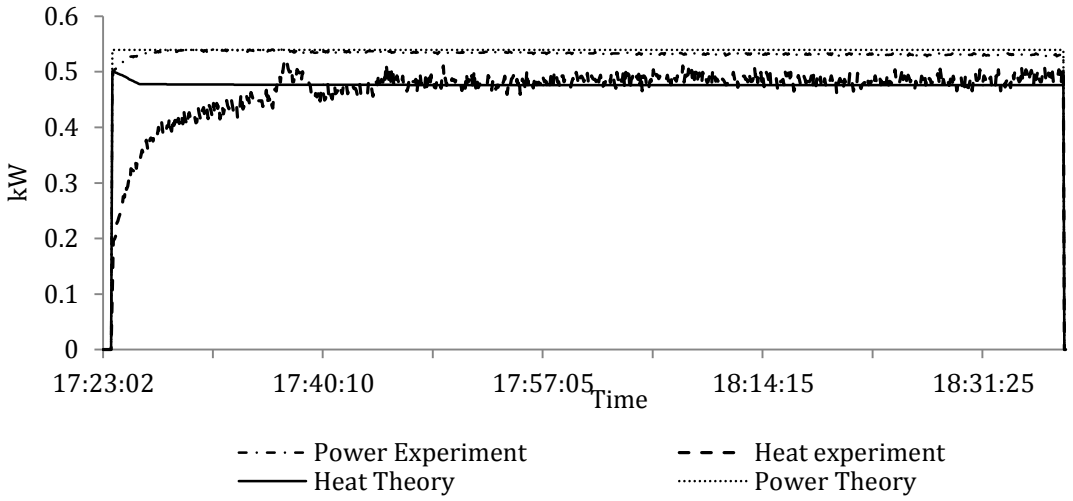

Figure 5.50 Experimental versus theoretical results in the operation of PEMFC

It can be seen in Figure 5.50 that the power generation prediction is in a good agreement with experimental results in terms of the maximum electric output. Marginally faster response of the power output was observed in the theoretical output. Small fluctuations around the nominal capacities can be seen for both the experimental electrical and thermal outputs. There is no significant difference between experimental results and model prediction for the heat output during the steady state operation but there is a significant deviation between the above curves in the early stage of operation. The transient response of the heat dissipated which was observed in physical tests was not captured in the modelling. Simulations predicted a particularly fast transitional regime in which the fuel cell reaches the nominal heating level within the first minutes of the operation. This deviation was partially attributed to the difference in the types of heat exchangers used in the model. Air heat exchanger was integrated into the real fuel cell whereas in simulations the water heat exchanger was incorporated. Overall, the modelling of a mCHP based on PEM fuel cell is a very challenging task. Some of the reasons behind the deviations in results are:

1. The fuel cell module and sub-models still have been under development which restricted modelling flexibility.
2. In the model the fuel cell was considered as a power generation device. Therefore only the electricity-led operation mode was available.
3. The integrated sub-model responsible for the auxiliary heater although was formally available in software was not actually functional.

Therefore the fuel cell was further simulated as a grey box which operates constantly at the steady state condition without accounting for the start-up transient processes but with averaged values of efficiencies, obtained during experiments for the whole cycle of operation (i.e. including transient processes).

Chapter 6 Theoretical Analysis of mCHP deployment in UK Dwellings

6.1 Introduction

The numerical modelling results on determination of economical and environmental impacts from deployment of various mCHP technologies in the range of UK dwellings are presented and analysed in this Chapter. Initially, the energy requirements in several UK buildings have been modelled using EnergyPlus. Then operation of a number of mCHP technologies based on ICE, Stirling engine and PEM fuel cell with various configurations and operating strategies has been simulated in order to assess the environmental and economic benefits for each scenario. Finally, the most feasible technology and operating strategy have been identified depending on the type of dwelling.

6.2 **Methodology description**

The evaluation of the deployment of mCHP systems in domestic environment initially requires the specification of property features such as the house type, construction details, occupancy pattern and electrical and space heating demand characteristics. Then experimental data obtained on certain mCHP technologies such the nominal capacity, partial efficiencies etc. is used to describe their operation inside dwelling in the theoretical models of EnergyPlus to reflect their realistic operational characteristics. In order to assess the performance of the Whispergen Stirling engine based mCHP in the dwellings two main different operating strategies were simulated:

- The generation of space heating and DHW occurs simultaneously (simultaneous heat generation);

- The DHW heat generation was separated from the space heating and the mCHP was programmed to start prior to each space heat demand event to fully charge a DHW tank before being switched to space heating mode (split heat generation).

The mCHP systems are used in domestic applications with the aim to replace conventional heating equipment such as condensing boilers. Therefore mCHP systems are commonly operate in the heat demand-led regime with the main purpose being a satisfaction of the household thermal requirements. In the heat demand-led regime of operation the mCHP firstly covers the thermal demand with a high partial efficiency (in the range of 60 %-70 %). Meeting the electrical demand is the secondary aim and this part takes place with a lower efficiency (10 %-20 %). The power generation therefore is considered to be a by-product. The operating regimes simulated in this section are considered to be realistic and feasible operating strategies in which the end-user decides whether the MCHP works to charge the domestic water tank simultaneously with the space heating or these processes can be separated in time if it offers greater benefits.

The experimental operational characteristics of the mCHP unit for simultaneous and split heat generations were determined previously and described in Chapter (5). Additionally, a range of hot water storage tank volumes were simulated to determine their effect on the system's performance. For the operating scenario, which offered best results, deployment of three alternative mCHP systems were compared to the reference case (conventional heating system with condensing boiler). The performance of a Honda Ecowill ICE based system, a Whispergen Stirling engine based mCHP and a PEM fuel cell based mCHP were compared in terms of the energy use and economics. Having established the validity of the theoretical results in the previous chapter, the modelling procedure was expanded to include mCHP systems with electrical capacities in the range of 1-3 kW_e for both Stirling and IC engine systems.

Table 6.1 Energy demand profiles applied throughout modelling process

Types of the houses and construction regulations	Electricity Consumption	DHW Consumption	Occupancy pattern
Semi-detached house (2006 Building Regulations)	4.6 MWh_e/annum	200 L/day	Working Adults
Semi-detached house (1996 Building Regulations) Detached house (2006 Building Regulations) Detached house (1996 Building Regulations)	4.6 MWh_e/annum 5.5 MWh_e/annum	200 L/day 250 L/day	
Bungalow house (2006 Building Regulations)	3.8 MWh_e/annum	100 L/day	Retired Adults

The effect of the construction standards and occupancy patterns on the primary energy consumption in several types of houses was investigated. Table 6.1 shows the construction standards together with the occupancy, electrical and hot water usage patterns used in simulations. Models describing a continuous operation of mCHP systems were also developed. Such operation can be achieved if mCHPs with small heat capacities are deployed in houses with larger heat requirements. In these cases additional (auxiliary) burners should be included into the modelling process.

6.3 Domestic energy demand modelling

6.3.1 Space heating demand and dwelling characteristics

The first selected building is a semi-detached two-storey dwelling with the overall floor area of 117 m^2, including a 16 m^2 garage, constructed under the UK's 2006 Building Regulations. Figure 6.1 and Figure 6.2 show the design of the semi-detached house used in simulations and the main features of the construction methods applied [147].

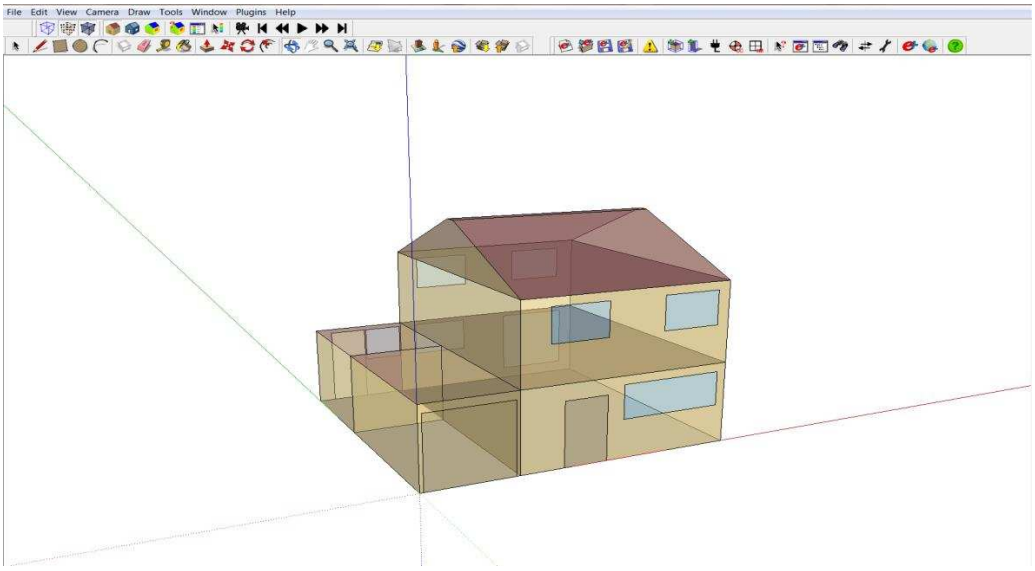

Figure 6.1 Design of the semidetached house

The dwelling has an overall window area of 16.3 m^2 which corresponds to 7 % of the gross external wall area, and a floor height is 2.5 m. It was modelled with five individual energy zones and was assumed to be located in the area of the Gatwick airport near London. All the simulations were performed using weather file in the IWEC format (which includes the ambient temperature, diffuse and direct solar radiations, etc.). The construction details can be found in [148].

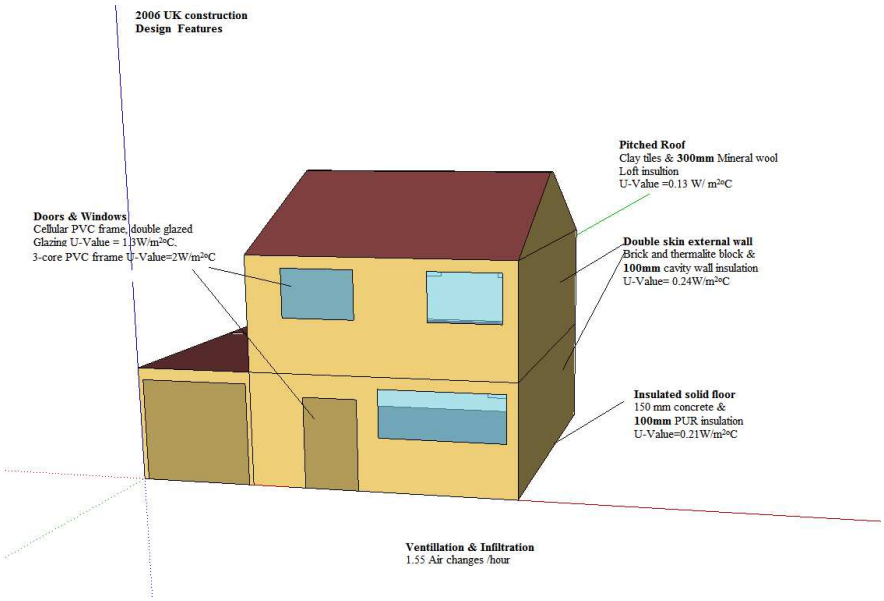

Figure 6.2 Main features of the construction (based on 2006 UK Building Regulations)

6.3.2 Occupancy characteristics

The energy consumption strongly depends on the occupancy pattern in the dwelling. Three working adults and a child of school age were assumed to occupy the house. There are two distinct occupancy patterns, namely during weekdays and weekends. The weekday's pattern is characterised by active occupancy for 2 hour period in the morning, followed by 9 hours of inactivity in the dwelling and 5 hours of active occupancy in the evening time. In the weekend day a long active occupancy lasting 13 consecutive hours is presumed. Table 6.2 shows the two heating system running schedules which have been simulated in accordance with the above occupancy patterns.

Table 6.2 Heating plant operation schedule for a typical winter day

Type of day	On (21 °C)	Off	On (21 °C)	Off
Weekday (Monday-Friday)	7:00	9:00	18:00	23:00
Weekend (Saturday, Sunday)	9:00			22:00

6.3.3 Electricity demand profiles

Two different electricity consumption profiles were derived for both weekday and weekend occupancy patterns. Typical electricity demand profiles, produced by the detailed analysis of all possible electricity events with their power consumption rates and lengths, were applied in modelling. Such the electricity demand profiles were calibrated against the average annual electricity demands in UK households and profiles previously developed in other research projects.

Figure 6.3 and Figure 6.4 show the distribution of the electricity consumption during weekdays and weekends, respectively, which then was used in the modelling process.

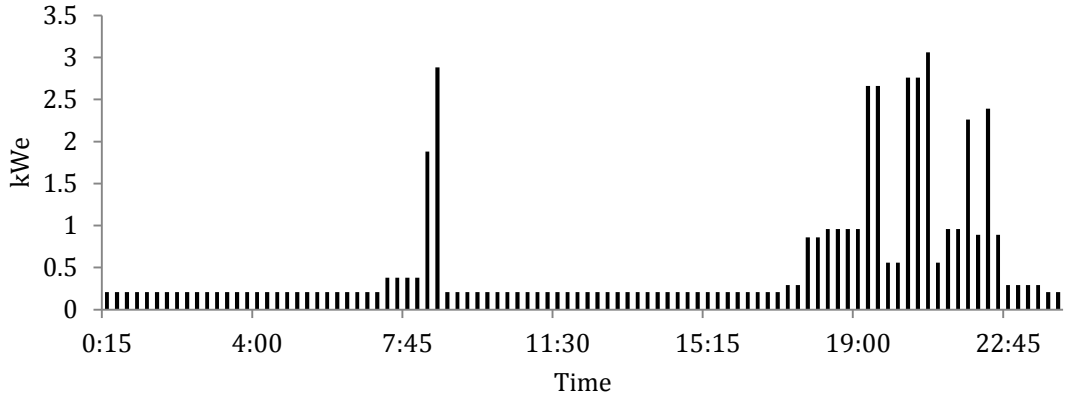

Figure 6.3 Typical electrical consumption distribution in weekdays

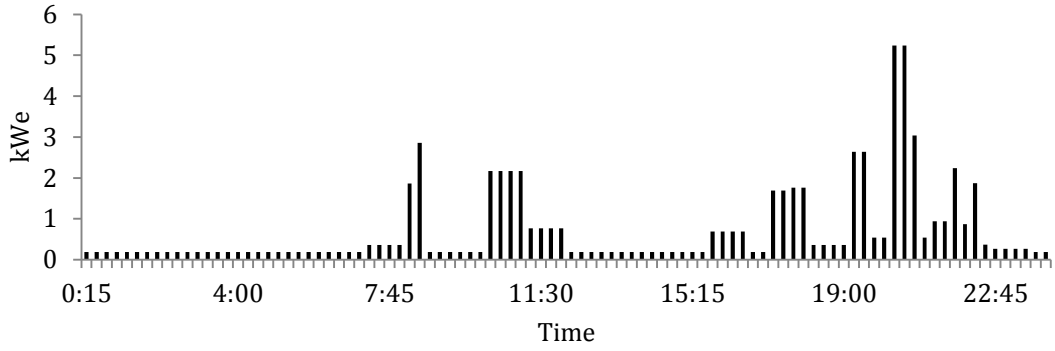

Figure 6.4 Typical electrical consumption in weekends

The electricity profiles were based on the average annual domestic electricity usage in the UK which is 4.6 MWh_e [37] and also on previous research data regarding the operation schedule and the type of appliances [37]. It can be seen in Figure 6.3 and in Figure 6.4 that the level of the electricity consumption coincides with the active occupancy periods with a small baseload at the periods when occupants are away. The electricity consumption is prolonged during weekends, whereas in a typical weekday it is concentrated in two distinct active periods in the morning and evening times.

6.3.4 Domestic hot water demand profiles

The modelled DHW system comprises a 150 litres insulated water tank with heat losses of 0.843 W/K [146]. The total daily consumption was estimated at 200 litres based on a 50 litres per person per day in accordance with [37]. The DHW tank in the model was controlled

by a thermostat which was set at 70 °C. The heat demand is signalled when the temperature inside the tank drops by 6 °C. The very modern energy saving measures have not been considered for the modelled house as this has been found to affect the carbon saving potential of mCHP [130]. Figure 6.5 and Figure 6.6 shows the hot water consumption profile during the weekdays and weekends.

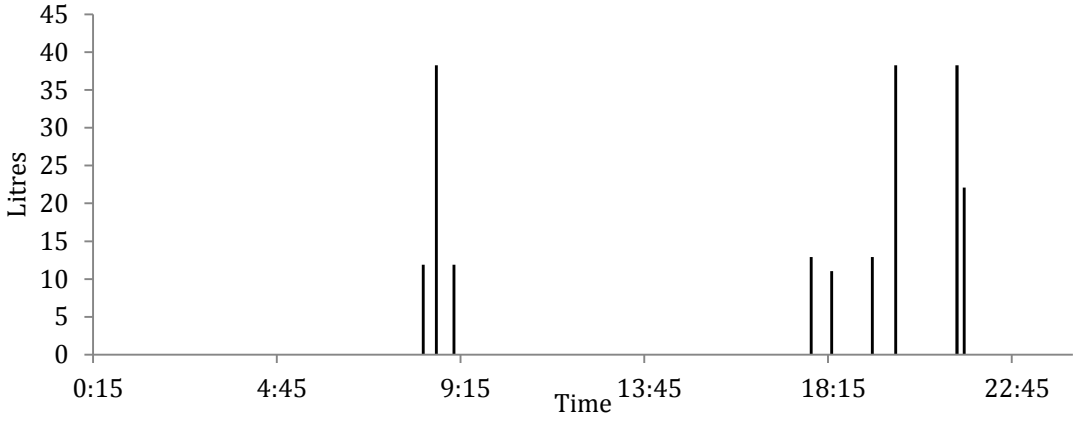

Figure 6.5 Typical hot water consumption distribution in weekdays

It can be seen in Figure 6.5 and in Figure 6.6 that the hot water demand follows the occupancy profile in the house with the higher demand coinciding with the active occupancy period (as was found for the electricity consumption).

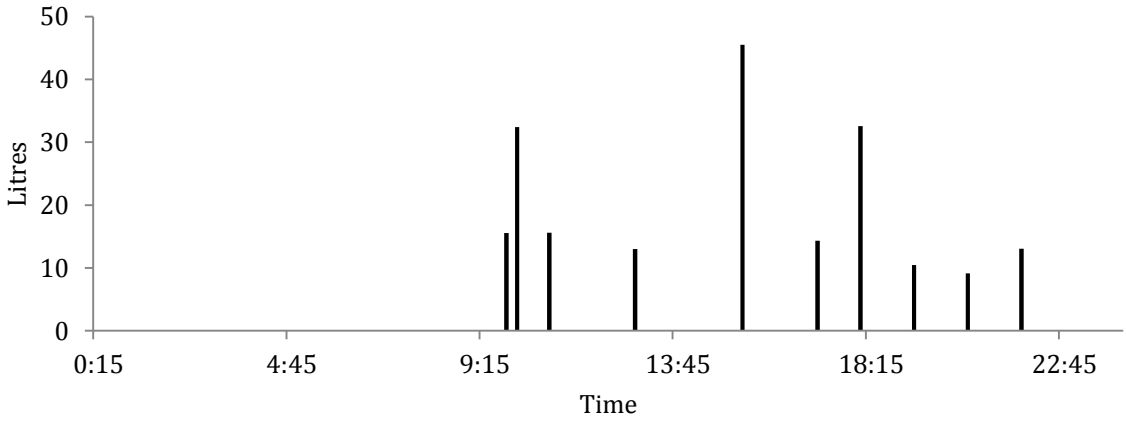

Figure 6.6 Typical hot water consumption distribution in weekends

6.4 Modelling conventional domestic heating system

A convective radiator space heating system had been set in the model to cover the thermal requirements within 3 active zones in the house, namely kitchen, ground and first floors. The heating system was regulated in the model by setting thermostats in each active zone, all maintaining the temperature of 21 °C. The sizing of the radiators, pipe – work and space heating water tank was performed by the software internal procedures. The conventional heating system to satisfy the heat demand in the house consisted of a condensing gas boiler and a 150 litres hot water tank. An efficiency value of 85 % was used for the modelling of the condensing boiler [122]. Additionally, the electricity consumption by the boiler was taken into account when estimating the annual electricity consumption in the house [122].

Initially, theoretical simulations were carried out using EnergyPlus to validate the applicability of the software. For this purpose, a real heating system with a non-condensing boiler with 75 % efficiency was modelled and the obtained results were compared against utility bills of the dwelling modelled and there was a satisfactory agreement between theoretical and real data. Hence EnergyPlus model was considered to be valid and it was modified to incorporate a condensing boiler with a higher efficiency (namely, 85 %). The annual heat demand predicted by the refined model, incorporating the condensing boiler, was 15 MWh_{th} which is close to that of the average domestic UK heat demand figures as provided in [130]. The condensing boiler supplied the thermal energy for both central heating and DHW during the colder period between November and April. During the summer period, namely between May and October only DHW heating was considered.

The electric demand in the house in the reference case throughout the year was assumed to be satisfied by importing the electric energy from the national grid. Figure 6.7 and Figure 6.8 show the obtained results on the operation of the boiler and the air temperature within a

heating zone corresponding to the ground floor for a winter weekday and winter weekend day, respectively.

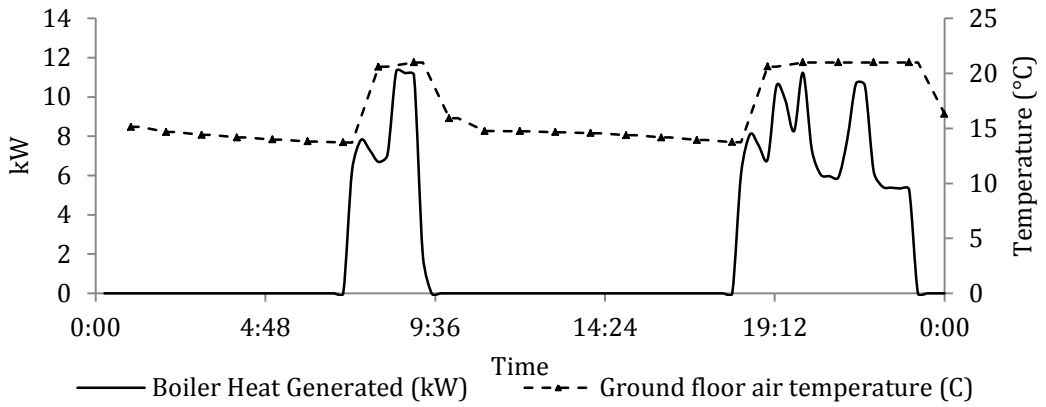

Figure 6.7 Boiler heat generation and zone air temperature during a winter weekday

It can be seen in Figure 6.7 and in Figure 6.8 that the conventional heating system was designed with the capability to modulate the thermal output in order to follow the heating requirement. The operation of the heating equipment was found to be consistent with the active occupancy patterns. The peaks in the heat generation on both design days can be attributed to the instantaneous domestic hot water demand. Hot water usage decreases the temperature in the hot water tank and results in the increased heat generation by the boiler. Space heating provides the adequate comfort temperature of 21 °C in all thermal zones.

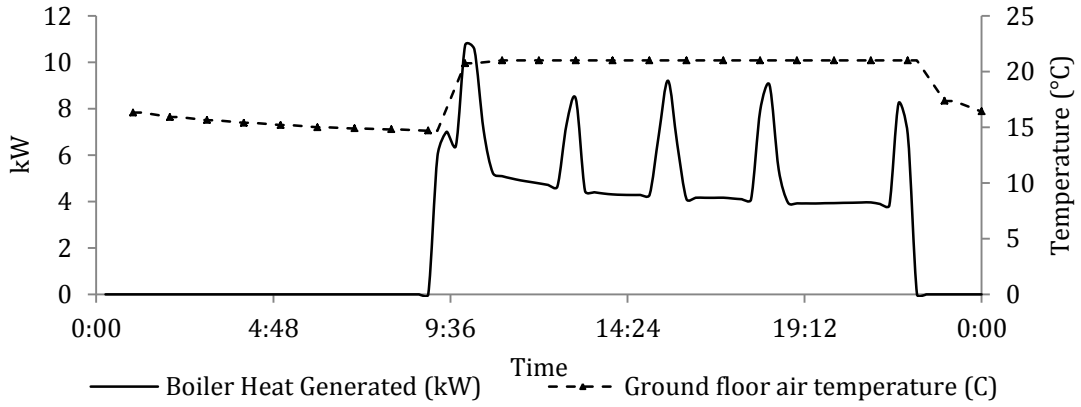

Figure 6.8 Boiler heat generation and zone air temperature during a winter weekend day

During the summer period the boiler generated heat in order to cover only the domestic hot water requirements. Figure 6.9 shows the boiler operation during such the summer day. It can be seen that the boiler cycles between "on" and "off" states more often on a typical summer day.

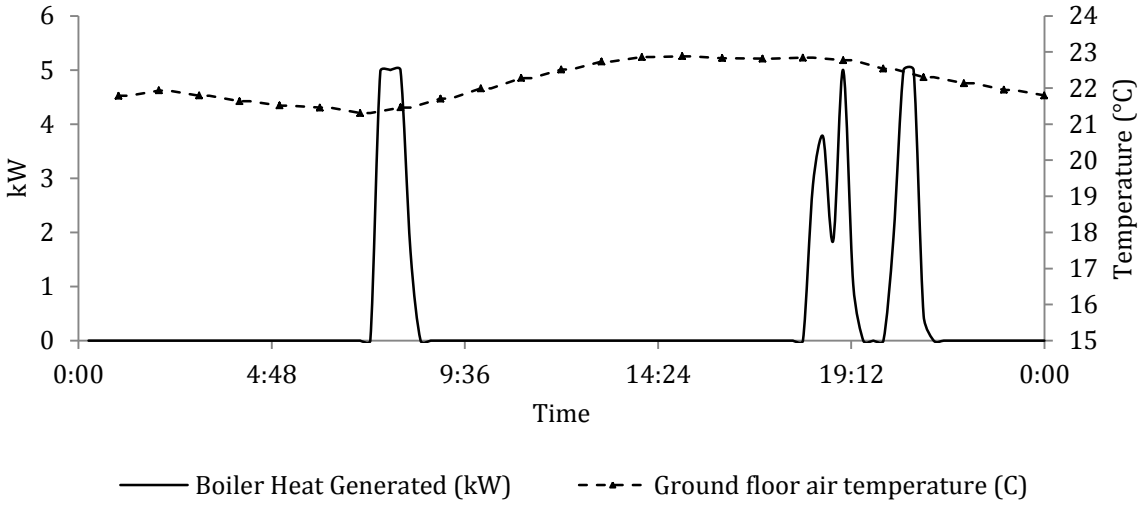

Figure 6.9 Boiler heat generation and zone air temperature in a summer weekday

6.5 Operating strategies for Whispergen 1 kWe Stirling engine base mCHP

6.5.1 Simultaneous heat generation mode

In the simultaneous heat generation mode the Stirling engine mCHP generates simultaneously heat for both space heating and domestic hot water circuits attempting to follow the thermal energy demand in the house. The Whispergen mCHP has a nominal electrical capacity of 1 kW_e and heat to power ratio of 6 (as described in Chapter 5). The modelling process of the operation of the Stirling engine based mCHP unit was described in Section 5.1.7 and, since some inflexibility was found in the operation of the auxiliary burner during tests, the additional burner was excluded from the current modelling procedure. Input parameters, requested in the modelling process, such as power and overall efficiencies in the steady state and transitional regimes of operation, were used from results obtained experimentally, as it was described in Chapter (5). Results of modelling the reference

scenario indicate that the thermal capacity of the Stirling engine unit might be just sufficient to cover the both space heating and hot water requirements. Figure 6.10 and Figure 6.11 show theoretical results on the operation of the Whispergen unit in simultaneous heat generation mode.

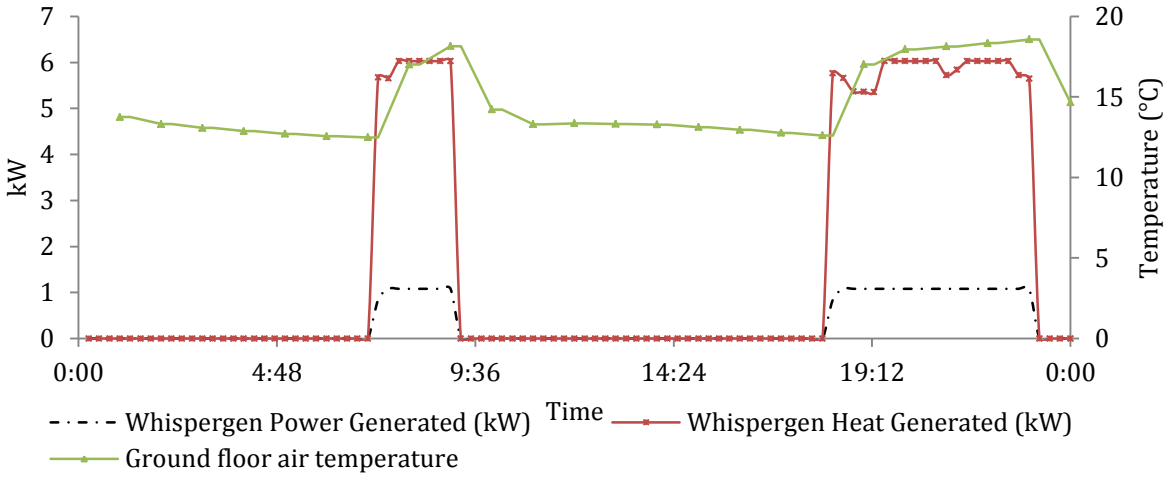

Figure 6.10 Heat and power generation by Stirling engine mCHP in a winter weekday simultaneous heat generation mode

It can be seen in Figure 6.10 that there is a delay in reaching the target thermal comfort level, particularly during the evening operation due to a need to supply heat to both radiators and DHW tank. However, it was found that during mild days there is a cyclic operation of the mCHP suggesting that the heat demand requirements were fully covered. Power is generated at the maximum capacity of 1 kW_e during mCHP's operation. There are small fluctuations in heat generation during the evening operation due to the interaction of space heating and DHW demand at this particular time period. It can be seen that during relatively short runs during winter week days the space heating requirement is not fully satisfied with the air temperature within zones being below the set point by approximately 2 K. Figure 6.11 shows that there is a constant operation at the rated output throughout the active occupancy period

during weekend design days in a winter period with a small variation in the heat generation in the early stage of operation.

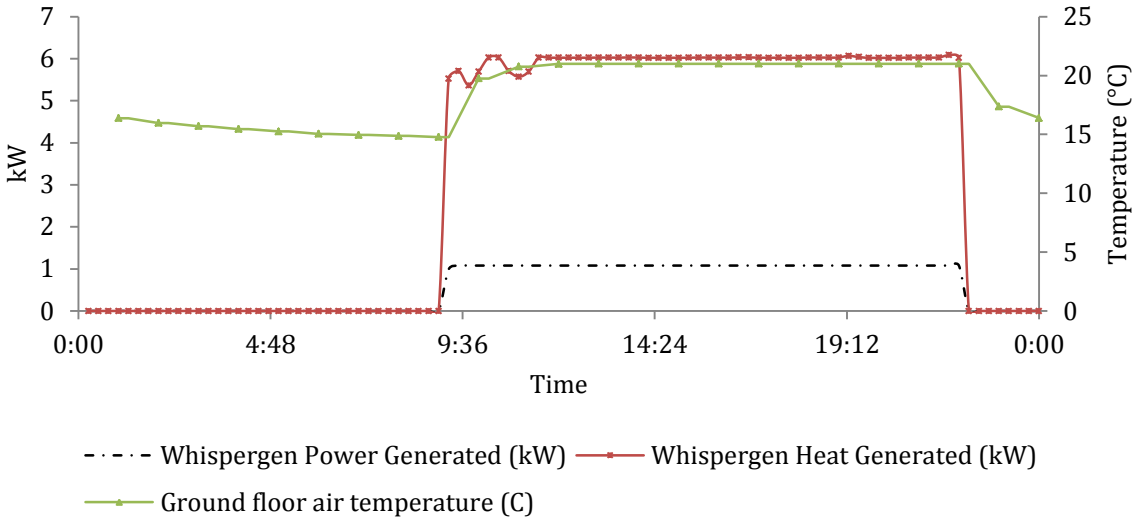

Figure 6.11 Heat and power generation by Stirling mCHP in a winter weekend day under in simultaneous heat generation mode

The continuous operation is due to significant continuous heat demand associated with both central heating and DHW requirements. The early fluctuation can be attributed to the start-up characteristics of the Whispergen system and to the variation of the return temperature in the system's circuit.

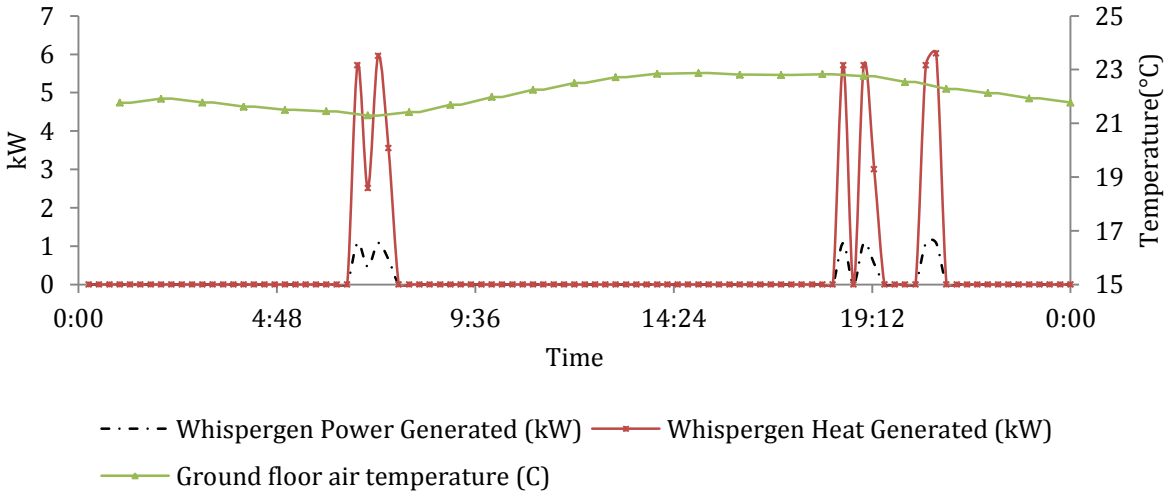

Figure 6.12 Heat and power generation by Stirling mCHP in a summer weekday

Figure 6.12 shows the operation of the Stirling mCHP unit in a summer week day. During the summer period the heating requirements are limited to only DHW requirements and therefore the mCHP operates with high cycling frequency. It can be seen that there are the "switch-off" events (when mCHP is switched off) and these were due to a lack of modulation capability of the mCHP unit: as soon as temperature in the hot water tank reaches the level of the thermostat setting the switch off sequence is triggered.

6.5.2 Split heat generation mode

A split heat generation mode strategy intended the prolonged mCHP operation which according to [18] could improve the operating performance and financial advantages of the Stirling engine mCHP system. In the theoretical simulations water in a 150 L hot water tank was warmed-up twice a day prior to the mCHP's morning and evening runs for satisfying the space heating demand. In simulations the mCHP operated for 45 minutes in the morning and another 30 minutes in the afternoon prior to heat demand periods. These additional operating periods were selected in the model based on the experimental results.

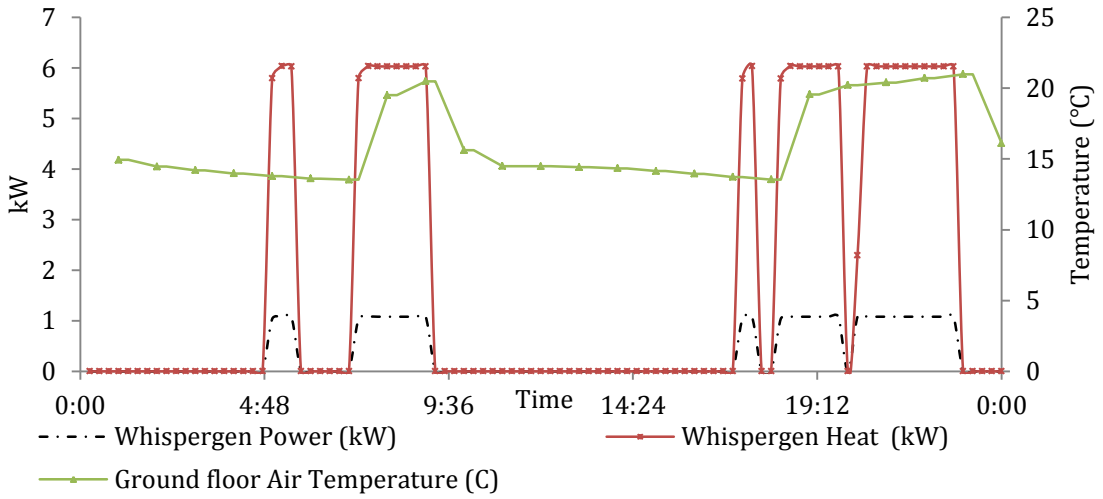

Figure 6.13 Heat and power generation by Stirling mCHP in a winter weekday in split heat generation mode with a 150 L hot water tank

Figure 6.13 shows the operation of the Stirling engine based mCHP in split heat generation mode in a week day during a winter period and the temperature fluctuation of the air in the ground floor. The thermal energy generated prior to the main heating demand was utilised for charging the water tank with bringing the temperature of water up to the level pre-set by tank's thermostat. A shorter time is needed to charge the water tank during the evening operation due to the higher initial water tank temperature. Once the zone comfort temperature was achieved, the mCHP is switched off during the evening space heating operation period. Figure 6.14 shows the variation of the water temperature in the hot water tank as well as the hot water consumption (from the tank) profile.

In Figure 6.14 it can be observed that the DHW charging prior to the space heating increases the water temperature in the tank to 70 °C, while hot water consumption events and thermal losses from the tank result in the tank water temperature drop during the both active occupancy and vacant periods, respectively. The hot water temperature at the user's end (sink tap, shower, etc.) is 45 °C. It is worth noticing that before the last demand event (a shower at 21:15 pm) the temperature inside the tank is 50 °C which suggests that the selected operating strategy is adequate for covering both central heating and DHW requirements.

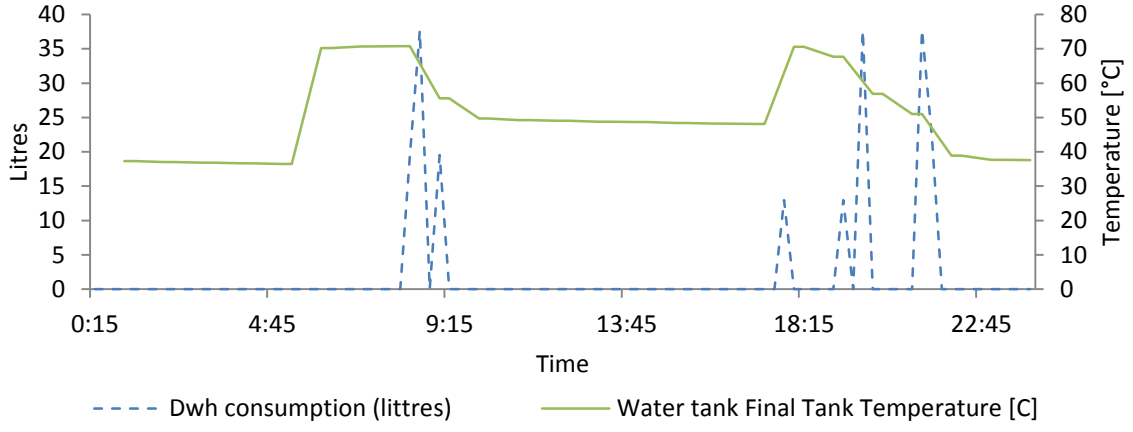

Figure 6.14 Hot water usage profile (150 L hot water tank) and temperature variation inside the tank in a winter weekday in split heat generation mode

6.5.3 Deployment of water tanks with increased capacity and of an auxiliary burner

6.5.3.1 Deployment of water tanks with increased capacity

Possibilities of deployment of hot water tanks with increased capacity and of an auxiliary burner together with the Whispergen unit were additionally investigated in the split heat generation mode of operation.

300L Domestic hot water tank

The increased volume of the DHW tank requires considerably more time to reach the thermostat setting, however a single charge might be sufficient for covering the daily DHW requirements. The 300 L DHW tank was incorporated into the model instead of the 150 L one and Figure 6.15 and Figure 6.16 show the operation of the system during a winter weekday.

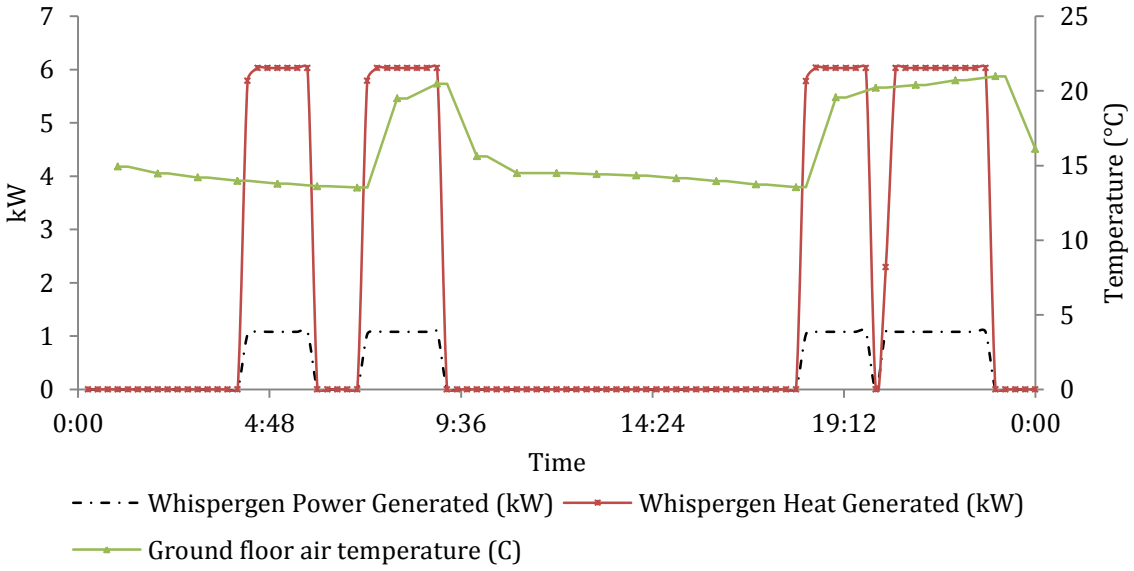

Figure 6.15 Heat and power generation by Stirling mCHP in winter weekday in split heat generation mode with a 300 L water tank

It can be seen in Figure 6.15 that a longer mCHP operation is required for charging a new hot water tank prior to the morning space heating. However, overall no significant variation in total tank charging time was observed compared to the case with 150 L water tank scenario.

Figure 6.16 shows the temperature variation of water in the new tank and the DHW consumption profiles during a winter weekday.

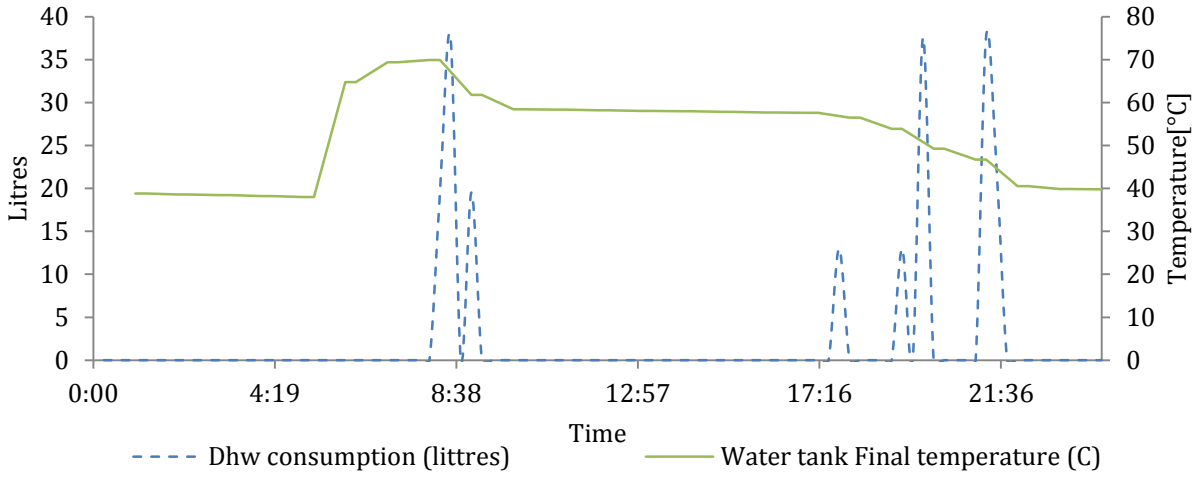

Figure 6.16 Hot water consumption from 300 L water tank and variation of the tank temperature in a winter weekday

It can be seen in this diagram that the water temperature is higher even after the last consumption event which means that additional DHW demand could therefore be met, if required.

380L Domestic hot water tank

An attempt was made in simulations to optimise the volume of the water tank so that the temperature of the water is maintained at the 45 °C level after the last consumption event. A number of tanks with different capacities were simulated. The obtained results predicted that for the above purpose the volume of the water tank should be further increased to 380 L. Figure 6.17 shows the operation of the Stirling engine mCHP unit with the 380 L water tank during a winter weekday.

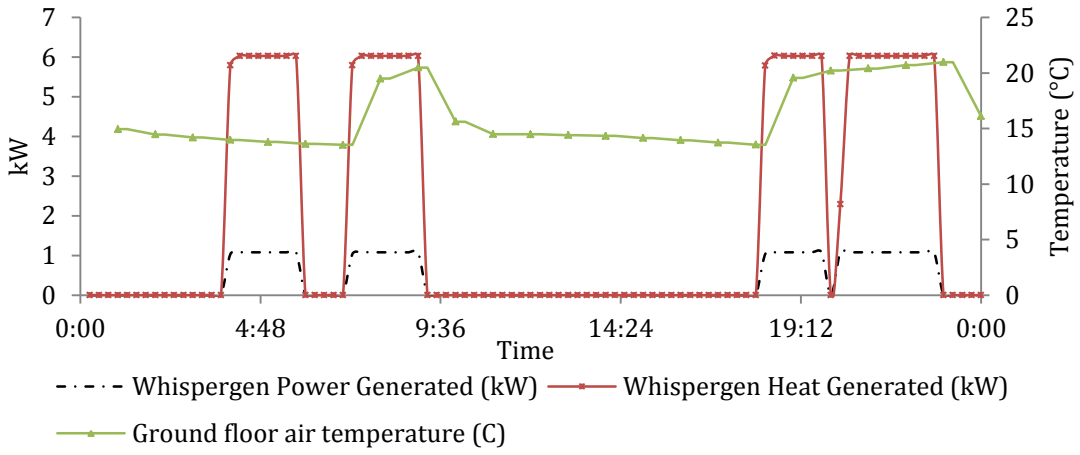

Figure 6.17 Heat and power generation by Stirling mCHP in a winter weekday in split heat generation mode with a 380 L water tank

Figure 6.17 shows that an operation for approximately 2 hours was required in order to reach requested water temperature (70 °C) within the 380 L water tank. Such a long operation enhances the power generation by the mCHP but with a significant drawback, namely it increases the fuel consumption. Figure 6.18 shows the temperature fluctuations inside the tank and the hot water consumption events. The temperature in the tank after the last hot water demand is still on the required level, as shown in Figure 6.18.

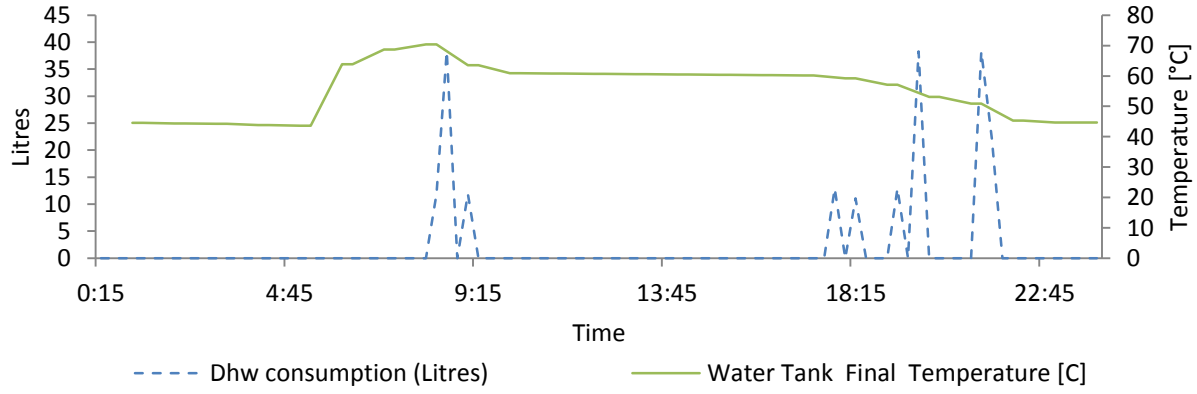

Figure 6.18 Hot water consumption events (with the 380 L water tank) and the temperature variation in the tank in a winter weekday

The Whispergen mCHP was able to satisfy the central heating demand slightly better than in the simultaneous heat generation operation scenario.

The air temperature within the active zones reached the pre-determined 21 °C level, however, during the long period of operation there is a higher cycling frequency can be observed.

6.5.3.2 1 kW_e Whispergen mCHP combined with and auxiliary burner for production DHW

In larger houses the capacity of the Whispergen mCHP will not be sufficient to satisfy both space heating and DHW demands. Therefore within the current model a further configuration where the Stirling engine mCHP is backed-up with an auxiliary boiler was modelled. The system consisted of a gas-fired DHW tank heating burner of the 5 kW_{th} rated output and constant efficiency of 75 %. This additional burner was used for DHW only and the mCHP was used only for the space heating demand.

Calculations show that such the supplementary heating equipment operates in frequent cycles to meet the DHW thermal requirements. Figure 6.19 and Figure 6.20 show the operating characteristics of both the Whispergen and the auxiliary equipment for designed days.

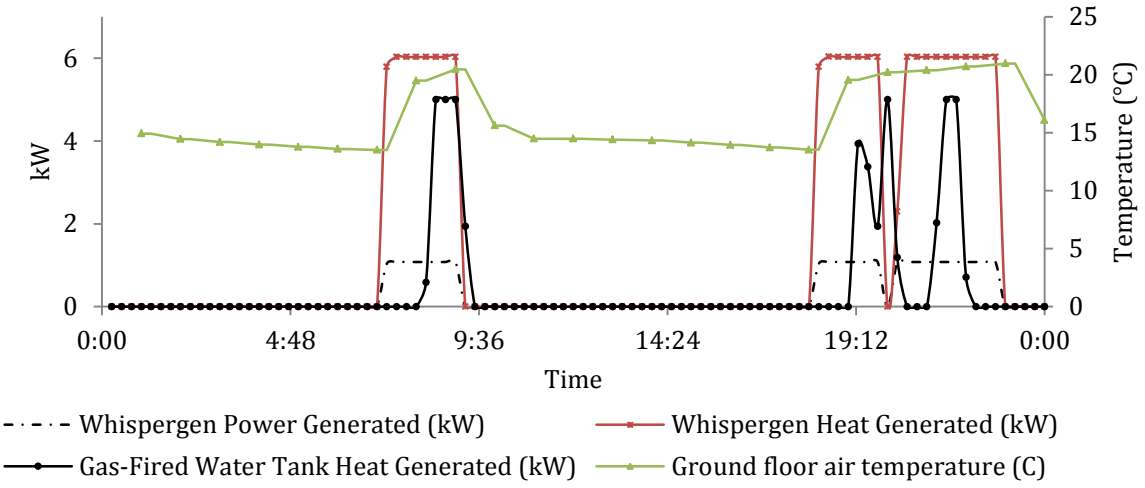

Figure 6.19 Heat and power generation by Stirling mCHP in a winter weekday with a DHW auxiliary burner

The space heating requirements were covered by the mCHP unit and its operation was identical to the split heat generation mode, as it can be seen in Figure 6.19 and in Figure 6.20. Hot water demand was satisfied using a 150 L gas-fired water tank.

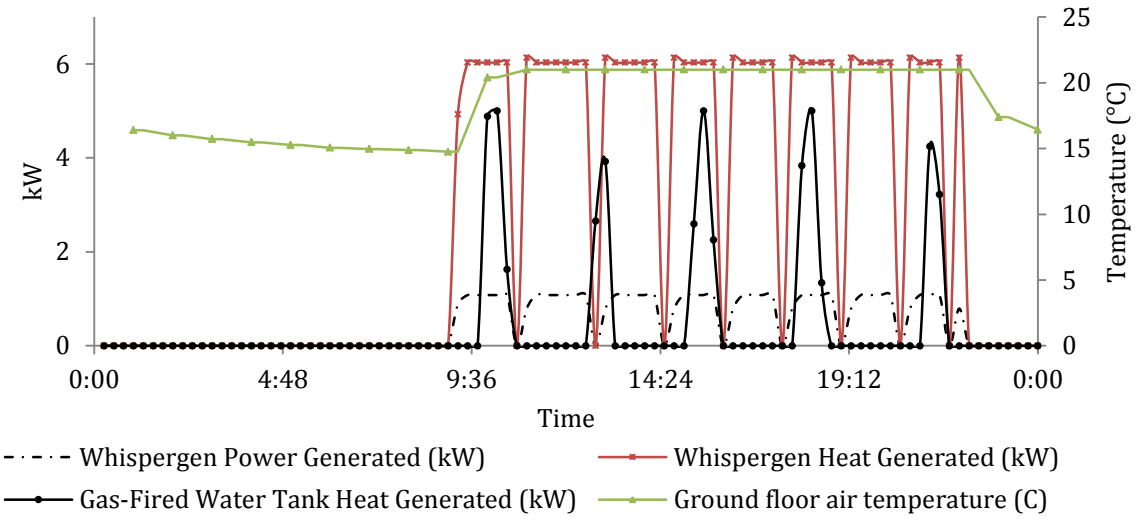

Figure 6.20 Heat and power generation by Stirling mCHP in a winter weekday with a DHW auxiliary burner

Figure 6.21 shows the operation of the gas-fired water tank during a summer period.

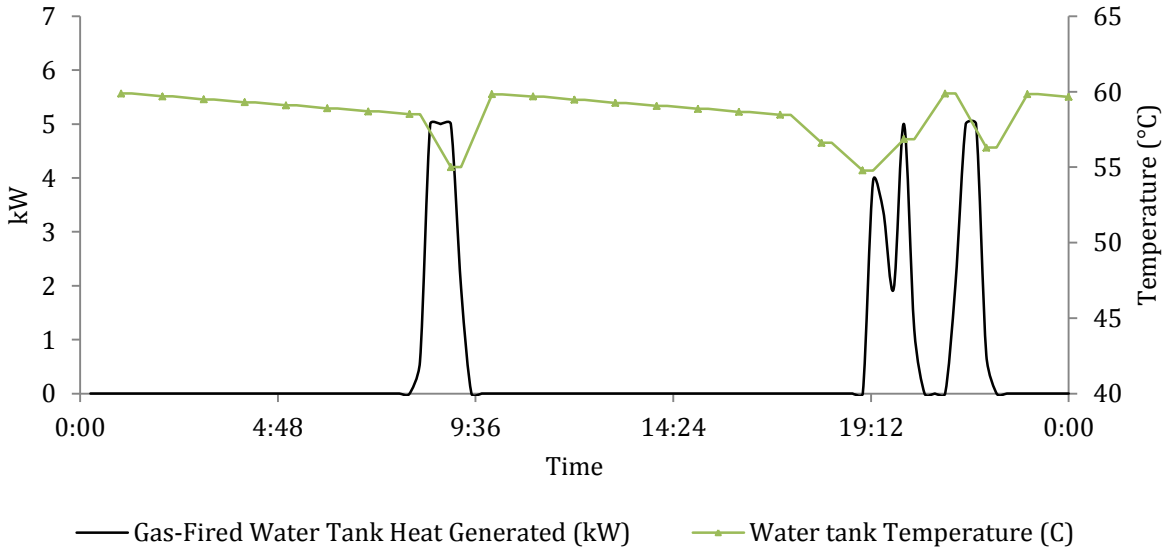

Figure 6.21 Operating of the 150 L gas-fired water tank in a summer week day

It can be seen in Figure 6.21 the auxiliary burner operates in cycles in order to maintain the requested temperature in the tank. It is worth mentioning that in such the system the operation of the Whispergen was limited during the heating season and it didn't operate at all during the summer period. Hence, the annual power generation is significantly decreased.

6.5.4 Power generation

Daily electricity demand profiles derived in Section 6.3.3 were incorporated into the model in order to analyse the flow of power between the dwelling and the local electricity grid. As mentioned above, the Whispergen unit was always was operated in the heat demand-led manner and, therefore, the power generation is a by-product.

Figure 6.22 and Figure 6.23 show the dynamics in the electricity generation, on site consumption and export to the grid for both simultaneous and split heat generation modes in the configuration with a plain (not gas-fired) 150 L DHW tank. A relatively high electricity generation level can be observed for this particular scenario. The thermal capacity of the unit is just enough to cover the total heating requirements and therefore the system is undersized. The continuous operation throughout the heating season and limited cycling frequency has resulted in the high level annual power generation.

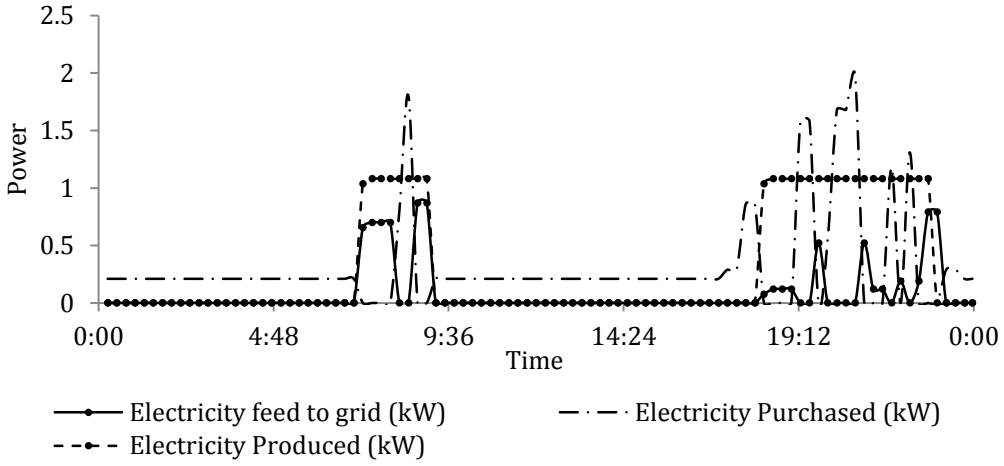

Figure 6.22 Power generation and flows in the dwelling in case of simultaneous heat generation mode in a winter weekday

Figure 6.22 shows that in average 12.25 kWh_e of electricity is consumed in a typical winter weekday with 7 hours of operation of the mCHP. Over that period, the mCHP satisfies 43 % of the daily electricity demand while the remaining amount is imported from the grid. The

electricity generation rate was found to be 0.27 kWh_e at the nominal capacity operation, consequently if consumption is above this rate, electricity was imported. It can be seen that there is a peak at 0.49 kWh_e for the purchased electricity. Despite the moderate electrical capacity of the mCHP, overall 2.2 kWh_e of electricity was exported during the off-peak demand period, which resulted in an electricity generation-to-onsite consumption ratio of 1.42. If the all power generated by the mCHP were utilised onsite, then the Whispergen unit would cover approximately 61 % of the electrical demand in the house.

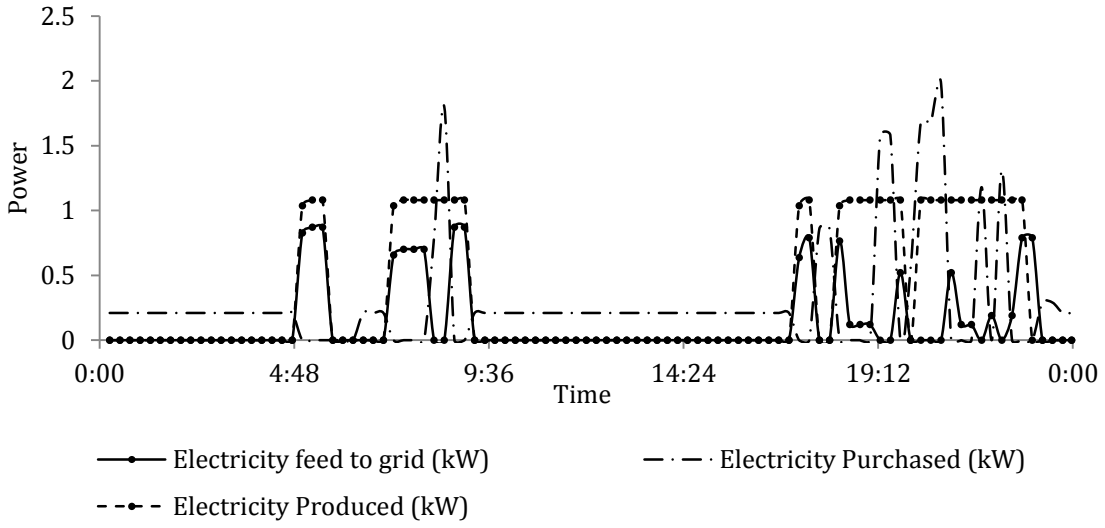

Figure 6.23 Power generation and flows in the dwelling in case of split heat generation mode in a winter weekday

It can be seen in Figure 6.23 that during the split heat generation mode of operation, the run of the Whispergen is extended by 45 minutes in the early morning and by 30 minutes in the early evening (prior to space heating). Therefore the power generated was increased by approximately 1.33 kWh_e. However, this excess of electricity was exported to the grid since the power production did not coincide with the electricity demand. The ratio of electricity production-to-onsite consumption is 1.48 and this is nearly the same as for simultaneous heat generation mode (1.42).

6.5.5 Annual financial benefits and carbon savings

6.5.5.1 Carbon emission reduction

An annual operation of the mCHP was modelled for various scenarios with estimation of environmental performance based on the calculated natural gas consumption and imported and exported amount of electricity. Emissions factors of 0.43 kg CO_2/kWh_e and 0.19 kg CO_2/kWh_{th} were used in calculations [123]. Table 6.3 summarise the environmental impact of deployment of the Whispergen mCHP in the analysed 3-bed semi-detached house.

Table 6.3 Annual carbon emissions

Heating System Configurations	Natural gas consumption related Carbon emissions (Kg)	Electricity consumption related Carbon emissions (kg)	Overall Annual Carbon emissions (Kg)	CO_2 Emission Savings in kg	CO_2 Emissions Savings in %
Condensing Boiler & 150 L WT	2888.29	2038.58	4926.87	/	/
mCHP split generation & 300 L WT	3747.01	1501.91	5248.92	-322.05	-6.54
mCHP simultaneous generation &150 L WT	4389.54	1322.14	5711.68	-784.81	-15.93
mCHP & gas-fired 150 L WT	3595.30	1559.75	5155.05	-228.17	-4.63
mCHP split generation & 150 L WT	3387.38	1507.77	4895.15	31.72	0.64
mCHP split generation & 380 L WT	3920.48	1493.65	5414.13	-165.21	-3.35

It can be seen in Table 6.3 that, in the reference scenario (using conventional condensing boiler) due to the electricity consumption during the operation of the boiler, there is the highest carbon emissions of 2038.6 kg. A very small reduction in the overall carbon emissions (0.64 %) was found for the case of the split heat generation strategy in the system with the mCHP and 150 L DHW tank.

For all other simulated cases the rise in the carbon emissions was predicted with the largest being almost 16 % for the simultaneous heat generation strategy in the system with the mCHP and 150 L DHW tank. In such the strategy the mCHP covers a bigger fraction of the

onsite electricity consumption resulting in the lower electricity related CO_2 emissions. However, overall annual carbon emissions are the highest due to the elevated gas consumption as a result of the continuous operation. When using larger hot water tanks the rise of carbon emissions is attributed to the higher water tank thermal losses and also to the prolonged daily operation [109].

6.5.5.2 Financial benefits

Implementation in the UK the feed-in-tariff rate of 10.5 p per kWh_e [149] has made domestic micro-power generation economically viable technology regardless of whether the electricity is exported to the grid or used on-site. The extended operation period of the mCHP increases the annual power generation and consequently raises the financial benefits, though the elevated gas consumption affects the overall economic performance. In calculation of financial benefits the electricity and gas tariff prices were used in accordance with [150]. It should be noted that the economic savings discussed throughout this work refer to the utility bill reductions only. These estimates were carried out without taking into account the higher capital cost of mCHPs and potentially higher maintenance costs. Table 6.4 summarises the annual results in terms of utility bills reductions compared to the reference system (the condensing boiler and 150 L DHW tank).

Table 6.4 Annual financial benefits

Heating System Configurations	**Gas Consumption** (£)	**Electricity Consumption** (£)	**Feed-in Tariff** (£)	**Net Annual Expenses** (£)	**Savings** (%)
Condensing Boiler & 150 L WT	616.24	617.16	/	1233.40	
mCHP split generation & 300 L WT	771.83	487.03	219.52	1258.86	15.73
mCHP simultaneous generation &150 L WT	888.25	443.44	261.38	1331.68	13.22
mCHP & gas-fired 150 L WT	744.34	501.05	147.31	1245.39	10.97
mCHP split generation & 150 L WT	706.67	488.45	198.35	1195.12	19.19
mCHP split generation & 380 L WT	803.26	485.03	229.90	1288.28	14.19

It can be seen in Table 6.4 that the deployment of the all systems with the Whispergen unit, as a replacement for the conventional condensing boiler, could provide savings from 10.97 % (the simultaneous heat generation mode with 150 L DHW tank) to 19.19 % (the simultaneous heat generation mode with 150 L DHW tank). In all cases gas bills are increased but overall saving are achieved due to implementation of the feed-in tariff. It should be highlighted that all above calculations were carried out using electricity and gas prices provided in [44]. The additional electricity consumption rate in the condensing boiler was taken in accordance with [38] and this adds approximately 3 % (154 kWh_e) to the electrical demand in the house.

Calculation of annual financial benefits for the scenario of the reduced feed-in tariff

Finally, hypothetical scenarios were investigated in which the feed-in-tariff is reduced to 75 %, 50 %, 25 % and 0 % of the current level. Table 6.5 shows the obtained results for the above reductions in the feed-in tariff.

Table 6.5 Effect of reduction in feed in tariff

Heating System Configurations	Annual Savings £ (75 % of feed-in tariff)	Annual Savings % (75 % of feed-in tariff)	Annual Savings £ (50 % of feed-in tariff)	Annual Savings % (50 % of feed-in tariff)	Annual Savings £ (25 % of feed-in tariff)	Annual Savings % (25 % of feed-in tariff)	Annual Savings £ (Without feed-in tariff)	Annual Savings % (Without feed-in tariff)
Condensing Boiler &150 L WT	/	/	/	/	/	/	/	/
mCHP split generation & 300 L WT	183.26	14.35	128.37	10.05	73.49	5.75	-25.46	-1.99
mCHP simultaneous generation & 150 L WT	141.82	11.10	76.48	5.99	11.13	0.87	-98.28	-7.69
mCHP & gas-fired 150 L WT	142.56	11.16	105.73	8.28	68.90	5.39	-11.99	-0.94
mCHP split generation & 150 L WT	231.12	18.09	181.53	14.21	131.94	10.33	38.28	3.00
mCHP split generation & 380 L WT	161.61	12.65	-24.24	-1.90	-26.83	-2.10	-29.43	-2.30

Reductions in the current feed-in-tariff (this scheme presumes that austerity measures could be applied in case of economic recession) result in a decrease in the annual expenditure savings. For the case when 75 % of the current feed-in tariff is implemented only the system with the mCHP operating in the split heat generation mode and with 380L DHW tank start to generate financial losses. Only the system with the mCHP operating in the split heat generation mode and with 150 L DHW tank will still provide small savings when the feed-in tariff is withdrawn but pay-back period would become unfeasible for end-users.

6.5.6 Conclusions

The deployment of the Whispergen MkVb 1 kW_e Stirling engine mCHP in a typical 3-bed 2 storey semi-detached house was investigated in different configurations of the heating system and modes of operation. Two main operating modes were modelled, namely the simultaneous space heating and DHW generation and split space heating and DHW heat generation. The annual performance of the mCHP system was evaluated and compared to the reference scenario (the conventional condensing boiler-based heating system). It was found that the rated output of the Whispergen unit was barely enough to fully satisfy space heating and DHW demands during the winter season (December-February) with delays in reaching the pre-set temperature of 21 °C in leaving zones. However, the unit demonstrated high cycling frequency during operation in winter weekends and in the spring-autumn periods.

- During simultaneous heat generation regime the system with the mCHP and 150 L DHW tank operating in the mode of the simultaneous heat generation provides economic savings of £261 at the current level of the UK feed-in-tariff but increases the carbon emissions by about 16 %;
- During split heat generation mode the system with the mCHP and 150 L DHW tank operates for longer periods thus generating more electricity but also consuming more fuel at lower efficiency. The economic savings were predicted to be £244 when the current

feed-in tariff is applied with very small carbon savings (0.64 %). This configuration of the system and mode of operation is found to be the most feasible of all system configurations analysed.

- If the feed-in tariff is withdrawn in future then using the Wispergen mCHP system will become fiscally unattractive.

6.6 Comparison of deployment of various mCHP technologies in a typical 3-bed semi-detached house

The Stirling engine mCHP features relatively high thermal efficiency and therefore is considered to be an attractive alternative for replacing a conventional boiler in domestic heating systems. mCHP technologies based on ICE and PEM fuel cell have considerably higher electrical efficiencies (up to 50 % for the fuel cell) and shorter transients processes which will affect performance of the heating systems and annual financial savings and carbon emissions of the house. Deployment of the commercially-available ICE based mCHP from Honda (Ecowill) [118] with the electrical output, identical to that of the Whispergen unit, but lower thermal output (2.8 kW_{th}) with very short transient processes is consider in this section. However, the low thermal output of this ICE mCHP requires an additional boiler to operate in parallel in order to satisfy dwellings heating requirements.

Furthermore, the deployment of the 1 kW_e PEM fuel cell based mCHP is also simulated. A substantial advantage of the fuel cell is zero carbon emissions when it is fuelled with pure hydrogen. It can be also operated using natural gas but in this case the gas-to-hydrogen reformer should be included into the system. Since the PEM fuel cell mCHP has very high electrical efficiency and low thermal output then an additional burner is also necessary to be included to satisfy heating demands in the house. Table 6.6 shows the technical specifications of these two mCHP unit systems, compared to those of the Whispergen mCHP.

Table 6.6 Specifications of mCHP systems

mCHP	Electrical output (kWe)	Thermal output (kWth)	η_e	η_{th}
Honda Ecowill	1	2.8	22.5	63
Whispergen	1	6	12	67
Hilton PEM FC	1	0.8	43	37

6.6.1 Deployment of the Honda Ecowill mCHP with the auxiliary boiler

Previous simulation results for the heating system with the Whispergen mCHP predicted that better performance would be obtained in the split heat generation mode. Prolonged operation increases the energy savings due to the higher level power generation. Analysis of the deployment of the Honda Ecowill mCHP was also conducted for the split heat generation mode since the thermal output of the ICE mCHP is not sufficient for operation in the simultaneous heat generation mode. The ICE mCHP by Honda has approximately twice the electrical efficiency of the Stirling engine mCHP, but significantly lower rated thermal output. A 10 kW_{th} auxiliary boiler (the efficiency of which is assumed to be 85 %) was used in simulations to cover the heating requirements. Figure 6.24 illustrate the schematic configuration of the domestic heating system with the ICE mCHP and auxiliary burner used for simulations.

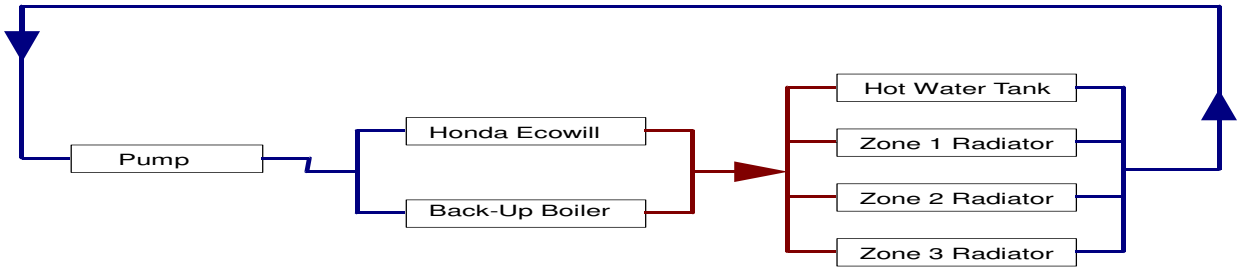

Figure 6.24 Schematic of the domestic heating system with the Honda mCHP and auxiliary boiler

One hour prior to both morning and evening space heating periods, the mCHP unit was run without the additional back-up boiler to generate heat for charging the hot water tank only.

For covering space heating demand, the back-up boiler was used in parallel with the mCHP. Results show that during relatively warm days (i.e. in September) the heating output from the Honda Ecowill was found to be maintain the zone temperature on the pre-set level. Figure 6.25 shows the operation of the ICE mCHP during a winter weekday.

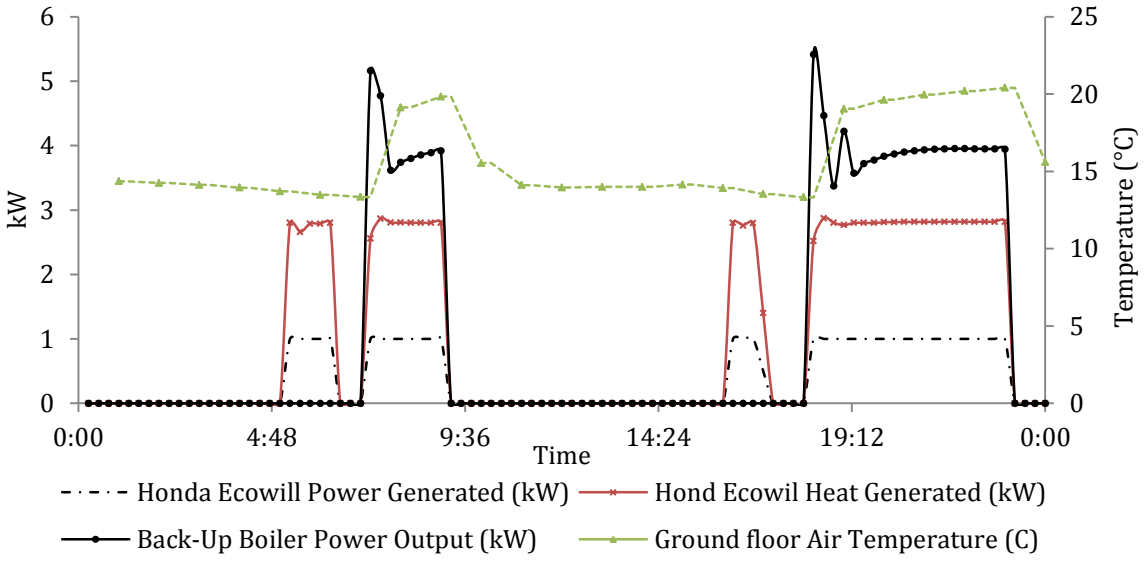

Figure 6.25 Operation of Honda Ecowill mCHP with auxiliary boiler on a winter weekday

Figure 6.25 show that the operation of the ICE mCHP unit dynamically follows the active occupancy pattern throughout the day. Small fluctuations in both thermal and electrical outputs were obtained in simulations. When heat is required for hot water tank charging only, the operation of the mCHP at a steady level to meet the demand was observed. When space heating was required, the auxiliary boiler generated additional heat in the range of 5-5.5 $kW_{th.}$ Such the particular operation resulted in a faster warm-up of the circulating water. Once the space heating set point was approached, a sharp drop in the boiler heat production occurred. Fluctuations in the thermal output of the boiler can be seen during its evening operation. Such unstable operation lasted for approximately 1 hour. Further investigations into the flow and return temperatures of both space and DHW heating systems explained this variation. The ICE mCHP unit was operating at its maximum electrical and thermal capacity and when the return temperature of the water dropped (due to the decrease in the air temperature inside the

heating zones during a rapid increase in ventilation, etc.), the thermal output of the boiler was increased. Figure 6.26 shows the water temperature fluctuations in the space heating circuit and it can be seen that peaks in the flow temperature of the boiler and boiler thermal output occur simultaneously.

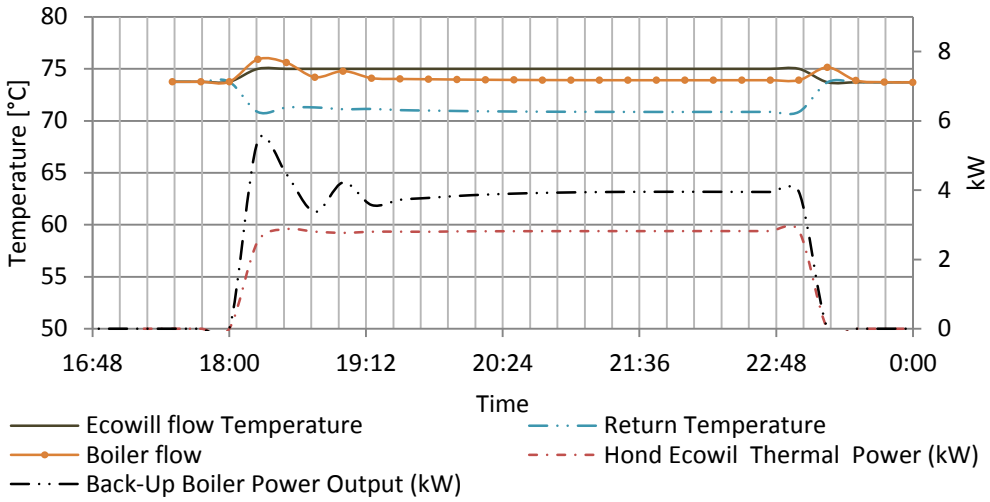

Figure 6.26 Fluctuation in the water loop temperature during the Honda Ecowill mCHP operation

However, the water flow temperature in the mCHP system remained constant during its operation and therefore fluctuations in the shared return water temperature mainly affected the boiler's heating output. Combining different heat supply equipment such as a boiler and mCHP or even different mCHP technologies may cause a prolonged transient start-up time period. Internal start-up diagnostic tools, individual capabilities of reaching the designed flow temperature, responses to changing in the thermal demand, could lead to a sharp decrease in the shared water return temperature and cause fluctuations in the thermal outputs. The precise pattern of output variations in a practical installation would depend on the plumbing and plant control. This was demonstrated in experimental results obtained on the Baxi SenerTec Dachs unit (presented in Section (5.3)).

6.6.2 Hilton PEM Fuel Cell and auxiliary burner

The use of pure hydrogen in PEM fuel cell mCHPs is not currently a feasible option therefore they should be equipped with a natural gas reformer. If a gas reformer is used there will be a significant drop in the overall system efficiency due to losses in the reforming process. In simulations hydrogen was used as fuel for the fuel cell and the annual performance results were summarised in terms of hydrogen and natural gas consumption. The conversion factor used in annual performance calculations was taken from experimental data obtained in a PEM FC coupled with a reformer as described in the following Sub-Section (selection of efficiency). The PEM fuel cell used in simulations is considered to have partial thermal and electrical efficiencies equal to 31 % and 43 %, respectively, and a heat-to-power ratio close to 1. The PEM fuel cell with a 1 kW_{th} thermal output was combined with the auxiliary boiler identical to that used for the ICE mCHP simulations. Figure 6.27 shows the operation of the PEM fuel cell mCHP with the auxiliary burner in a winter weekday for space heating.

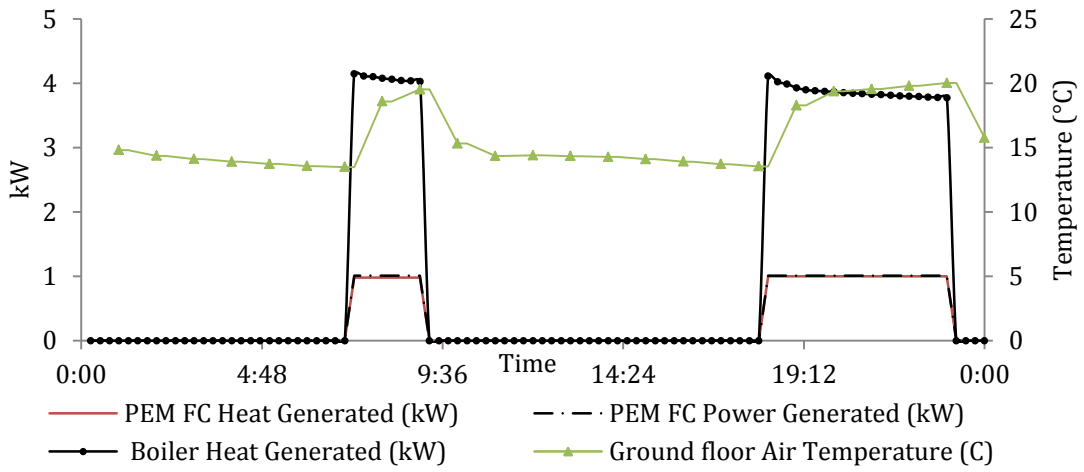

Figure 6.27 Operation of PEM FC mCHP with additional boiler for space heating in a winter weekday

Small fluctuations in heat produced by the boiler can be observed in Figure 6.27 because the heat generated by the FC mCHP does not cause sharp changes in the flow and return water temperatures. Simulations of the operation of the FC mCHP charging only the 150 L hot

water tank also was carried out, indicating a continuous operation of the FC throughout the day in order to maintain the pre-set temperature in the domestic hot water. For this reason the split heat generation mode (which was used for previously considered mCHPs) could not be implemented and thus was excluded from the fuel cell mCHP simulations. The fuel cell based mCHP in conjunction with the auxiliary boiler was used only for space heating instead. The domestic hot water demand was covered by a gas-fired water tank as described in Section (6.5.3.2)

Reforming process: Selection of efficiency

When PEM FC mCHPs are deployed domestic heating systems they normally should be coupled to a natural gas reformer. Several reforming processes in which natural gas is converted into hydrogen are available. The steam gas reforming process, auto thermal and membrane reforming processes are considered to have good market potential. The steam gas reforming process is commonly used in the PEM fuel cells for domestic applications. The low temperature FCs that are used in mCHP systems have a low tolerance for a CO content and only the steam reforming process can provide reach in hydrogen syngas.

A number of research projects have been performed on the reforming process evaluations. Experimental results obtained indicate that in steady-state conditions the efficiency of reforming processes are between 70 and 83 % [102-104, 107]. However, a long time is required in order for a reformer to reach the operating temperature of more than 600 °C. During the start-up transient process which lasts for about 90-100 minutes there is no hydrogen production [101, 103, 105]. When the whole cycle is taken into consideration, the efficiency of the process is reduced to 55 % [101]. The heat released during the start-up time from the combustion of the natural gas could be used for space heating. The heat that could be recovered during the reforming process can increase the co-generating efficiency by 14.8-

15.5 %, depending on the operating capacity of the reformer (20 %-100 %) [100]. Assuming that all the heat from the reforming process could be recovered and using the dynamic efficiency of 55 % [101], the overall efficiency of the reforming process can be taken as 70 %. This reforming efficiency value can be then used to convert the hydrogen consumption into natural gas consumption.

6.6.3 Annual financial benefits and carbon savings

6.6.3.1 Carbon emission reduction

Table 6.7 presents obtained results on the environmental performance of the mCHP units based on different technologies including the fuel cell mCHP. The obtained annual hydrogen consumption was converted into the natural gas consumption using the conversion factor of 0.70, as it was discussed above.

Table 6.7 Carbon emissions reduction for different mCHPs

mCHP system configurations	Natural gas Related Carbon emissions (kg)	Electricity Related Carbon emissions (kg)	Annual Carbon emissions (Kg)	Emission Savings (%)
Boiler & 150 L DHW tank	2888.29	2038.58	4926.87	/
1 kW_e Whispergen & 150 L DHW tank	3387.38	1507.77	4895.15	0.64
1 kW_e Honda Ecowill with Back-up Boiler & 150 L DHW tank	2949.06	1335.15	4284.21	13.04
1 kW_e Hilton PEM FC with Back-up Boiler & 150 L DHW tank	3453.56	1443.51	4897.07	0.60

It can be seen that from the range of mCHP technologies, only the 1 kW_e Honda Ecowill unit with a back-up boiler and 150 L DHW tank in the domestic heating system provides noticeable carbon savings (about 13 %) with other two technologies making a negligible positive impact on the environment.

6.6.3.2 Financial benefits

Table 6.8 shows results obtained the annual financial benefits calculated for different mCHP technologies deployed in a typical 3-bed 2 storey semi-detached house. The current UK feed-in tariff rate was used in estimations. The natural gas and electricity prices are the same as used in Section 6.5.5.

Table 6.8 Annual utility cost savings using different mCHPs

mCHP system configurations	Gas Consumption (£)	Electricity Consumption (£)	Feed-in tariff (£)	Annual Expenses with feed-in tariff included (£)	Savings (%)
Boiler & 150 L DHW tank	616.24	617.16	/	1233.40	/
1 kW_e Whispergen & 150 L DHW tank	706.67	488.45	198.35	1195.12	19.19
1 kW_e Honda Ecowill with Back-up Boiler & 150L DHW tank	627.25	446.59	267.80	1073.85	34.65
1 kW_e Hilton PEM FC with Back-up Boiler & 150 L DHW tank	718.66	472.87	217.20	1191.53	21.00

It can be seen in Table 6.8 that the highest amount of power generation is achieved using the Honda mCHP resulting in 34.65 % savings in gas and electricity bills compared to about 20 % savings achieved by the PEM FC and Whispergen mCHPs. Lower saving are due to the longer start-up in the SE mCHP and the low conversion efficiency of the reforming process in the FC mCHP.

6.7 Modelling of deployment of IC and Stirling engine mCHP technologies in dwellings with increased heat and electricity demands

The advantages of replacing a conventional heating system with three mCHP technologies have been previously established in this work for a typical 3-bed 2-storey semi-detached house in the UK. There is a broad diversity of dwellings in the UK in terms of satisfying Building regulations and electricity and heat demands. In this section an attempt has been made to consider deployment of various IC and Stirling engine mCHP technologies in such different types of dwellings and evaluate economical and environmental impacts. A number

of cases in which the electricity demand is increased by 20 % and the hot water demand is increased by 50 L per day (i.e. incorporating a 200 L water tank) were analysed. The scenarios aimed to simulate a higher energy requirement in the buildings. Energy demand profiles were applied to two different dwellings, namely a detached house satisfying 2006 construction regulations and a semi-detached house satisfying 1996 construction regulations. mCHP systems deployed in models are based either on Stirling or IC engines and featuring a nominal electrical capacity in the range of 2-3 kW_e. Table 6.9 shows the details of scenarios investigated in this section.

Table 6.9 Matrix of scenarios of mCHP deployment

Electricity Demand	**Annual Electricity demand of 4.6 MWh_e**		**Hot Water Demand 200L Daily 150 L water tank**
Heat Demand	**Detached house, 2006 building regulations**	**Semi-detached house, 1996 building regulations**	
Heating system configuration	Boiler	Boiler	
	2 kW_e Stirling mCHP	2 kW_e Stirling mCHP	
	3 kW_e ICE mCHP	3 kW_e ICE mCHP	
	3 kW_e Disenco Stirling mCHP	3 kW_e Disenco Stirling mCHP	
Electricity Demand	**20 % increase in Electricity demand**		
Heat Demand	**Detached house, 2006 building regulations**	**Semi-detached house, 1996 building regulations**	
Heating system configuration	2 kW_e Stirling mCHP	2 kW_e Stirling mCHP	
	3 kW_e ICE mCHP	3 kW_e ICE mCHP	
	3 kW_e Disenco Stirling mCHP	3 kW_e Disenco Stirling mCHP	

Electricity Demand	**Annual Electricity demand of 4.6 MWh**		**200 L Water Tank**
Heat Demand	**Detached house, 2006 building regulations**	**Semi-detached house, 1996 building regulations**	
Hot Water Demand	**25 % increased Hot water profile**	**25 % Increased Hot water profile**	
Configuration	2 kW_e Stirling mCHP	2 kW_e Stirling mCHP	
	3 kW_e ICE mCHP	3 kW_e ICE mCHP	
	3 kW_e Disenco Stirling mCHP	3 kW_e Disenco Stirling mCHP	

6.7.1 Proposed Cogeneration units

There are two commercially IC engine based mCHPs, namely 1kWe Honda Ecowill and 5.5 kW_e SenerTech Dachs. Two additional IC engine based mCHP were considered in the modelling process, namely with 2 and 3 kW_e outputs, respectively (Proposed 1 and Proposed 2 mCHPs in Table 6.10 with 5.3 kW_{th} and 7.5 kW_{th} thermal outputs). These proposed mCHPs, as 1 kW_e Honda Ecowill, were assumed to have the same dynamic characteristics as experimentally tested 5.5 kW_e SenerTech Dachs.

There are two commercially available Stirling mCHPs, namely 1 kW_e Whispergen and 3 kW_e Disenco, see Table 6.10. An additional Stirling engine based mCHP was considered in simulations, namely with 2 kW_e output (Proposed 3 mCHP in Table 6.10 with 10 kW_{th} thermal output). Proposed 3 and Disenco mCHPs were assumed the same dynamic characteristics as the tested 1kW_e Whispergen unit).

Table 6.10 Specifications of available and proposed mCHP systems based on Stirling and IC engines

ICE mCHP	Electrical output (kW)	Thermal output (kW)	Electrical Efficiency	Thermal Efficiency	Heat/Power
Honda Ecowill	1	2.8	22.5	63	2.8
SenerTechDachs	5.5	12.3	27	66	2.3
Proposed 1	2	5.3	23.7	63	2.68
Proposed 2	3	7.5	24.5	64.7	2.57

Stirling mCHP	Electrical output (kW)	Thermal output (kW)	Electrical Efficiency	Thermal Efficiency	Heat/Power
Whispergen	1	6	12	67	6
Disenco	3	12	18.4	73.6	4
Proposed 3	2	10	15.2	70.3	5

The specifications of the market available units are shown in grey shaded cells in Table 6.10 and the proposed mCHP capacities were determined using linearly interpolated capacities of the commercially-available equipment.

6.7.2 Simulations of the detached house with the annual electricity demand of 4.6 MWhe and satisfying 2006 UK construction regulations

A detached two-storey house with 160 m2 of total floor area and 6.1% glazing of the gross external wall area was used in simulations. Figure 6.28 shows the design of the building. It was modelled with five individual energy zones and insulation levels in accordance with the UK building regulation of 2006 [147]. The design was based on the actual house for witch details can be found in [151]. The simulation results throughout a year of the house with the conventional heating system produced data on annual gas and electricity costs which were compared with the owners' utilities bills and results were found to be in good agreement. The alternative heating systems incorporating 2 kW_e Stirling engine mCHP, 3 kW_e ICE mCHP and 3 kW_e Stirling mCHP (Disenco) theoretically modelled.

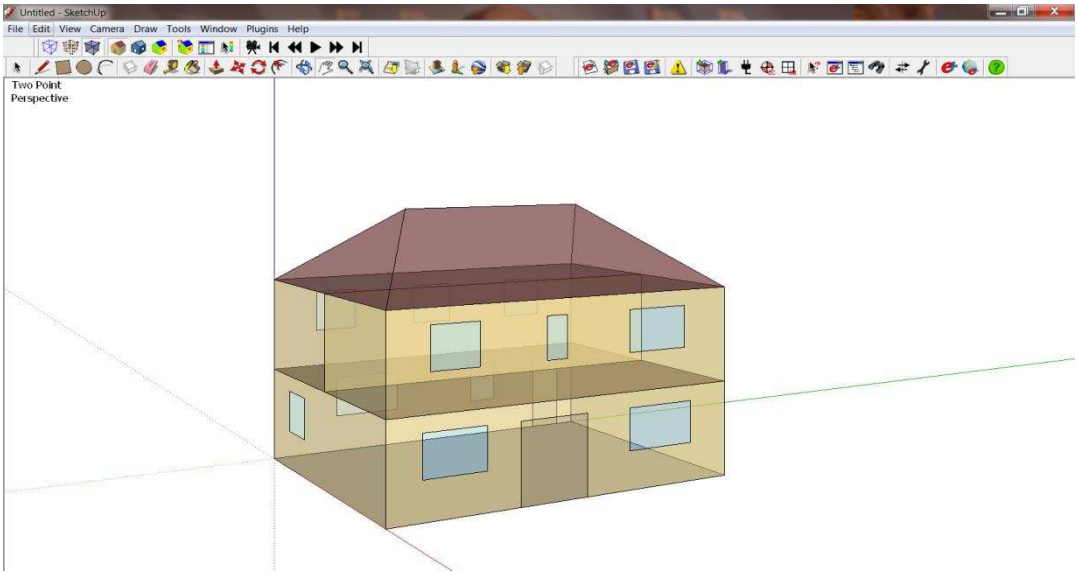

Figure 6.28 Detached house satisfying 2006 UK construction regulation used for theoretical modelling

Figure 6.29 shows results on the operation of the conventional heating system in the detached house. Simulations of a conventional heating system were conducted on both a daily and annual basis. In the average winter design day, 9 kW_{th} of thermal output is required to satisfy the space heating demand. However, in colder winter days peaks between 13-14 kW_{th} in the

thermal output of the boiler were necessary to maintain 21 °C air temperature in living spaces. These results are found to be in good agreement with the data presented in [151].

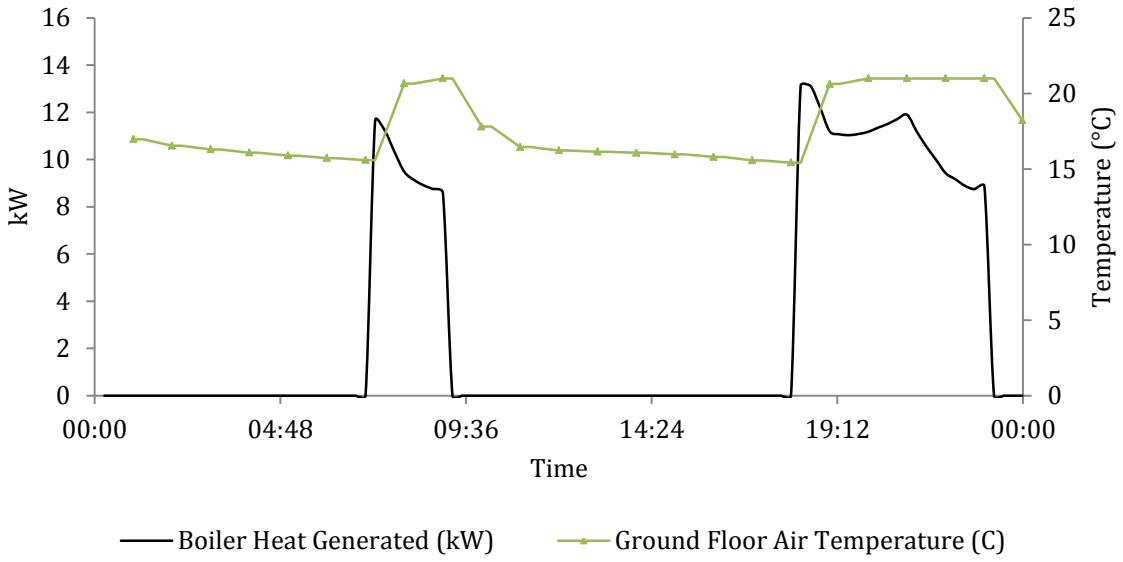

Figure 6.29 Boiler heat generation and ground floor air temperature in the detached building satisfying 2006 construction regulations

6.7.3 Modelling of operation of mCHP units in the detached house with the annual electricity demand of 4.6 MWhe and satisfying 2006 UK construction regulations

Using the details in the Table 6.10, the operation of cogeneration systems was modelled. Figures 6.30-6.32 show results of simulations during the heating season for all mCHP alternatives in Table 6.10. All simulations were conducted for operation in the split heat generation pattern mode in a winter week day.

For the sake of simplicity and due to the fact that both buildings have the similar space heating requirement, the operation of the cogeneration units in the detached house satisfying the 2006 building regulations are presented. The operation of the mCHP systems in the semi-detached house satisfying the 1996 building regulations was found to be very close (the obtained results are presented in the Appendix (B)).

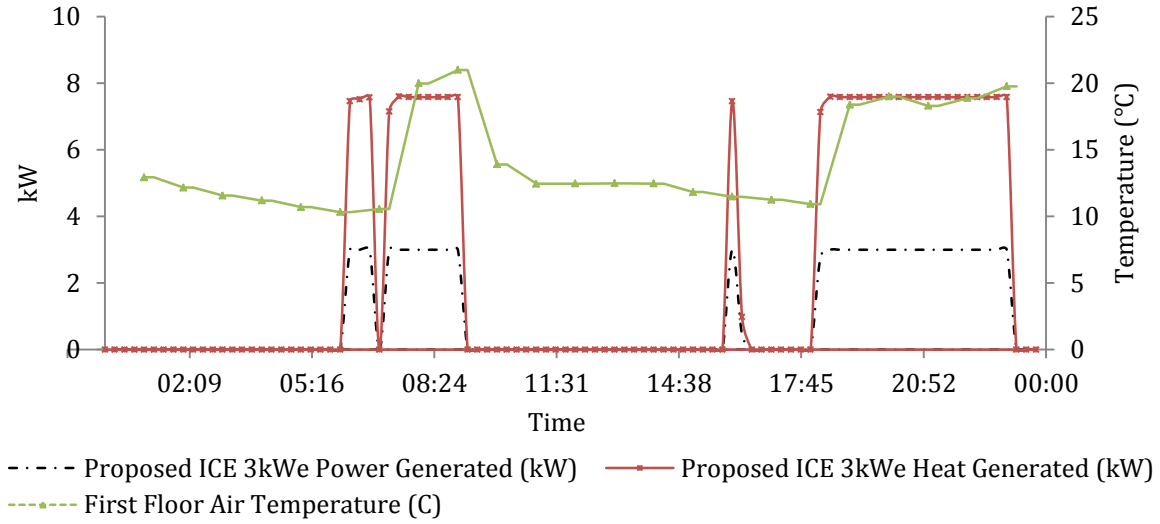

Figure 6.30 Operation of the 3 kW_e IC engine mCHP in a winter weekday in split heat generation mode with a 150 L water tank and water consumption of 200 L per day

It can be seen in Figure 6.30 that there is a continuous operation at nominal electrical and thermal capacities of 3 kW_e and 7.8 kW_{th}, respectively, in the winter design weekday.

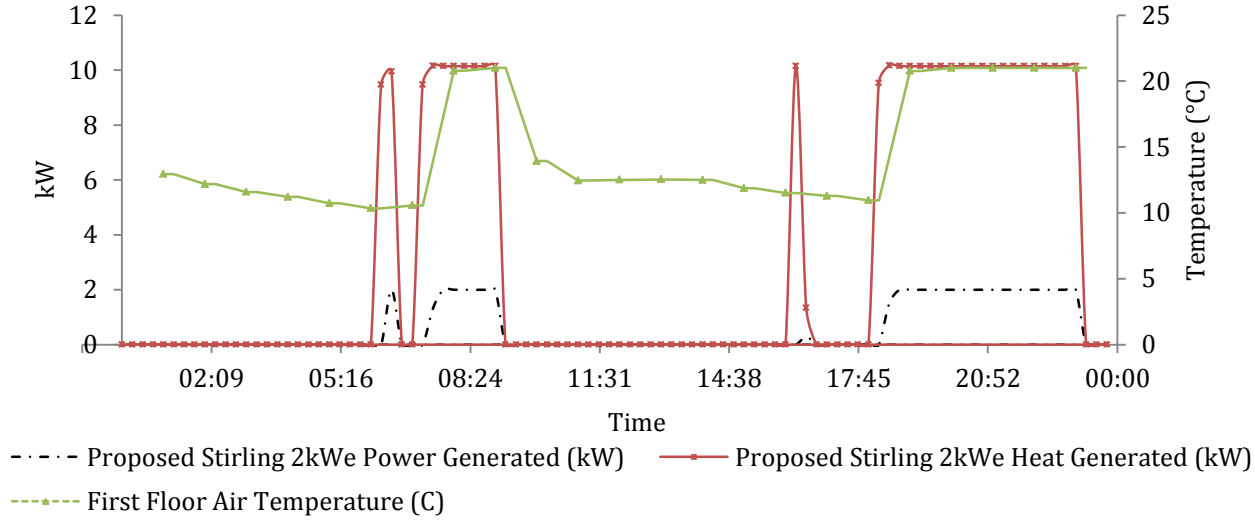

Figure 6.31 Operation of the 2 kW_e Stirling engine mCHP in a winter weekday in split heat generation mode with a 150 L water tank and water consumption of 200 L per day

It was also noted in Figure 6.31 that there is no switch-off events (excluding the switch off after tank was charged) and this suggests that the space heating requirements are not

completely covered because the thermal comfort within zones was not quite reached, especially during the evening period.

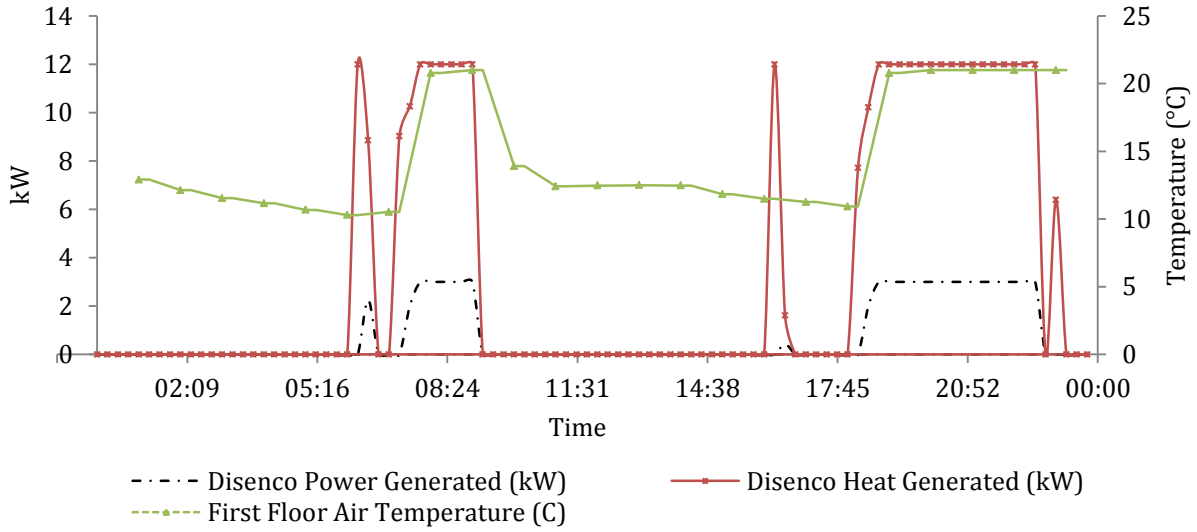

Figure 6.32 Operation of the 3 kWe Disenco Stirling engine mCHP in a winter weekday in the split heat generation mode in the detached house with a 150 L water tank and water consumption of 200 L per day

In Figure 6.31 and in Figure 6.32 it can be observed that both Stirling engine based mCHP systems feature the higher heat-to-power ratio**.** Approximately 10 kW_{th} heat is generated by the 2 kW_e Stirling mCHP, whereas the Disenco mCHP generates a 12 kW_{th} heat output. Both units operate consistently following the occupancy period and there are no fluctuations in heat and power generation. One switching-off event can be seen at the end of evening space heating operation in Figure 6.32, suggesting that Disenco mCHP has a capacity to easily satisfy the heating requirement in the house.

From results presented in Figure 6.30 to Figure 6.32 it is evident that all mCHP systems considered operate at the maximum capacity and switch-off events are avoided with the thermal demand fully covered in case of Stirling mCHPs.

6.7.3.1 Calculation of economical and ecological benefits from deployment of the mCHPs in the detached house with the annual electricity demand of 4.6 MWhe and satisfying 2006 UK construction regulations

The energy demand profiles described in Sections (6.3.3) and (6.3.4) were applied for modelling in the previous section (i.e. the base house scenario – the 4.6 MWh_e annual electricity demand and 200 L per day of the hot water demand). Simulations were performed in the split heat generation mode and for the heating system with the 150L DHW tank. Table 6.11 shows the annual reductions in the carbon emissions and natural gas and electricity cost savings for the considered mCHPs. The current feed-in-tariff scheme can be applied for mCHPs with the nominal electrical output of ≤ 2 kW_e. Therefore, in calculations of the FIT payments for the 3 kW_e mCHP units the summative power generation was 33 % decreased.

Table 6.11 Prediction of the annual CO_2 and fuel & electricity cost reductions for the base house scenario

Heating system configuration	Savings in costs (%)	Savings in carbon emissions (%)
Boiler & 150 L DHW tank	/	/
2 kW_e Stirling mCHP & 150 L DHW tank	**20.99**	**-1.99**
3 kW_e ICE mCHP & 150 L DHW tank	**33.05**	**-1.85**
3 kW_e Disenco mCHP & 150L DHW tank	**20.96**	**-0.059**

It can be seen in Table 6.11 that the prolonged operation of the 3 kW_e IC engine mCHP resulted in the highest reduction in fuel & electricity costs (due to increased power generation). The higher thermal efficiency of the 3 kW_e Disenco Stirling mCHP explains the lowest negative environmental impact.

6.7.4 Simulations of the detached house with the increased electricity demand and satisfying 2006 UK construction regulations

To simulate such the scenario the nature of the electricity demand distribution throughout a typical day was kept unchanged but the amplitude of energy consumption at each time-step was multiplied by a factor of 25 % to explore how economical and ecological impacts are

sensitive to the increase in the electrical consumption. Such procedure resulted in the increase in the annual electricity consumption to 5.5 MWh_e. Figure 6.33 and Figure 6.34 show the increased electricity consumption graphs for weekdays and weekends, respectively.

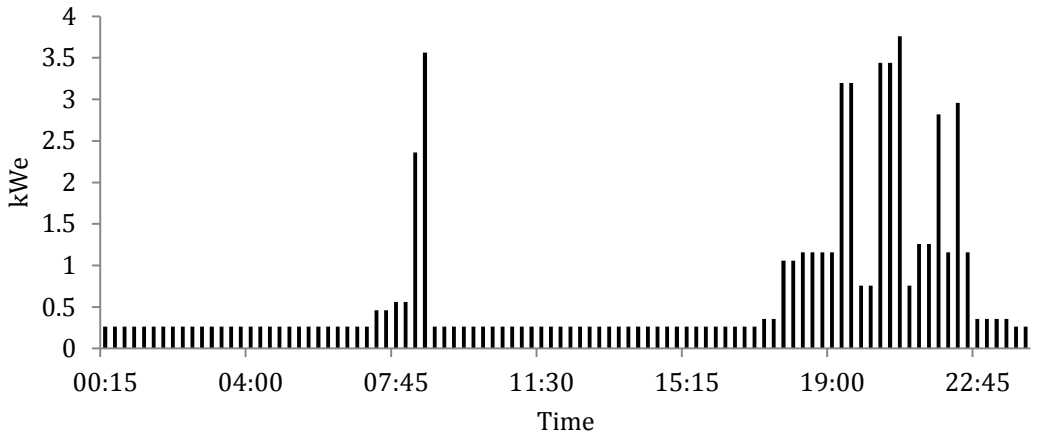

Figure 6.33 Increased electricity consumption profile during a weekday

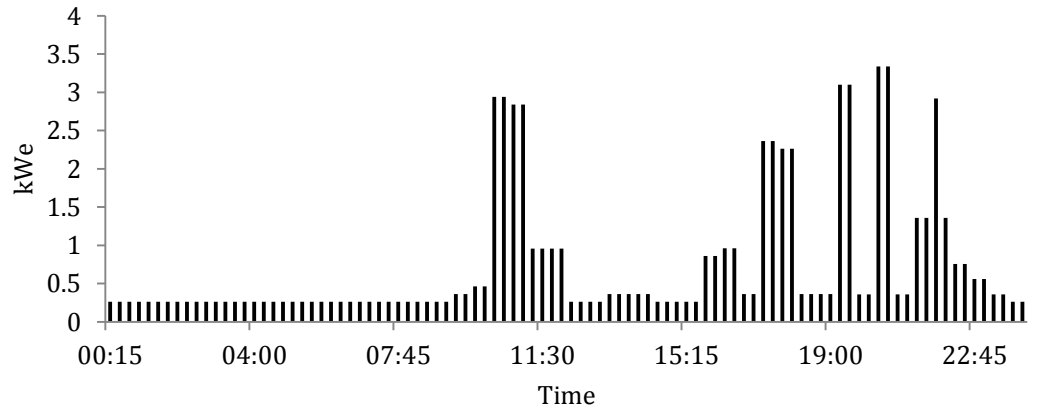

Figure 6.34 Increased electricity consumption profile during weekends

A new peak of consumption is approximately 0.94 kWh_e (see Figure 6.33) whereas the maximum electricity consumption peak in the base scenario was 0.76 kWh_e. In addition the base load is now increased by 0.01 kWh_e for both design days. The operation of mCHP systems was unaffected by the increase in the electricity consumption since they are heat-lead. However, the on-site electricity utilisation and the import and export of electricity were significantly affected. Figure 6.35 to Figure 6.37 show the variation in the on-site electricity

consumption and electricity imported and received from the grid for the 3 kW_e Disenco, 3 kW_e ICE and 2 kW_e Stirling engine mCHPs.

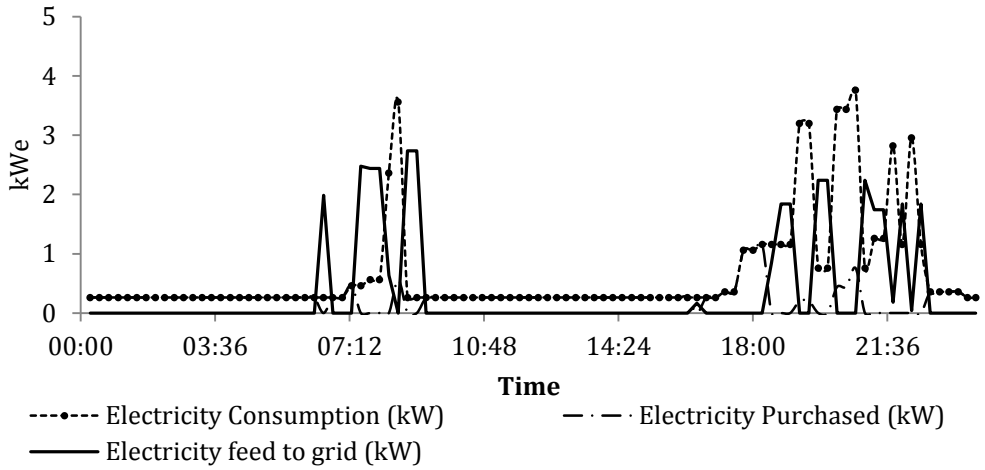

Figure 6.35 Power generation and flows in the detached house satisfying 2006 building regulations and with increased electricity consumption in a winter weekday (Disenco mCHP)

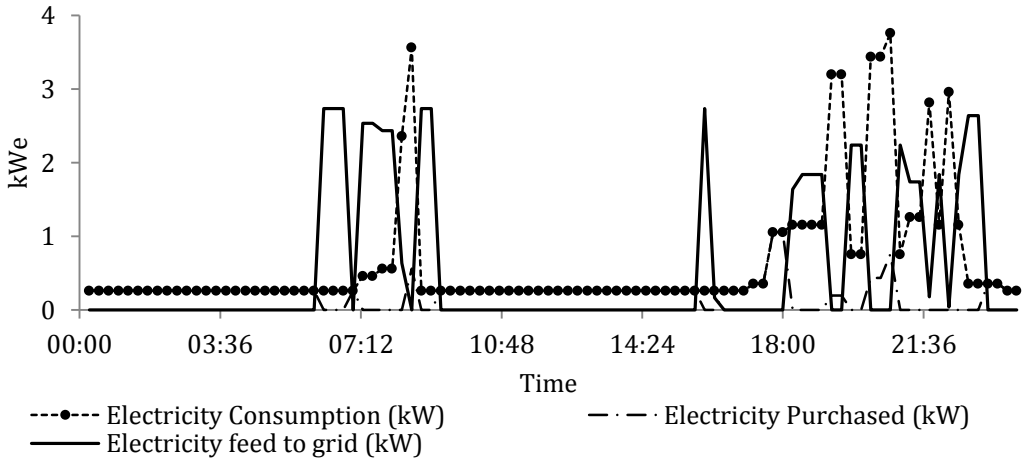

Figure 6.36 Power generation and flows in the detached house satisfying 2006 building regulations and with increased electricity consumption in a winter weekday (3 kW_e ICE mCHP)

It can be seen in Figure 6.35 to Figure 6.37 that the increased load resulted in a higher percentage of produced electricity on-site utilisation. This improves economical and ecological impacts from the deployment of the mCHPs. Table 6.12 shows the annual

reductions in both carbon emissions and fuel and electricity costs for the increased electricity demand in the house.

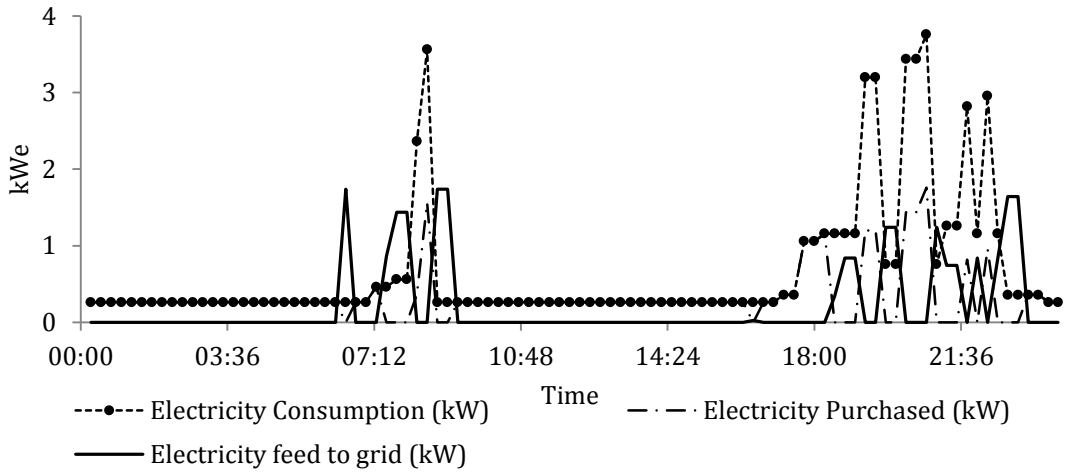

Figure 6.37 Power generation and flows in the detached house satisfying 2006 building regulations and with increased electricity consumption in a winter weekday (2 kW_e Stirling mCHP)

Table 6.12 Annual CO_2 and fuel & electricity cost savings for the detached house with the increased electricity consumption

Heating system configuration	Savings in costs (%)	Savings in carbon emissions (%)
Boiler & 150 L DHW tank	/	/
2 kW_e Stirling mCHP & 150 L DHW tank	**22.34**	**1.04**
3 kW_e ICE mCHP & 150 L DHW tank	**34.57**	**2.03**
3 kW_e Disenco mCHP & 150 L DHW tank	**21.10**	**1.58**

It can be seen in Table 6.12 that the reduction in the energy cost is insignificant compared to the base scenario case (see Table 6.11). However, there is a noticeable improvement in the carbon emission reductions with all mCHP systems providing small carbon emission savings due to the higher on-site electricity utilisation. The 3 kW_e ICE mCHP provides the highest reduction in carbon emissions of approximately 2 %.

6.7.5 Simulations of the detached house satisfying 2006 UK construction regulations with the annual electricity demand of 4.6 MWhe and increased domestic hot water demand

In this case the daily domestic hot water consumption was increased to 250 L per day to assess the effect of this on both the fuel & electricity costs and emission savings. The increase in hot water consumption corresponds to an additional occupant in the house [29]. Figure 6.38 and Figure 6.39 show the increased DHW consumption profiles during weekdays and weekends.

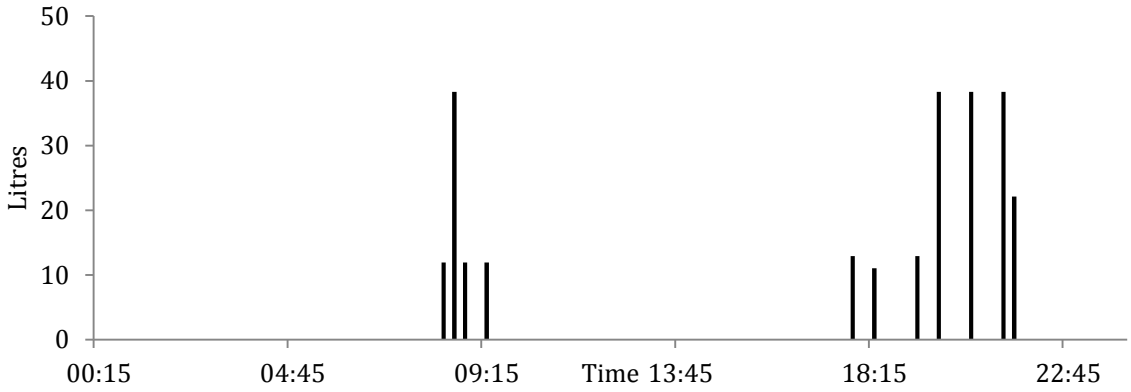

Figure 6.38 Distribution of the increased domestic hot water consumption in a typical weekday

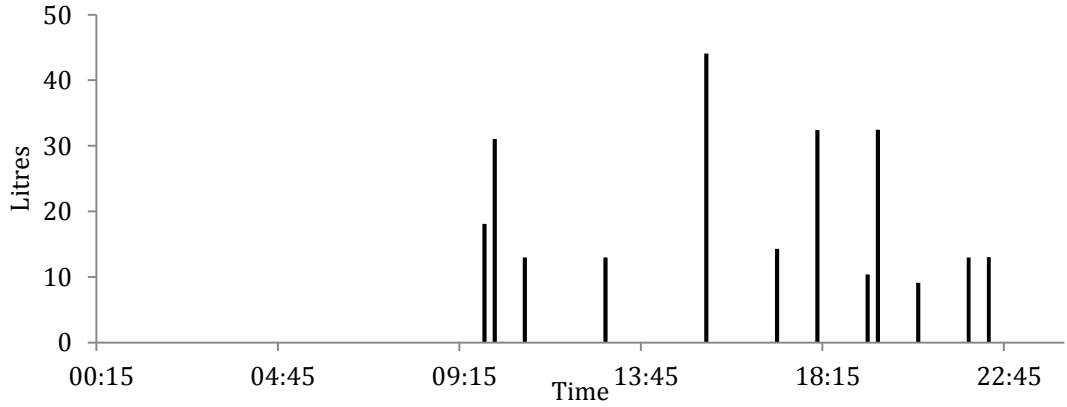

Figure 6.39 Distribution of the increased domestic hot water consumption in a typical weekend

These diagrams (Figure 6.38 and Figure 6.39) include additional two (sink) and one (shower) consumption events during the active occupancy period to increase the hot water consumption by 50 litres a day. Finally, the capacity of the DHW tank was increased from

150 L to 200 L in the simulations. Figure 6.40 to Figure 6.42 show, as an example, the operation of the 3 kW_e ICE, 2 kW_e Stirling and 3 kW_e Disenco mCHP units for the case of increased DHW consumption during winter weekdays.

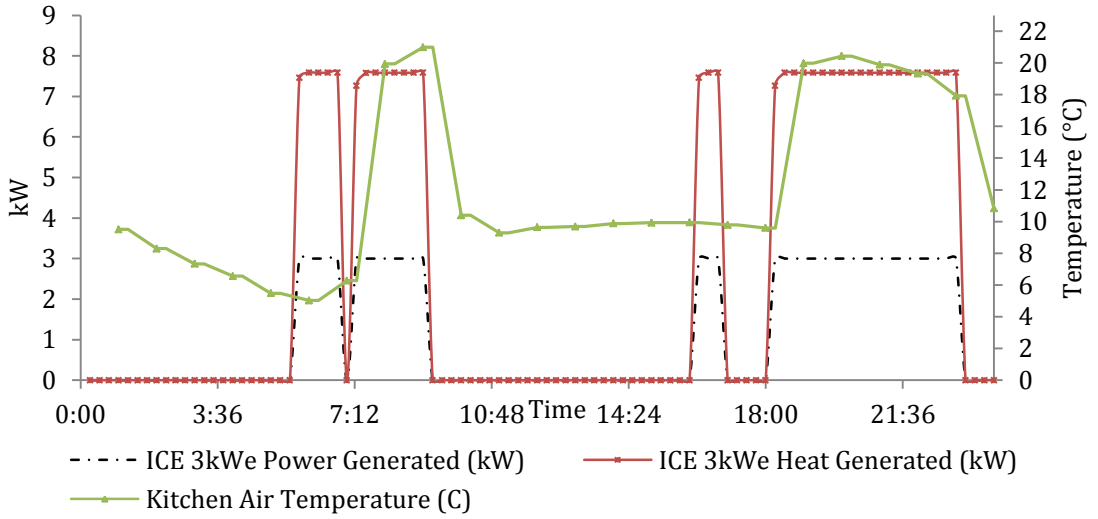

Figure 6.40 Operation of the 3 kWe ICE mCHP in a winter weekday in the detached house with a 200 L DHW tank

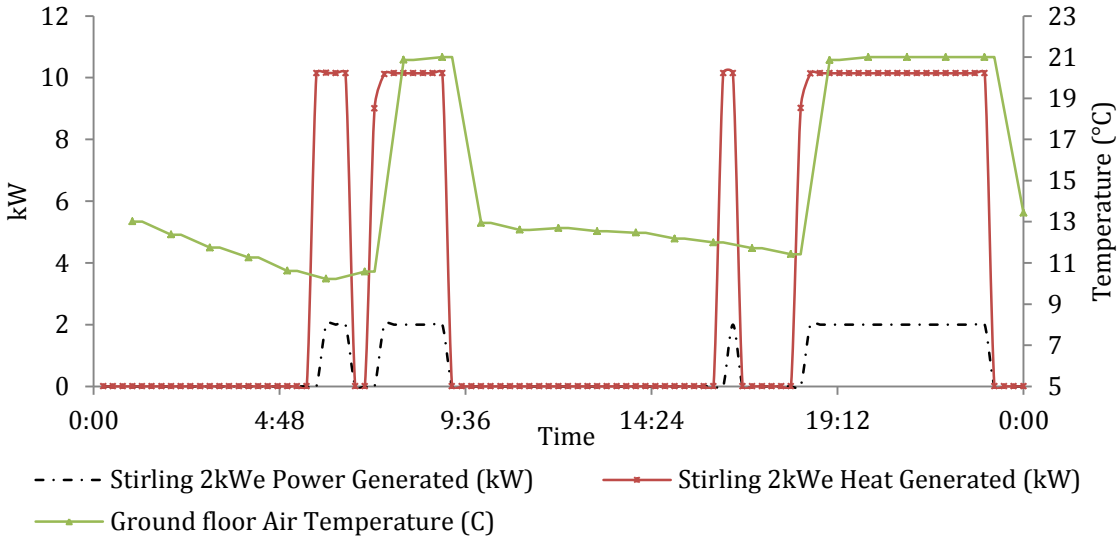

Figure 6.41 Operation of the 2 kWe Stirling mCHP in a winter weekday in the detached house with a 200 L DHW tank

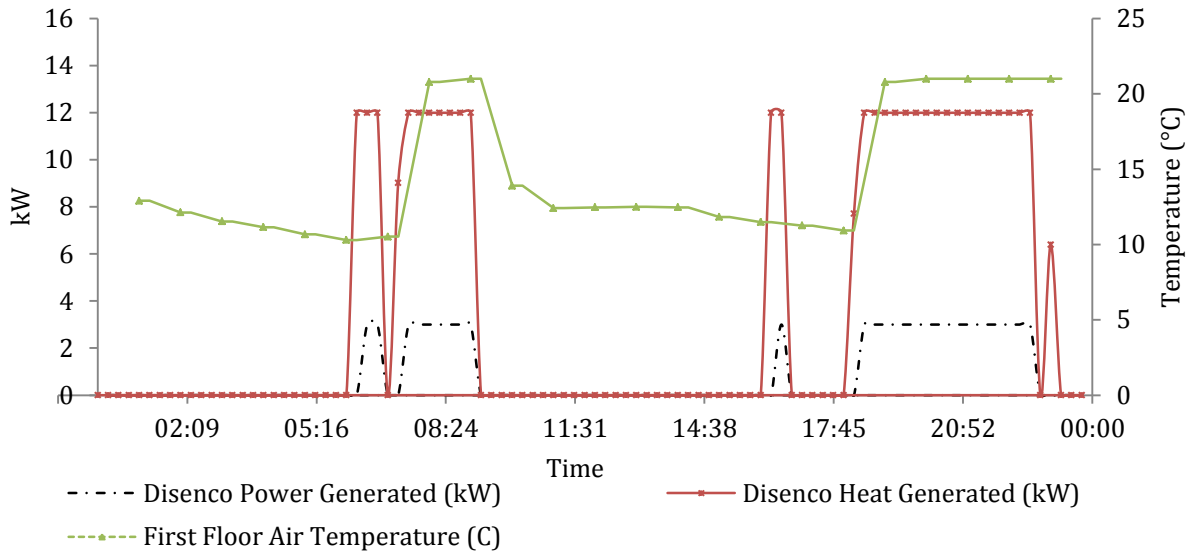

Figure 6.42 Operation of the 3 kWe Disenco mCHP in a winter weekday in the detached house with a 200 L DHW tank

It can be seen in Figure 6.40 to Figure 6.42 that the mCHPs operate for a longer period during the DHW tank charging phase (prior to the space heating) since the tank has the larger capacity. During the space heating operation phase, there are no differences compared to the system with a 150 L DHW tank. Table 6.13 summarises the annual economic and environmental impacts for this new scenario compared to the conventional heating system with condensing boiler and 200 L DHW tank satisfying the 200 L hot water demand a day

Table 6.13 Annual CO_2 and fuel & electricity cost reductions for the case of the detached house with the increased DHW consumption

Heating system configuration	Savings in costs (%)	Savings in carbon emissions (%)
Boiler & 200 L DHW tank	/	/
2 kW_e Stirling mCHP & 200 L DHW tank	**18.66**	**-9.88**
3 kW_e ICE mCHP & 200 L DHW tank	**30.72**	**-11.25**
3 kW_e Disenco mCHP & 200 L DHW tank	**17.54**	**-6.97**

It can be seen in Table 6.13 that the increase in the DHW demand and installing a larger volume water tank results in increased carbon emissions for all the mCHP system options.

The annual carbon emissions are increased by approximately 7 to11 %. This is mainly attributed to the higher fuel consumption. At the same time, all co-generation units provide a reduction in the fuel & electricity costs with the 3 kWe ICE mCHP option offering the highest reduction of approximately 31 %.

6.7.6 Simulations of the semi-detached house satisfying 1996 UK building regulations with deployment of 3 kW_e ICE, 2 kW_e Stirling and 3 kW_e Disenco mCHP units

Two Stirling engine mCHPs (2 kW_e and 3 kW_e) and the 3 kW_e ICE mCHP were deployed in the model to cover the space heating and DHW demands in the semi-detached house of the same design, as described in Section (6.2.1) but with its energy performance parameters to satisfy the 1996 UK building regulations. Figure 6.43 shows the characteristics of the 1996 UK building regulations. Simulations were performed for the yearly period for the base scenario of the electricity consumption and then for cases with the increased domestic hot water and electricity consumptions.

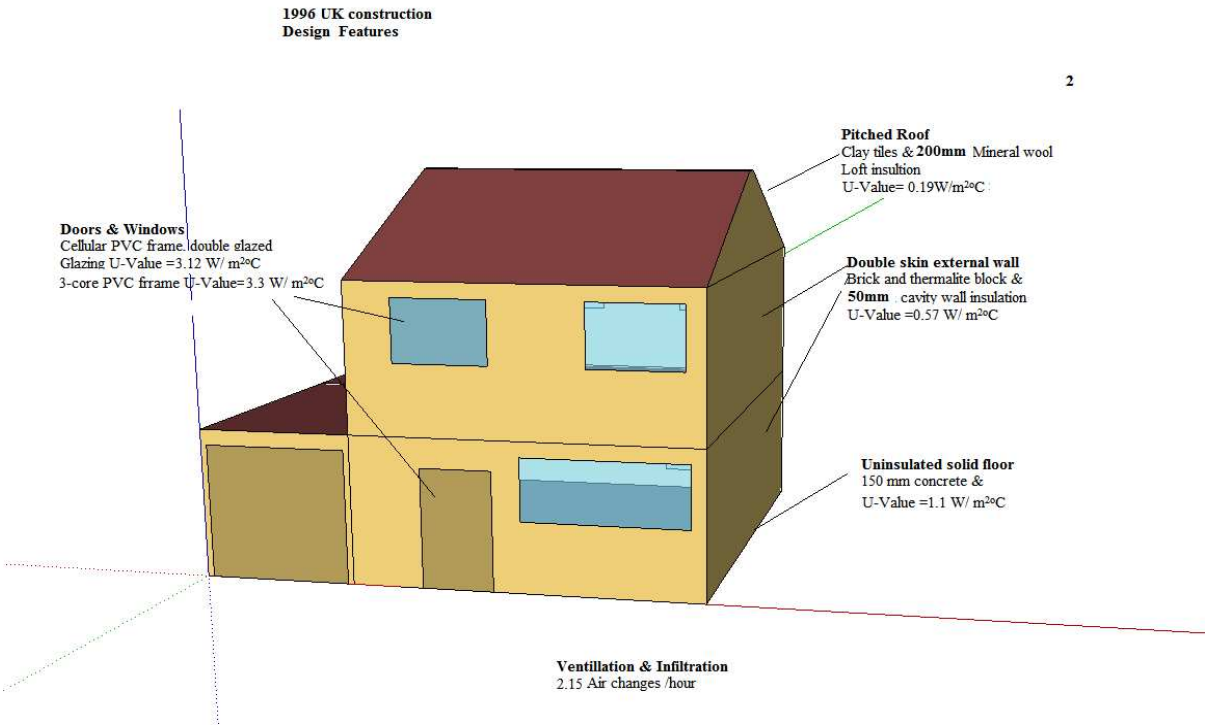

Figure 6.43 Main features of 1996 UK building regulations

6.7.6.1 Simulation of the base electricity consumption scenario

The base electricity consumption scenario considers the case of 4.6 MWh_e of the annual electricity consumption and 200 L per day of the DHW and the heating system with a 150 L DHW tank and. A split generation strategy was used in the modelling Table 6.14 shows the results obtained on annual carbon emissions and fuel & electricity cost savings.

Table 6.14 Annual CO_2 and fuel & cost savings for the base scenario

Heating system configuration	Savings in costs (%)	Savings in carbon emissions (%)
Boiler & 150 L DHW tank	/	/
2 kW_e Stirling mCHP & 150 L DHW tank	**23.03**	**0.07**
3 kW_e ICE mCHP & 150 L DHW tank	**35.09**	**-0.10**
3 kW_e Disenco mCHP & 200 L DHW tank	**21.98**	**1.02**

Co-generation systems commonly work in the heat-led mode, in which they are controlled by the heat demand in much the same way as a conventional boiler with electricity surpluses exported to the grid and electricity shortfalls imported from the grid. Consequently, the heat capacity of the unit was used as criterion for coupling with the appropriate space heating requirements. Boiler simulation results suggested that approximately the 10 kWth rated output of the heating equipment would be sufficient for covering dwelling's requirements. The proposed 3 kW_e ICE mCHP has a rated thermal output of 7.5 kW_{th} (considerably lower than the required capacity).

A delay in reaching the desirable thermal comfort threshold has been noted for the ICE mCHP option; in particularly during cold days when the room air temperature did not exceed 19 °C. Thermostat settings with no apparent effort were attained within the energy zones due to high thermal capacity in the case of both the Stirling based mCHP. The operation of individual mCHP units are presented in the Appendix (B). From Table 6.14 it can be seen that the carbon saving with all options is marginal (in the range of 0.1 to1 %). The negative

impact of the 3 kW_e ICE mCHP unit is due to the lowest thermal efficiency among the systems. The highest annual power generation and rapid transient response account for the highest reduction in the utility bills estimated for the same scenario.

6.7.6.2 Simulation of the case with the increased electricity consumption

The increased electricity consumption described in Section (6.7.4) was re-used throughout for the semi-detached house modelling. The operation of the various mCHP units was found to deviate little from that described in Section (6.7.4) for the detached house (however these results are presented graphically in Appendix (B)). Table 6.15 shows the annual simulation results in respect of the carbon emission and utility cost savings.

Table 6.15 Annual CO_2 and fuel & electricity costs reduction for the increased electricity consumption scenario

Heating system configuration	Savings in costs (%)	Savings in carbon emissions (%)
Boiler & 150 L DHW tank	/	/
2 kW_e Stirling mCHP & 150 L DHW tank	**22.57**	**1.23**
3 kW_e ICE mCHP & 150 L DHW tank	**35.88**	**3.10**
3 kW_e Disenco mCHP & 200 L DHW tank	**21.25**	**1.82**

The annual consumption in the electricity was increased from 4.6 MWh_e based on [29] to 5.5 MWh_e which augmented the fraction of the power generation that was utilised onsite. From Table 6.15 it is evident that the reduction in utility costs compared to the base scenario is negligible however greater savings in carbon emissions were found for all mCHP options. There was a lower import of electricity from national grid compared to the base scenario. The highest carbon reduction was estimated for the proposed 3 kWe ICE mCHP option.

6.7.6.3 Simulations of the case with the increased hot water consumption

As described in Section (6.7.5) for the detached house the hot water consumption was again increased by 50 L per day for the semi-detached house. The operation of the various co-generation units options did not deviate from those of the detached house presented in Section 6.6.3.3. Table 6.16 shows the annual results with respect to the emissions and utility costs.

Table 6.16 Annual CO_2 and fuel & electricity cost reductions for the case with the increased DHW consumption

Heating system configuration	Savings in costs (%)	Savings in carbon emissions (%)
Boiler & 150 L DHW tank	/	/
2 kW_e Stirling mCHP & 150 L DHW tank	**19.47**	**-8.79**
3 kW_e ICE mCHP & 150 L DHW tank	**31.44**	**-10.38**
3 kW_e Disenco mCHP & 200 L DHW tank	**18.93**	**-5.87**

Results in Table 6.16 show a significant saving in annual utility costs, however this is followed by the increase in carbon emission in the range of 6 % - 10 %.

6.7.7 Conclusions

The following conclusions can be made from analysis of theoretical results obtained in Sections (6.2 to 6.7):

- The condensing boiler efficiency can exceed 85 % whilst the efficiency of existing co-generation systems is currently limited to approximately 75 %. Considering that carbon emissions are associated with both electricity and gas consumption, then equilibrium between nominal electrical and thermal capacities and efficiencies in mCHP systems must be achieved in order to deliver and maximise environmental benefits.
- Simulation results predicted that if a cogeneration unit operates on its maximum capacity throughout the heating season, then significant utility cost savings can be achieved. The latter was observed in the case of undersized systems (the 3 kWe ICE in the semi-

detached house satisfying the 1996 building regulation or detached house satisfying 2006 building regulations).

- Prolonged operation in the split heat generation operating strategy results in the higher power generation and consequently, in the higher financial savings (when FIT is taken into consideration) and lower electricity-related carbon savings.
- The time delay in power generation that characterises the Stirling engine mCHP units constrains the annual electricity production, especially when an oversized unit is selected. The introduction of a regulated operation mode (modulation) can be beneficial for oversized mCHPs.
- Higher savings are obtained in cases in which mCHP units are deployed in dwellings with high thermal requirements. This conclusion very well agrees with [130]. Marginally better performance regarding CO_2 emissions reduction was demonstrated by Stirling engine mCHPs due to the higher thermal efficiency; however further investigation should be conducted to confirm this.
- The increased electricity consumption resulted in better performance of all mCHPs. However the increase by 25 % in the domestic hot water usage resulted in lower performance. This was attributed to increased natural gas consumption which negates the reduction of electricity-related carbon emission savings and marks down the overall performance.

6.8 Modelling of deployment of small capacity mCHP systems with auxiliary burners in houses with increased heat demand

Dwelling energy demand profiles and individual mCHP specification strongly affect the advantages of the mCHP deployment, which means that the sizing and selection of the system is of vital importance for achieving positive economical and ecological impacts. If the energy supply and demand balance is correctly considered, it should be possible to minimise

the cycling in the operation of the mCHP unit resulting in greater performance and decrease maintenance costs due to reduced wear.

By incorporating an auxiliary burner into the mCHP system, as described in Section (6.6.1), it is possible to cover higher heating demands. The mCHPs can operate at nominal capacities throughout the heating season while the additional burner modulates the heating output when needed.

Simulations were carried out using the 1 kWe Whispergen Stirling engine and the Honda Ecowill ICE mCHP systems, both equipped with an auxiliary burner. The houses considered were the detached house meeting 2006 and 1996 building regulations and a semi-detached house satisfying 1996 building regulations. With respect to the primary energy requirements, two electricity demand profiles were applied whereas the DHW consumption was kept constant at 200 L per day in all simulations.

Table 6.17 shows all cases modelled in this section.

Table 6.17 Matrix for theoretical simulations

Electricity Demand	**Annual Electricity consumption at 4.6 MWh_e and 5.5 MWh_e levels**		
Space Heating Demand	**Detached house, 2006 building regulations**	**Semi-detached house, 1996 building regulations**	**Detached house, 1996 building regulations**
Hot Water Demand	**200 L/day**	**200 L/day**	**200 L/day**
mCHP configuration	Whispergen & Additional burner	Whispergen & Additional burner	Whispergen & Additional burner
	Honda Ecowill & Additional burner	Honda Ecowill & Additional burner	Honda Ecowill & Additional burner

The control priority in the model is that the primary heating system is considered to be the mCHP unit whilst the additional heat demand is covered by the auxiliary boiler if needed.

6.8.1 Simulations of the detached house satisfying the 2006 construction regulations

Figure 6.44 and Figure 6.45 show, as an example, the operation of the ICE and Stirling engine mCHPs fitted with the auxiliary burner.

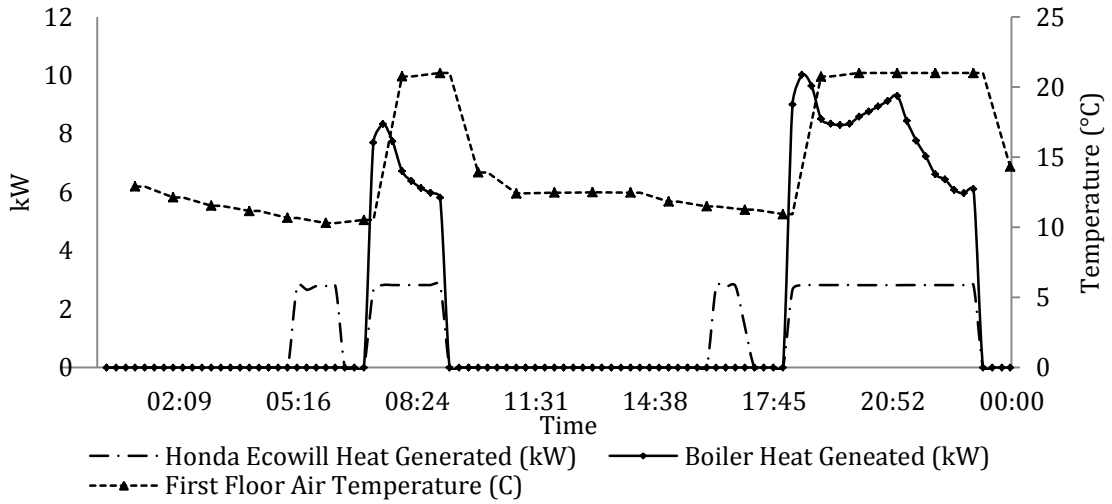

Figure 6.44 Heat generation by the Honda mCHP system with the back-up boiler in the split heat generation mode during a winter weekday

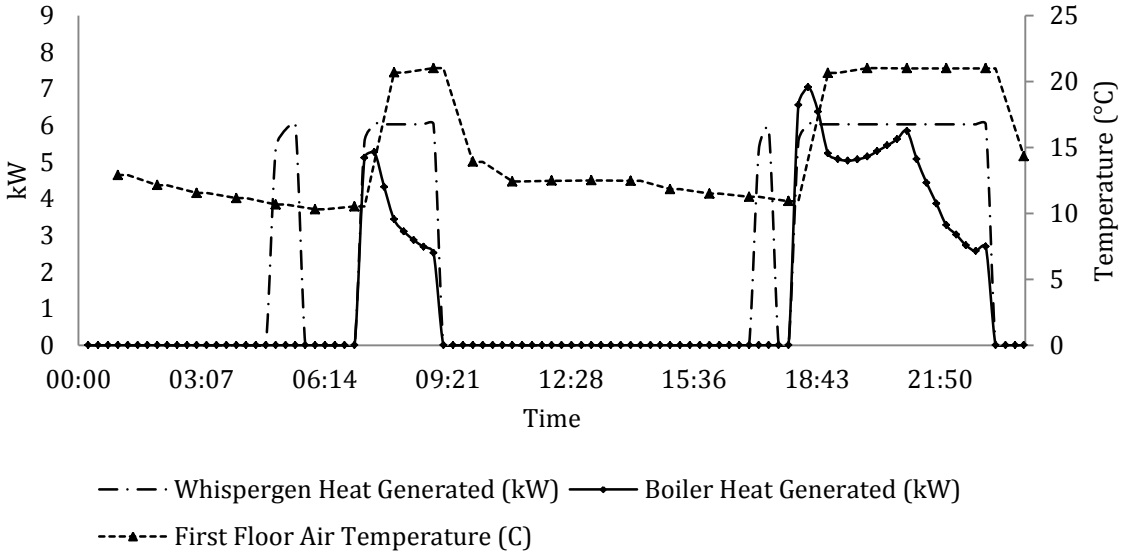

Figure 6.45 Heat generation by the Whispergen mCHP system with the back-up boiler in the split heat generation mode during a winter weekday

All simulations were conducted for the split heat generation mode, as being most advantageous. The operation of the mCHP systems prior to the space heating during which the hot water tank charged is present in all cases of modeling. From Figure 6.44 and Figure 6.45 it can be seen that both the mCHP systems generate heat at their maximum thermal output during both the space heating and DHW operation. The operation of both units follows the active occupancy pattern with little to no variation in respect to the heat generated. The additional heating requirements for the living space zones are covered by the gas-fired boiler. The sharp rise in the output curve of the thermal output in both mCHPs occurs in the evening occupancy period and is attributed to an instantaneous space heating load caused by ventilation/ infiltration. It can be seen in Figure 6.45 that the higher thermal capacity of the Whispergen mCHP unit results in the lower heat generation rate of the auxiliary boiler. The respective boiler heat generation curve is shifted downwards by approximately 3 kW_{th}.

6.8.2 Simulations of the detached house satisfying the 1996 construction regulations

The U-values of the building envelope corresponding to the 1996 building regulation, as described in Section 6.7.6 and presented in detail in Figure 6.43, together with the corresponding infiltration/ventilation parameters were applied in the modelling of the detached dwelling. These changes resulted in the increased space heating requirements. Figure 6.46 and Figure 6.47 show the operation of the ICE and Stirling engine mCHPs, respectively. The same trends can be observed in Figure 6.46 and Figure 6.47 as in Section (6.8.1). There is a consistent operation of both the mCHP units following the occupancy pattern and with small variations in respect of the heat generated. Any additional space heating demand is covered by the auxiliary boilers when needed. Nevertheless, in this particular scenario, the higher thermal demand during evening operation can be observed due to features in the evening occupancy period. This was attributed to the environmental conditions and to the infiltration/ventilation characteristics.

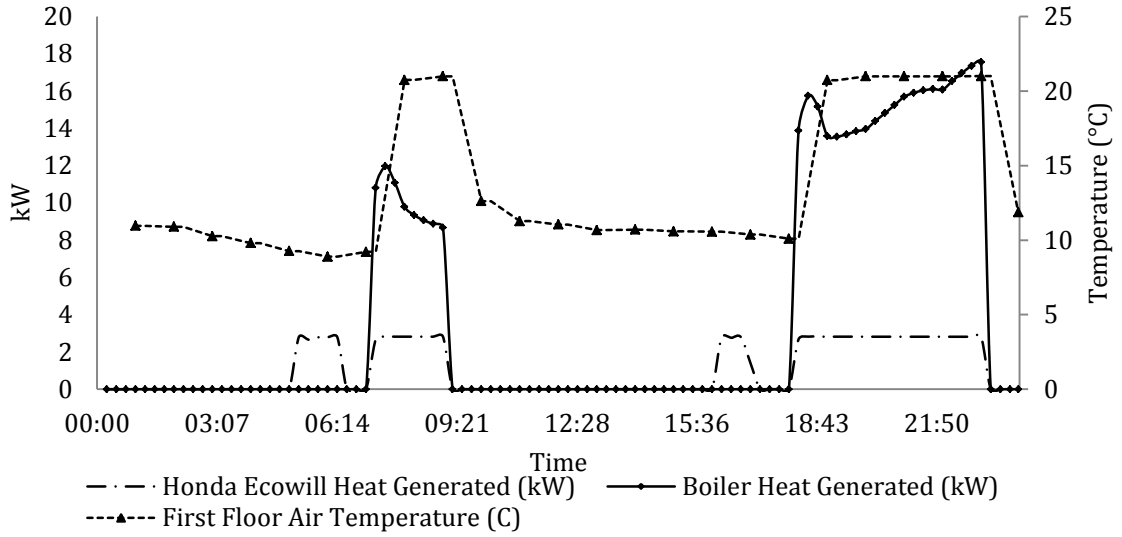

Figure 6.46 Heat generation by the Honda mCHP system with the back-up boiler in split heat generation mode during a winter weekday

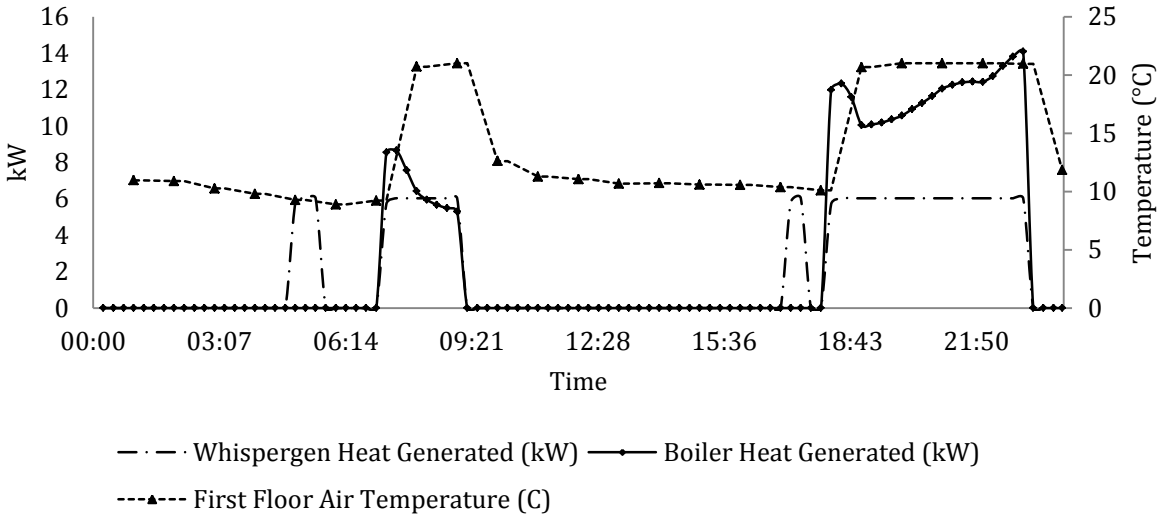

Figure 6.47 Heat generation by the Whispergen mCHP system with the back-up boiler in the split heat generation mode during a winter weekday

6.8.3 Simulations of the semi-detached house satisfying the 1996 construction regulations

The building's layout and construction details used for simulations in this scenario were described in Section (6.7.6). Figure 6.48 and Figure 6.49 show the operation of the ICE and Stirling engine mCHPs.

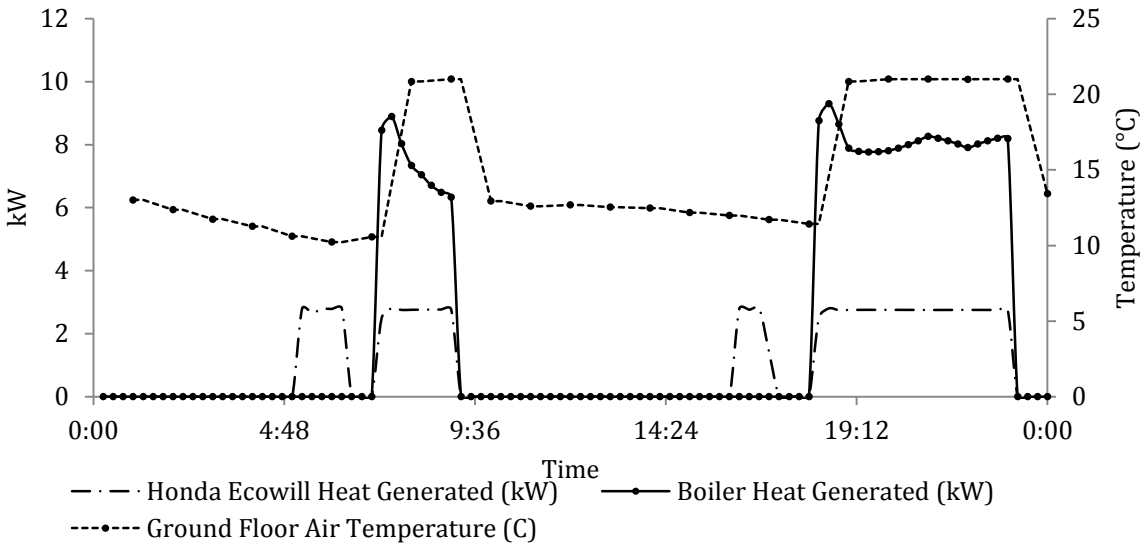

Figure 6.48 Heat generation by the Honda mCHP system with back-up boiler in split generation mode during a winter weekday

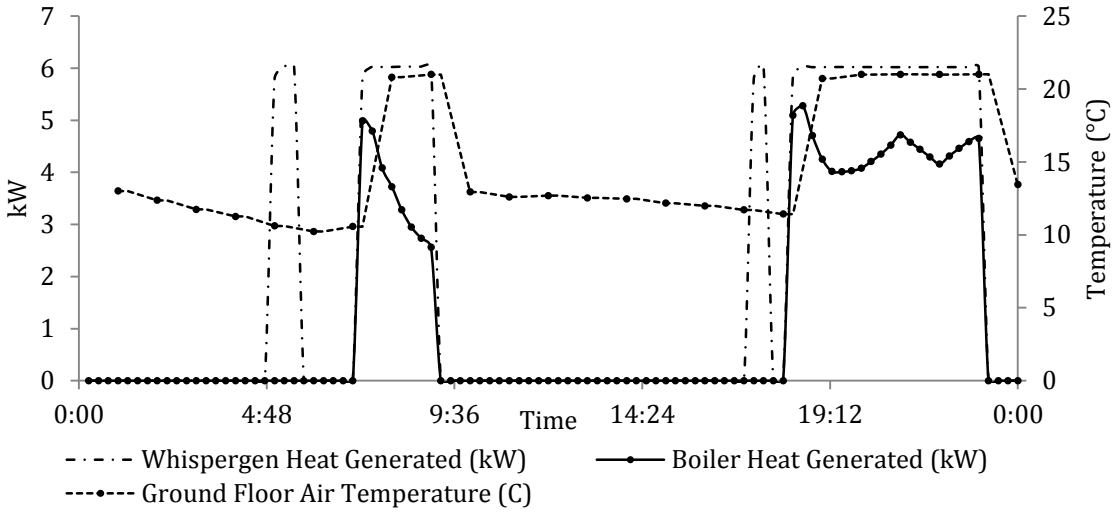

Figure 6.49 Heat generation by the Whispergen mCHP system with back-up boiler in split generation mode during a winter weekday

It can be seen in Figure 6.48 and in Figure 6.49 that the space heating requirements of the semi-detached house satisfying the 1996 building regulations is similar to those in the detached house constructed to the same building regulations. No significant variation was observed regarding the mCHP operation from previous scenarios. During the evening

operation it can be observed that the boiler maintains the heat generation at an average rate of 8 kW_{th} with small fluctuations around this value in the ICE mCHP (see Figure 6.48). For the same period much considerable fluctuations occur in the Stirling engine mCHP (see Figure 6.49).

6.8.4 Calculations of annual carbon emission and utility bill reductions

Results on the annual economic and carbon emission savings are summarised and presented in this section for the two 1 kW_e mCHPs equipped with the auxiliary boiler. Electricity and gas prices, the feed-in tariff rate and carbon emission factors as described in Section (6.5.5) were used in performing calculations.

6.8.4.1 The detached house satisfying 2006 building regulations

In the base scenario case the 4.6 MWh_e annual electricity consumption and DHW consumption equal to 200 L per day were used with the heating system based on the condensing boiler and a 150 L DHW tank. Table 6.18 shows the summary on the annual utility bill and carbon emission savings. Table 6.19 shows the summary on the annual utility bill and carbon emission savings. The increased electricity consumption case considered in the earlier models was modelled whereas the domestic hot water consumption was kept unchanged at 200 L per day.

Table 6.18 The annual utility bill and carbon emission savings for the base scenario case

Heating system configuration	Savings in costs (%)	Savings in carbon emissions (%)
Boiler & 150 L DHW	/	/
Whispergen with the additional burner & 150 L DHW	**19.61**	**-0.34**
Honda Ecowill with the additional burner & 150 L DHW	**31.54**	**10.62**

Table 6.19 The annual utility bill and carbon emission savings for the increased electricity consumption case

Heating system configuration	Savings in costs (%)	Savings in carbon emissions (%)
Boiler & 150 L DHW	/	/
Whispergen with the additional burner & 150 L DHW	**19.24**	**0.67**
Honda Ecowill with the additional burner & 150 L DHW	**30.68**	**11.22**

The negative carbon saving in the case of the Stirling mCHP option (see Table 6.18) in the base scenario case becomes a marginal carbon saving in the case of the increased electricity consumption though the utility cost saving remains virtually the same. There is a little change in annual performance with regards to the ICE mCHP option due to the increased electrical demand.

6.8.4.2 Detached house satisfying the 1996 building regulations

The 1996 UK building regulation requirements were applied to the detached building resulting in the increased annual gas consumption by approximately 34 %. Table 6.20 shows the annual reduction in carbon emission and utility costs for the case of the base scenario. Table 6.21 shows the same information for the case when there is the increased electricity consumption in the house.

Table 6.20 The annual utility bill and carbon emission savings for the base scenario case

Heating system configuration	Savings in costs (%)	Savings in carbon emissions (%)
Boiler & 150 L DHW	/	/
Whispergen with the additional burner & 150 L DHW	**20.84**	**2.74**
Honda Ecowill with the additional burner & 150 L DHW	**29.29**	**10.35**

Table 6.21 The annual utility bill and carbon emission savings for the increased electricity consumption case

Heating system configuration	Savings in costs (%)	Savings in carbon emissions (%)
Boiler & 150 L DHW	/	/
Whispergen with the additional burner & 150 L DHW	**19.78**	**2.84**
Honda Ecowill with the additional burner & 150 L DHW	**27.93**	**10.51**

Savings in case of both mCHPs and scenarios can be seen in Table 6.20 and in Table 6.21. The increased electricity consumption resulted in a small increase in the carbon emission and utility cost reduction compared with the base scenario.

6.8.4.3 Semi-detached house satisfying the 1996 building regulations

Space heating requirements of the semi-detached house satisfying the 1996 building regulations were found to be similar to those of the detached house constructed to 2006 building regulations. Table 6.22 and Table 6.23 show the annual reduction in carbon emission and utility costs for the cases of the base scenario is the increased electricity consumption in the house. Results obtained for the above two cases are similar to estimations made for the detached house satisfying 2006 building regulations. However the higher electricity utilisation due to the increased electricity consumption had a little effect on the carbon emission savings in the case of the Stirling engine mCHP.

Table 6.22 The annual utility bill and carbon emission savings for the base scenario case

Heating system configuration	Savings in costs (%)	Savings in carbon emissions (%)
Boiler & 150 L DHW	/	/
Whispergen with the additional burner & 150 L DHW	**18.85**	**-1.62**
Honda Ecowill with the additional burner & 150 L DHW	**31.07**	**9.37**

Table 6.23 The annual utility bill and carbon emission savings for the increased electricity consumption case

Heating system configuration	Savings in costs (%)	Savings in carbon emissions (%)
Boiler & 150 L DHW	/	/
Whispergen with the additional burner & 150 L DHW	**18.75**	**-0.32**
Honda Ecowill with the additional burner & 150 L DHW	**30.22**	**10.04**

6.8.5 Conclusions on modelling of deployment of small capacity mCHP systems with auxiliary burners in houses with increased heat demand

The following conclusions were made from results obtained on modelling of deployment of small capacity mCHP systems with auxiliary burners in houses with increased heat demand:

- The 1 kW_e Honda Ecowill mCHP unit was found to provide greater better utility cost and carbon emission reductions over the 1 kW_e Whispergen mCHP option. The ICE unit's auxiliary boiler provided a smaller fraction to the total heat generated rather than Whispergen mCHP's auxiliary burner and this resulted in the higher combined (mCHP/boiler) thermal efficiency, resulting in better performance.
- Although savings in utility costs were found in all scenarios in respect of the Stirling engine mCHP system, the small carbon emission savings were predicted only in the half of the simulated scenarios.
- In respect of the overall performance, the increased electricity consumption resulted in the higher carbon emission savings compared the base scenario case. This was attributed to the increased on-site utilisation of the electricity produced.

6.9 Bungalow Simulations

All previous simulations were conducted using an occupancy pattern matching working adult residents schedule. In respect to a weekday this profile was characterised by two active

occupancies periods in mornings and evenings respectively and a vacancy period in-between. The occupancy pattern was proved to affect significantly the performance of the mCHP systems. In this section retired resident's occupancy pattern was investigated in the bungalow type of buildings.

6.9.1 Bungalow Design

A bungalow building with the floor area of 66 m^2 including a 17 m^2 garage was used in simulations and this was constructed to the UK 2006 regulations. Figure 6.50 shows the design layout of the bungalow building.

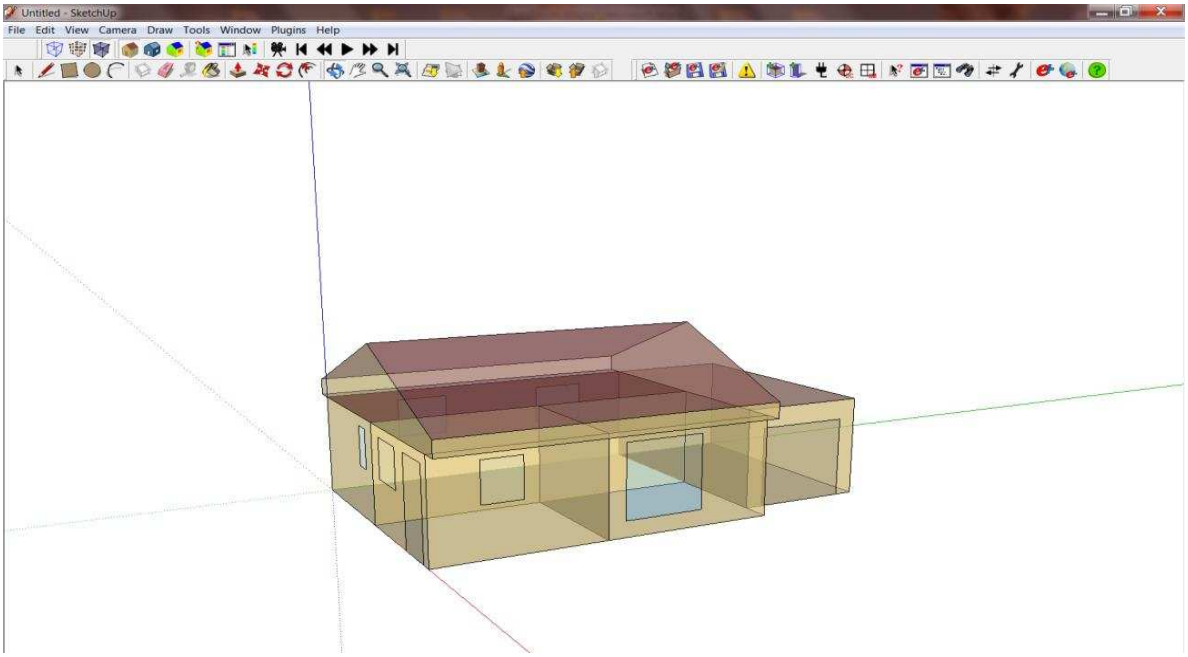

Figure 6.50 Design of the bungalow building

The building envelope was designed with a 7.13 m^2 glazing which corresponds to 4.2 % of the gross external surface area, and a floor height of 2.5 m.

It was modelled with five individual energy zones and was assumed to reside in the area of the Gatwick airport near London. The building matches requirements of retired residents due to a smaller size and lower energy requirements

6.9.2 Occupancy pattern

Resident of the building is a retired couple with a single occupancy pattern throughout the whole week as shown in Table 6.24.

Table 6.24 The heating plant's operation schedule for a typical winter day

Design Day	On (21°C)	Off
Monday to Sunday	9:00	22:00

6.9.3 Electricity consumption profile

A reduction by approximately 22 % in the annual electricity consumption was modelled in the bungalow compared to the basic scenario case so it matches the bungalow energy requirements. Since a single design day was simulated then the same electricity consumption distribution was used in the modelling throughout the year. Figure 6.51 shows the such electricity consumption distribution in the design day.

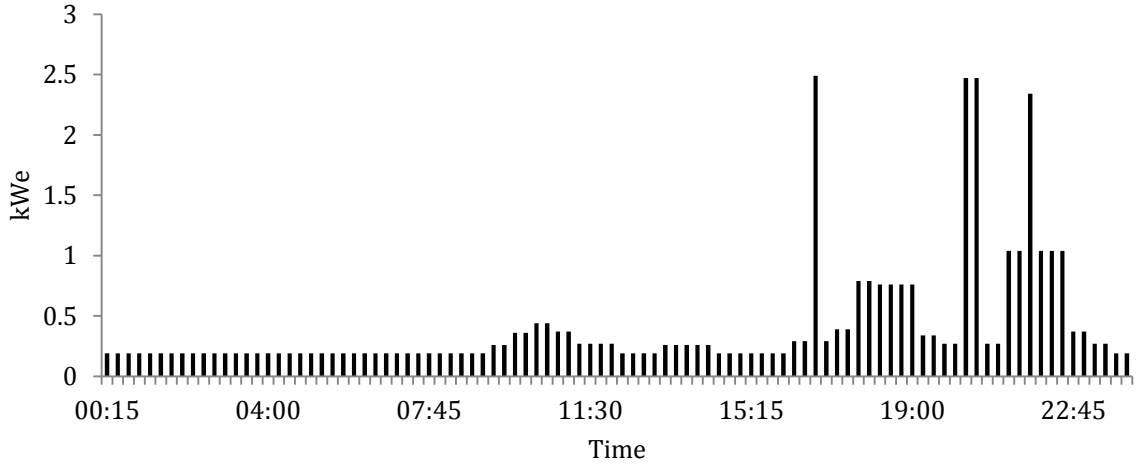

Figure 6.51 Electricity consumption distribution during the design day

6.9.4 Domestic hot water consumption distribution

The domestic hot water system in the bungalow is equipped with a standard 150 L tank. A 100 L daily hot water demand was implemented in the model assuming that each of the occupant requires 50 L of hot water per day as described in Section (6.3.4).

Figure 6.52 shows the hot water consumption distribution during the design day.

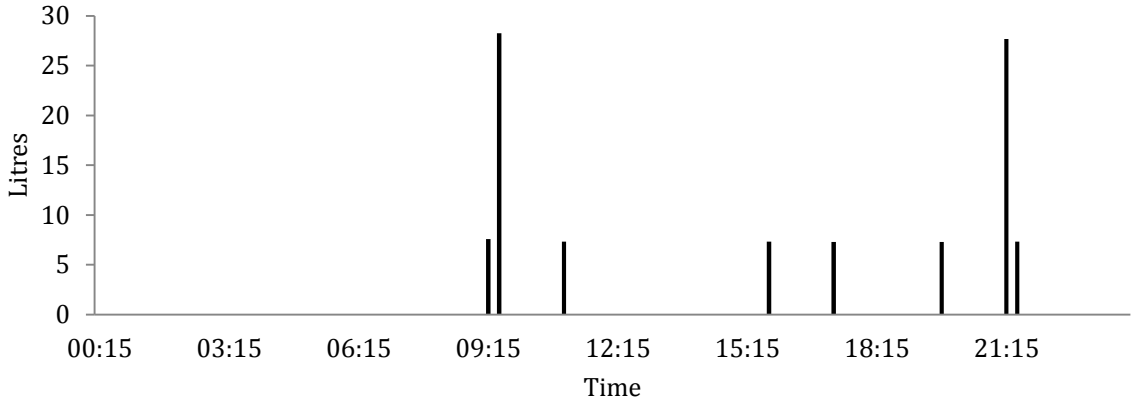

Figure 6.52 DHW consumption profile during the design day

It can be seen in Figure 6.52 that there are two peaks corresponding to showering and 6 equally distributed events attributed to hot water consumption at the sink.

6.9.5 Modelling of the operation of the heating systems

6.9.5.1 The heating system with a conventional condensing boiler

Due to the reduced heating requirements a 10 kW_{th} condensing boiler with the 85 % thermal efficiency was used in the modelling process for the heating system of the house. Figure 6.53 shows the operation of the boiler and the air temperature variation within the lounge energy zone.

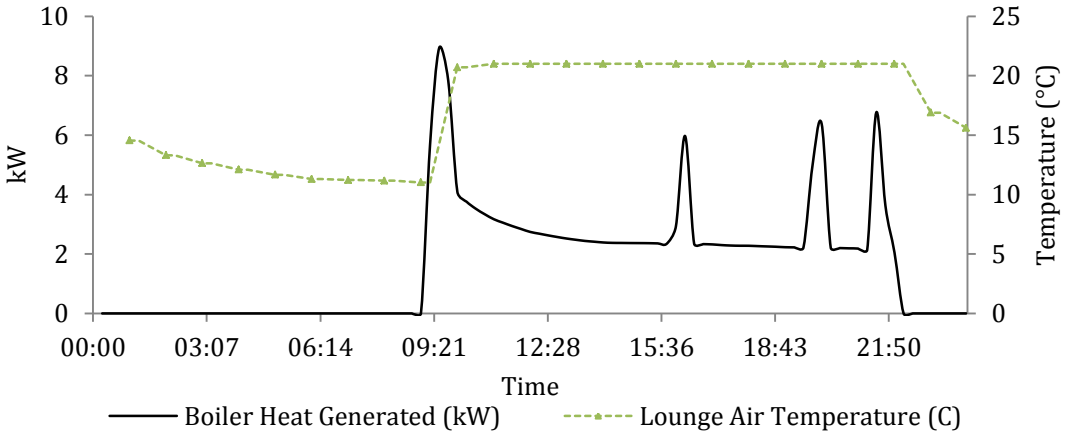

Figure 6.53 Operation of the boiler during the winter design day

Details of the system were described in Section (6.4). The boiler operation is set to start at 9.00 am and to switch off at 22.00 to follow the occupancy pattern presented in Table 6.24. The peaks in the boiler heat generation curve were attributed to the domestic hot water consumption events which trigger the boiler to switch to the higher heat generation rate. It can be seen that such heating system consistently maintains the air-temperature on pre-set level (21 °C).

6.9.5.2 The heating system with 1kWe Whispergen Stirling Based mCHP

Figure 6.54 shows the operation of the Whispergen mCHP in the bungalow in the split heat generation mode during a winter day. It can be seen that the operation of the Whispergen unit is characterised by a high frequency of switching events due to the to the low heat requirements of the dwelling.

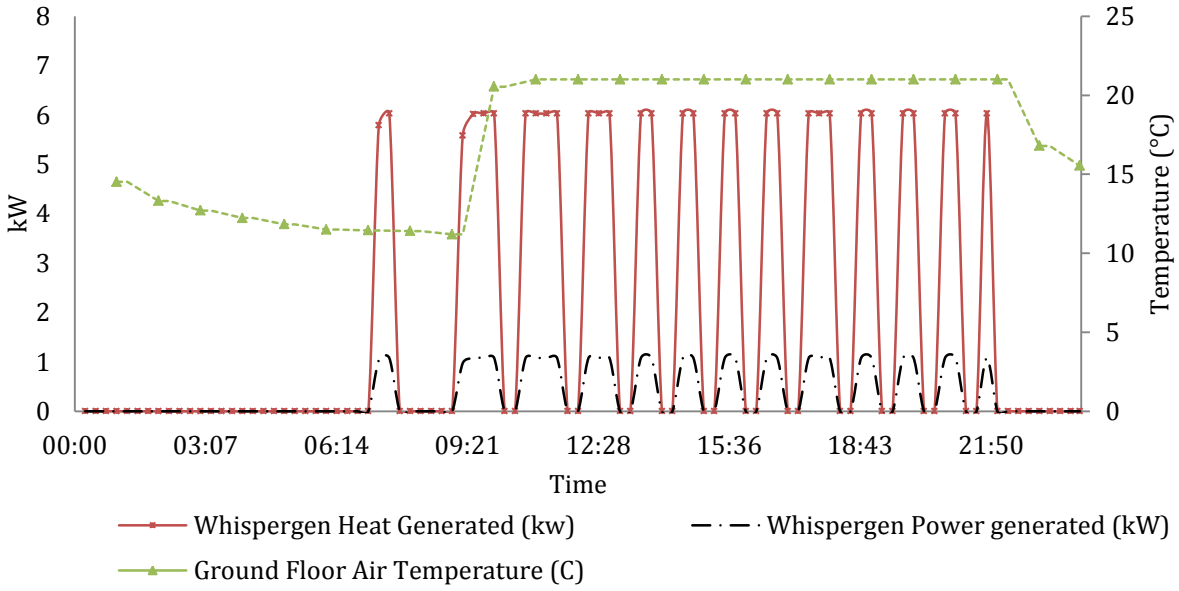

Figure 6.54 Heat and Power generation by the Whispergen mCHP during a winter design day

Figure 6.55 shows the hot water consumption events and the temperature fluctuation inside the domestic hot water tank.

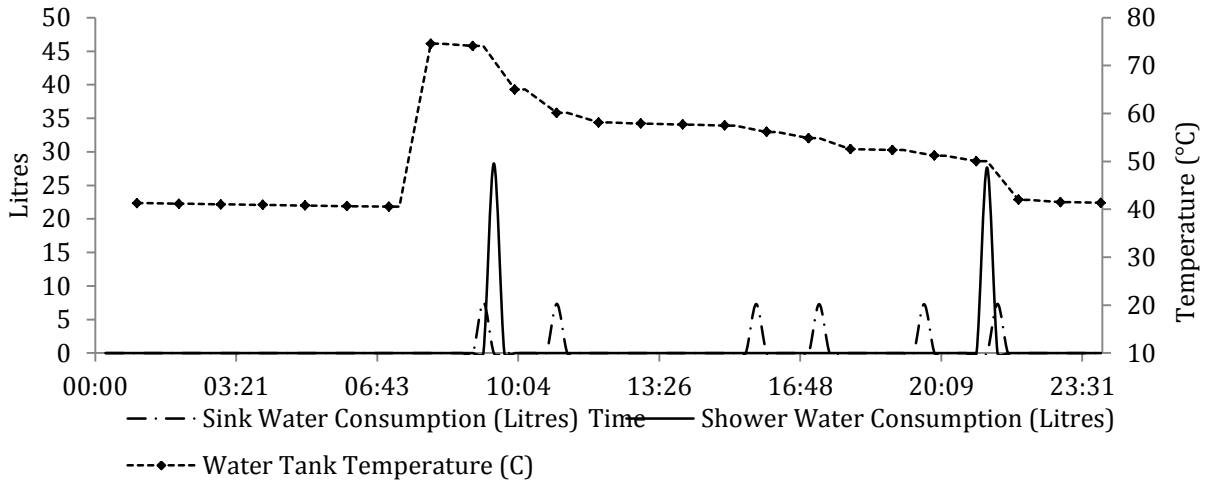

Figure 6.55 Hot water consumption events and the temperature fluctuations inside the tank during a winter weekday.

It can be seen in Figure 6.55 that the 100 L daily consumption is covered by a single charging event and the water temperature is sufficient to even compensate for extra hot water consumption event.

6.9.5.3 The heating system with the 1 kWe ICE based mCHP

The 1kWe ICE based mCHP was simulated with incorporation of the auxiliary burner and Figure 6.56 shows the operation of such the system during the winter design day.

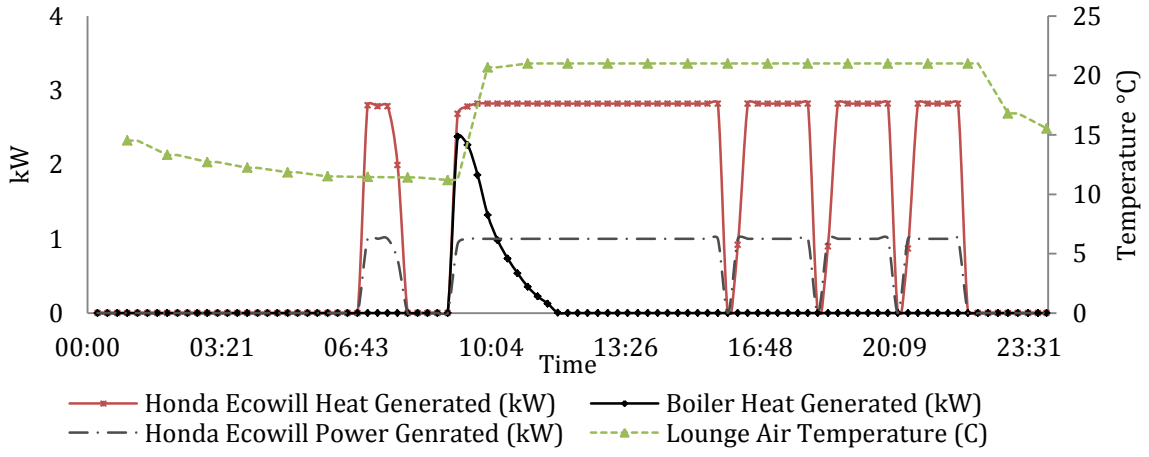

Figure 6.56 Heat and Power generation by the Honda Ecowill mCHP during a winter design day

A longer operation for the warm-up of the DHW tank can be observed in Figure 6.56. The operation of the auxiliary boiler is limited to approximately 3 hours as afterwards the heat generated by the mCHP is sufficient to maintain the requested temperature within the living zones. There is the cycling in the operation of the mCHP which takes place later in the design day.

6.9.5.4 The heating system with the 1 kW_e PEM FC mCHP and auxiliary boiler

The PEM fuel cell based mCHP unit which was described in Section (6.6.2) is used for modelling of the heating system of the bungalow. In simulations hydrogen was used as fuel whilst the calculations of the annual benefits were then carried out using the conversion factor to estimate the consumption of natural gas. Two configurations were investigated for the PEM fuel cell mCHP based heating system. In the first configuration the heat generated by the mCHP was used for space heating, whereas in the second configuration this heat was utilised to cover only the domestic hot water demand.

The heat generated by the mCHP is used for space heating

Figure 6.57 shows the operation of the 1 kWe PEM fuel cell based mCHP with the auxiliary burner. The space heating demand is covered by the mCHP together the auxiliary boiler whilst the DHW demand is covered by the auxiliary burner only. It can be seen in Figure 6.57 that the fuel cell mCHP is operating at its maximum capacity throughout the day. The split heat generation operating strategy is not applicable in this scenario due to the fact that the 1 kW_{th} heat produced by mCHP is used only for space heating. The peaks in the heat generation by the auxiliary are due to the boiler covering heat demands both for space heating and DHW demands.

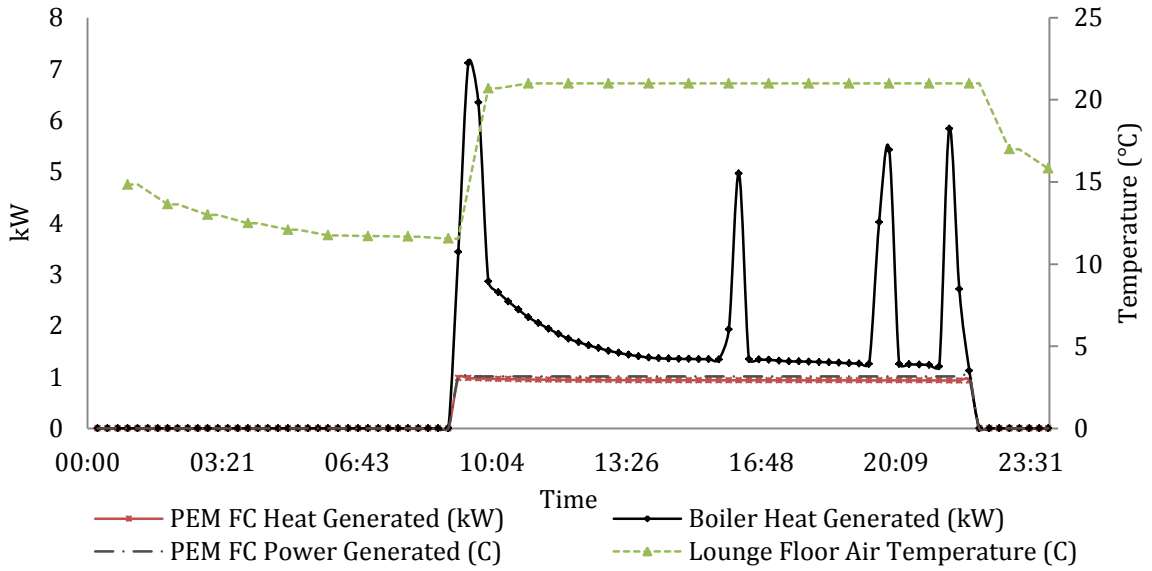

Figure 6.57 Heat and Power generation by the PEM FC unit during a winter design day

The heat generated by the mCHP is used to cover the domestic hot water demand

In this scenario the space heating demand was covered by the auxiliary boiler. Figure 6.58 shows the operation of such the system.

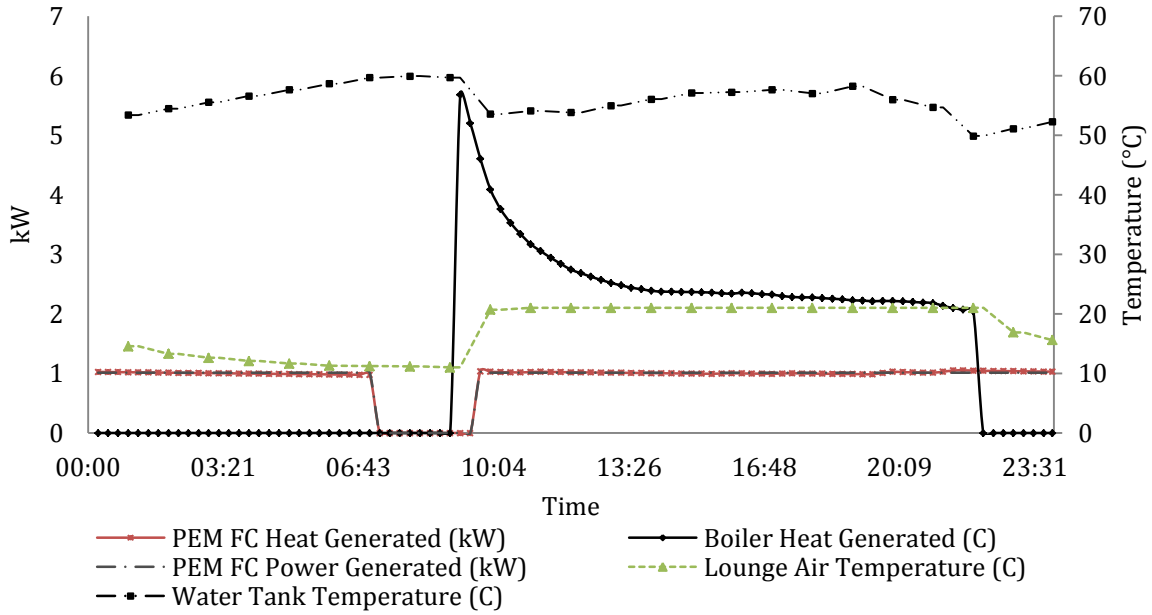

Figure 6.58 Heat and Power generation by the PEM FC unit during a winter design

In order to maintain the pre-set water temperature in the DHW tank (which was reduced from typical 70 °C to 60 °C due to the low temperature heat recovering from the fuel cell) the PEM

fuel cell mCHP operates continuously for almost whole day. The system is switched off only for few hours before the space heating demand is triggered in the morning. Such type of operation of the mCHP should enhance the annual power generation and annual cost savings. The major advantage of this configuration is prolonged electricity generation even during the summer period. Nevertheless, the highest fuel consumption was calculated for this scenario of operation.

6.9.6 Calculations of annual utility cost and carbon emission savings

Results from calculations of the annual ecological and economic performance are summarised in Table 6.25.

Table 6.25 Calculations of annual utility cost and carbon emission savings

Heating system configuration	Savings in costs (%)	Savings in carbon emissions (%)
Boiler & 150 L DHW	/	/
Whispergen with the additional burner & 150 L DHW	**10.37**	**-13.01**
Honda Ecowill with the additional burner & 150 L DHW	**38.41**	**8.7**
FC (for CH) with the additional burner & 150 L DHW	**-44.18**	**-13.95**
FC (for DHW) with the additional burner & 150 L DHW	**-38.86**	**-89.45**

It can be seen in Table 6.25 that only the Honda ICE based mCHP performs well in the bungalow environment for the adapted occupancy pattern and energy and heating demand profiles. The ICE mCHP provides about 38 and 9 % savings in utility costs and carbon emissions, respectively. The high cycling frequency in the operation of the Whispergen unit resulted in the increased fuel consumption due to the long warm-up transient regime and, consequently, resulted in the rise in carbon emissions. In respect to the fuel cell mCHP

system deployment, the highest amount in the annual power generation was achieved at the cost of the highest fuel consumption due to low efficiency of the fuel reforming process.

6.10 Analysis of the trend in variation of annual benefits with the thermal requirements of the house and size of mCHPs

The simulation results obtained in Chapter (6) are summarised with reference to the economic (utility costs) and environmental (carbon emission) impact in relation to the thermal requirements of the house types analysed. An overall analysis was carried out in order to assess the performance trends of each mCHP technology considered in respect of the thermal demand.

6.10.1 Cases when the house heating systems are based only on mCHPs as heating equipment

This section considers cases in which mCHPs are used as the sole heating equipment in the houses (i.e. configurations with additional heating boilers are not included).

Carbon savings summary

The carbon savings values (as percentage) are plotted against the thermal demand of the two simulated buildings, namely the semi-detached house satisfying the 1996 building regulations and the detached house meeting the 2006 building regulations. Both cases are considered with two alternative DHW demand profiles, so in a total there are four domestic thermal demand patterns.

Heat demands were met by the 3 kW_e Stirling and IC mCHP systems and the 2 kW_e Stirling based mCHP. Figure 6.59 shows the reduction in the carbon emissions and the level of the electricity utilisation in the heating system with the 2 kW_e Stirling based mCHP in respect of the above four heat demand requirements.

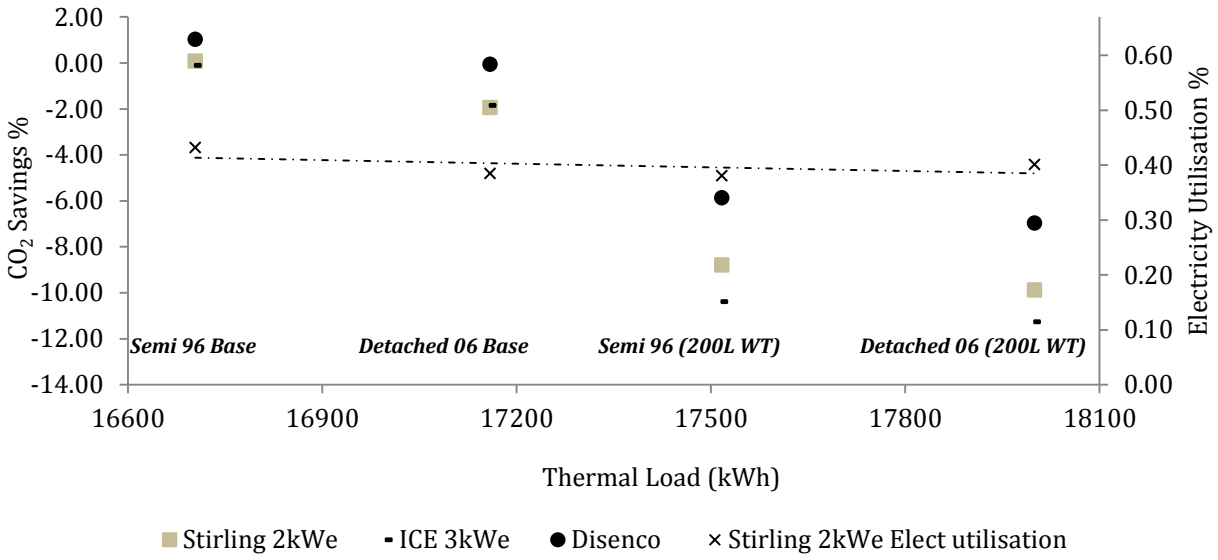

Figure 6.59 Carbon emission reduction and electricity utilisation versus thermal demand in houses

It can be seen in Figure 6.59 that the emission savings decrease with increasing the thermal load. The electricity utilisation level is found to be almost independent on the thermal load. The sharp drop in the emissions (which occurs for thermal loads between 17,200 kWh_{th} and 17,500 kWh_{th}) is attributed to the increased gas consumption and thermal losses in the larger water tanks. In respect of the carbon emissions, the Disenco mCHP demonstrates better performance due to its higher thermal efficiency and the highest (among other mCHPs) electricity utilisation. Overall, the above mCHPs provide only marginal carbon savings in houses with low thermal requirements.

Economic summary

Figure 6.60 shows the reduction in utility costs in respect to the four demand requirements. It can be seen in Figure 6.60 that utility cost savings are gradually decreasing with the rise in the thermal demand of the houses. The higher thermal requirements require the prolonged operation of the mCHP systems resulting in the higher power generation. However, the increased electricity generation does not compensate for the higher natural gas consumption.

All technologies provide the significant cost savings in the range between 17 and 35% with 3 kW_e ICE mCHP having advantages over Stirling engine mCHPs.

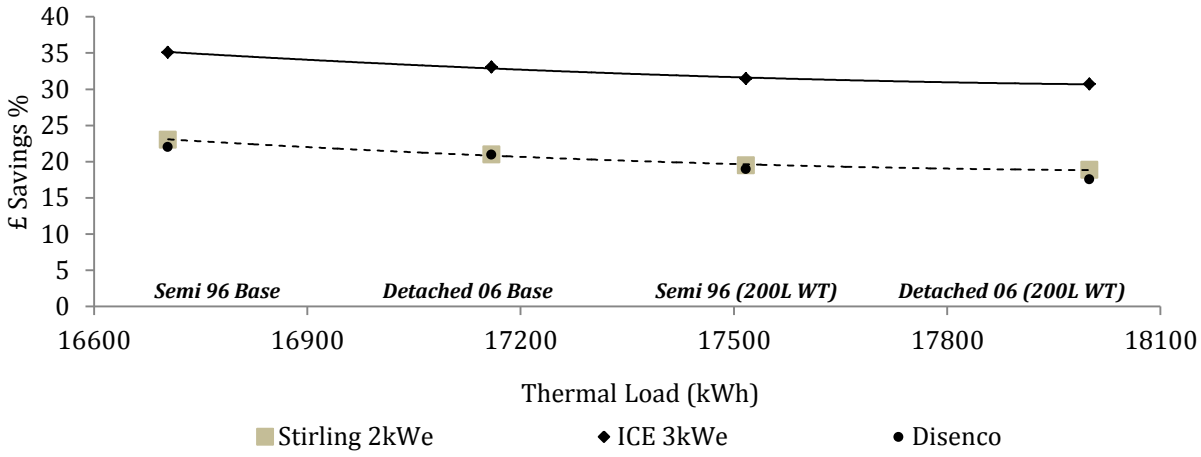

Figure 6.60 Utility cost reductions versus thermal demand

6.10.1.1 Individual mCHP systems

Simulation results were also summarised in respect to Stirling and IC engine mCHPs and PEM fuel cell mCHPs.

Stirling engine mCHPs

The savings in utility costs and the reduction of carbon emissions as functions of the thermal load for all Stirling engine mCHP units are shown in Figure 6.61 and Figure 6.62.

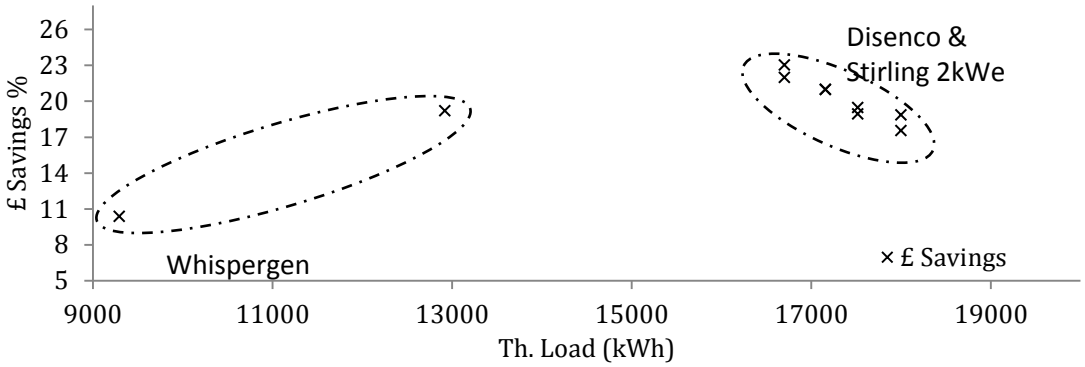

Figure 6.61 Utility costs reductions as a function of the thermal demand with Stirling based mCHPs

In general, in cases in which Stirling engine mCHPs are deployed then utility cost savings decrease as the thermal load increases.

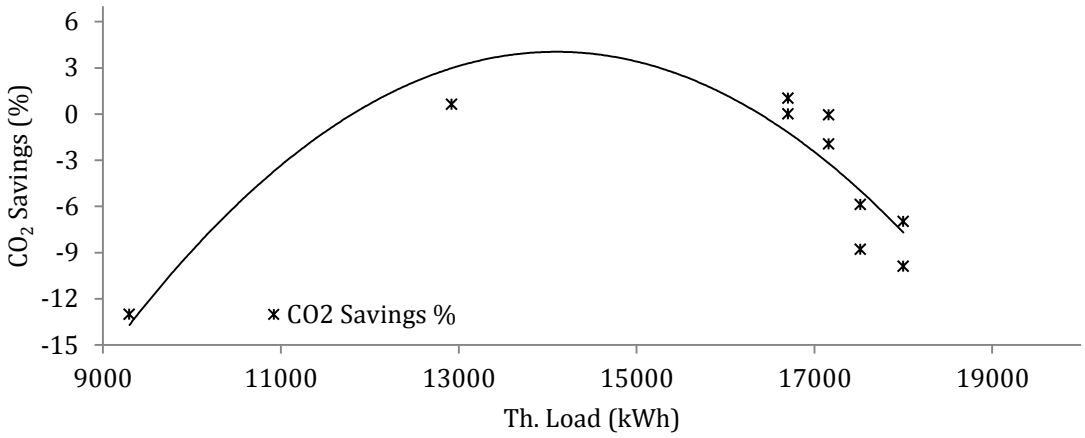

Figure 6.62 Carbon emission reduction as function of the thermal demand with Stirling based mCHPs

Figure 6.62 shows that for very large and very small thermal demands Stirling mCHPs, with their current technical specifications, do not provide carbon savings compared to the conventional gas boiler heating system and grid-connected electricity supply in houses. However, it appears possible to obtain small carbon savings using Stirling mCHPs in houses with average thermal requirements on the 14,000 kWh_{th} level.

IC engine based mCHPs

Figure 6.63 and Figure 6.64 show the utility costs reduction and carbon emissions variations as functions of the thermal load in cases in which ICE engine mCHPs were employed. From Figure 6.63 the utility cost savings decline with the rise in the thermal load. The increased gas consumption at the high thermal demands has a negative impact on the overall economic performance regardless of the increased power generation. Figure 6.64 shows that there are noticeable carbon savings for the thermal demands up to 15,000 kWh which exist in a majority of UK houses. Savings would reach maximum in houses with thermal demand of

about 11,500 kWh. For houses with large thermal demands, the ICE based mCHPs do not provide carbon savings.

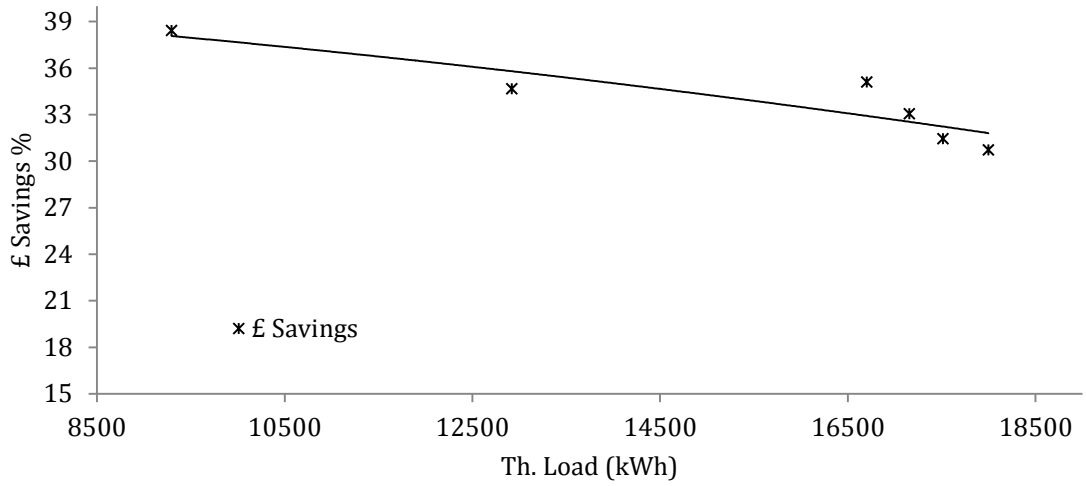

Figure 6.63 Utility cost reductions as a function of the thermal demand with ICE based mCHPs

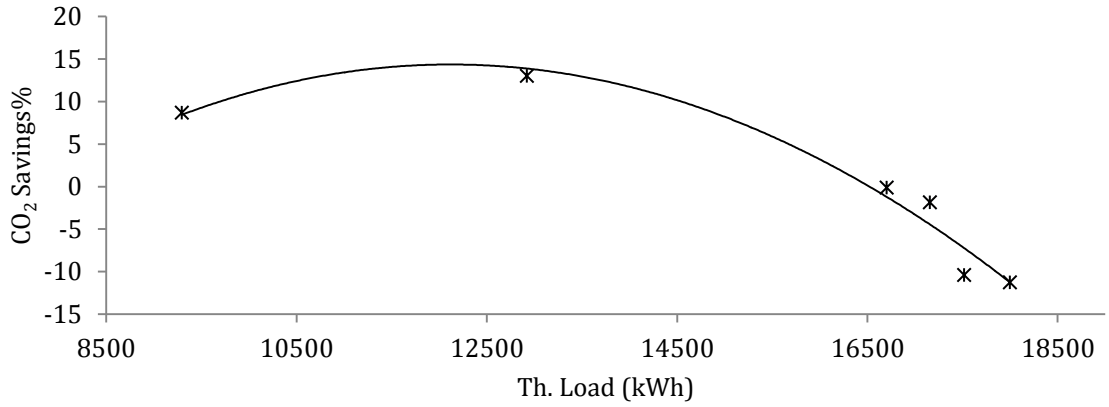

Figure 6.64 Carbon emission reductions as a function of the thermal demand with ICE based mCHPs

PEM Fuel cell based mCHPs

Figure 6.65 presents results on carbon emission and utility cost savings as a function of the thermal load for the PEM fuel cell mCHPs. Thermal requirements of two building only were used in simulations.

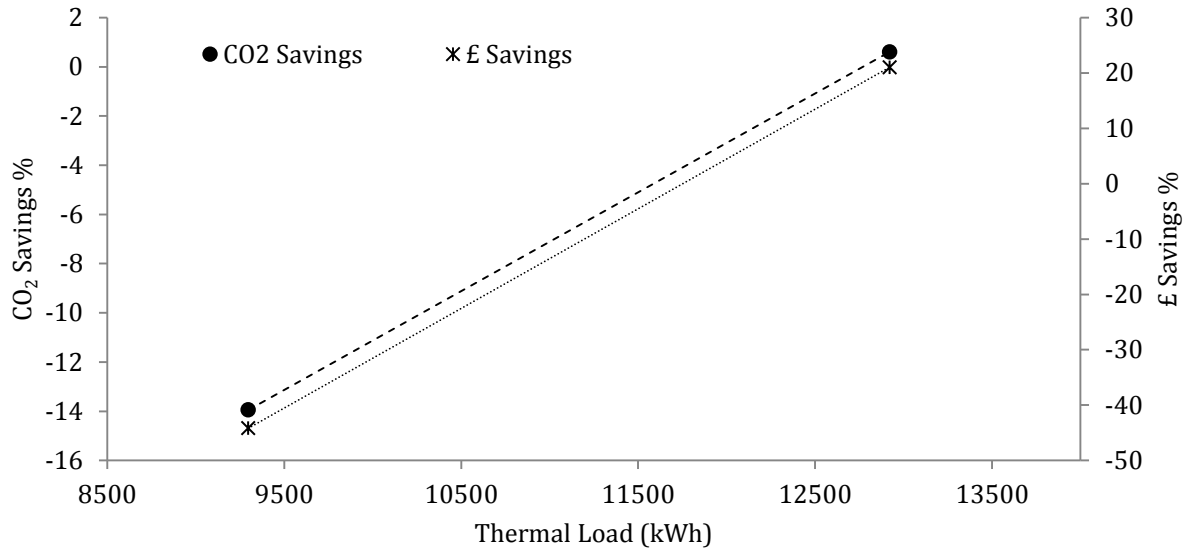

Figure 6.65 Reduction in carbon emissions and utility costs as functions of the thermal demand with PEM fuel cell mCHPs

It can be seen that the rise in the thermal loads increases both carbon emission and utility cost savings. This is attributed to the increase in both electricity utilisation and combined thermal efficiency of the fuel cell system. But overall, the PEM FC mCHP provides carbon savings for houses with small and medium thermal loads. The utility savings are not achieved in the houses with the small thermal load.

6.10.1.2 Carbon emission and utility cost savings in houses with full utilisation of electricity generated by mCHPs

The electricity utilisation rate significantly affects both the economic and environmental performance of the mCHP systems. A hypothetical scenario, in which all the power generated by mCHPs is utilised inside the house, was investigated.

Stirling based mCHPs

Figure 6.66 and Figure 6.67 show the utility cost and carbon emission savings as a function of the thermal load in the house for all cases in which the Stirling engine mCHPs were deployed. It can be seen that both types of savings are considerably improved when the all power produced by mCHPs is fully utilised in the house. The utility savings are provided in the range between 20 and 40 % for the whole range of thermal loads and carbon savings are achieved in houses with thermal loads starting at about 10,000 kW_{th}.

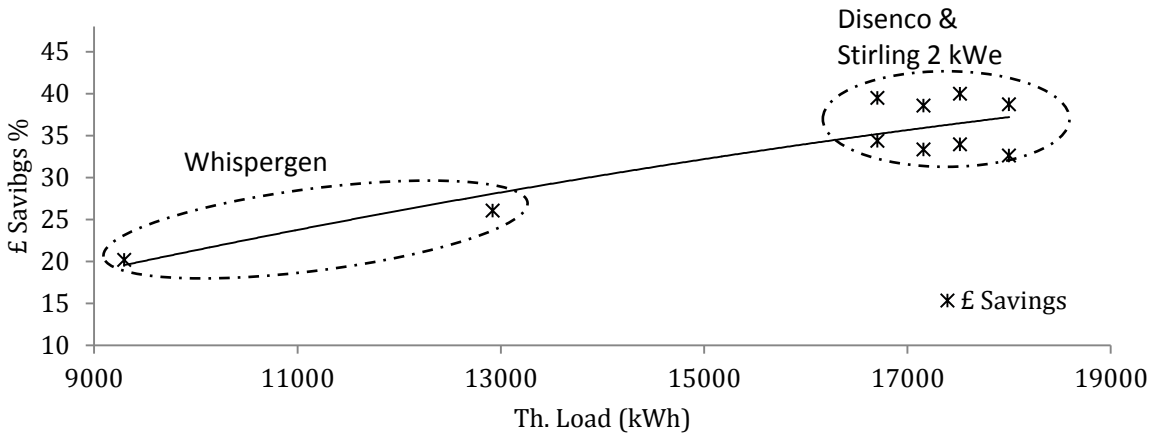

Figure 6.66 Utility cost reductions as a function of the thermal demand with Stirling engine mCHPs

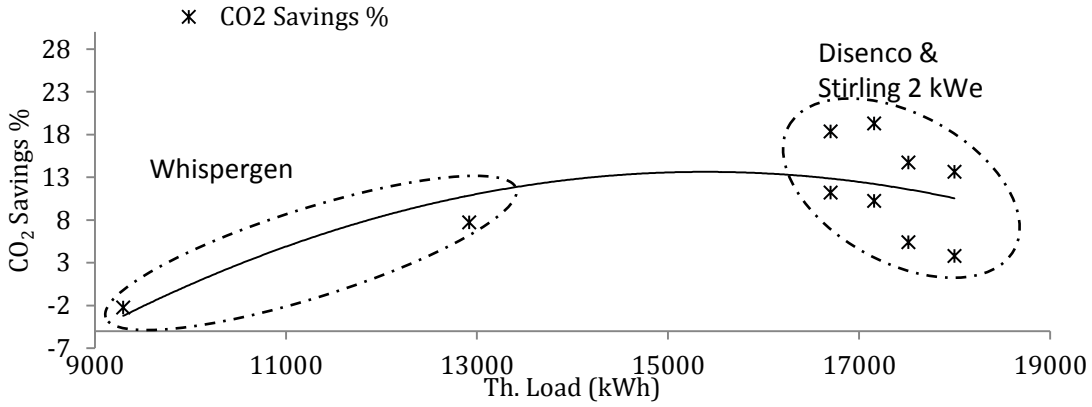

Figure 6.67 Carbon emission reductions as a function of the thermal demand with Stirling engine mCHPs

ICE based mCHPs

Figure 6.68 and Figure 6.69 shows the results obtained on utility and carbon emission savings in cases in which the ICE mCHPs are deployed. As in the case with Stirling engine mCHPs, savings are significantly improved if all power generated by mCHPs is fully utilised in the house.

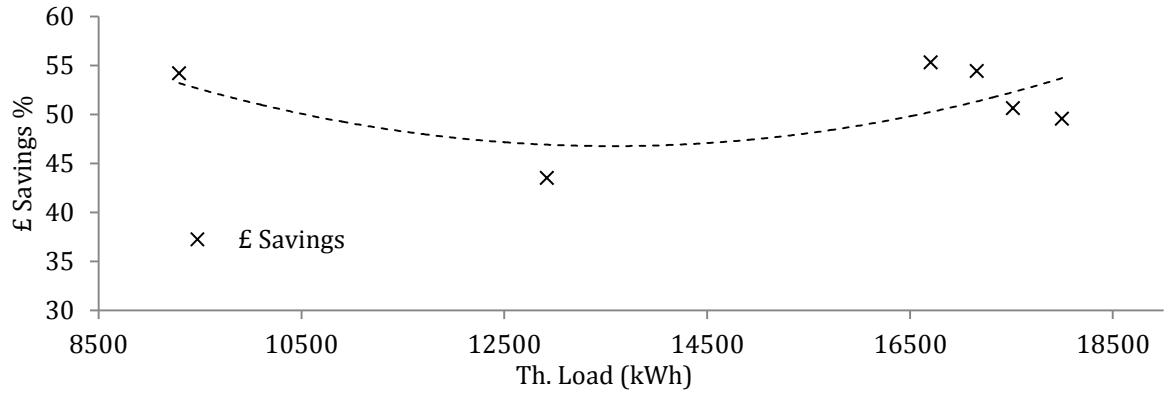

Figure 6.68 Utility cost reductions as a function of the thermal demand with Stirling engine mCHPs

Figure 6.68 shows that utility cost savings are now on the level of 42-55 % with greater savings being achieved for houses with the small and large thermal loads. The carbon savings decrease with the rise of the thermal load in the house, see Figure 6.69.

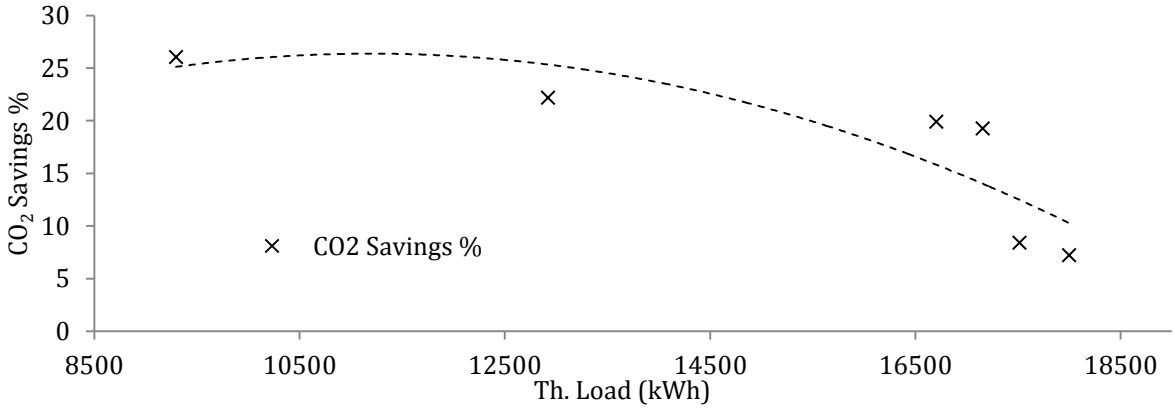

Figure 6.69 Carbon emission reductions as a function of the thermal demand with ICE mCHPs

PEM Fuel cell based mCHPs

Figure 6.70 shows the utility cost and carbon emission savings as functions of the thermal load for PEM fuel cell mCHPs.

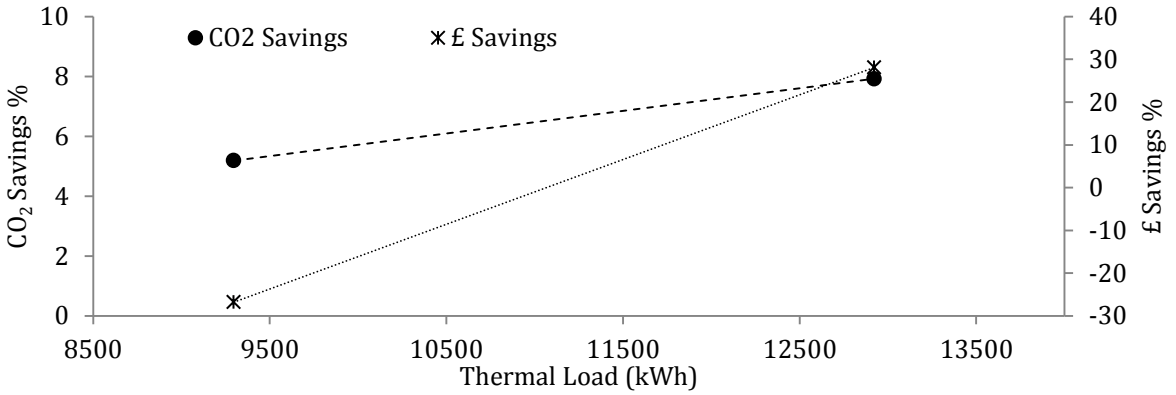

Figure 6.70 Reduction in carbon emissions and utility costs as functions of the thermal demand with PEM fuel cell mCHPs

Assumming that all the electricity generated is consumed on site, Figure 6.70 show that the carbon emission and utility savings practically improve very little.

6.10.2 Cases when the house heating systems are based on 1 kWe ICE and Stirling engine mCHPs with auxiliary burners

The simulation results are presented in this section for cases when mCHPs with auxiliary burners are deployed in the house heating systems with reference to their economic and environmental performance. Figure 6.71 and Figure 6.72 show the carbon emission and utility cost savings as functions of the thermal load for the detached house satisfying 1996 and 2006 building regulations and semi-detached house meeting 1996 building regulations. The level of the carbon savings are determined by the rate of electricity generation utilisation inside the house and the amount of natural gas consumption. It can be seen in Figure 6.71 that a small increase in the thermal demand resulted in a reduction in carbon emissions due to the rise in the electricity related CO_2 savings. However, whilst the noticeable carbon savings are

achieved with the ICE mCHP, there are a very marginal carbon savings (or, indeed, a slight carbon emissions increase) with the Stirling engine mCHP deployed in the house with the high thermal demand.

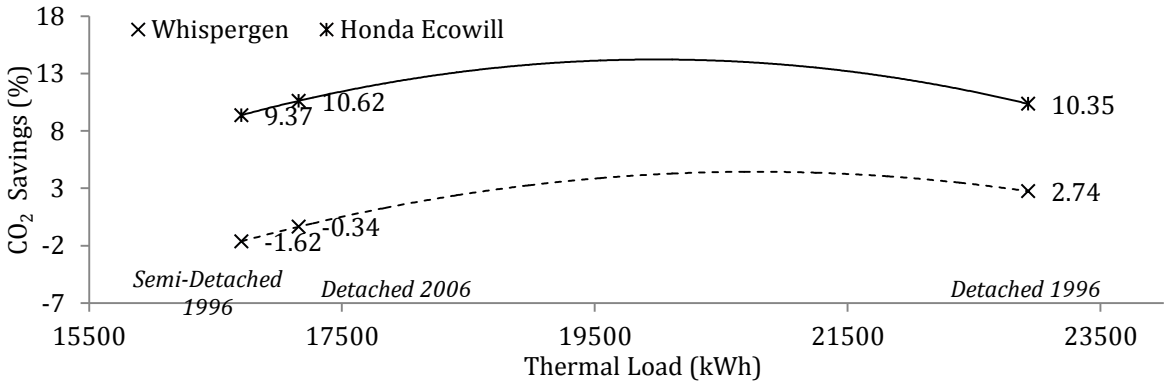

Figure 6.71 Carbon emissions reduction as a function of the thermal demand for Stirling engine and ICE mCHPs combined with the auxiliary boiler

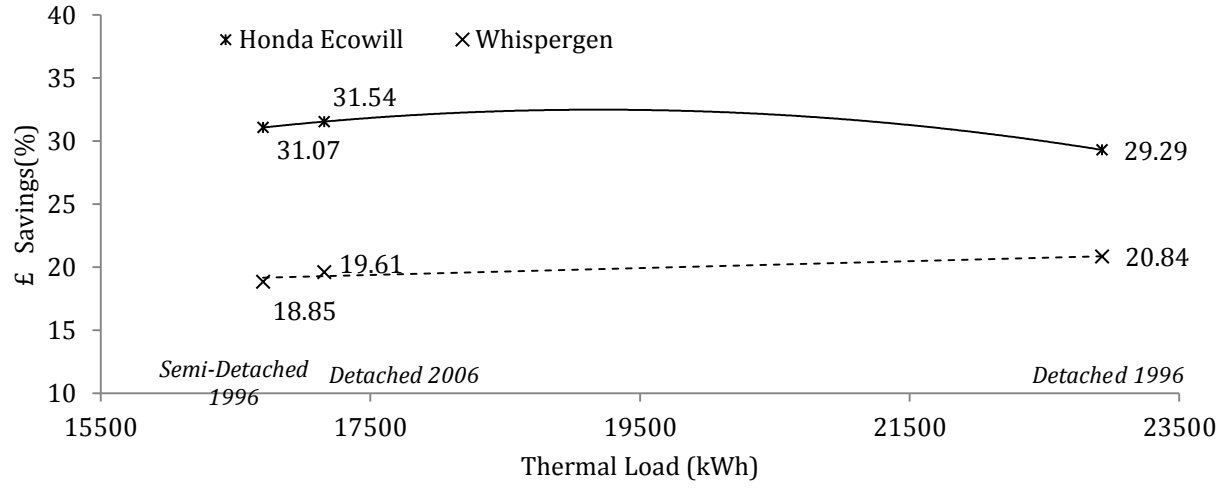

Figure 6.72 Utility cost reductions as a function of thermal load for Stirling engine and ICE mCHPs combined with the auxiliary boiler

In respect of the ICE mCHP unit, it can be seen in Figure 6.72 that the utility cost savings are marginally increased with the thermal load. However for the detached house meeting 1996 building regulations an increased gas consumption brings down the overall utility cost savings. In respect of the Stirling engine mCHP unit, both increased electricity utilisation and

power generation were observed and these compensated for the gas consumption. Therefore savings in utility bills increase linearly with the thermal load in the house.

The effect of the Auxiliary Boiler/mCHP thermal outputs ratio

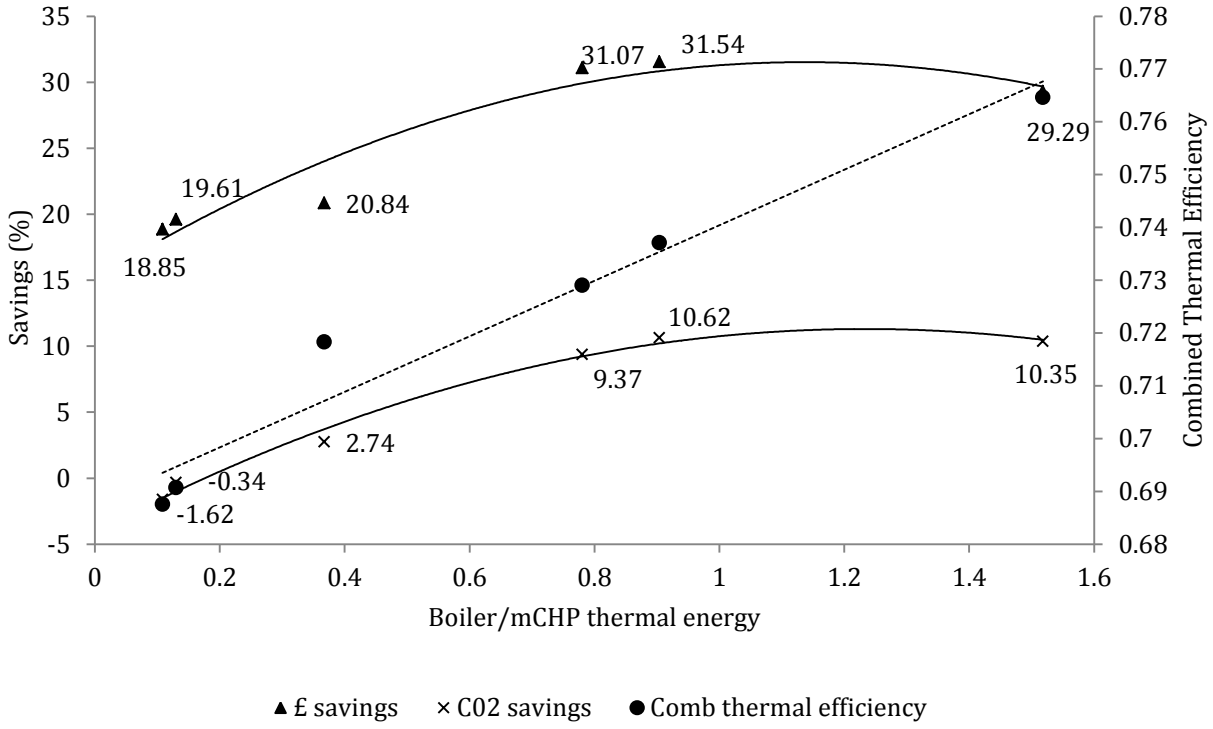

Figure 6.73 shows the utility cost and carbon emission savings as functions of the auxiliary Boiler/mCHP thermal outputs ratio.

For both utility costs and carbon emissions, an increase in savings with increasing of the auxiliary Boiler/mCHP thermal outputs ratio is evident, which can be attributed to an increase in the combined thermal efficiency of the auxiliary boiler/mCHP system. Maximum savings were predicted the auxiliary Boiler/mCHP thermal outputs ratios between 1 and 1.2.

Chapter 7 Deployment on a district/street level of a random set of mCHPs based on different technologies

7.1 Introduction

The advantages of replacing convectional heating system with mCHPs, with reference to energy cost and carbon emissions, in individual dwellings have been analysed in previous two Chapters. If mCHPs will reach the market and become commercially available, then it is most likely that a random mix of such technologies will be deployed. In this Chapter such the deployment on a district/street level of a random set of mCHPs based on different technologies is modelled and resulting annual economic and carbon emission savings are estimated. In this modelling process it was assumed that the district/street will consist of a combination of different type houses with various thermal and power requirements.

Table 7.1 and Table 7.2 show the details of various house heat and power demands considered in the modelling process.

Table 7.1 Simulated houses in which mCHPs are used as a single heating source

House type	Electricity requirements (MWh_e)	DHW requirements (L/Day)	Deployed mCHP
Bungalow 2006	3.7	150	1 kW_e Whispergen
Semi-Detached 2006	4.6	200	1) 1 kW_e Whispergen 2) 2 kW_e ICE
Semi-Detached 1996	4.6 5.5 4.6	200 200 250	1) 3 kW_e Disenco, 2) 2 kW_e Stirling 3) 3 kW_e ICE
Detached 2006	4.6 5.5 4.6	200 200 250	1) 3 kW_e Disenco, 2) 2 kW_e Stirling 3) 3 kW_e ICE

Table 7.2 Simulated houses in which mCHPs are combined with auxiliary burners

House type	Electricity requirements (MWh_e)	DHW requirements (L/Day)	Deployed mCHP
Bungalow 2006	3.7	150	1) 1 kW_e Ecowill 2) 1 kW_e PEM FC
Semi-Detached 2006	4.6	200	1) 1 kW_e Ecowill 2) 1 kW_e PEM FC
Semi-Detached 1996	4.6 5.5	200	1) 1 kW_e Whispergen 2) 1 kW_e Ecowill
Detached 2006	4.6 5.5	200	1) 1 kW_e Whispergen 2) 1 kW_e Ecowill
Detached 1996	4.6 5.5	200	1) 1 kW_e Whispergen 2) 1 kW_e Ecowill

These demands are covered by the mCHP technologies in scenarios in which they are used as a single source of heat (Table 7.1) or used in combination with auxiliary boilers (Table 7.2). Additionally, these tables show the range of mCHP systems considered for each type of houses. In house with the 250 L per day DHW demand the heating system is equipped with a 200 L DHW tank. All houses with other DHW demands were simulated with the heating system having the 150 L DHW tank

7.2 Sizes of streets simulated

7.2.1 The 61-house street

A mixture of houses, including detached, semi-detached and bungalow buildings, was assumed to make up the street with a total of 61 dwellings. The generation of houses and of their primary energy requirements could be performed randomly, however, the number of dwellings in the street was considered to be relatively small and therefore the even distribution in the street in respect to the energy demand (building) and supply (mCHP technology) was selected. Thus, in half of the houses a mCHP was used as a single source of heat generation, whilst in the remaining half of houses mCHPs combined with auxiliary

burners were deployed. Table 7.3 shows the mixture of houses which was used in the modelling process of the 61-house street.

Table 7.3 The mixture of houses and mCHP technologies which was used in the modelling process of the 61-house street

Type of Dwelling	Number of Dwellings	mCHP # Dwellings	mCHP & Back-up Boiler # Dwellings
Bungalow		2	2
	4	Whispegen	Honda Ecowill & Boiler PEMFC & Boiler
Semi-Detached 2006		2	2
	4	Whispegen 2 kWe ICE	Honda Ecowill & Boiler PEMFC & Boiler
Detached 2006		6	4
	10	3 kWe ICE 2 kWe Stirling 3 kWe Disenco	Whispergen & Boiler Honda Ecowill & Boiler
Semi Detached 1996		6	4
	10	3 kWe ICE 2 kWe Stirling 3 kWe Disenco	Whispergen & Boiler Honda Ecowill & Boiler
Detached 2006; Increased Electricity consumption		3	6
	9	3 kWe ICE 2 kWe Stirling 3 kWe Disenco	Whispergen & Boiler Honda Ecowill & Boiler
Semi Detached 1996 Increased Electricity consumption		6	4
	10	3 kWe ICE 2 kWe Stirling 3 kWe Disenco	Whispergen & Boiler Honda Ecowill & Boiler
Detached 2006; Increased Electricity consumption		3	
	3	3 kWe ICE 2 kWe Stirling 3 kWe Disenco	/
Semi-Detached 1996 Increased Electricity consumption		3	
	3	3 kWe ICE 2 kWe Stirling 3 kWe Disenco	/
Detached 1996			4
	4	/	Whispergen & Boiler Honda Ecowill & Boiler
Detached 1996; Increased Electricity consumption			4
	4		Whispergen & Boiler Honda Ecowill & Boiler
Total	***61***	***31***	***30***

After generating the above mixture of houses and mCHP technologies the whole street was simulated and results were compared with results from a street in which all houses are equipped with conventional heating systems and use grid-imported electricity. Table 7.4 shows the results in respect of the economic and environmental performance of a mixture of mCHP technologies in such the 61-house street.

Table 7.4 Annual CO_2 emissions and utility costs for the 61-house street

Configuration of the house heating system	**CO_2 emission (t)**	**Annual Expenses (£k)**
Conventional heating systems	364.6	74.4
A mixture of mCHPs	346.5	68.2

It can be seen in Table 7.4, that a reduction in both carbon emissions and utility costs of approximately 5 % and 32 %, respectively, is achieved when the street made of a mixture of 61 houses is equipped with different mCHP technologies. The relatively low thermal efficiency in all cogeneration systems resulted in the increased gas consumption by the street residents. However, the power generated compensates for emissions related to the fuel usage.

7.2.2 The 120-house street

A Street consisting of 120 houses was considered. The selection of supply technologies and demand mix implemented for the 61-house street was scaled up for application in this case. Table 7.5 shows the mixture of houses which was used in the modelling process of the 120 dwellings street. Half of the total number of houses was supplied from a single heating equipment while the remaining half was supplied by a mCHP combined with an auxiliary boiler.

Table 7.5 The mixture of houses and mCHP technologies which was used in the modelling process of the 120-house street.

Type of Dwelling	Number of Dwellings	mCHP # Dwellings	mCHP & Back-up Boiler # Dwellings
Bungalow		2	4
	6	Whispegen	Honda Ecowill & Boiler PEMFC & Boiler
Semi-Detached 2006		4	4
	8	Whispegen 2 kWe ICE	Honda Ecowill & Boiler PEMFC & Boiler
Detached 2006		12	8
	20	3 kWe ICE 2 kWe Stirling 3 kWe Disenco	Whispergen & Boiler Honda Ecowill & Boiler
Semi Detached 1996		12	8
	20	3 kWe ICE 2 kWe Stirling 3 kWe Disenco	Whispergen & Boiler Honda Ecowill & Boiler
Detached 2006; Increased Electricity consumption		6	12
	18	3 kWe ICE 2 kWe Stirling 3 kWe Disenco	Whispergen & Boiler Honda Ecowill & Boiler
Semi Detached 1996 Increased Electricity consumption		12	8
	20	3 kWe ICE 2 kWe Stirling 3 kWe Disenco	Whispergen & Boiler Honda Ecowill & Boiler
Detached 2006; Increased Electricity consumption		6	
	6	3 kWe ICE 2 kWe Stirling 3 kWe Disenco	/
Semi-Detached 1996 Increased Electricity consumption		6	
	6	3 kWe ICE 2 kWe Stirling 3 kWe Disenco	/
Detached 1996			8
	8	/	Whispergen & Boiler Honda Ecowill & Boiler
Detached 1996; Increased Electricity consumption			8
	8		Whispergen & Boiler Honda Ecowill & Boiler
Total	***120***	***60***	***60***

Table 7.6 shows the results in respect of the economic and environmental performance of a mixture of mCHP technologies in such the 120-house street.

Table 7.6 Annual CO_2 emissions and utility costs for the 120-house street

Configuration of the house heating system	**CO_2 emission (t)**	**Annual Expenses (£k)**
Conventional heating systems	721.8	147.1
A mixture of mCHPs	708	103.6

The obtained results presented in Table 7.6, indicate a reduction in carbon emissions of approximately 13 tonnes per annum (corresponding to 2 %) in respect of the 120-house street powered by a mixture of mCHP systems, whereas the utility bills were reduced by 29.5 %.

7.2.3 The 240-house street

Finally, a street which consisted of 240 houses was simulated. Table 7.7 shows the mixture of houses which was used in the modelling process of the 240-house street. Table 7.8 shows the results in respect of the economic and environmental performance of a mixture of mCHP technologies in such the 240-house street.

If the above mixture of mCHP systems replace the conventional heating systems in the street of 240 houses then a 28.5 % overall reduction in the utility costs can be achieved as presented in Table 7.8. In respect of the CO_2 emission, a reduction of 15.6 tonnes per annum (about 1 %) is estimated to be achieved in such the street.

Table 7.7 The mixture of houses and mCHP technologies which was used in the modelling process of the 240-house street.

Type of Dwelling	Number of Dwellings	mCHP # Dwellings	mCHP & Back-up Boiler # Dwellings
Bungalow		4	8
	12	Whispegen	Honda Ecowill & Boiler PEMFC & Boiler
Semi-Detached 2006		8	8
	16	Whispegen 2 kWe ICE	Honda Ecowill & Boiler PEMFC & Boiler
Detached 2006		24	16
	40	3 kWe ICE 2 kWe Stirling 3 kWe Disenco	Whispergen & Boiler Honda Ecowill& Boiler
Semi Detached 1996		24	16
	40	3 kWe ICE 2 kWe Stirling 3 kWe Disenco	Whispergen & Boiler Honda Ecowill & Boiler
Detached 2006; Increased Electricity consumption		12	24
	36	3 kWe ICE 2 kWe Stirling 3 kWe Disenco	Whispergen & Boiler Honda Ecowill& Boiler
Semi Detached 1996 Increased Electricity consumption		24	16
	40	3 kWe ICE 2 kWe Stirling 3 kWe Disenco	Whispergen & Boiler Honda Ecowill & Boiler
Detached 2006; Increased Electricity consumption		12	
	12	3 kWe ICE 2 kWe Stirling 3 kWe Disenco	/
Semi-Detached 1996 Increased Electricity consumption		12	
	12	3 kWe ICE 2 kWe Stirling 3 kWe Disenco	/
Detached 1996			16
	16	/	Whispergen & Boiler Honda Ecowill & Boiler
Detached 1996; Increased Electricity consumption			16
	16		Whispergen & Boiler Honda Ecowill & Boiler
Total	***240***	***120***	***120***

Table 7.8 Annual CO_2 emissions and utility costs for the 240-house street

Configuration	CO_2 emission (t)	Annual Expenses (£k)
Conventional heating system Street scheme	1443.7	293.8
mCHP based Street scheme	1428.1	209.9

7.3 Annual CO_2 and utility cost reductions from deployment of mCHP technologies on the street level

Obtained simulation results are summarised in order to assess the merits of the installation of mCHP systems on the district/street level. Figure 7.1 shows the reduction in carbon emissions and utility cost (in percentages) for all simulated street scenarios.

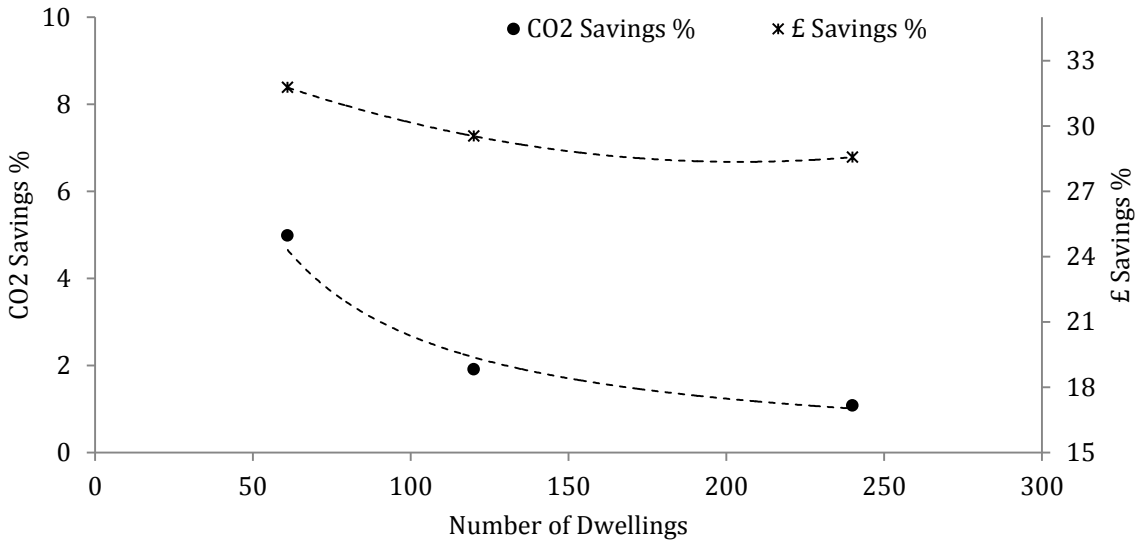

Figure 7.1 CO_2 and utility cost reductions from deployment of mCHPs on the street level

It can be noted from Figure 7.1 that as the number of houses on the street increases, the carbon emissions and cost savings decline. This is attributed to an increase in the number of mCHP units with poorer performance appearing in the mix of systems as the total number of houses goes up. The total annual carbon emissions in all scenarios was analysed in its

component parts, namely fuel-related and electricity-related. Figure 7.2 shows the annual carbon emissions components related to the number of houses.

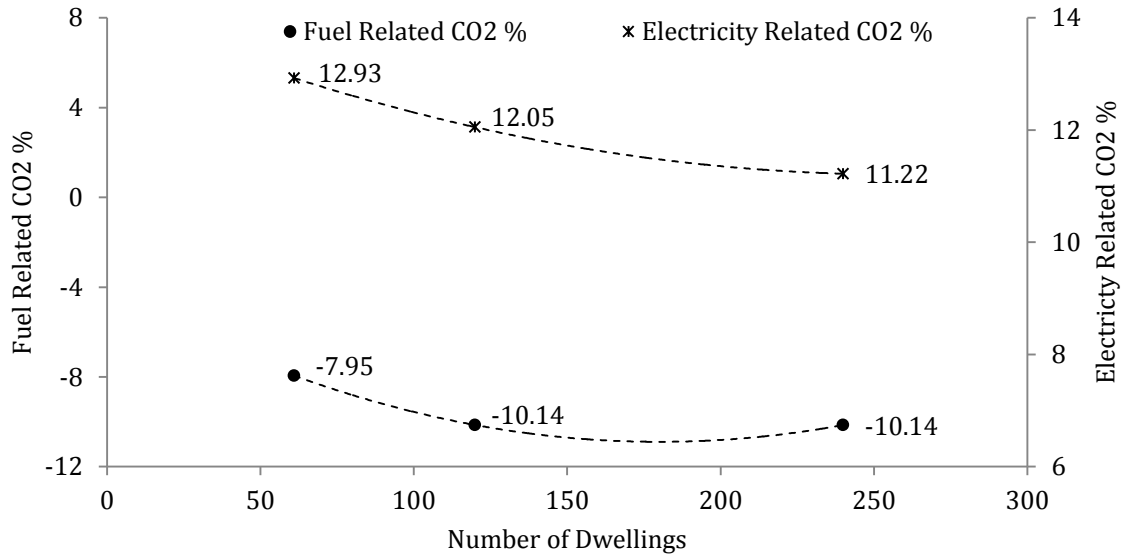

Figure 7.2 CO_2 emissions related to both fuel and electricity from deployment of mCHPs on the street level

In all cases cogeneration systems featured a lower thermal efficiency than the condensing boiler, which results in the increased fuel consumption. Therefore, carbon emissions related to fuel consumption were found to be higher compared to the reference scenario as it can be seen in Figure 7.2. In the 61-house street the carbon emissions were found to be almost 8% higher than the base scenario case whereas for 120- and 240-houses carbon emissions were increased by 10 %. The increase of the fuel related CO_2 emissions combined with the gradual drop in the electricity related emissions, resulted in a steep drop in the carbon emission savings as shown in Figure 7.1 (particularly in the transition from the 61- to 120-house street). The marginal saving in carbon emissions in both the 120- and 240- house streets was attributed to a higher number of low performance mCHP units which were allocated in the distribution pattern.

The savings in the utility costs were found to consist of three components: the fuel consumption, the electricity purchased and the economic incentives under the feed-in tariff

scheme. Figure 7.3 shows savings in the utility costs related to all three components over the total number of houses in the street.

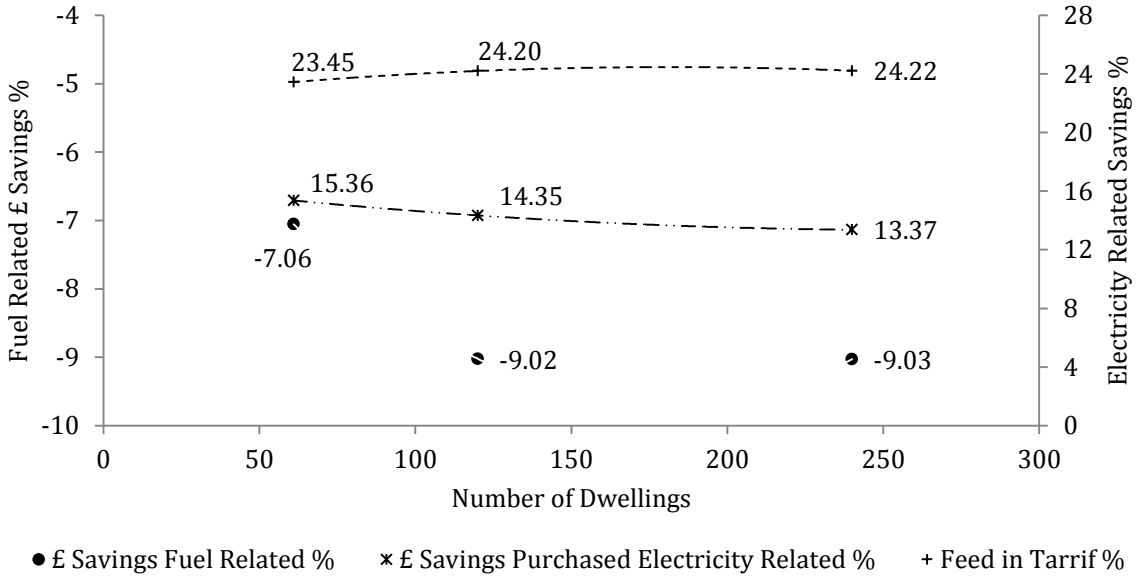

Figure 7.3 Utility cost savings split between the fuel and electricity from deployment of mCHPs on the street level

From Figure 7.3 it can be seen that the reduction in the electricity bills due to the feed- in tariff (FIT) was approximately unchanged in all three scenarios; the FIT contribution accounted for the 23.4 % to 24.2 % reduction of the gross utility costs. The savings related to the electricity imported from the national grid were found to gradually decrease. The gas related savings show a steep increase in the transition from the 61- to 120-house street whilst it remained constant in transition from the 120- to 240-street houses. This supports the suggestion that more "low performance" mCHPs are participating in 120- and 240-house street schemes. Under all scenarios the increased fuel consumption was translated to higher utility bills.

7.4 Equipping Street houses with best mCHP technologies

Overall results from deployment of a mix of different mCHP technologies on the street scale are significantly affected by the selection of the energy supply-demand mix distribution. The

approach which was followed in the previous modelling of the three streets was based on an even distribution of technologies which in return could constrain overall mix mCHP performance. In this section, since data on the individual mCHP system's performance is available, the only technologies that demonstrated the best performance were selected to replace the conventional heating systems in given dwellings. Table 7.8 shows the best units selected for replacement of the conventional heating systems in the 61-house street.

Table 7.8 The best units selected for replacement of the conventional heating systems in the 61-house street.

Type of Dwelling	Number of Dwellings	mCHP # Dwellings	mCHP & Back-up Boiler # Dwellings
Bungalow		2	2
	4	Whispegen	Honda Ecowill & Boiler
Semi-Detached 2006		2	2
	4	Whispegen	Honda Ecowill & Boiler
Detached 2006		6	4
	10	3 kWe Disenco	Honda Ecowill & Boiler
Semi Detached 1996		6	4
	10	3 kWe Disenco	Honda Ecowill & Boiler
Detached 2006; Increased Electricity consumption		3	6
	9	3 kWe ICE	Honda Ecowill & Boiler
Semi Detached 1996; Increased Electricity consumption		6	4
	10	3 kWe ICE	Honda Ecowill & Boiler
Detached 2006; Increased Electricity consumption		3	
	3	3 kWe Disenco	/
Semi-Detached 1996; Increased Electricity consumption		3	
	3	3 kWe Disenco	/
Detached 1996			4
	4	/	Honda Ecowill & Boiler
Detached 1996; Increased Electricity consumption			4
	4	/	Honda Ecowill & Boiler
Total	***61***	***31***	***30***

The similar selection of the mCHP technologies offering the best performance then was carried out for 120- and 240-house streets following the methodology and distribution as summarised in Table 7.8. Table 7.9 shows the annual results on CO2 emissions and utility costs obtained for all three streets (in percentage) with reference to the base scenario in which conventional heating systems were used in all houses.

Table 7.9 Annual results on CO_2 emissions and utility costs savings obtained for all three streets with reference to the base scenario in which conventional heating systems were used in all houses

Configuration	Emission Savings %	Expenses Savings %
61-house street	5.22	32.85
120-house street	5.21	32.96
240-house street	3.6	31.01

The allocation of the best mCHP technology in houses improved the overall performance on the street level in terms of both carbon emissions and utility costs. It can be seen in Table 7.9 that CO_2 emission savings are increased compared to the original mCHP technology mix distribution and are in the range between 3.6 to 5.2 %. This was achieved as the least feasible units were excluded from the mCHP mix. The utility costs are decreased by approximately 32 % in all cases. The improvement in the performance was due to the higher on-site utilisation of the electricity and lower gas consumption by more efficient mCHPs.

7.5 A possibility of "electrical power" coupling of adjacent houses with different occupancy patterns

In all previous modelling of street scenarios, it is assumed that there is no electrical interaction between the houses and surplus of electricity, generated in each house, is exported to the national grid. In this section, a hypothetical situation in which a power interaction between the dwellings is carried out is considered with expectation that this will result in better performance due to higher on-site electricity utilisation. In a coupled houses scenario, an excess of produced electricity is assumed to be utilised in the adjacent houses, rather than be exported into the grid. Due to different operating profiles in the street mix, any overlapping in the power generation through the day is expected to enhance the advantages of

mCHP. The selected pair of houses represents bungalows meeting the 2006 building regulations and equipped with the ICE engine mCHPs. The energy requirement profiles for the house with two retired residents were selected for the first bungalow and the energy requirement profiles for the house with a pair of working adults were applied for the second bungalow. In this way, the operation of the mCHP throughout the day could be attained. All simulations were performed in the split heat generation mode. Figure 7.4 shows the layout of the coupled bungalow buildings.

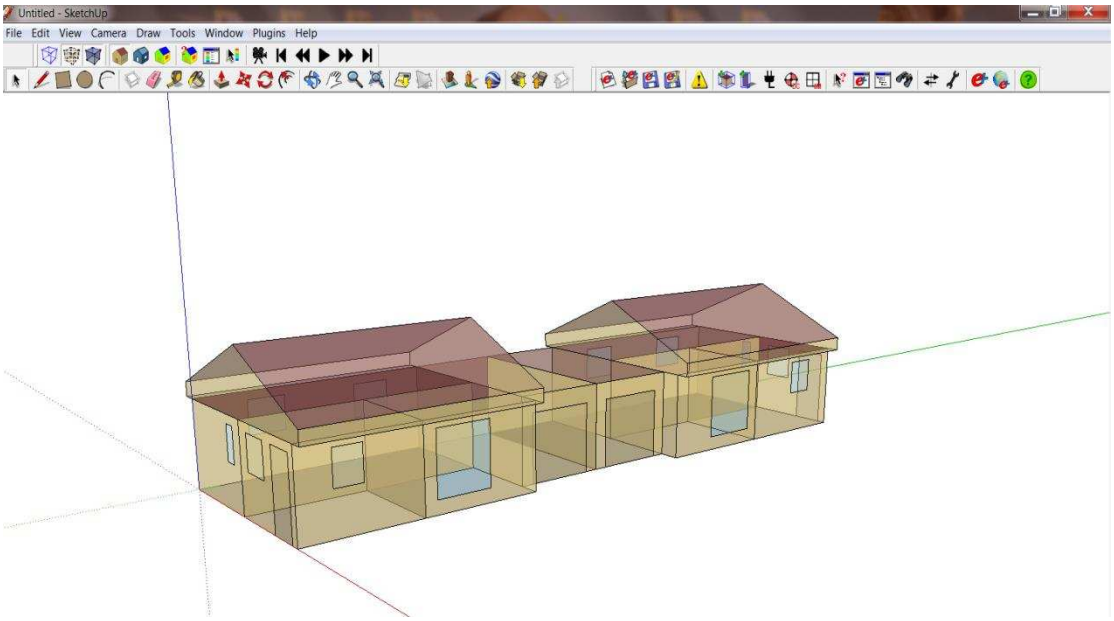

Figure 7.4 The layout of the coupled bungalows

Figure 7.5 shows the operation of both cogeneration units with the back-up boilers in a winter weekday. It can be seen in Figure 7.5 that the Honda Ecowill_1 mCHP combined with its auxiliary Boiler_1 was used to meet the thermal demand of the bungalow house with two retired residents, whereas the Honda-Ecowill_2 mCHP combined with its auxiliary Boiler_2 was used in the adjacent bungalow in which two working adults reside.

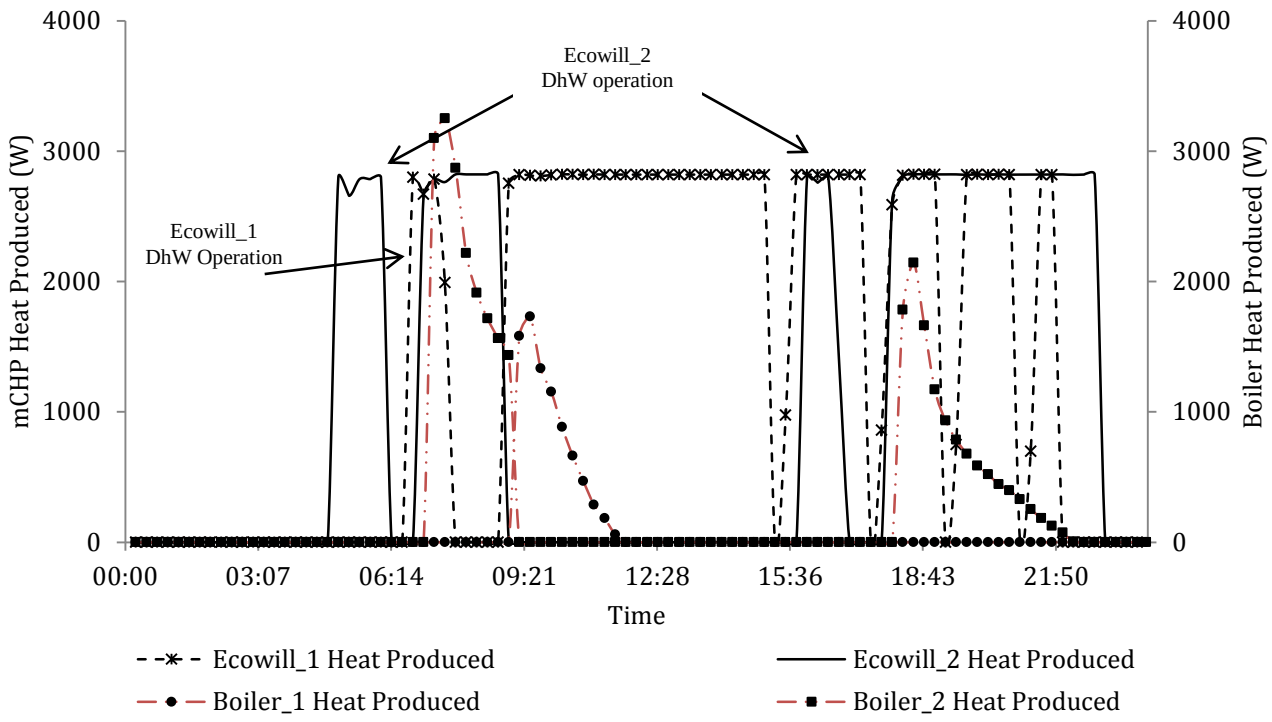

Figure 7.5 Heat generation by two mCHPs with auxiliary boilers in the coupled bungalows in the split heat generation mode in a winter weekday

Heat generated by both mCHP units prior to the space heating (indicated by arrows in the diagram) was used for charging corresponding 150 L DHW tanks. The lower exterior temperature during early morning resulted in the increased thermal output from the Boiler_1 during the morning space heating operation compared to the corresponding operation of the Boiler_2 two hours later in the day (when the exterior temperature was higher). Once the zones thermal comfort temperature was reached, both boilers were switched off and the mCHP unit was operating in cycles. This can be observed starting after 15.30 during the long operation of the Ecowill_1 mCHP in the bungalow of the retired couple.

The obtained simulation results were compared against the scenario in which the adjacent bungalows do not exchange generated electricity. Table 7.10 shows the results on annual carbon and utility cost savings for both scenarios.

Table 7.10 Annual carbon and utility cost savings

House configuration	CO_2 emission savings %	Utility costs Savings %
Bungalows with power Interaction	13.71	45.29
Bungalows without power Interaction	9.91	41.17

It can be seen in Table 7.10 that the power interaction between buildings enhances both economic and emission savings by about 4 %. Despite the fact that in both scenarios, the power generated and the natural gas consumption were identical, the purchased electricity amount was decreased by 819 kWh_e which corresponds to 14 % of the total electricity imported. The on-site electricity utilisation rate was increased from 50 % for the scenario without power interaction to a 66 %.

If such power interaction is extended to the street level then the overall performance of buildings in streets may improve beyond 4 % enhancement.

7.6 Conclusions

- In all street scenarios savings in annual carbon emissions and utility costs are achieved. Savings in the carbon emissions are in the range of 1-5 % whilst reductions in the utility costs are between 28.5 and 31.7 %

- The negative ecological impact of individual mCHP units with poorer performance was compensated by mCHPs with better performance in the mix.

- In the scenario in which all conventional heating equipment was replaced with the mCHP technologies, which demonstrated the best performance, both carbon and utility cost savings were enhanced. Reductions are in the range of 3.6-5.2 % and 31-32.5 % for the carbon emissions and utility costs, respectively.

- Simulations of two bungalows with different occupancy patterns and with power interaction indicate that both economic and environmental performance of buildings were enhanced by about 4 % as a result of the higher rate of on-site electricity utilisation.

Chapter 8 Conclusions and Recommendations for Future work

8.1 Conclusions

The outcomes and the main findings of the experimental and theoretical analysis of deployment of a number of mCHP systems based on various technologies along with recommendations for future investigations are presented in this Chapter.

Conclusion from the experimental setups of Whispergen Mk Vb 1 kW_e Stirling engine, Hilton PEM fuel cell 0.75 kW_e and Baxi SenerTech Dachs 5.5 kW_e ICE

Conclusion from the theoretical simulation of several configuration and operating regimes of the Stirling engine based mCHP system applied in a semi-detached building under 2006 construction regulations

Conclusion from the theoretical simulation of a number mCHP units with nominal capacity in the range of 1-3 kW_e based on Stirling, ICE engines and PEM fuel cell prime mover technology.

Conclusion from theoretical simulation of a mass installation scheme which used a mixture of different micro scale co-generation technologies (Stirling, ICE engines, PEMFC)

8.1.1 Conclusions from the experimental part of investigations

The performances of three mCHP units, namely 1 kW_e Whispergen MkVb Stirling engine, 0.75 kW_e Hilton PEM fuel cell and 5.5 kW_e Baxi SenerTech Dachs ICE, were determined for steady-state and dynamic (transient) regimes of the operation, including start-up and shut-down regimes.

The experimentally obtained performance of the units were then used as input data for modelling house heating systems in EnergyPlus software for analysing the energy performance of different types of buildings over a yearly period.

the Stirling based mCHP unit

1. The unit was found to operate at relatively low average thermal and electrical efficiencies of 67 % and 12 %, respectively. The lower level of efficiencies is observed during start-up transient regimes.
2. The unit still generates heat (at a lower rate) for few minutes after it is switched off and this has a positive effect on the overall efficiency of the unit.

The PEM fuel cell unit

1. The maximum electrical efficiency is calculated at 49 % during 'low load' operation and the highest thermal efficiency is 36 % when the stack operates at high power densities. The average efficiency values are 43 % and 31 % for the electrical and thermal efficiencies, respectively, when hydrogen is used as a fuel.

2. The warm star-up of the unit improves both the electrical and thermal performance due to the increased stack temperature and, consequently, to enhanced kinetics of the cell reactions.

3. Each change of the load is associated with a voltage transient behaviour and the magnitude of it's undershoot/overshoot depends on the load variation. No significance difference in the recovery time was noticed during the overshoot voltage response. The absence of the current undershoot/overshoot phenomena suggests that the water content in the self-humidifying membrane is insufficient for provoking the transient voltage behaviour.

4. Despite the fact that purging of hydrogen decreased the stack efficiency, it improves the water management within the fuel cells. In addition hydrogen purging frequency increases with rise in the load since the possibility of water flooding is enhanced at high power densities operation.

the ICE mCHP

1. The average thermal and electrical efficiencies of the unit are 70 % and 20 %, respectively.
2. The unit demonstrates a poor thermal performance during the start-up period.
3. There is a very little delay in full power generation during start-up period (few minutes only).
4. Due to the increased heating requirements of the building in which experiment were conducted the cycling operation did not take place.

8.1.2 Conclusions from simulations of deployment of the Stirling engine based unit with different house heating system configurations and operating strategies

For the estimation of the annual performance two main operating scenarios were identified, and simulated; simultaneous CH and DHW heat generation and split CH and DHW heat generation.

simultaneous heat generation mode

1. The economic savings of **£**261 is predicted, which is attributed to the current UK feed-in-tariff rate.
2. The carbon savings are not achieved, in fact there is a rise in carbon emissions by about 16 %;
3. Such the operating regime was the least feasible in all scenarios investigated.

split heat generation mode

The mCHP operates for longer periods in this mode thus generating more electricity but also consuming more fuel at the lower efficiency.

1. The economic savings for this mode of operation is £244 and are due to the feed-in tariff scheme.
2. The carbon savings are marginal at 0.64 %, compared to a conventional domestic heating system.
3. This mode of operation was the most feasible in all scenarios investigated.

the effect of DHW tank capacity

The rise in the DHW tank capacity is detrimental to annual performance of the mCHP system due to higher thermal losses in the tank and due to an extended operation on a daily basis with increased consumption of fuel.

the effect of the rise in electricity requirements

The rise in electricity requirements in the house result in a higher carbon emission savings due to higher on-site power utilisation, but marginally decreased the utility cost savings due to the higher cost of the imported fraction of electricity.

the effect of the rise in thermal requirements

1. Both Stirling and ICE mCHP systems provide the highest CO_2 emission savings in the buildings with average thermal demand (13-15 MWh_{th}). In buildings with good insulation and higher DHW demand mCHP exhibit a poor performance in terms of carbon savings.

2. In respect to the utility savings, regardless the technology, increasing the thermal load results in deterioration of the mCHP's economic performance.
3. In buildings with high thermal demand the 1 kW_e PEM FC mCHP exhibits the strong economic and environmental performance.
4. For both utility costs and carbon emissions, an increase in savings with increasing of the auxiliary Boiler/mCHP thermal outputs ratio is evident, which can be attributed to an increase in the combined thermal efficiency of the auxiliary boiler/mCHP system. Maximum savings were predicted the auxiliary Boiler/mCHP thermal outputs ratios between 1 and 1.2.

8.1.3 Conclusion from the theoretical simulations of various mCHP units

1 kW_e mCHP units

1. The PEM FC mCHP cannot be used on its own to meet heating demand in even small houses due to its low HPR.
2. The Stirling engine mCHP is the only unit which can be deployed in buildings without an additional burner due to the highest HPR. The low thermal efficiency results in the high fuel consumption and therefore marginal CO_2 savings can be achieved. The system provides the lowest utility cost savings.
3. Best performance was predicted for the ICE engine based mCHP unit which is attributed to the quick start-up transient process, moderate electricity import and the highest combined thermal (CHP/Boiler) efficiency.

mCHP units in the range of 2-3 kW_e

The best performance is demonstrated by the 3 kW_e ICE and Stirling base mCHP units depending on the energy requirements of the building

8.1.4 Conclusions from simulations of deployment of a mix of mCHP technologies on a district/street scale

The ecological and economical impacts of deployment of a mix of mCHP technologies on a district/street levels (61, 120 and 240-house streets). Technologies considered for a mix are Stirling and ICE engines and PEM fuel cells.

1. In all street scenarios savings in annual carbon emissions and utility costs are achieved. Savings in the carbon emissions are in the range of 1-5 % whilst reductions in the utility costs are between 28.5 and 31.7 %

2. The negative ecological impact of individual mCHP units with poorer performance was compensated by mCHPs with better performance in the mix.

3. In the scenario in which all conventional heating equipment was replaced with the mCHP technologies, which demonstrated the best performance, both carbon and utility cost savings were enhanced. Reductions are in the range of 3.6-5.2 % and 31-32.5 % for the carbon emissions and utility costs, respectively.

4. Simulations of two bungalows with different occupancy patterns and with power interaction indicate that both economic and environmental performance of buildings were enhanced by about 4 % as a result of the higher rate of on-site electricity utilisation.

8.2 Recommendations for future work

In respect to the experimental work

1. The effect of the water tank volumes should be assessed experimentally on the test rig.

2. DHW usage profile during the operation of the mCHP should be implemented in experimental investigations.
3. Experimental evaluation of a PEM FC mCHP system with fuel reformer should be carried out in order to improve the accuracy of theoretical simulations of energy performance of houses.

In respect to the theoretical work:

1. The EnergyPlus software should be improved in order to accurately present the dynamic behaviour of all mCHP systems. This can be implemented by activating an empirical power generation equation.
2. Further improvements in the Fuel Cell module in EnergyPlus are required to include interaction with the auxiliary burner. Additionally, an explicit heat-led operation option should be included in the modelling procedure in software.
3. The effect of the power interaction should be assessed on the street level.

References

[1] G. Baiocchi, J. Minx, and K. Hubacek, "The Impact of Social Factors and Consumer Behavior on Carbon Dioxide Emissions in the United Kingdom," Journal of Industrial Ecology, vol. 14, pp. 50-72, 2010.

[2] M. Chitnis, A. Druckman, L. C. Hunt, T. Jackson, and S. Milne, "Forecasting scenarios for UK household expenditure and associated GHG emissions: Outlook to 2030," Ecological Economics, vol. 84, pp. 129-141, 2012.

[3] R. B. Beith, Small and micro combined heat and power (CHP) systems: advanced design, performance, materials and applications. Oxford: Woodhead, 2011.

[4] I. B. Mike Knowles, Bob Beith, Micro Energy Systems: Review of Technology, Issues of Scale and Integration: Professional Engineering Publishing, 2004.

[5] G. Walker, Stirling Engines. United States, New York: Oxford University Press, 1980.

[6] "Stirling Engines Assessment," EPRI, Palo, Alto, CA:2002. 1007317.

[7] http://www.microchap.info/.

[8] http://www.baxi.co.uk/index.htm.

[9] http://www.inspirit-energy.com/index.php.

[10] "http://www.qnergy.com/."

[11] http://www.whispergen-europe.com/stirling_en.php.

[12] J. B. Heywood, Internal combustion engine fundamental: Mc Graw Hill, 1988.

[13] http://web.mit.edu/16.unified/www/SPRING/propulsion/notes/node25.html.

[14] http://www.baxi-senertec.co.uk/html/baxi_senertec.htm.

[15] http://www.vaillant.com/.

[16] http://world.honda.com/power/cogenerator/.

[17] http://www.proenvis.de/.

[18] R. P. O'Hayre, Fuel cell fundamentals. Hoboken, N.J. : Wiley2006, 2006.

[19] Y. Wang, K. S. Chen, J. Mishler, S. C. Cho, and X. C. Adroher, "A review of polymer electrolyte membrane fuel cells: Technology, applications, and needs on fundamental research," Applied Energy, vol. 88, pp. 981-1007, 2011.

[20] http://www.tokyo-gas.co.jp/techno/stp1/00h1_e.html.

[21] http://www.elcore.com/de/home.html.

[22] http://panasonic.co.jp/ap/FC/en_index.html.

[23] http://www.hexis.com/.

[24] H. N. S. Michael J. Moran, Fundamentals of Engineering Thermodynamics, Sixth ed.: John Wiley & Sons, Inc, 2010.

[25] [http://www.learnthermo.com/T1-tutorial/ch09/lesson-D/pg05.php].

[26] M. Farrokhi, S. H. Noie, and A. A. Akbarzadeh, "Preliminary experimental investigation of a natural gas-fired ORC-based micro-CHP system for residential buildings," Applied Thermal Engineering.

[27] G. Qiu, Y. Shao, J. Li, H. Liu, and S. B. Riffat, "Experimental investigation of a biomass-fired ORC-based micro-CHP for domestic applications," Fuel, vol. 96, pp. 374-382, 2012.

[28] J. Li, G. Pei, Y. Li, and J. Ji, "Analysis of a novel gravity driven organic Rankine cycle for small-scale cogeneration applications," Applied Energy, vol. 108, pp. 34-44, 2013.

[29] G. Valenti, P. Silva, N. Fergnani, G. Di Marcoberardino, S. Campanari, and E. Macchi, "Experimental and Numerical Study of a Micro-cogeneration Stirling Engine for Residential Applications," Energy Procedia, vol. 45, pp. 1235-1244, 2014.

[30] S. Karmacharya, G. Putrus, C. P. Underwood, K. Mahkamov, S. McDonald, and A. Alexakis, "Simulation of energy use in buildings with multiple micro generators," Applied Thermal Engineering, vol. 62, pp. 581-592, 2014.

[31] G. Conroy, A. Duffy, and L. M. Ayompe, "Validated dynamic energy model for a Stirling engine μ-CHP unit using field trial data from a domestic dwelling," Energy and Buildings, vol. 62, pp. 18-26, 2013.

[32] M. N. David Kane, "Scenarios for Carbon Abatement in Dwellings by Implementation of Stirling Engine Micro-CHP Systems," The Fourth International Conference on Energy Efficiency in Domestic Appliances and Lighting (EEDAL), 2006.

[33] J. E. Thorsen, Bovin, J. And Carlsen, H., "3KW Stirling Engine for power and Heat Production," Proceedings of the International Energy Conversion Engineering Conference, 1996.

[34] S. Bell M., M., Entchev, E., Gusdorf, J., Kalbfleisch, W., Marchand, R., and Szadkowski, F. , "Testing Residential Combined Heat and Power Systems at the Canadian Centre for Housing Technology."

[35] A. A. Aliabadi, M. J. Thomson, J. S. Wallace, T. Tzanetakis, W. Lamont, and J. Di Carlo, "Efficiency and Emissions Measurement of a Stirling-Engine-Based Residential Microcogeneration System Run on Diesel and Biodiesel," Energy & Fuels, vol. 23, pp. 1032-1039, 2009.

[36] S. Thiers, B. Aoun, and B. Peuportier, "Experimental characterization, modeling and simulation of a wood pellet micro-combined heat and power unit used as a heat source for a residential building," Energy and Buildings, vol. 42, pp. 896-903, 2010.

[37] D. C. G. Veitch and K. Mahkamov, "Assessment of economical and ecological benefits from deployment of a domestic combined heat and power unit based on its

experimental performance," Proceedings of the Institution of Mechanical Engineers, Part A: Journal of Power and Energy, vol. 223, pp. 783-798, 2009.

[38] M. A. Ehyaei, P. Ahmadi, F. Atabi, M. R. Heibati, and M. Khorshidvand, "Feasibility study of applying internal combustion engines in residential buildings by exergy, economic and environmental analysis," Energy and Buildings, vol. 55, pp. 405-413, 2012.

[39] F. Caresana, C. Brandoni, P. Feliciotti, and C. M. Bartolini, "Energy and economic analysis of an ICE-based variable speed-operated micro-cogenerator," Applied Energy, vol. 88, pp. 659-671, 2011.

[40] C. D. Aussant, A. S. Fung, V. I. Ugursal, and H. Taherian, "Residential application of internal combustion engine based cogeneration in cold climate—Canada," Energy and Buildings, vol. 41, pp. 1288-1298, 2009.

[41] H. I. Onovwiona, V. Ismet Ugursal, and A. S. Fung, "Modeling of internal combustion engine based cogeneration systems for residential applications," Applied Thermal Engineering, vol. 27, pp. 848-861, 2007.

[42] A. Rosato and S. Sibilio, "Energy performance of a micro-cogeneration device during transient and steady-state operation: Experiments and simulations," Applied Thermal Engineering, vol. 52, pp. 478-491, 2013.

[43] An Experimental and Simulation-Based Investigation of the Performance of Small-Scale Fuel Cell and Combustion-Based Cogeneration Devices Serving Residential Buildings. Canada, , 2008.

[44] A. Rosato and S. Sibilio, "Performance assessment of a micro-cogeneration system under realistic operating conditions," Energy Conversion and Management, vol. 70, pp. 149-162, 2013.

[45] A. Rosato and S. Sibilio, "Calibration and validation of a model for simulating thermal and electric performance of an internal combustion engine-based micro-cogeneration device," Applied Thermal Engineering, vol. 45–46, pp. 79-98, 2012.

[46] E. Entchev, L. Yang, F. Szadkowski, M. Armstrong, and M. Swinton, "Application of hybrid micro-cogeneration system—Thermal and power energy solutions for Canadian residences," Energy and Buildings, vol. 60, pp. 345-354, 2013.

[47] A. Algieri and P. Morrone, "Techno-economic Analysis of Biomass-fired ORC Systems for Single-family Combined Heat and Power (CHP) Applications," Energy Procedia, vol. 45, pp. 1285-1294, 2014.

[48] S. R. Wood and P. N. Rowley, "A techno-economic analysis of small-scale, biomass-fuelled combined heat and power for community housing," Biomass and Bioenergy, vol. 35, pp. 3849-3858, 2011.

[49] M. Uris, J. I. Linares, and E. Arenas, "Techno-economic feasibility assessment of a biomass cogeneration plant based on an Organic Rankine Cycle," Renewable Energy, vol. 66, pp. 707-713, 2014.

[50] A. Stoppato, "Energetic and economic investigation of the operation management of an Organic Rankine Cycle cogeneration plant," Energy, vol. 41, pp. 3-9, 5// 2012.

[51] P. Ahmadi, I. Dincer, and M. A. Rosen, "Exergo-environmental analysis of an integrated organic Rankine cycle for trigeneration," Energy Conversion and Management, vol. 64, pp. 447-453, 2012.

[52] H. Liu, Y. Shao, and J. Li, "A biomass-fired micro-scale CHP system with organic Rankine cycle (ORC) – Thermodynamic modelling studies," Biomass and Bioenergy, vol. 35, pp. 3985-3994, 2011.

[53] S. Quoilin, M. Orosz, H. Hemond, and V. Lemort, "Performance and design optimization of a low-cost solar organic Rankine cycle for remote power generation," Solar Energy, vol. 85, pp. 955-966, 2011.

[54] B. C. H. Steele, "Material science and engineering: The enabling technology for the commercialisation of fuel cell systems," Journal of Materials Science, vol. 36, pp. 1053-1068, 2001.

[55] K. B. Prater, "Solid polymer fuel cells for transport and stationary applications," Journal of Power Sources, vol. 61, pp. 105-109, 1996.

[56] S. J. C. Cleghorn, X. Ren, T. E. Springer, M. S. Wilson, C. Zawodzinski, T. A. Zawodzinski, et al., "Pem fuel cells for transportation and stationary power generation applications," International Journal of Hydrogen Energy, vol. 22, pp. 1137-1144, 1997.

[57] M. W. Ellis, American Society of Heating, Refrigerating and Air-Conditioning Engineers, Fuel cells for building applications, 2002.

[58] Y. Hou, Z. Yang, and X. Fang, "An experimental study on the dynamic process of PEM fuel cell stack voltage," Renewable Energy, vol. 36, pp. 325-329, 2011.

[59] C. Kunusch, P. F. Puleston, M. A. Mayosky, and J. J. Moré, "Characterization and experimental results in PEM fuel cell electrical behaviour," International Journal of Hydrogen Energy, vol. 35, pp. 5876-5881, 2010.

[60] Y. Tang, W. Yuan, M. Pan, Z. Li, G. Chen, and Y. Li, "Experimental investigation of dynamic performance and transient responses of a kW-class PEM fuel cell stack under various load changes," Applied Energy, vol. 87, pp. 1410-1417, 2010.

[61] A. Ferguson and V. Ismet Ugursal, "Fuel cell modelling for building cogeneration applications," Journal of Power Sources, vol. 137, pp. 30-42, 2004.

[62] L. Wang, A. Husar, T. Zhou, and H. Liu, "A parametric study of PEM fuel cell performances," International Journal of Hydrogen Energy, vol. 28, pp. 1263-1272, 2003.

[63] A. Iranzo, M. Muñoz, E. López, J. Pino, and F. Rosa, "Experimental fuel cell performance analysis under different operating conditions and bipolar plate designs," International Journal of Hydrogen Energy, vol. 35, pp. 11437-11447, 2010.

[64] J. Cho, H.-S. Kim, and K. Min, "Transient response of a unit proton-exchange membrane fuel cell under various operating conditions," Journal of Power Sources, vol. 185, pp. 118-128, 2008.

[65] Q. Yan, H. Toghiani, and H. Causey, "Steady state and dynamic performance of proton exchange membrane fuel cells (PEMFCs) under various operating conditions and load changes," Journal of Power Sources, vol. 161, pp. 492-502, 2006.

[66] S. Kim, S. Shimpalee, and J. W. Van Zee, "The effect of reservoirs and fuel dilution on the dynamic behavior of a PEMFC," Journal of Power Sources, vol. 137, pp. 43-52, 2004.

[67] G.-B. Jung, K.-F. Lo, A. Su, F.-B. Weng, C.-H. Tu, T.-F. Yang, et al., "Experimental evaluation of an ambient forced-feed air-supply PEM fuel cell," International Journal of Hydrogen Energy, vol. 33, pp. 2980-2985, 2008.

[68] S. Kim, S. Shimpalee, and J. W. Van Zee, "The effect of stoichiometry on dynamic behavior of a proton exchange membrane fuel cell (PEMFC) during load change," Journal of Power Sources, vol. 135, pp. 110-121, 2004.

[69] J. Benziger, E. Chia, J. F. Moxley, and I. G. Kevrekidis, "The dynamic response of PEM fuel cells to changes in load," Chemical Engineering Science, vol. 60, pp. 1743-1759, 2005.

[70] J. Chen and B. Zhou, "Diagnosis of PEM fuel cell stack dynamic behaviors," Journal of Power Sources, vol. 177, pp. 83-95, 2008.

[71] J. Hamelin, K. Agbossou, A. Laperrière, F. Laurencelle, and T. K. Bose, "Dynamic behavior of a PEM fuel cell stack for stationary applications," International Journal of Hydrogen Energy, vol. 26, pp. 625-629, 2001.

[72] K. Jiao, J. Park, and X. Li, "Experimental investigations on liquid water removal from the gas diffusion layer by reactant flow in a PEM fuel cell," Applied Energy, vol. 87, pp. 2770-2777, 2010.

[73] D. Spernjak, A. K. Prasad, and S. G. Advani, "Experimental investigation of liquid water formation and transport in a transparent single-serpentine PEM fuel cell," Journal of Power Sources, vol. 170, pp. 334-344, 2007.

[74] W.-M. Yan, X.-D. Wang, D.-J. Lee, X.-X. Zhang, Y.-F. Guo, and A. Su, "Experimental study of commercial size proton exchange membrane fuel cell performance," Applied Energy, vol. 88, pp. 392-396, 2011.

[75] T. Kim, C. Sim, and M. Kim, "Research on water discharge characteristics of PEM fuel cells by using neutron imaging technology at the NRF, HANARO," Applied Radiation and Isotopes, vol. 66, pp. 593-605, 2008.

[76] A. Arsalis, M. P. Nielsen, and S. K. Kær, "Modeling and parametric study of a 1 kWe HT-PEMFC-based residential micro-CHP system," International Journal of Hydrogen Energy, vol. 36, pp. 5010-5020, 2011.

[77] E.-D. Wang, P.-F. Shi, and C.-Y. Du, "Novel self-humidifying MEA with water transfer region for PEM fuel cells," Fuel Cells Bulletin, vol. 2008, pp. 12-16, 2008.

[78] Z. Qi and A. Kaufman, "PEM fuel cell stacks operated under dry-reactant conditions," Journal of Power Sources, vol. 109, pp. 469-476, 2002.

[79] T. E. Springer, T. A. Zawodzinski, and S. Gottesfeld, "Polymer Electrolyte Fuel Cell Model," Journal of The Electrochemical Society, vol. 138, pp. 2334-2342, 1991.

[80] D. M. Bernardi and M. W. Verbrugge, "A Mathematical Model of the Solid-Polymer-Electrolyte Fuel Cell," Journal of The Electrochemical Society, vol. 139, pp. 2477-2491, 1992.

[81] D. M. Bernardi and M. W. Verbrugge, "Mathematical model of a gas diffusion electrode bonded to a polymer electrolyte," AIChE Journal, vol. 37, pp. 1151-1163, 1991.

[82] O. Shamardina, A. Chertovich, A. A. Kulikovsky, and A. R. Khokhlov, "A simple model of a high temperature PEM fuel cell," International Journal of Hydrogen Energy, vol. 35, pp. 9954-9962, 2010.

[83] M. Tohidi, S. H. Mansouri, and H. Amiri, "Effect of primary parameters on the performance of PEM fuel cell," International Journal of Hydrogen Energy, vol. 35, pp. 9338-9348, 2010.

[84] A. Rowe and X. Li, "Mathematical modeling of proton exchange membrane fuel cells," Journal of Power Sources, vol. 102, pp. 82-96, 2001.

[85] G. Karimi and X. Li, "Electroosmotic flow through polymer electrolyte membranes in PEM fuel cells," Journal of Power Sources, vol. 140, pp. 1-11, 2005.

[86] P. K. Das, X. Li, and Z.-S. Liu, "Analysis of liquid water transport in cathode catalyst layer of PEM fuel cells," International Journal of Hydrogen Energy, vol. 35, pp. 2403-2416, 2010.

[87] S. M. Sharifi Asl, S. Rowshanzamir, and M. H. Eikani, "Modelling and simulation of the steady-state and dynamic behaviour of a PEM fuel cell," Energy, vol. 35, pp. 1633-1646, 2010.

[88] S. P. Philipps and C. Ziegler, "Computationally efficient modeling of the dynamic behavior of a portable PEM fuel cell stack," Journal of Power Sources, vol. 180, pp. 309-321, 2008.

[89] T. Yalcinoz and M. S. Alam, "Dynamic modeling and simulation of air-breathing proton exchange membrane fuel cell," Journal of Power Sources, vol. 182, pp. 168-174, 2008.

[90] D. S. Falcão, P. J. Gomes, V. B. Oliveira, C. Pinho, and A. M. F. R. Pinto, "1D and 3D numerical simulations in PEM fuel cells," International Journal of Hydrogen Energy, vol. 36, pp. 12486-12498, 2011.

[91] A. Arsalis, M. P. Nielsen, and S. K. Kær, "Application of an improved operational strategy on a PBI fuel cell-based residential system for Danish single-family households," Applied Thermal Engineering, vol. 50, pp. 704-713, 2013.

[92] L. Barelli, G. Bidini, F. Gallorini, and A. Ottaviano, "Dynamic analysis of PEMFC-based CHP systems for domestic application," Applied Energy, vol. 91, pp. 13-28, 2012.

[93] S. Sevencan, T. Guan, G. Lindbergh, C. Lagergren, P. Alvfors, and B. Ridell, "Fuel cell based cogeneration: Comparison of electricity production cost for Swedish conditions," International Journal of Hydrogen Energy, vol. 38, pp. 3858-3864, 2013.

[94] S.-D. Oh, K.-Y. Kim, S.-B. Oh, and H.-Y. Kwak, "Optimal operation of a 1-kW PEMFC-based CHP system for residential applications," Applied Energy, vol. 95, pp. 93-101, 2012.

[95] G. Gigliucci, L. Petruzzi, E. Cerelli, A. Garzisi, and A. La Mendola, "Demonstration of a residential CHP system based on PEM fuel cells," Journal of Power Sources, vol. 131, pp. 62-68, 2004.

[96] B. Shabani and J. Andrews, "An experimental investigation of a PEM fuel cell to supply both heat and power in a solar-hydrogen RAPS system," International Journal of Hydrogen Energy, vol. 36, pp. 5442-5452, 2011.

[97] N. Briguglio, M. Ferraro, G. Brunaccini, and V. Antonucci, "Evaluation of a low temperature fuel cell system for residential CHP," International Journal of Hydrogen Energy, vol. 36, pp. 8023-8029, 2011.

[98] J. J. Hwang and M. L. Zou, "Development of a proton exchange membrane fuel cell cogeneration system," Journal of Power Sources, vol. 195, pp. 2579-2585, 2010.

[99] Y. Hamada, R. Goto, M. Nakamura, H. Kubota, and K. Ochifuji, "Operating results and simulations on a fuel cell for residential energy systems," Energy Conversion and Management, vol. 47, pp. 3562-3571, 2006.

[100] J. Geraldo de Melo Furtado, G. C. Gatti, E. T. Serra, and S. C. Anibal de Almeida, "Performance analysis of a 5 kW PEMFC with a natural gas reformer," International Journal of Hydrogen Energy, vol. 35, pp. 9990-9995, 2010.

[101] M. Radulescu, O. Lottin, M. Feidt, C. Lombard, D. L. Noc, and S. L. Doze, "Experimental results with a natural gas cogeneration system using a polymer exchange membrane fuel cell," Journal of Power Sources, vol. 159, pp. 1142-1146, 2006.

[102] D. Dalle Nogare, P. Baggio, C. Tomasi, L. Mutri, and P. Canu, "A thermodynamic analysis of natural gas reforming processes for fuel cell application," Chemical Engineering Science, vol. 62, pp. 5418-5424, 2007.

[103] E. Calò, A. Giannini, and G. Monteleone, "Small stationary reformers for H2 production from hydrocarbons," International Journal of Hydrogen Energy, vol. 35, pp. 9828-9835, 2010.

[104] A. Heinzel, B. Vogel, and P. Hübner, "Reforming of natural gas—hydrogen generation for small scale stationary fuel cell systems," Journal of Power Sources, vol. 105, pp. 202-207, 2002.

[105] H.-J. Jahn and W. Schroer, "Dynamic simulation model of a steam reformer for a residential fuel cell power plant," Journal of Power Sources, vol. 150, pp. 101-109, 2005.

[106] S. Campanari, E. Macchi, and G. Manzolini, "Innovative membrane reformer for hydrogen production applied to PEM micro-cogeneration: Simulation model and thermodynamic analysis," International Journal of Hydrogen Energy, vol. 33, pp. 1361-1373, 2008.

[107] N. Zuliani and R. Taccani, "Microcogeneration system based on HTPEM fuel cell fueled with natural gas: Performance analysis," Applied Energy, vol. 97, pp. 802-808, 2012.

[108] R.-F. Horng, C.-R. Chen, T.-S. Wu, and C.-H. Chan, "Cold start response of a small methanol reformer by partial oxidation reforming of hydrogen for fuel cell," Applied Thermal Engineering, vol. 26, pp. 1115-1124, 2006.

[109] A. Rosato, S. Sibilio, and G. Ciampi, "Energy, environmental and economic dynamic performance assessment of different micro-cogeneration systems in a residential application," Applied Thermal Engineering, vol. 59, pp. 599-617, 2013.

[110] D. Pineau, P. Rivière, P. Stabat, P. Hoang, and V. Archambault, "Performance analysis of heating systems for low energy houses," Energy and Buildings, vol. 65, pp. 45-54, 2013.

[111] S. Cao, A. Mohamed, A. Hasan, and K. Sirén, "Energy matching analysis of on-site micro-cogeneration for a single-family house with thermal and electrical tracking strategies," Energy and Buildings, vol. 68, Part A, pp. 351-363, 2014.

[112] B. C. M. Arteconi Alessia, Brandoni Caterina "Energy and economic analysis of small-scale distributed generation in the residential sector," 14th International Stirling Engine Conference, 2009.

[113] J. Cockroft and N. Kelly, "A comparative assessment of future heat and power sources for the UK domestic sector," Energy Conversion and Management, vol. 47, pp. 2349-2360, 2006.

[114] A. D. Peacock and M. Newborough, "Impact of micro-CHP systems on domestic sector CO2 emissions," Applied Thermal Engineering, vol. 25, pp. 2653-2676, 2005.

[115] V. Dorer and A. Weber, "Energy and CO2 emissions performance assessment of residential micro-cogeneration systems with dynamic whole-building simulation programs," Energy Conversion and Management, vol. 50, pp. 648-657, 2009.

[116] V. Kuhn, J. Klemeš, and I. Bulatov, "MicroCHP: Overview of selected technologies, products and field test results," Applied Thermal Engineering, vol. 28, pp. 2039-2048, 2008.

[117] C. Roselli, M. Sasso, S. Sibilio, and P. Tzscheutschler, "Experimental analysis of microcogenerators based on different prime movers," Energy and Buildings, vol. 43, pp. 796-804, 2011.

[118] E. S. Barbieri, P. R. Spina, and M. Venturini, "Analysis of innovative micro-CHP systems to meet household energy demands," Applied Energy.

[119] B. Thomas, "Benchmark testing of Micro-CHP units," Applied Thermal Engineering, vol. 28, pp. 2049-2054, 2008.

[120] V. Dorer, R. Weber, and A. Weber, "Performance assessment of fuel cell micro-cogeneration systems for residential buildings," Energy and Buildings, vol. 37, pp. 1132-1146, 2005.

[121] K. R. Voorspools and W. D. D'Haeseleer, "The evaluation of small cogeneration for residential heating," International Journal of Energy Research, vol. 26, pp. 1175-1190, 2002.

[122] C. Trust, "Micro-CHP Accelerator," 2011.

[123] A. Reacock, Newborough, M. , "Micro Generation Opportunities in the UK Residential Sector," World Renewable Energy Congress VIII (WREC), 2004.

[124] A. D. Hawkes and M. A. Leach, "Cost-effective operating strategy for residential micro-combined heat and power," Energy, vol. 32, pp. 711-723, 2007.

[125] F. Lin and J. Yi, "Optimal operation of a CHP plant for space heating as a peak load regulating plant," Energy, vol. 25, pp. 283-298, 2000.

[126] M. De Paepe, P. D'Herdt, and D. Mertens, "Micro-CHP systems for residential applications," Energy Conversion and Management, vol. 47, pp. 3435-3446, 2006.

[127] H. Zhao, J. Holst, and L. Arvastson, "Optimal operation of coproduction with storage," Energy, vol. 23, pp. 859-866, 1998.

[128] D. Haeseldonckx, L. Peeters, L. Helsen, and W. D'haeseleer, "The impact of thermal storage on the operational behaviour of residential CHP facilities and the overall CO2 emissions," Renewable and Sustainable Energy Reviews, vol. 11, pp. 1227-1243, 2007.

[129] B. Rolfsman, "Combined heat-and-power plants and district heating in a deregulated electricity market," Applied Energy, vol. 78, pp. 37-52, 2004.

[130] A. D. Peacock and M. Newborough, "Effect of heat-saving measures on the CO2 savings attributable to micro-combined heat and power (μCHP) systems in UK dwellings," Energy, vol. 33, pp. 601-612, 2008.

[131] A. D. Hawkes and M. A. Leach, "The capacity credit of micro-combined heat and power," Energy Policy, vol. 36, pp. 1457-1469, 2008.

[132] A. Hawkes and M. Leach, "Impacts of temporal precision in optimisation modelling of micro-Combined Heat and Power," Energy, vol. 30, pp. 1759-1779, 2005.

[133] M. Newborough and P. Augood, "Demand-side management opportunities for the UK domestic sector," Generation, Transmission and Distribution, IEE Proceedings-, vol. 146, pp. 283-293, 1999.

[134] K. R. Voorspools and W. D. D'Haeseleer, "The impact of the implementation of cogeneration in a given energetic context," Energy Conversion, IEEE Transactions on, vol. 18, pp. 135-141, 2003.

[135] T. Oda, Akisawa, A. and Kashiwagi T, "A Theoretical Evaluation of a Cogeneration System's Total Energy Efficiency Considering Fluctuation in Heat and Power Demands," World Renewable Energy Congress VIII (WREC), 2004.

[136] N. L. Truong, A. Dodoo, and L. Gustavsson, "Effects of heat and electricity saving measures in district-heated multistory residential buildings," Applied Energy, vol. 118, pp. 57-67, 2014.

[137] J. Duquette, P. Wild, and A. Rowe, "The potential benefits of widespread combined heat and power based district energy networks in the province of Ontario," Energy, vol. 67, pp. 41-51, 2014.

[138] A. Boyano, P. Hernandez, and O. Wolf, "Energy demands and potential savings in European office buildings: Case studies based on EnergyPlus simulations," Energy and Buildings, vol. 65, pp. 19-28, 2013.

[139] N. Fumo, P. Mago, and R. Luck, "Methodology to estimate building energy consumption using EnergyPlus Benchmark Models," Energy and Buildings, vol. 42, pp. 2331-2337, 2010.

[140] N. M. Mateus, A. Pinto, and G. C. d. Graça, "Validation of EnergyPlus thermal simulation of a double skin naturally and mechanically ventilated test cell," Energy and Buildings, vol. 75, pp. 511-522, 2014.

[141] D. B. Crawley, L. K. Lawrie, F. C. Winkelmann, W. F. Buhl, Y. J. Huang, C. O. Pedersen, et al., "EnergyPlus: creating a new-generation building energy simulation program," Energy and Buildings, vol. 33, pp. 319-331, 2001.

[142] R. F. Michael Stadler, Dimitri Curtil, Chris Marnay, "On-Site Generation Simulation with EnergyPlus for Commercial Buildings," LBNL, p. 12, 2006.

[143] http://apps1.eere.energy.gov/buildings/energyplus/?utm_source=EnergyPlus&utm_medium=redirect&utm_campaign=EnergyPlus%2Bredirect%2B1.

[144] http://www.doe2.com/.

[145] O. M. Al-Rabghi and D. C. Hittle, "Energy simulation in buildings: overview and BLAST example," Energy Conversion and Management, vol. 42, pp. 1623-1635, 2001.

[146] http://apps1.eere.energy.gov/buildings/energyplus/energyplus_documentation.cfm.

[147] EDSL, Construction Materials Database, 2011.

[148] G. Gkounis, "Impact of micro CHP on the energy performance of a typical UK house using EnergyPlus software," 2009.

[149] Information related to the feed in tariff scheme available at www.fitariffs.co.uk.

[150] Rates in electricty and gas available at www.Eonenergy.com.

[151] D. Jack, "Experimental and theoretical analysis of the performance of a Whispergen MkVb μCHP unit in a UK 4 bed detached house," Durham University, 2011.

Appendix A

Validation of the Stirling based mCHP power delay modelling approach

The modelling method used for description of the operation of the Stirling engine based mCHP assumes that the heat generation depends on the engine's temperature. This approach is in a good agreement with experimental results described in (Section 5.2.6). This approach was suggested by EnergyPlus developers as the most adequate method for simulating particularly Stirling engine based mCHPs. Additionally, the operation of the Stirling engine is simulated using a power delay method (normally used with IC engines). Figure A.1 shows theoretical and experimental results on simulation of the dynamic operation of the Stirling engine mCHP.

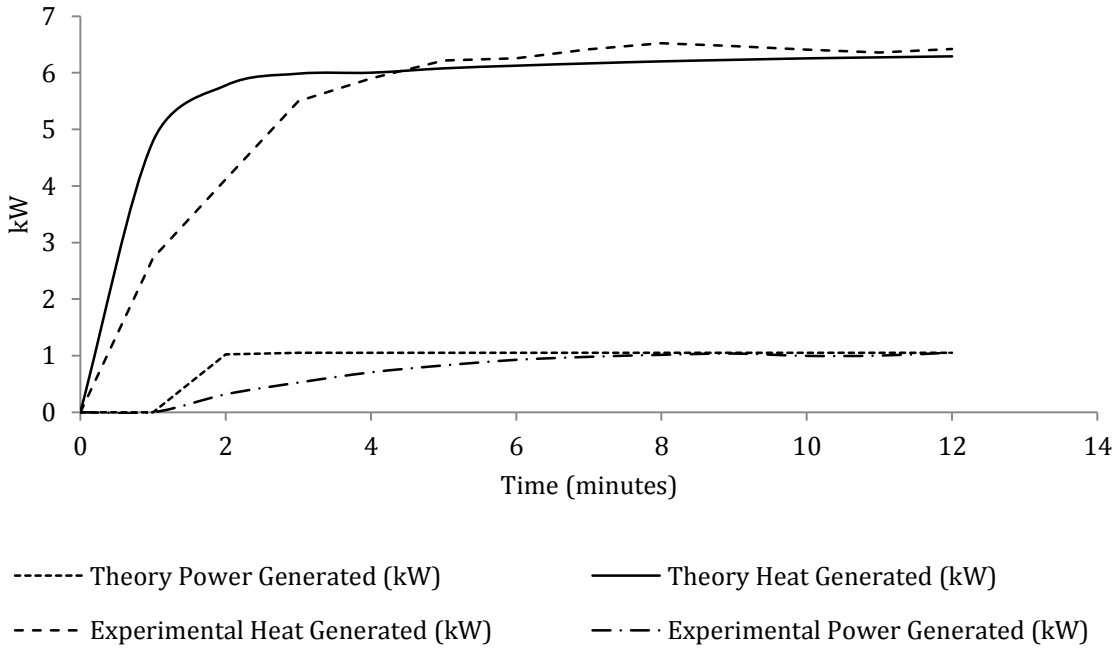

Figure A.1 Validation of theoretical modelling of operation of Stirling engine based mCHP using "Power delay" approach

It can be seen in Figure A.1 that the theoretical modelling predicts a significantly faster response to the heat requirements. Dynamic characteristics during the start-up resume are not included in this approach and the engine reaches the steady state significantly sooner that in

real conditions. In respect to the power generation it can be seen that there is a delay period during start-up (2 minutes). The mCHP reaches the nominal electric capacity within 1 minute period, i.e. significantly faster than in experimental conditions. There is no a noticeable difference in results during the steady state operation for both heat and power generation. Overall, this theoretical method produces less accurate results and therefore was not deployed in the current research.

Appendix B

Operation of mCHP systems in a semi-detached building satisfying 1996 constructions regulations

The operation of 2 and 3 kW_e ICE and 3 kW_e Stirling mCHP units in base scenario case demand profiles, and DHW profiles are presented in Figures B.1-B.6

Base Demand profiles (Electricity - 4.6 MWh_e, DHW – 200 L/day)

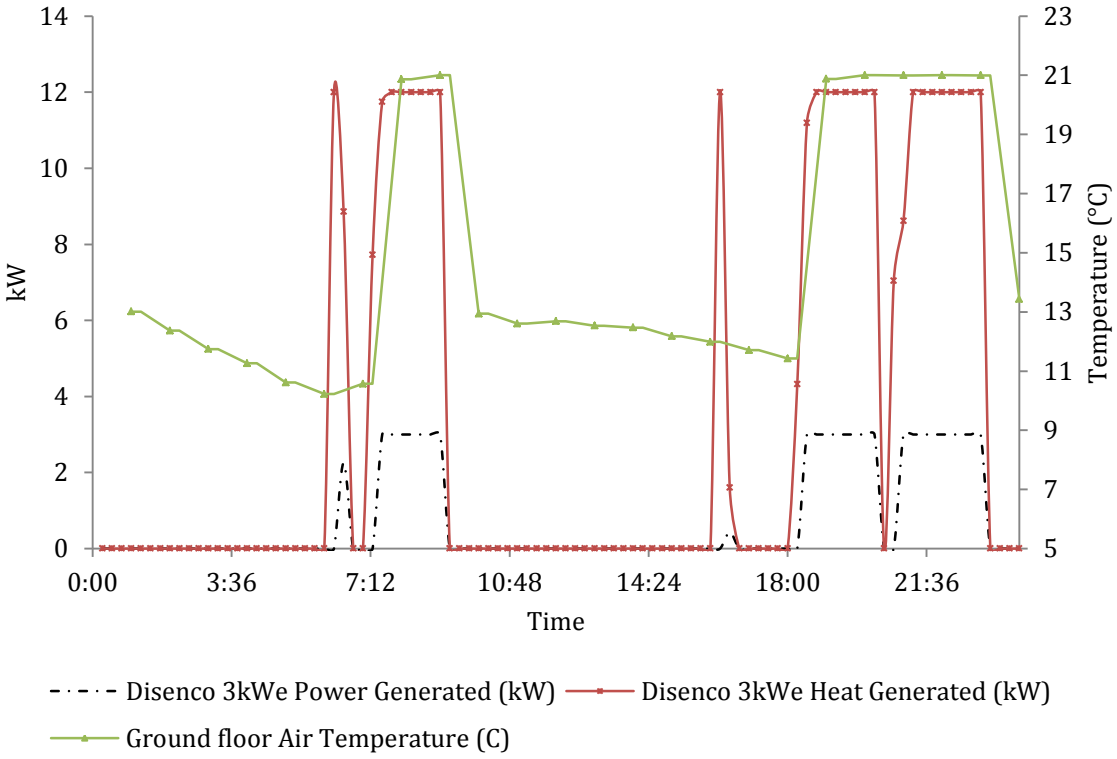

Figure B.1 Heat and Power generation by 3 kWe Disenco mCHP combined with a 150 L DHW tank in winter weekday

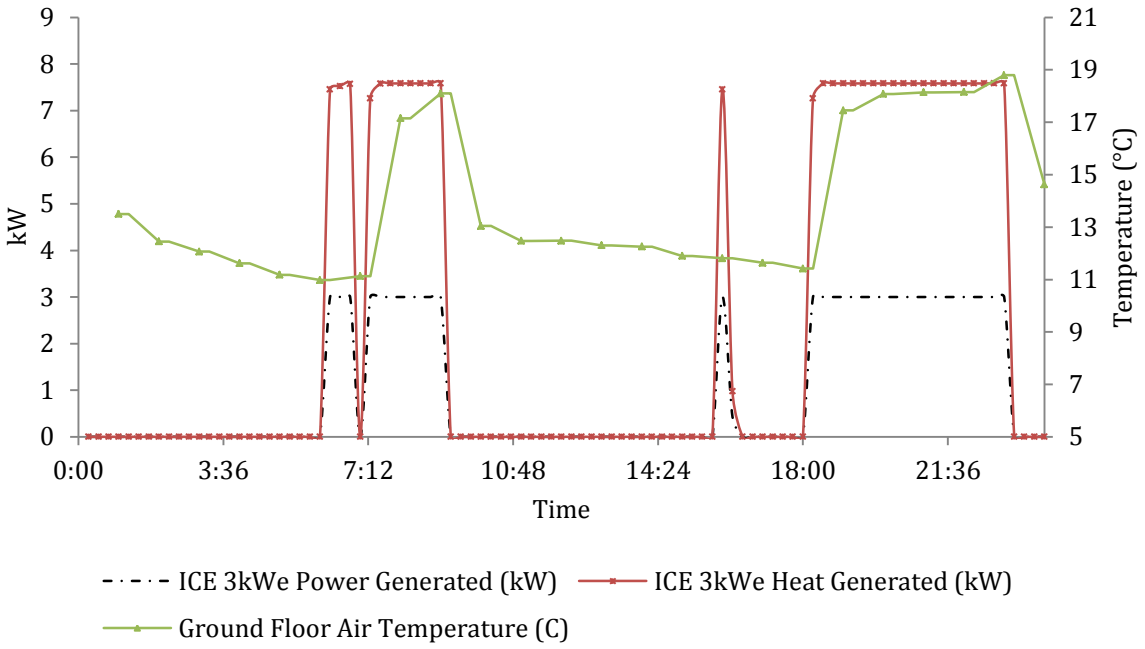

Figure B.2 Heat and Power generation by 3 kWe ICE mCHP combined with a 150 L DHW tank in winter weekday

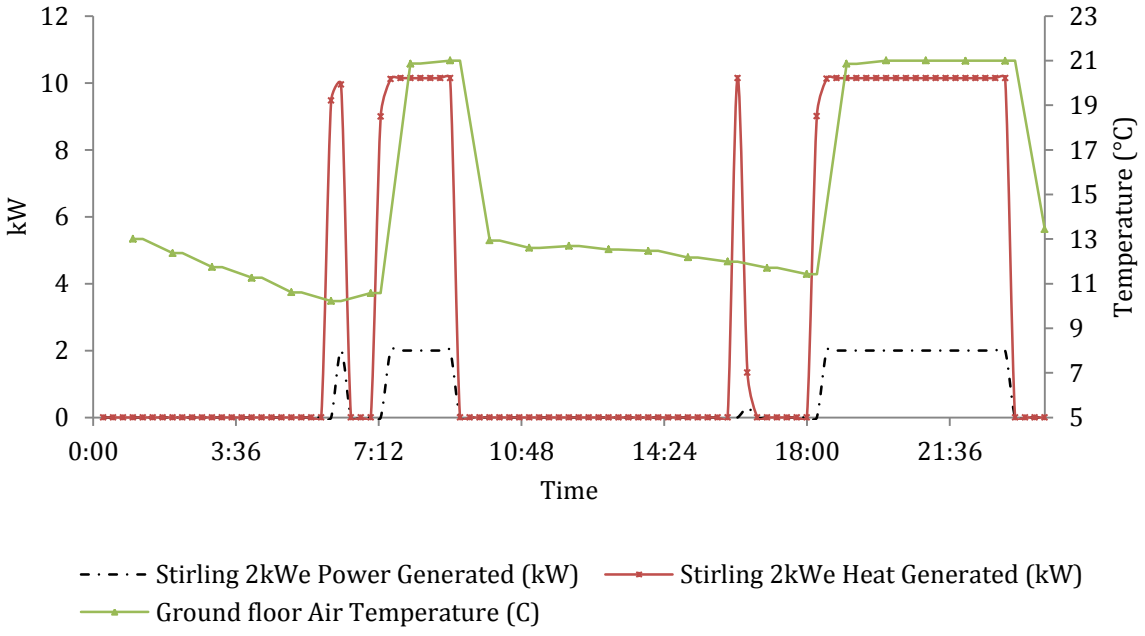

Figure B.3 Heat and Power generation by 2 kWe Stirling engine mCHP combined with a 150 L DHW tank in winter weekday

Increased DHW demand (Electricity - 4.6 MWh$_e$, DHW – 250 L/day)

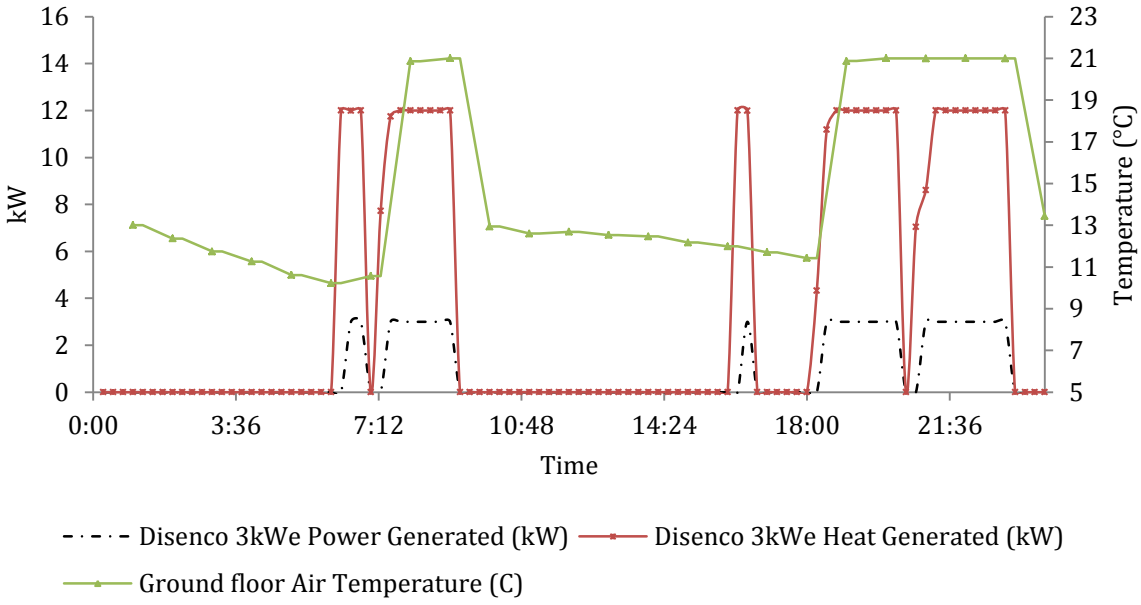

Figure B.4 Heat and Power generation by 3 kWe Disenco mCHP combined with a 200 L DHW tank in winter weekday

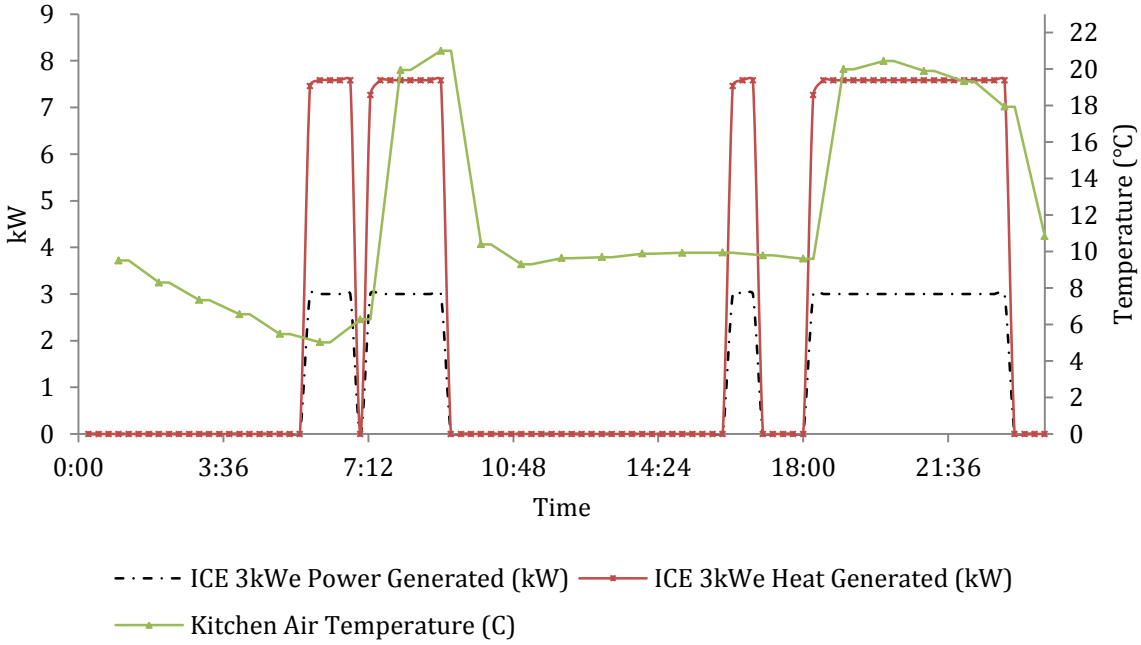

Figure B.5 Heat and Power generation by 3 kWe ICE mCHP combined with a 200 L DHW tank in winter weekday

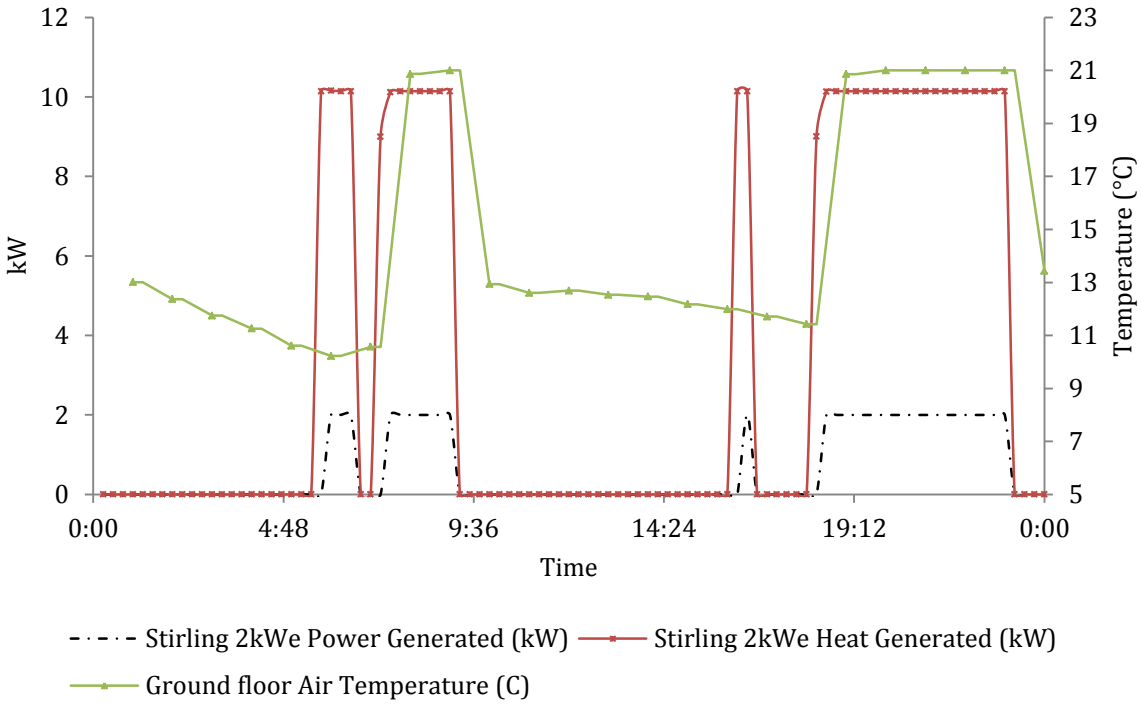

Figure B.6 Heat and Power generation by 2 kWe Stirling engine mCHP combined with a 200 L DHW tank in winter weekday